学位論文

Curvature Perturbations and Primordial Black Hole Formation in the Inflationary Universe

(インフレーション宇宙における曲率ゆらぎと原始ブラックホール形成)

平成 28 年 12 月博士（理学）申請

東京大学大学院理学系研究科

物理学専攻

多田 祐一郎

Ph.D. thesis

Curvature Perturbations and Primordial Black Hole Formation in the Inflationary Universe

Yuichiro Tada

Department of Physics, The University of Tokyo, Bunkyo-ku, Tokyo 113-0033, Japan
Kavli Institute for the Physics and Mathematics of the Universe (WPI), UTIAS, The University of Tokyo, 5-1-5 Kashiwanoha, Kashiwa, Chiba 277-8583, Japan
Institute for Cosmic Ray Research, The University of Tokyo, 5-1-5 Kashiwanoha, Kashiwa, Chiba 277-8582, Japan

E-mail: yuichiro.tada@ipmu.jp

Referees

Dr. Masahiro Kawasaki	Supervisor
Dr. Hitoshi Murayama	Supervisor
Dr. Koichi Hamaguchi	Chief Examiner
Dr. Aya Bamba	Examiner
Dr. Masahiro Ibe	Examiner
Dr. Shinji Miyoki	Examiner
Dr. Jun'ichi Yokoyama	Examiner

February 10, 2017

Abstract

In this thesis, we discuss the generation of the curvature perturbations during inflation beyond the linear perturbation theory as well as the primordial black hole formation in two classes of double inflation. We proposed the non-perturbative algorithm called *stochastic-δN formalism* for the calculation of the power spectrum of the curvature perturbations, combining the stochastic and δN formalism. This algorithm can be applied for generic classes of inflation. Also the interpretation of the so-called local observer effect of the squeezed bispectrum is shown with use of the δN formalism. Then we concretely discuss the PBH formation in chaotic-new double inflation and hybrid inflation. In the chaotic-new inflation model which is supported in terms of supergravity, both abundant PBHs for dark matter and massive PBHs for LIGO's gravitational wave events can be realized simultaneously. The expected secondary gravitational waves are marginally consistent with the current pulsar timing array constraints. On the other hand, with use of the stochastic-δN formalism, we prove that the detectably massive PBHs cannot be produced in hybrid inflation with appropriate abundance, but rather they are inevitably overproduced. The specific power spectra of the curvature perturbations are also shown as an example of the stochastic-δN formalism.

To Hiroko,

Hitoshi and Yumiko

Contents

Notation

We adopt the natural unit $c = \hbar = k_\mathrm{B} = 1$ unless otherwise noted, and in Chapters 3, 5, 6 and Appendix C the reduced Planck mass $M_\mathrm{Pl} = \sqrt{\frac{\hbar c}{8\pi G}} = 4.341 \times 10^{-6}\,\mathrm{g} = 2.435 \times 10^{18} c^{-2}\,\mathrm{GeV} = (2.814 \times 10^{-43} c^2 \hbar^{-1}\,\mathrm{s})^{-1}$ is also set to unity.

Latin indices i, j, k, and so on generally run over the three spatial coordinate labels, usually taken as 1, 2, 3. Greek indices μ, ν, etc. generally run over the four spacetime coordinate labels 1, 2, 3, 0, with x^0 the time coordinate.

The flat spacetime metric is $\eta_{\mu\nu} = \mathrm{diag}(-1, 1, 1, 1)$.

Variables in boldface characters ($\mathbf{p}$, $\mathbf{k}$, and so on) indicate three-vectors. For them, variables in normal characters represent their three-norm ($p = \sqrt{p_1^2 + p_2^2 + p_3^2}$ etc.).

The Fourier transformation and its inverse are defined by

$$f(\mathbf{x}) = \int \frac{\mathrm{d}^3 k}{(2\pi)^3} f_\mathbf{k} \mathrm{e}^{i\mathbf{k}\cdot\mathbf{x}}, \qquad f_\mathbf{k} = \int \mathrm{d}^3 x\, f(\mathbf{x}) \mathrm{e}^{-i\mathbf{k}\cdot\mathbf{x}}. \tag{0.0.1}$$

Acronyms & Symbols

FLRW	···	Friedmann–Lemaître–Robertson–Walker
CMB	···	cosmic microwave background
BBN	···	big-bang nucleosynthesis
NG	···	non-Gaussianity
PBH	···	primordial black hole
SMBH	···	supermassive black hole
DM	···	dark matter
GW	···	gravitational wave
PTA	···	pulsar timing array
vev	···	vacuum expectation value
w.r.t.	···	with respect to
PDF	···	probability distribution function
EoM	···	equation of motion
EoS	···	equation of state

CR	$\cdots$	consistency relation
SUSY	$\cdots$	supersymmetry
SUGRA	$\cdots$	supergravity

$M_\odot$	$\cdots$	The solar mass $\sim 2 \times 10^{33}$ g.
$P_\mathcal{O}(k)$	$\cdots$	The power spectrum of the operator $\mathcal{O}$. $\langle \mathcal{O}_\mathbf{k} \mathcal{O}_\mathbf{p} \rangle = (2\pi)^3 \delta^{(3)}(\mathbf{k}+\mathbf{p}) P_\mathcal{O}(k)$, or $P_\mathcal{O}(k) = \int \mathrm{d}^3x \, \langle \mathcal{O}(\mathbf{x})\mathcal{O}(\mathbf{y})\rangle \, \mathrm{e}^{-i\mathbf{k}\cdot(\mathbf{x}-\mathbf{y})}$.
$\mathcal{P}_\mathcal{O}(k)$	$\cdots$	The power spectrum of the operator $\mathcal{O}$ per logarithmic k interval: $\mathcal{P}_\mathcal{O}(k) = \frac{k^3}{2\pi^2} P_\mathcal{O}(k)$. Indeed, if $P_\mathcal{O}(k)$ is a function only of the norm k due to the rotational invariance, it satisfies $\int \frac{\mathrm{d}^3k}{(2\pi)^3} P_\mathcal{O}(k) = \int \mathrm{d}k \frac{k^2}{2\pi^2} P_\mathcal{O}(k) = \int \mathrm{d}\log k \, \mathcal{P}_\mathcal{O}(k)$.
$B_\mathcal{O}(k_1, k_2, k_3)$	$\cdots$	The bispectrum of the operator $\mathcal{O}$. $\langle \mathcal{O}_{\mathbf{k}_1} \mathcal{O}_{\mathbf{k}_2} \mathcal{O}_{\mathbf{k}_3} \rangle = (2\pi)^3 \delta^{(3)}(\mathbf{k}_1+\mathbf{k}_2+\mathbf{k}_3) B_\mathcal{O}(k_1, k_2, k_3)$, or $B_\mathcal{O}(k_1, k_2, k_3) = \int \mathrm{d}^3x \mathrm{d}^3y \, \langle \mathcal{O}(\mathbf{x})\mathcal{O}(\mathbf{y})\mathcal{O}(\mathbf{z})\rangle \, \mathrm{e}^{-i\mathbf{k}_1\cdot(\mathbf{x}-\mathbf{z})-i\mathbf{k}_2\cdot(\mathbf{y}-\mathbf{z})}$.
∇^2	$\cdots$	The Laplacian $\frac{\partial^2}{\partial(x^1)^2} + \frac{\partial^2}{\partial(x^2)^2} + \frac{\partial^2}{\partial(x^3)^2}$.
∇_i	$\cdots$	The covariant derivative.

Introduction

0.1 Overview of modern cosmology

The standard model of the cosmology has greatly succeeded to describe a lot of phenomena of the universe. Among them, inflation has been a key topic for more than 30 years. Inflation [1–6], namely the accelerated expansion phase in the early universe, can at least postpone the singularity of the beginning of the universe to the far past. Also it can solve several problems of the big-bang theory such as the horizon problem, flatness problem, monopole problem, and so on. Furthermore, as its most important role, the inflationary universe can produce almost scale-invariant primordial perturbations as seeds of the cosmological structures from the quantum fluctuations. On the large scale ($\gtrsim 1\,\mathrm{Mpc}$), the assumptions of such scale-invariant primordial perturbations are favored by the observation of the large scale structure, and moreover recent Planck collaboration's results for the temperature and polarization perturbations of the cosmic microwave backgrounds can be fitted well only by 6 parameters if one assumes the almost scale-invariant primordial perturbations [7].

However, despite its great success, the precise mechanism of inflation is still unknown and there is no strongly favored inflationary model. The Planck collaboration has not detected the significant non-Gaussianity of the primordial perturbations as [8]

$$f_{\mathrm{NL}}^{\mathrm{local}} = 0.8 \pm 5.0, \qquad f_{\mathrm{NL}}^{\mathrm{equil}} = -4 \pm 43, \qquad f_{\mathrm{NL}}^{\mathrm{ortho}} = -26 \pm 21, \qquad (68\%\ \mathrm{CL}). \tag{0.1.1}$$

That is, no signal of the deviation from the simple single field inflation model was found. On the other hand, the primordial tensor perturbations also have not been detected. The obtained constraints on the tensor-to-scalar ratio is $r_{0.002} < 0.11$ (95% CL) [9], disfavoring the simplest single field large field inflation with a polynomial potential. Even for the models consistent with the Planck's observation, generally several problems are involved [9]. For example, natural inflation assumes the super Planckian symmetry breaking scale, while small scale inflation suffers from a severe initial condition problem. The CMB observation itself favors the R^2 inflationary model, but there is no physical origin of the large R^2 term.

In these situations, we need further observational information. One direction is the small scale perturbations about which we have little knowledge now. Several future observational projects in this direction are planned: 21 cm line observations by SKA [10], galaxy surveys by Euclid [11], and so on. As an interesting signal related with small scale perturbations, the primordial black hole has been refocused on more and more recently. Recent remarkable development on observational instruments allows us to close in on the scenario that dark matter consists of PBHs, while the first direct detection of gravitational waves by LIGO/Virgo collaboration sheds light on the possibility that the observed massive black holes might be primordial ones.

On the other hand, the prospect future survey plans call for the development of robust techniques for computing the primordial perturbations. Such techniques are also required for the PBH prediction. In this thesis, we derive some non-perturbative algorithm to calculate the power spectrum of the primordial perturbations. Also we give the new interpretation of the so-called local observer effect of the squeezed bispectrum with use of the δN formalism. Further we discuss the PBH formation in several inflationary models, partially using the above algorithm.

The rest of the thesis is as follows. In the next subsection, we briefly summarize the fundamental equations in the homogeneous universe and inflation at first. Part I is devoted to the theory of fluctuations in the inflationary universe. In Chapter 1, we review the linear perturbation theory, and then we discuss the approach beyond the linear theory in Chapter 2. In Chapter 3, we discuss the calculation algorithm of the squeezed bispectrum in the δN formalism. Then Part II is a part for the primordial black hole. After several basics of PBH are described in Chapter 4, we concretely discuss the PBH formation in two types of inflation in Chapters 5 and 6. In Chapter 5, we consider the double inflation whose energy scales are separated and successfully realize abundant PBHs as a main component of dark matter and origins of LIGO's gravitational events. On the other hand, in Chapter 6, we generically analyze the hybrid-type inflation models with use of the non-perturbative algorithm described in Chapter 2, and exclude the appropriate formation of the detectably massive PBHs in this class of inflation.

0.2 Homogeneous universe and inflation

Let us summarize several basic equations for the homogeneous universe and inflation. The most generic homogeneous isotropic metric is given by the Friedmann–Lemaître–Robertson–Walker metric [12–15]:

$$\mathrm{d}s^2 = -\mathrm{d}t^2 + a^2(t)\left(\mathrm{d}\mathbf{x}^2 + k\frac{(\mathbf{x}\cdot\mathrm{d}\mathbf{x})^2}{1-k\mathbf{x}^2}\right) = -\mathrm{d}t^2 + a^2(t)\left(\frac{\mathrm{d}r^2}{1-kr^2} + r^2\mathrm{d}\Omega\right). \tag{0.2.1}$$

Here the scale factor a represents the time dependence of the physical scale between two fixed points. k represents the three-curvature. On the other hand, under the homogeneous isotropic assumption, the background energy-momentum tensor should be the perfect fluid form as

$$T_{\mu\nu} = pg_{\mu\nu} + (\rho + p)u_\mu u_\nu, \tag{0.2.2}$$

where ρ and p are the energy density and pressure. The four-velocity u_μ is normalized by $g^{\mu\nu}u_\mu u_\nu = -1$, and for the comoving coordinate, $u_0 = -1$ and $u_i = 0$. For them, the $(0,0)$ component of the Einstein equation reads

$$\left(\frac{\dot{a}}{a}\right)^2 + \frac{k}{a^2} = \frac{\rho}{3M_{\mathrm{Pl}}^2}. \tag{0.2.3}$$

This equation is called *Friedmann equation* [12]. The expansion rate $H = \dot{a}/a$ is often referred to as *Hubble parameter*. The (i,j) component of the Einstein equation gives the following equation of acceleration.

$$\ddot{a} = -\frac{1}{6M_{\mathrm{Pl}}^2}(\rho + 3p)a. \tag{0.2.4}$$

The energy conservation:

$$0 = \nabla_\mu T^{0\mu} = \frac{\partial T^{0\mu}}{\partial x^\mu} + \Gamma^0_{\mu\nu} T^{\mu\nu} + \Gamma^\mu_{\mu\nu} T^{0\nu}, \tag{0.2.5}$$

leads the continuity equation as

$$\frac{\mathrm{d}(a^3\rho)}{\mathrm{d}t} = -p\frac{\mathrm{d}a^3}{\mathrm{d}t}, \quad \Leftrightarrow \quad \frac{\mathrm{d}\rho}{\mathrm{d}t} + 3\frac{\dot{a}}{a}(\rho + p) = 0. \tag{0.2.6}$$

Since the curvature component $\propto k$ is known to be negligibly small by e.g. CMB observations [7], hereafter we assume the flat universe $k = 0$.

Now let us consider some concrete fluid for the component of the universe. Assuming the EoS of such a fluid as $p = w\rho$, the continuity equation (0.2.6) reads

$$\frac{\mathrm{d}\rho}{\rho} = 3(1+w)\frac{\mathrm{d}a}{a}. \tag{0.2.7}$$

It can be solved as

$$\rho \propto a^{-3(1+w)}. \tag{0.2.8}$$

Substituting it to the Friedmann equation (0.2.3), one can also obtain

$$a \propto t^{\frac{2}{3(1+w)}}. \tag{0.2.9}$$

Therefore, if the universe is filled by the non-relativistic matter component $w = 0$, its energy density merely decays as a particle number dilution $\rho \propto a^{-3}$ and the time dependence of the scale factor is $a \propto t^{2/3}$. On the other hand, the relativistic radiation component $w = 1/3$ decays faster as $\rho \propto a^{-4}$ because not only its number density but also its wavenumber do decay by the expansion. The scale factor grows as $a \propto t^{1/2}$. Finally for the component of $w < -1/3$, the acceleration equation (0.2.4) shows the positive acceleration as

$$\ddot{a} = -\frac{1}{6M_{\mathrm{Pl}}^2}(1+3w) > 0. \tag{0.2.10}$$

Therefore it leads the accelerated expansion of the universe. Such a component is called *dark energy*. In particular, for $w \sim -1$, the energy density becomes constant. In this case, the Hubble parameter is also constant as shown in the Friedmann equation, and then the universe expands exponentially $a \propto \mathrm{e}^{Ht}$.

The inflationary mechanism assumes such an exponential expansion in the early universe and generally it is realized by the homogeneous scalar field called *inflaton*. Let us consider a simple example with the following action:

$$S = \int \mathrm{d}^4x\sqrt{-g}\left[-\frac{1}{2}g^{\mu\nu}\partial_\mu\phi\partial_\nu\phi - V(\phi)\right]. \tag{0.2.11}$$

Assuming the FLRW metric, it reads

$$S = \int \mathrm{d}^4x a^3(t)\left[-\frac{1}{2}g^{\mu\nu}\partial_\mu\phi\partial_\nu\phi - V(\phi)\right]. \tag{0.2.12}$$

For the homogeneous isotropic scalar field $\phi = \phi(t)$, the corresponding EoM can be obtained as

$$\ddot{\phi} + 3H\dot{\phi} + V'(\phi) = 0. \tag{0.2.13}$$

Compared with the Minkowski background case, there is an additional friction term $3H\dot{\phi}$ called *Hubble friction* due to the dilution by the expansion.

The energy-momentum tensor is given by

$$T_{\mu\nu} = -\frac{2}{\sqrt{-g}}\frac{\delta S}{\delta g^{\mu\nu}} = g_{\mu\nu}\left[-\frac{1}{2}g^{\rho\sigma}\partial_\rho\phi\partial_\sigma\phi - V(\phi)\right] + \partial_\mu\phi\partial_\nu\phi. \tag{0.2.14}$$

Comparing it with the perfect fluid form (0.2.2), the energy density and pressure for the homogeneous scalar can be written as

$$\rho = \frac{1}{2}\dot{\phi}^2 + V(\phi), \qquad p = \frac{1}{2}\dot{\phi}^2 - V(\phi). \tag{0.2.15}$$

Therefore the Hubble parameter is given by

$$H = \sqrt{\frac{\rho}{3M_{\rm Pl}^2}} = \sqrt{\frac{1}{3M_{\rm Pl}^2}\left(\frac{1}{2}\dot{\phi}^2 + V(\phi)\right)}. \tag{0.2.16}$$

Its time derivative has a simple form, with use of the EoM (0.2.13), as

$$\dot{H} = -\frac{\dot{\phi}^2}{2M_{\rm Pl}^2}. \tag{0.2.17}$$

Therefore the decay rate of the Hubble parameter per Hubble time H^{-1} is given by

$$\epsilon_H = -\frac{\dot{H}}{H^2} = \frac{\dot{\phi}^2}{\frac{2}{3}\left(\frac{1}{2}\dot{\phi}^2 + V(\phi)\right)}, \tag{0.2.18}$$

and the condition of the exponential expansion $\epsilon_H \ll 1$ can be rewritten as $\dot{\phi}^2 \ll V(\phi)$. Namely, if the potential is sufficiently flat and the Hubble friction works enough, the momentum energy can be negligible compared to the potential energy and it realizes the exponential expansion of the universe. This mechanism is called *slow-roll inflation* and the decay rate parameter ϵ_H is referred to as *slow-roll parameter*.

In the slow-roll approximation, the Hubble parameter is almost given by the potential energy as

$$H \simeq \sqrt{\frac{V}{3M_{\rm Pl}^2}}. \tag{0.2.19}$$

Assuming that its time derivative is also a good approximation as

$$\dot{H} \simeq \frac{1}{6M_{\rm Pl}^2}\frac{V'\dot{\phi}}{H} \tag{0.2.20}$$

one can obtain, with use of Eq. (0.2.17),

$$3H\dot{\phi} \simeq -V'(\phi). \tag{0.2.21}$$

This is the form of the EoM with the neglected $\ddot{\phi}$ term and it is called *slow-roll EoM*. This approximation is equivalent to imposing the condition

$$|\ddot{\phi}| \ll |H\dot{\phi}|. \tag{0.2.22}$$

It is also another slow-roll condition.

Let us rewritten these slow-roll conditions in terms of the potential. First we define the first slow-roll parameter as

$$\epsilon_V = \frac{M_{\rm Pl}^2}{2}\left(\frac{V'}{V}\right)^2. \tag{0.2.23}$$

It is equivalent to the previous slow-roll parameter ϵ_H in the slow-roll limit:

$$\epsilon_V = \frac{M_{\rm Pl}^2}{2}\left(\frac{V'}{V}\right)^2 \simeq \frac{M_{\rm Pl}^2}{2}\left(\frac{3H\dot{\phi}}{3M_{\rm Pl}^2H^2}\right)^2 = \frac{\dot{\phi}^2}{2M_{\rm Pl}^2H^2} = -\frac{\dot{H}}{H^2} = \epsilon_H. \tag{0.2.24}$$

The other slow-roll parameter can be found by the time derivative of the slow-roll EoM (0.2.21):

$$\ddot{\phi} \simeq -\frac{\dot{H}}{H}\dot{\phi} - \frac{V''}{3H}\dot{\phi}. \tag{0.2.25}$$

Substituting it to the slow-roll condition (0.2.21), it reads

$$\left|-\epsilon_H + \frac{V''}{3H^2}\right| \ll 1. \tag{0.2.26}$$

Since the first term ϵ_H is already smaller enough than unity, the remained condition is

$$|\eta_V| = \left|M_{\rm Pl}^2\frac{V''}{V}\right| \ll 1. \tag{0.2.27}$$

This $\eta_V = M_{\rm Pl}^2 V''/V$ is also the slow-roll parameter. The slow-roll condition $\epsilon_V \ll 1$ requires the sufficient flatness of the potential, while $|\eta_V| \ll 1$ indicates the smallness of the scalar mass term $m^2 = V''$.

Part I

Inflationary Perturbation Theory

Chapter 1

Linear Perturbation Theory

One of the most important subjects of the modern cosmology is to test the perturbations as the origin of the structures in the universe. Since our observable universe seems to be almost homogeneous and little perturbed at least on the large scale, the linear perturbation theory is a strong tool as the lowest order analysis. In this chapter, let us review this linear perturbation theory, particularly focusing on the perturbation during the inflationary universe. We basically follow Ref. [16].

1.1 Generic description of cosmological perturbation

1.1.1 Field equations

The fundamental cosmology is based on general relativity and the cosmological principle, that is, our observable universe is homogenous and isotropic on the large scale. Therefore, at the zeroth order, the universe can be described by the homogenous and isotropic metric, i.e., the Friedmann–Lemaître–Robertson–Walker metric, and the components of the universe are also homogeneous and isotropic. In other words, the zeroth background metric $\bar{g}_{\mu\nu}$ is given by

$$\bar{g}_{00} = -1, \qquad \bar{g}_{0i} = \bar{g}_{i0} = 0, \qquad \bar{g}_{ij} = a^2(t)\delta_{ij}, \tag{1.1.1}$$

and the background energy-momentum tensor should take the perfect fluid form as

$$\bar{T}_{\mu\nu} = \bar{p}\bar{g}_{\mu\nu} + (\bar{p} + \bar{\rho})\bar{u}_\mu\bar{u}_\nu, \tag{1.1.2}$$

from the rotational and translational invariance.

Then let us consider the linear deviation from the zeroth solution. That is, for the perturbed metric and energy-momentum tensor:

$$g_{\mu\nu} = \bar{g}_{\mu\nu} + h_{\mu\nu}, \qquad T_{\mu\nu} = \bar{T}_{\mu\nu} + \delta T_{\mu\nu}. \tag{1.1.3}$$

we want the explicit expression of the Einstein equation

$$R_{\mu\nu} - \frac{1}{2} g_{\mu\nu} g^{\lambda\kappa} R_{\lambda\kappa} = -M_{\rm Pl}^{-2} T_{\mu\nu}, \tag{1.1.4}$$

at the linear order w.r.t. the perturbations $h_{\mu\nu}$ and $\delta T_{\mu\nu}$. Here the Ricci tensor $R_{\mu\nu}$ is defined by

$$R_{\mu\nu} = \frac{\partial \Gamma^{\lambda}_{\mu\lambda}}{\partial x^{\nu}} - \frac{\partial \Gamma^{\lambda}_{\mu\nu}}{\partial x^{\lambda}} + \Gamma^{\kappa}_{\mu\lambda}\Gamma^{\lambda}_{\nu\kappa} - \Gamma^{\kappa}_{\mu\nu}\Gamma^{\lambda}_{\lambda\kappa}, \tag{1.1.5}$$

with the affine connection

$$\Gamma^{\mu}_{\nu\kappa} = \frac{1}{2} g^{\mu\lambda} \left[\frac{\partial g_{\lambda\nu}}{\partial x^{\kappa}} + \frac{\partial g_{\lambda\kappa}}{\partial x^{\nu}} - \frac{\partial g_{\nu\kappa}}{\partial x^{\lambda}} \right]. \tag{1.1.6}$$

Instead of using the Einstein equation (1.1.4) directly, the other equivalent expression is often considered since the concrete expression of the left-hand side of the original Einstein equation becomes quite messy. The trace of the Einstein equation gives

$$g^{\mu\nu} R_{\mu\nu} = M_{\rm Pl}^{-2} T^{\lambda}{}_{\lambda}, \tag{1.1.7}$$

and then, substituting it the original Einstein equation, one obtains the other form of the equation as

$$R_{\mu\nu} = -M_{\rm Pl}^{-2} S_{\mu\nu}, \tag{1.1.8}$$

where the source tensor $S_{\mu\nu}$ is expressed as

$$S_{\mu\nu} = T_{\mu\nu} - \frac{1}{2} g_{\mu\nu} T^{\lambda}{}_{\lambda}. \tag{1.1.9}$$

The linear order Einstein equation is

$$\delta R_{\mu\nu} = -M_{\rm Pl}^{-2} \delta S_{\mu\nu}. \tag{1.1.10}$$

With use of the explicit forms of $\delta R_{\mu\nu}$ and $\delta S_{\mu\nu}$ which we summarize in Appendix A, one obtains the full expressions of (ij), $(i0)$, and (00) components of the linear order Einstein equation as

$$\begin{aligned}
-M_{\rm Pl}^{-2} \left(\delta T_{jk} - \frac{a^2}{2} \delta_{jk} \delta T^{\lambda}{}_{\lambda} \right) &= -\frac{1}{2} \partial_j \partial_k h_{00} - (2\dot{a}^2 + a\ddot{a}) \delta_{jk} h_{00} \\
&\quad - \frac{1}{2} a\dot{a} \delta_{jk} \dot{h}_{00} + \frac{1}{2a^2} (\nabla^2 h_{jk} - \partial_i \partial_j h_{ik} - \partial_i \partial_k h_{ij} + \partial_j \partial_k h_{ii}) \\
&\quad - \frac{1}{2} \ddot{h}_{jk} + \frac{\dot{a}}{2a} (\dot{h}_{jk} - \delta_{jk} \dot{h}_{ii}) + \left(\frac{\dot{a}^2}{a^2} + \frac{3\ddot{a}}{a} \right) h_{jk} + \left(\frac{\dot{a}^2}{a^2} \right) \delta_{jk} h_{ii} \\
&\quad + \frac{\dot{a}}{a} \delta_{jk} \partial_i h_{i0} + \frac{1}{2} (\partial_j \dot{h}_{k0} + \partial_k \dot{h}_{j0}) + \frac{\dot{a}}{2a} (\partial_j h_{k0} + \partial_k h_{j0}),
\end{aligned} \tag{1.1.11}$$

$$\begin{aligned}
-M_{\rm Pl}^{-2} \delta T_{j0} &= \frac{\dot{a}}{a} \partial_j h_{00} + \frac{1}{2a^2} (\nabla^2 h_{j0} - \partial_j \partial_i h_{i0}) + \left(\frac{\dot{a}^2}{a^2} + \frac{2\ddot{a}}{a} \right) h_{j0} \\
&\quad + \frac{1}{2} \frac{\partial}{\partial t} \left[\frac{1}{a^2} (\partial_j h_{kk} - \partial_k h_{kj}) \right],
\end{aligned} \tag{1.1.12}$$

$$\begin{aligned}
-M_{\rm Pl}^{-2} \left(\delta T_{00} + \frac{1}{2} \delta T^{\lambda}{}_{\lambda} \right) &= \frac{1}{2a^2} \nabla^2 h_{00} + \frac{3\dot{a}}{2a} \dot{h}_{00} - \frac{1}{a^2} \partial_i \dot{h}_{i0} \\
&\quad + \frac{1}{2a^2} \left[\ddot{h}_{ii} - \frac{2\dot{a}}{a} \dot{h}_{ii} + 2 \left(\frac{\dot{a}^2}{a^2} - \frac{\ddot{a}}{a} \right) h_{ii} \right] + 3 \left(\frac{\dot{a}^2}{a^2} + \frac{\ddot{a}}{a} \right) h_{00}.
\end{aligned} \tag{1.1.13}$$

The conservation laws for perturbations also can be derived from these equations, but they can be obtained more easily from the linear perturbation of the full conservation law $T^{\mu}{}_{\nu;\mu} = 0$. The energy and momentum conservations are given by the temporal and spatial components as

$$\partial_0 \delta T^0{}_0 + \partial_i \delta T^i{}_0 + \frac{3\dot{a}}{a}\delta T^0{}_0 - \frac{\dot{a}}{a}\delta T^i{}_i - \left(\frac{\bar{\rho}+\bar{p}}{2a^2}\right)\left(-\frac{2\dot{a}}{a}h_{ii} + \dot{h}_{ii}\right) = 0 \tag{1.1.14}$$

$$\partial_0 \delta T^0{}_j + \partial_i \delta T^i{}_j + \frac{2\dot{a}}{a}\delta T^0{}_j - a\dot{a}\delta T^j{}_0 - (\bar{\rho}+\bar{p})\left(\frac{1}{2}\partial_j h_{00} - \frac{\dot{a}}{a}h_{j0}\right) = 0, \tag{1.1.15}$$

whose detailed derivations are described in Appendix A.

These results are too complicated to be directly used. So now let us decompose them into the scalar, transverse vector, and traceless-transverse tensor components. The metric perturbations can always be decomposed into the following forms.

$$h_{00} = -E, \tag{1.1.16}$$

$$h_{i0} = a\left[\frac{\partial F}{\partial x^i} + G_i\right], \tag{1.1.17}$$

$$h_{ij} = a^2\left[A\delta_{ij} + \frac{\partial^2 B}{\partial x^i \partial x^j} + \frac{\partial C_i}{\partial x^j} + \frac{\partial C_j}{\partial x^i} + D_{ij}\right]. \tag{1.1.18}$$

Here A, B, C_i, $D_{ij} = D_{ij}$, E, F, and G_i are functions of t and $\mathbf{x}$ respectively, and satisfy the following conditions.

$$\frac{\partial C_i}{\partial x^i} = \frac{\partial G_i}{\partial x^i} = 0, \qquad \frac{\partial D_{ij}}{\partial x^i} = 0, \qquad D_{ii} = 0. \tag{1.1.19}$$

Similarly the energy-momentum tensor can be also decomposed. First let us begin by the perfect fluid form:

$$T_{\mu\nu} = p g_{\mu\nu} + (\rho + p)u_\mu u_\nu. \tag{1.1.20}$$

Since the four-velocity is normalized as

$$g^{\mu\nu}u_\mu u_\nu = -1, \tag{1.1.21}$$

recalling that $\bar{u}_i = 0$, $\bar{u}_0 = -1$, one can derive the constraint

$$\delta u^0 = \delta u_0 = h_{00}/2, \tag{1.1.22}$$

but δu_i are still independent dynamical variables. Accordingly the linear perturbation of the perfect fluid reads

$$\delta T_{ij} = \bar{p}h_{ij} + a^2\delta_{ij}\delta p, \qquad \delta T_{i0} = \bar{p}h_{i0} - (\bar{\rho}+\bar{p})\delta u_i, \qquad \delta T_{00} = -\bar{\rho}h_{00} + \delta\rho. \tag{1.1.23}$$

Generic fluids will give more complicated expressions. Indeed the original symmetric $\delta T_{\mu\nu}$ has 10 d.o.f., though we still have only 5 d.o.f. as $\delta\rho$, δp, and δu_i. Then, decomposing δu_i into the scalar component δu and the transverse vectors δu_i^{V} and adding insufficient d.o.f. similarly to the metric perturbation, one obtains the following expressions.

$$\delta T_{ij} = \bar{p}h_{ij} + a^2[\delta_{ij}\delta p + \partial_i\partial_j\pi^{\mathrm{S}} + \partial_i\pi_j^{\mathrm{V}} + \partial_j\pi_i^{\mathrm{V}} + \pi_{ij}^{\mathrm{T}}], \tag{1.1.24}$$

$$\delta T_{i0} = \bar{p}h_{i0} - (\bar{\rho}+\bar{p})(\partial_i\delta u + \delta u_i^{\mathrm{V}}), \tag{1.1.25}$$

$$\delta T_{00} = -\bar{\rho}h_{00} + \delta\rho, \tag{1.1.26}$$

where $\pi_i^{\rm V}$, $\pi_{ij}^{\rm T}$, and $\delta u_i^{\rm V}$ satisfy the following constraints.

$$\partial_i \pi_i^{\rm V} = \partial_i \delta u_i^{\rm V} = 0, \qquad \pi_{ji}^{\rm T} = \pi_{ij}^{\rm T}, \qquad \partial_i \pi_{ij}^{\rm T} = 0, \qquad \pi_{ii}^{\rm T} = 0. \tag{1.1.27}$$

Here the additional d.o.f. $\pi^{\rm S}$, $\pi^{\rm V}$, and $\pi^{\rm T}$ called *anisotropic inertia* characterize the deviation from the perfect fluid.

Then the perturbed Einstein equations (1.1.11)–(1.1.13) can be also decomposed into the scalar, vector, and tensor modes. The EoM for scalar modes are given by the terms proportional to δ_{jk} and $\partial_j\partial_k S$ form ones of Eq. (1.1.11), $\partial_j S$ form terms of Eq. (1.1.12), and the whole part of Eq. (1.1.13) as[1]

$$\begin{aligned}
&-\frac{a^2}{2M_{\rm Pl}^2}[\delta\rho - \delta p - \nabla^2\pi^{\rm S}] \\
&\quad = \frac{1}{2}a\dot{a}\dot{E} + (2\dot{a}^2 + a\ddot{a})E + \frac{1}{2}\nabla^2 A - \frac{1}{2}a^2\ddot{A} - 3a\dot{a}\dot{A} - \frac{1}{2}a\dot{a}\nabla^2\dot{V} + \dot{a}\nabla^2 F, && (1.1.28)\\
&\partial_j\partial_k[2M_{\rm Pl}^{-2}a^2\pi^{\rm S} + E + A - a^2\ddot{B} - 3a\dot{a}\dot{B} + 2a\dot{F} + 4\dot{a}F] = 0, && (1.1.29)\\
&M_{\rm Pl}^{-2}a(\bar{\rho}+\bar{p})\partial_j\delta u = -\dot{a}\partial_j E + a\partial_j\dot{A}, && (1.1.30)\\
&-\frac{1}{2M_{\rm Pl}^2}(\delta\rho + 3\delta p + \nabla^2\pi^{\rm S}) \\
&\quad = -\frac{1}{2a^2}\nabla^2 E - \frac{3\dot{a}}{2a}\dot{E} - \frac{1}{a}\nabla^2\dot{F} - \frac{\dot{a}}{a^2}\nabla^2 F + \frac{3}{2}\ddot{A} + \frac{3\dot{a}}{a}\dot{A} - \frac{3\ddot{a}}{a}E + \frac{1}{2}\nabla^2\ddot{B} + \frac{\dot{a}}{a}\nabla^2\dot{B}. && (1.1.31)
\end{aligned}$$

The conservation laws for the scalar components are also useful. They can be derived by the whole part of the energy conservation (1.1.14) and the $\partial_j S$ terms of the momentum conservation (1.1.15) as

$$\begin{aligned}
&\delta\dot{\rho} + \frac{3\dot{a}}{a}(\delta\rho + \delta p) + \nabla^2\left[-a^{-1}(\bar{\rho}+\bar{p})F + a^{-2}(\bar{\rho}+\bar{p})\delta u + \frac{\dot{a}}{a}\pi^{\rm S}\right] \\
&\qquad + \frac{1}{2}(\bar{\rho}+\bar{p})\partial_0[3A + \nabla^2 B] = 0, && (1.1.32)\\
&\partial_j\left[\delta p + \nabla^2\pi^{\rm S} + \partial_0[(\bar{\rho}+\bar{p})\delta u] + \frac{3\dot{a}}{a}(\bar{\rho}+\bar{p})\delta u + \frac{1}{2}(\bar{\rho}+\bar{p})E\right] = 0. && (1.1.33)
\end{aligned}$$

The vector part comes from the $\partial_k V_j$ terms of Eq. (1.1.11) and V_j terms of Eq. (1.1.12) with some transverse vector V_j as

$$\begin{aligned}
&\partial_k[2M_{\rm Pl}^{-2}a^2\pi_j^{\rm V} - a^2\ddot{C}_j - 3a\dot{a}\dot{C}_j + a\dot{G}_j + 2\dot{a}G_j] = 0, && (1.1.34)\\
&M_{\rm Pl}^{-2}(\bar{\rho}+\bar{p})a\delta u_j^{\rm V} = \frac{1}{2}\nabla^2 G_j - \frac{a}{2}\nabla^2\dot{C}_j. && (1.1.35)
\end{aligned}$$

The transverse vectorial part of the momentum conservation (1.1.15) gives the conservation law for the vector components as,

$$\nabla^2\pi_j^{\rm V} + \partial_0[(\bar{\rho}+\bar{p})\delta u_j^{\rm V}] + \frac{3\dot{a}}{a}(\bar{\rho}+\bar{p})\delta u_j^{\rm V} = 0. \tag{1.1.36}$$

[1]These decompositions are validated in a similar way as the decomposition of the original perturbations (1.1.16)–(1.1.18).

Note that, for the perfect fluid $\pi_i^{\rm V} = 0$, this momentum conservation indicates that $(\bar{\rho} + \bar{p})\delta u_i^{\rm V}$ decays as a^{-3}. In this case, both Eqs. (1.1.34) and (1.1.35) show that $G_j - a\dot{C}_j$ decays as a^{-2}. Actually this $G_j - a\dot{C}_j$ is the only gauge-invariant combination of the vector components of the metric perturbations (see the next subsection). Then vector modes have not played a large role in cosmology, and hereafter we basically neglect the vector modes.

Finally the EoM for the tensor components is given by the traceless-transverse tensorial terms of Eq. (1.1.11) as

$$-2M_{\rm Pl}^{-2}a^2\pi_{ij}^{\rm T} = \nabla^2 D_{ij} - a^2\ddot{D}_{ij} - 3a\dot{a}\dot{D}_{ij}. \tag{1.1.37}$$

The above equations do not form a complete set. This is in part because we still have the freedom of the coordinate transformation (gauge d.o.f.). In the next subsection, we review the gauge transformation of the linear perturbation and introduce the useful Newtonian gauge.

1.1.2 Gauge transformation

The EoM derived in the previous subsection still include the unphysical components due to the gauge d.o.f. and this problem is usually solved by fixing the gauge. In this subsection, we consider the gauge transformation of the perturbations and introduce the useful Newtonian gauge.

First, let us consider the spacetime coordinate transformation:

$$x^\mu \to x'^\mu = x^\mu + \epsilon^\mu(x), \tag{1.1.38}$$

and study the modulation at the linear order w.r.t. $\epsilon^\mu(x)$ as well as other perturbations. The metric is transformed as

$$g'_{\mu\nu}(x') = g_{\lambda\kappa}(x)\frac{\partial x^\lambda}{\partial x'^\mu}\frac{\partial x^\kappa}{\partial x'^\nu}, \tag{1.1.39}$$

but we impose the constraints that the zeroth order metric and coordinate points do not change and instead all modifications are pressed into the perturbations. In this case, the modulations of the perturbations are called *gauge transformations*. That is, the gauge transformation of the metric perturbation $h_{\mu\nu}$ is given by

$$\Delta h_{\mu\nu}(x) = g'_{\mu\nu}(x) - g_{\mu\nu}(x). \tag{1.1.40}$$

Here the field equations should be invariant under the gauge transformation $h_{\mu\nu} \to h_{\mu\nu}(x) + \Delta h_{\mu\nu}(x)$. At the linear order w.r.t. $\epsilon^\mu(x)$ and $h_{\mu\nu}(x)$, it reads

$$\begin{aligned}\Delta h_{\mu\nu}(x) &= g'_{\mu\nu}(x') - \frac{\partial g_{\mu\nu}(x)}{\partial x^\lambda}\epsilon^\lambda(x) - g_{\mu\nu}(x) \\ &= -\bar{g}_{\lambda\mu}(x)\frac{\partial\epsilon^\lambda(x)}{\partial x^\nu} - \bar{g}_{\lambda\nu}(x)\frac{\partial\epsilon^\lambda(x)}{\partial x^\mu} - \frac{\partial\bar{g}_{\mu\nu}(x)}{\partial x^\lambda}\epsilon^\lambda(x),\end{aligned} \tag{1.1.41}$$

The energy-momentum tensor is also transformed similarly as

$$\Delta\delta T_{\mu\nu} = -\bar{T}_{\lambda\mu}(x)\frac{\partial\epsilon^\lambda(x)}{\partial x^\nu} - \bar{T}_{\lambda\nu}(x)\frac{\partial\epsilon^\lambda(x)}{\partial x^\mu} - \frac{\partial\bar{T}_{\mu\nu}(x)}{\partial x^\lambda}\epsilon^\lambda(x), \tag{1.1.42}$$

Their concrete expressions are shown in Appedix A. Finally, decomposing the spatial part of ϵ^μ into the scalar and the transverse vector modes as

$$\epsilon_i = \partial_i \epsilon^{\rm S} + \epsilon_i^{\rm V}, \qquad \partial_i \epsilon_i^{\rm V} = 0, \tag{1.1.43}$$

One can obtain the gauge transformations of each component of the metric perturbations as

$$\begin{cases} \Delta A = \dfrac{2\dot{a}}{a}\epsilon_0, \quad \Delta B = -\dfrac{2}{a^2}\epsilon^{\rm S}, \quad \Delta E = 2\dot{\epsilon}_0, \quad \Delta F = \dfrac{1}{a}\left(-\epsilon_0 - \dot{\epsilon}^{\rm S} + \dfrac{2\dot{a}}{a}\epsilon^{S}\right) \\ \Delta C_i = -\dfrac{1}{a^2}\epsilon_i^{\rm V}, \qquad \Delta G_i = \dfrac{1}{a}\left(-\dot{\epsilon}_i^{\rm V} + \dfrac{2\dot{a}}{a}\epsilon_i^{\rm V}\right) \\ \Delta D_{ij} = 0, \end{cases} \tag{1.1.44}$$

and of the perturbations to the pressure, energy density, and velocity potential as

$$\Delta\delta p = \dot{\bar{p}}\epsilon_0, \qquad \Delta\delta\rho = \dot{\bar{\rho}}\epsilon_0, \qquad \Delta\delta u = -\epsilon_0. \tag{1.1.45}$$

The other ingredients of the energy-momentum tensor do not change by the gauge transformation.

$$\Delta\pi^{\rm S} = \Delta\pi_i^{\rm V} = \Delta\pi_{ij}^{\rm T} = \Delta\delta u_i^{\rm V} = 0. \tag{1.1.46}$$

Therefore the perfect fluid conditions $\pi^{\rm S} = \pi_i^{\rm V} = \pi_{ij}^{\rm T} = 0$ or the irrotational condition $\delta u_i^{\rm V} = 0$ are gauge-invariant.

Newtonian gauge

Now we obtain the gauge transformations of the perturbations, so let us introduce the Newtonian gauge. Here we consider only the scalar modes (vector modes are decaying and tensor modes are gauge-invariant). In the Newtonian gauge, $\epsilon^{\rm S}$ is chosen so that $B = 0$ and ϵ_0 is chosen so that $F = 0$. After that, there remains no gauge d.o.f. Conventionally E and A are written in this gauge as

$$E = 2\Phi, \qquad A = -2\Psi. \tag{1.1.47}$$

Therefore the perturbed metric is

$$g_{00} = -1 - 2\Phi, \qquad g_{0i} = 0, \qquad g_{ij} = a^2\delta_{ij}[1 - 2\Psi]. \tag{1.1.48}$$

The field equations (1.1.28)–(1.1.31) are given by

$$-\frac{1}{2M_{\rm Pl}^2}a^2[\delta\rho - \delta p - \nabla^2\pi^{\rm S}] = a\dot{a}\dot{\Phi} + (4\dot{a}^2 + 2a\ddot{a})\Phi - \nabla^2\Psi + a^2\ddot{\Psi} + 6a\dot{a}\dot{\Psi}, \tag{1.1.49}$$

$$-M_{\rm Pl}^{-2}a^2\partial_i\partial_j\pi^{\rm S} = \partial_i\partial_j[\Phi - \Psi], \tag{1.1.50}$$

$$\frac{1}{2M_{\rm Pl}^2}a(\bar{\rho} + \bar{p})\partial_i\delta u = -\dot{a}\partial_i\Phi - a\partial_i\dot{\Psi}, \tag{1.1.51}$$

$$\frac{1}{2M_{\rm Pl}^2}(\delta\rho + 3\delta p + \nabla^2\pi^{\rm S}) = \frac{1}{a^2}\nabla^2\Phi + \frac{3\dot{a}}{a}\dot{\Phi} + 3\ddot{\Psi} + \frac{6\dot{a}}{a}\dot{\Psi} + \frac{6\ddot{a}}{a}\Phi, \tag{1.1.52}$$

and the conservations of energy (1.1.32) and momentum (1.1.33) are

$$\delta p + \nabla^2 \pi^{\rm S} + \partial_0[(\bar{\rho}+\bar{p})\delta u] + \frac{3\dot{a}}{a}(\bar{\rho}+\bar{p})\delta u + (\bar{\rho}+\bar{p})\Phi = 0, \tag{1.1.53}$$

$$\delta\dot{\rho} + \frac{3\dot{a}}{a}(\delta\rho+\delta p) + \nabla^2\left[a^{-2}(\bar{\rho}+\bar{p})\delta u + \frac{\dot{a}}{a}\pi^{\rm S}\right] - 3(\bar{\rho}+\bar{p})\dot{\Psi} = 0. \tag{1.1.54}$$

By subtracting $3/a^2$ times Eq. (1.1.49) from Eq. (1.1.52) and using Eqs. (1.1.50) and (1.1.51) to remove $\pi^{\rm S}$ and Φ, one can obtain

$$a^3\delta\rho - 3Ha^3(\bar{\rho}+\bar{p})\delta u - 2M_{\rm Pl}^2 a\nabla^2\Psi = 0. \tag{1.1.55}$$

Then let us define the gauge-invariant density perturbation by

$$\Delta_\rho = \frac{\delta\rho}{\bar{\rho}} - 3H(1+w)\delta u. \tag{1.1.56}$$

Its gauge-invariance can be checked with use of the gauge transformations of $\delta\rho$ and δu and the continuity equation (0.2.6), $\dot{\rho} = -3H(1+w)\rho$. This quantity is indeed the density perturbation on the so-called comoving time slice where δu is fixed to zero. With use of this density perturbation, Eq. (1.1.55) reads the Poisson-like form as

$$\nabla^2\Psi = \frac{1}{2M_{\rm Pl}^2}a^2\bar{\rho}\Delta_\rho. \tag{1.1.57}$$

With use of the Friedmann equation, its Fourier expression is given by

$$\Delta_{\rho,k} = -\frac{2}{3}\left(\frac{k}{aH}\right)^2\Psi_k. \tag{1.1.58}$$

1.1.3 Conservation outside the horizon

The cosmological perturbations are generally assumed to be generated in inflation. However there are many uncertainties in the physics after inflation, so naively the prediction of the current perturbations seems to lose its reliability. In this subsection, we show that there is a solution of the perturbation with which gauge-invariantly composed curvature perturbations are conserved on the superhorizon scale irrespectively of the details of the state of the universe. In the next chapter, we will also review the proof of this conservation beyond the linear perturbation theory.

One example specific of the gauge-invariant perturbations is defined as

$$\zeta_k = -\Psi_k + \frac{\delta\rho_k}{3(\bar{\rho}+\bar{p})}, \tag{1.1.59}$$

in the Newtonian gauge. It is referred to as the curvature perturbation on the uniform density slice ($\delta\rho = 0$). Another gauge-invariant quantity:

$$\mathcal{R}_k = -\Psi_k + H\delta u_k, \tag{1.1.60}$$

which is called the curvature perturbation on the comoving slice ($\delta u = 0$), is also often used. Their deference is given by the comoving density perturbation (1.1.56)

$$\zeta_k - \mathcal{R}_k = 3(1+w)\Delta_{\rho,k} = -2(1+w)\left(\frac{k}{aH}\right)^2 \Psi_k. \tag{1.1.61}$$

Therefore they asymptote to each other in the superhorizon limit $k \ll aH$.

From the energy conservation (1.1.54), one can indeed see $\dot{\zeta}_k = 0$ in the superhorizon limit $k \to 0$ if $\delta p/\dot{\bar{p}} = \delta\rho/\dot{\bar{\rho}}$. These solutions for δp and $\delta\rho$ can be related with the additionally appearing gauge d.o.f. in the long-wavelength limit. Let us review this below. Hereafter we neglect the vector modes.

$k = 0$ limit

Let us first consider the $k = 0$ limit, i.e., the perfectly homogeneous and isotropic perturbations. Note that there remains the gauge d.o.f. in this case even after the Newtonian gauge is adopted.

The spatially homogeneous linear metric perturbations are given by

$$h_{00} = -2\Phi(t), \qquad h_{i0} = 0, \qquad h_{ij} = -2\delta_{ij}a^2(t)\Psi(t) + a^2(t)D_{ij}, \tag{1.1.62}$$

in the Newtonian gauge. Here D_{ij} is constrained by the condition $D_{ii} = 0$. Let us show that there remains gauge d.o.f. which satisfies the spatially homogeneity and the condition of the Newtonian gauge. At first, from the gauge transformation (A.0.38), for h_{00} to stay spatially homogeneous, the temporal component of such a gauge transformation should be the form of

$$\epsilon_0(\mathbf{x}, t) = \epsilon(t) + \chi(\mathbf{x}). \tag{1.1.63}$$

Accordingly

$$\Delta\Phi = \frac{1}{2}\Delta E = \dot{\epsilon}. \tag{1.1.64}$$

Also from the gauge transformation (A.0.37), for h_{i0} to remain homogeneous, the spatial component should be

$$\epsilon_i(\mathbf{x}, t) = a^2(t)f_i(\mathbf{x}) - a^2(t)\frac{\partial\chi(x)}{\partial x^i}\int\frac{\mathrm{d}t}{a^2(t)}. \tag{1.1.65}$$

Therefore Eq. (A.0.36) gives

$$\Delta h_{ij} = -a^2\left(\frac{\partial f_i}{\partial x^j} + \frac{\partial f_j}{\partial x^i}\right) + 2\delta_{ij}a\dot{a}[\epsilon + \chi] + 2a^2\frac{\partial^2\chi}{\partial x^i\partial x^j}\int\frac{\mathrm{d}t}{a^2}. \tag{1.1.66}$$

Now χ should be constant so that h_{ij} does not depend on $\mathbf{x}$, and in this case, one can take $\chi = 0$ by shifting ϵ. Similarly f_i should be written as $f_i(\mathbf{x}) = \omega_{ij}x^j$ with a constant matrix ω_{ij}. We neglect a constant offset of f_i since it does not affect the metric at all. Accordingly

$$\Delta h_{ij} = -a^2[\omega_{ij} + \omega_{ji}] + 2\delta_{ij}a\dot{a}\epsilon. \tag{1.1.67}$$

On the other hand, from the Newtonian gauge conditions $B = 0$ and $A = -2\Psi$, h_{ij} should keep the following form.

$$\Delta h_{ij} = -2a^2\delta_{ij}\Delta\Psi + a^2\Delta D_{ij}. \tag{1.1.68}$$

Comparing them, one obtains

$$\begin{cases} \Delta\Psi = \dfrac{1}{3}\omega_{ii} - H\epsilon, \\ \Delta D_{ij} = -\omega_{ij} - \omega_{ji} + \dfrac{2}{3}\delta_{ij}\omega_{kk}. \end{cases} \tag{1.1.69}$$

They are explicit forms of the remained gauge d.o.f.

If the combination $(h_{\mu\nu}, T_{\mu\nu})$ is the solution of EoM, $(h_{\mu\nu} + \Delta h_{\mu\nu}, T_{\mu\nu} + \Delta T_{\mu\nu})$ should also be the solution and then so is their difference $(-\Delta h_{\mu\nu}, -\Delta T_{\mu\nu})$. Therefore, for the scalar modes, one can obtain the following special solution from Eqs. (1.1.45), (1.1.46), (1.1.64), and (1.1.69).

$$\begin{cases} \Psi = H\epsilon - \dfrac{\omega_{ii}}{3}, \qquad \Phi = -\dot{\epsilon}, \\ \delta p = -\dot{\bar{p}}\epsilon, \qquad \delta\rho = -\dot{\bar{\rho}}\epsilon, \qquad \delta u = \epsilon, \qquad \pi^{\mathrm{S}} = 0. \end{cases} \tag{1.1.70}$$

Also for the tensor modes

$$D \propto \omega_{ij} - \frac{1}{3}\delta_{ij}\omega_{kk}, \qquad \pi^{\mathrm{T}}_{ij} = 0. \tag{1.1.71}$$

To $k \neq 0$ modes

Actually the above solutions for the scalar modes cannot be continued smoothly to the non-zero wavenumber one. That is because, for $k = 0$, EoM (1.1.50) is trivially satisfied and the required constraints have not been completely imposed. That is, the above solutions include ones which cannot be obtained by the $k \to 0$ limit of the non-zero wavenumber modes. Since now $\pi^{\mathrm{S}} = 0$, one has to impose $\Phi = \Psi$ by hand. Namely

$$\dot{\epsilon} = -H\epsilon + \frac{\omega_{kk}}{3}. \tag{1.1.72}$$

Incidentally, Eq. (1.1.51) is also trivially satisfied, but we have already obtained the required condition $\delta u = \epsilon$. From the above results, it is shown that there is the solution where the curvature perturbation asymptote to

$$\zeta = \mathcal{R} = \frac{\omega_{kk}}{3} = \text{const.} \tag{1.1.73}$$

Inversely ϵ can be solved as

$$\epsilon(t) = \frac{\zeta}{a(t)}\int_{\mathcal{T}}^{t} a(t')\mathrm{d}t', \tag{1.1.74}$$

then

$$\Psi = \Phi = \zeta \left[-1 + \frac{H(t)}{a(t)} \int_{\mathcal{T}}^{t} a(t') \mathrm{d}t' \right], \tag{1.1.75}$$

$$\frac{\delta p}{\dot{\bar{p}}} = \frac{\delta \rho}{\dot{\bar{\rho}}} = -\delta u = -\frac{\zeta}{a(t)} \int_{\mathcal{T}}^{t} a(t') \mathrm{d}t'. \tag{1.1.76}$$

Note in particular that these scalar modes have equal values for $\delta\rho_\alpha / \dot{\bar{\rho}}_\alpha$ for all individual constituents α of the universe, whether or not energy is separately conserved for these constituents. For this reason, such perturbations are called *adiabatic* and any other solutions are called *entropic*. Adiabatic perturbations are related with the additional gauge d.o.f. in the homogeneous limit.

Assuming the time dependence of the scale factor as

$$a \propto t^{\frac{2}{3(1+w)}}, \tag{1.1.77}$$

where $w = \bar{p}/\bar{\rho}$ is the EoS of the fluid, the concrete solutions for non-zero ζ are given by

$$\Psi = \Phi = -\frac{3(1+w)}{5+3w}\zeta, \qquad \frac{\delta\rho}{\dot{\bar{\rho}}} = \frac{\delta p}{\dot{\bar{p}}} = -\frac{3(1+w)}{5+3w} t\zeta. \tag{1.1.78}$$

Also the comoving density perturbation is

$$\Delta_{\rho,k} = \frac{2(1+w)}{5+3w} \left(\frac{k}{aH} \right)^2 \zeta_k. \tag{1.1.79}$$

1.2 Perturbation in inflation

So far we have seen the generic properties of cosmological perturbations. In this section, let us concentrate on the perturbation generated in the inflationary universe. Several useful expressions for scalar fields are summarized in Appendix A.

1.2.1 Generic formulation

Let us begin by generic prescriptions. Considering $\mathcal{N}$ scalar fields $\phi^n(x)$ $(n = 1, \cdots, \mathcal{N})$, the most generic action with GR gravity can be written as

$$S = \int \mathrm{d}^4x \sqrt{-g} \left[-\frac{1}{2} g^{\mu\nu} \gamma_{nm}(\phi) \partial_\mu \phi^n \partial_\nu \phi^m - V(\phi) \right], \tag{1.2.1}$$

where $V(\phi)$ is an arbitrary real potential and $\gamma_{nm}(\phi)$ is an arbitrary real symmetric positive-definite matrix called *field space metric*. For this action, the Euler-Lagrange equation w.r.t. ϕ^n takes the form of

$$\partial_\mu \left(\sqrt{-g} g^{\mu\nu} \gamma_{nm}(\phi) \partial_\nu \phi^m \right) = \sqrt{-g} \left(\frac{1}{2} g^{\mu\nu} \frac{\partial \gamma_{lm}(\phi)}{\partial \bar{\phi}^n} \partial_\mu \phi^l \partial_\nu \phi^m + V_n \right), \tag{1.2.2}$$

where $V_n = \partial V / \partial \phi^n$.

We take each scalar field $\phi^n(x)$ as an unperturbed homogeneous background $\bar{\phi}(t)$ plus a linear order perturbation $\delta\phi^n(\mathbf{x},t)$:

$$\phi^n(\mathbf{x},t) = \bar{\phi}^n(t) + \delta\phi^n(\mathbf{x},t). \tag{1.2.3}$$

The unperturbed field equation (1.2.2) reads

$$\ddot{\bar{\phi}}^n + \gamma^n_{ml}(\bar{\phi})\dot{\bar{\phi}}^m\dot{\bar{\phi}}^l + 3H\dot{\bar{\phi}}^n + \gamma^{nm}(\bar{\phi})V_m(\bar{\phi}) = 0, \tag{1.2.4}$$

where γ^{nm} is the inverse of γ_{nm} and γ^n_{ml} is the affine connection in the field space given by

$$\gamma^n_{ml}(\bar{\phi}) = \frac{1}{2}\gamma^{nk}(\bar{\phi})\left(\frac{\partial\gamma_{km}(\bar{\phi})}{\partial\bar{\phi}^l} + \frac{\partial\gamma_{kl}(\bar{\phi})}{\partial\bar{\phi}^m} - \frac{\partial\gamma_{ml}(\bar{\phi})}{\partial\bar{\phi}^k}\right). \tag{1.2.5}$$

By differentiate the unperturbed energy density w.r.t. t and using EoM, one can obtain

$$\dot{H} = -\frac{1}{2M_{\rm Pl}^2}\gamma_{nm}(\bar{\phi})\dot{\bar{\phi}}^n\dot{\bar{\phi}}^m, \tag{1.2.6}$$

related to Eq. (0.2.17).

For more than one scalar field $T_{\mu\nu}$ is not of the perfect fluid form to all orders in perturbations, but at least in the linear order, one can see that the anisotropic inertia actually vanishes (see Appendix A). Since there is no first order anisotropic inertia, in the Newtonian gauge one has $\Phi = \Psi$, so $h_{00} = -2\Psi$, and the Einstein equation (1.1.51) takes the form

$$\dot{\Psi} + H\Psi = \frac{1}{2M_{\rm Pl}^2}\gamma_{nm}(\bar{\phi})\dot{\bar{\phi}}^n\delta\phi^m. \tag{1.2.7}$$

The first order terms in the field equation (1.2.2) give

$$\begin{aligned}\frac{D^2}{Dt^2}\delta\phi^n + 3H\frac{D}{Dt}\delta\phi^n + \gamma^{nm}(\bar{\phi})V_{ml}(\bar{\phi})\delta\phi^l - \left(\frac{\nabla^2}{a^2}\right)\delta\phi^n \\ = -2\gamma^{nm}(\bar{\phi})\Psi V_m(\bar{\phi}) + 4\dot{\Psi}\dot{\bar{\phi}}^n - \gamma^n{}_{lmk}(\bar{\phi})\dot{\bar{\phi}}^l\dot{\bar{\phi}}^m\delta\phi^k,\end{aligned} \tag{1.2.8}$$

where $\gamma^n{}_{lmk}(\bar{\phi})$ is the Riemann tensor in field space defined by

$$\gamma^n{}_{lmk}(\bar{\phi}) = \frac{\partial\gamma^n_{lm}(\bar{\phi})}{\partial\bar{\phi}^k} - \frac{\partial\gamma^n_{lk}(\bar{\phi})}{\partial\bar{\phi}^m} + \gamma^r_{lm}(\bar{\phi})\gamma^n_{kr}(\bar{\phi}) - \gamma^r_{lk}(\bar{\phi})\gamma^n_{mr}(\bar{\phi}), \tag{1.2.9}$$

and we use the covariant derivative:

$$\frac{D}{Dt}v^n = \frac{\partial}{\partial t}v^n + \gamma^n_{lm}(\bar{\phi})\dot{\bar{\phi}}^l v^m, \tag{1.2.10}$$

for any contravariant vector v^n. Also the Poisson-like constraint (1.1.55) is here

$$\left(\dot{H} - \frac{\nabla^2}{a^2}\right)\Psi = \frac{1}{2M_{\rm Pl}^2}\gamma_{nm}(\bar{\phi})\left(-\dot{\bar{\phi}}^n\frac{D}{Dt}\delta\phi^m + \delta\phi^m\frac{D}{Dt}\dot{\bar{\phi}}^n\right). \tag{1.2.11}$$

Before moving to the Fourier space, note that we would like to treat $\delta\phi^n$ and Ψ as quantum field operators. With $\mathcal{N}$ scalar fields, there are $\mathcal{N}$ pairs of annihilation and creation

operators, but Ψ is just a auxiliary field and does not increase physical d.o.f. Therefore the decompositions of $\delta\phi^n$ and Ψ to plane waves can be written as

$$\delta\hat{\phi}^n(\mathbf{x},t) = \sum_{N=1}^{\mathcal{N}} \int \frac{\mathrm{d}^3q}{(2\pi)^3} \left[\delta\phi^n_{Nq}(t)\mathrm{e}^{i\mathbf{q}\cdot\mathbf{x}}\hat{a}_{N\mathbf{q}} + \delta\phi^{n*}_{Nq}(t)\mathrm{e}^{-i\mathbf{q}\cdot\mathbf{x}}\hat{a}^\dagger_{N\mathbf{q}}\right], \tag{1.2.12}$$

$$\hat{\Psi}(\mathbf{x},t) = \sum_{N=1}^{\mathcal{N}} \int \frac{\mathrm{d}^3q}{(2\pi)^3} \left[\Psi_{Nq}(t)\mathrm{e}^{i\mathbf{q}\cdot\mathbf{x}}\hat{a}_{N\mathbf{q}} + \Psi^*_{Nq}(t)\mathrm{e}^{-i\mathbf{q}\cdot\mathbf{x}}\hat{a}^\dagger_{N\mathbf{q}}\right]. \tag{1.2.13}$$

Since each annihilation or creation operator is independent, the each coefficient should satisfy the field equations. Therefore the field equations read

$$\dot{\Psi}_{Nq} + H\Psi_{Nq} = \frac{1}{2M_{\mathrm{Pl}}^2}\gamma_{nm}(\bar{\phi})\dot{\bar{\phi}}^n\delta\phi^m_{Nq}, \tag{1.2.14}$$

$$\begin{aligned}&\frac{D^2}{Dt^2}\delta\phi^n_{Nq} + 3H\frac{D}{Dt}\delta\phi^n_{Nq} + \gamma^{nm}(\bar{\phi})V_{ml}(\bar{\phi})\delta\phi^l_{Nq} + \left(\frac{q}{a}\right)^2\delta\phi^n_{Nq}\\ &\quad = -2\gamma^{nm}(\bar{\phi})\Psi_{Nq}V_m(\bar{\phi}) + 4\dot{\Psi}_{Nq}\dot{\bar{\phi}}^n - \gamma^n{}_{lmk}(\bar{\phi})\dot{\bar{\phi}}^l\dot{\bar{\phi}}^m\delta\phi^k_{Nq},\end{aligned} \tag{1.2.15}$$

with the constraint

$$\left(\dot{H} + \frac{q^2}{a^2}\right)\Psi_{Nq} = \frac{1}{2M_{\mathrm{Pl}}^2}\gamma_{nm}(\bar{\phi})\left(-\dot{\bar{\phi}}^n\frac{D}{Dt}\delta\phi^m_{Nq} + \delta\phi^m_{Nq}\frac{D}{Dt}\dot{\bar{\phi}}^n\right). \tag{1.2.16}$$

If the constraint is satisfied once, the field equations do not spoil this constraint. Therefore it is used only for the determination of the initial condition. Noting that one can take the massless limit as $q^2/a^2 \gg V_{nm}$ well inside the horizon $q \gg aH$, let us look for the WKB solutions:

$$\delta\phi^n_{Nq}(t) \to f^n_{Nq}(t)\exp\left(-iq\int_{t_1}^t\frac{\mathrm{d}t'}{a(t')}\right), \tag{1.2.17}$$

$$\Psi_{Nq}(t) \to g_{Nq}(t)\exp\left(-iq\int_{t_1}^t\frac{\mathrm{d}t'}{a(t')}\right), \tag{1.2.18}$$

where $\dot{f}^n_{Nq}(t)$ and $\dot{g}_{Nq}(t)$ are negligible compared to q/a. Eqs. (1.2.14) and (1.2.16) are both satisfied to leading order in q/a if one takes

$$g_{Nq} = \frac{ia}{2M_{\mathrm{Pl}}^2 q}\gamma_{nm}(\bar{\phi})\dot{\bar{\phi}}^n f^m_{Nq}. \tag{1.2.19}$$

The terms in Eq. (1.2.15) of first order in q/a then give

$$\frac{D}{Dt}f^n_{Nq} + Hf^n_{Nq} = 0. \tag{1.2.20}$$

To solve this, we note that, because $\gamma^{nm}(\bar{\phi}(t))$ is positive-definite, it can be written in terms of a set of vielbeins $e^n_N(t)$ as

$$\gamma^{nm}(\bar{\phi}(t)) = \sum_N e^n_N(t)e^m_N(t). \tag{1.2.21}$$

These vielbeins can be defined to satisfy the equation of parallel transport[2]

$$\frac{D}{Dt}e^n_{Nq} = 0, \tag{1.2.22}$$

so the solutions of Eq. (1.2.20) can be given by

$$f^n_{Nq}(t) \propto a^{-1}(t)e^n_N(t). \tag{1.2.23}$$

The total normalization is determined by the canonical quantization. If one imposes the commutation relation as

$$\begin{cases} [\phi^n(\mathbf{x},t), \dot{\phi}^m(\mathbf{y},t)] = ia^{-3}(t)\gamma^{nm}(\bar{\phi}(t))\delta^{(3)}(\mathbf{x}-\mathbf{y}), \\ [\phi^n(\mathbf{x},t), \phi^m(\mathbf{y},t)] = [\dot{\phi}^n(\mathbf{x},t), \dot{\phi}^m(\mathbf{y},t)] = 0, \end{cases} \tag{1.2.24}$$

and assumes that the creation-annihiliation operators are normalized as

$$[\hat{a}_{N\mathbf{q}}, \hat{a}^\dagger_{N'\mathbf{q}'}] = (2\pi)^3\delta^{(3)}(\mathbf{q}-\mathbf{q}')\delta_{NN'}, \qquad [\hat{a}_{N\mathbf{q}}, \hat{a}_{N'\mathbf{q}'}] = [\hat{a}^\dagger_{N\mathbf{q}}, \hat{a}^\dagger_{N'\mathbf{q}'}] = 0, \tag{1.2.25}$$

one obtains the normalized initial condition

$$\delta\phi^n_{Nq}(t) \to \frac{1}{a(t)\sqrt{2q}}e^n_N(t)\exp\left(-iq\int_{t_1}^t \frac{\mathrm{d}t'}{a(t')}\right), \tag{1.2.26}$$

$$\Psi_{Nq} \to \frac{i\gamma_{nm}(\bar{\phi})e^m_N(t)\dot{\bar{\phi}}^n(t)}{2M^2_{\rm Pl}\sqrt{2q^3}}\exp\left(-iq\int_{t_q}^t \frac{\mathrm{d}t'}{a(t')}\right). \tag{1.2.27}$$

Finally let us show the expression of the curvature perturbation. Since the curvature perturbation on the uniform density slice has a little complicated expression, we here use the curvature perturbation on the comoving slice $\mathcal{R}$. It is given by, with use of Eq. (A.1.8),

$$\begin{aligned} \mathcal{R}(\mathbf{x},t) &= -\Psi(\mathbf{x},t) + H(t)\delta u(\mathbf{x},t) \\ &= -\Psi(\mathbf{x},t) + \frac{H(t)}{2M^2_{\rm Pl}\dot{H}(t)}\gamma_{nm}(\bar{\phi}(t))\dot{\bar{\phi}}^n(t)\delta\phi^m(\mathbf{x},t) \\ &= \sum_N \int \frac{\mathrm{d}^3q}{(2\pi)^3}\left[\mathrm{e}^{i\mathbf{q}\cdot\mathbf{x}}\hat{a}_{N\mathbf{q}}\mathcal{R}_{Nq}(t) + \mathrm{e}^{-i\mathbf{q}\cdot\mathbf{x}}\hat{a}^\dagger_{N\mathbf{q}}\mathcal{R}^*_{Nq}(t)\right], \end{aligned} \tag{1.2.28}$$

where

$$\mathcal{R}_{Nq}(t) = -\Psi_{Nq}(t) + \frac{H(t)}{2M^2_{\rm Pl}\dot{H}(t)}\gamma_{nm}(\bar{\phi}(t))\dot{\bar{\phi}}^n(t)\delta\phi^m_{Nq}(t). \tag{1.2.29}$$

Its power spectrum is given by

$$\mathcal{P}_\mathcal{R}(k) = \frac{k^3}{2\pi^2}\sum_N |\mathcal{R}_{Nk}|^2. \tag{1.2.30}$$

At least numerically one can calculate the perturbation in inflation with use of the results obtained in this subsection, and we follow such a procedure in Chapter 5. In the next subsection, let us proceed the analytic study in the simplest case.

[2]For example, if the field metric is diagonalized as $\gamma_{nm}(\phi) = C_n(\phi)\delta_{nm}$ where the summation w.r.t. n is not taken, the simple realization of vielbeins is $e^n_N(t) = C_n^{-1/2}(\bar{\phi})\delta^n_N$ and it satisfies the parallel transport equation.

1.2.2 Canonical single field case

In this subsection, we illustrate several analytic results in the simplest case, that is, the canonical single field case:

$$S = \int \mathrm{d}^4x\sqrt{-g}\left[-\frac{1}{2}g^{\mu\nu}\partial_\mu\phi\partial_\nu\phi - V(\phi)\right]. \tag{1.2.31}$$

In this case, the field equations, constraint, and initial conditions read

$$\dot{\Psi}_q + H\Psi_q = \frac{1}{2M_{\rm Pl}^2}\dot{\bar{\phi}}\delta\phi_q, \tag{1.2.32}$$

$$\delta\ddot{\phi}_q + 3H\delta\dot{\phi}_q + V''(\bar{\phi})\delta\phi_q + \left(\frac{q}{a}\right)^2\delta\phi_q = -2\Psi_q V'(\bar{\phi}) + 4\dot{\Psi}_q\dot{\bar{\phi}}, \tag{1.2.33}$$

$$\left(\dot{H} + \frac{q^2}{a^2}\right)\Psi_q = \frac{1}{2M_{\rm Pl}^2}(-\dot{\bar{\phi}}\delta\dot{\phi}_q + \ddot{\bar{\phi}}\delta\phi_q), \tag{1.2.34}$$

$$\delta\phi_q \to \frac{1}{a(t)\sqrt{2q}}\exp\left(-iq\int_{t_1}^{t}\frac{\mathrm{d}t'}{a(t')}\right), \tag{1.2.35}$$

$$\Psi_q \to \frac{i\dot{\bar{\phi}}}{2M_{\rm Pl}^2\sqrt{2q^3}}\exp\left(-iq\int_{t_1}^{t}\frac{\mathrm{d}t'}{a(t')}\right). \tag{1.2.36}$$

The Friedmann equation and the decay rate of the Hubble parameter can be written as

$$3M_{\rm Pl}^2H^2 = \frac{1}{2}\dot{\bar{\phi}}^2 + V(\bar{\phi}), \qquad \dot{H} = -\frac{\dot{\bar{\phi}}^2}{2M_{\rm Pl}^2}. \tag{1.2.37}$$

The curvature perturbation on the comoving slice is given by

$$\mathcal{R}_q = -\Psi_q + H\delta u_q = -\Psi - \frac{H}{\dot{\bar{\phi}}}\delta\phi_q. \tag{1.2.38}$$

One can show that it satisfies the following EoM with use of the above field equations.

$$\ddot{\mathcal{R}}_q + \left(3H - \frac{2\dot{H}}{H} + \frac{\ddot{H}}{\dot{H}}\right)\dot{\mathcal{R}}_q + \frac{q^2}{a^2}\mathcal{R}_q = 0. \tag{1.2.39}$$

Since there is only one physical d.o.f., we need not to calculate two dynamical variables $\delta\phi$ and Ψ and this single equation involves all necessary information.

Let us consider the gauge-invariant scalar perturbation similar to $\mathcal{R}$. We define such a quantity by [17, 18]

$$Q = \delta\phi + \frac{\dot{\bar{\phi}}}{H}\Psi. \tag{1.2.40}$$

Q is related with $\mathcal{R}$ by $\mathcal{R} = -HQ/\dot{\bar{\phi}}$. One can derive the EoM for this variable as

$$\ddot{Q}_q + 3H\dot{Q}_q + \left[\left(\frac{q}{a}\right)^2 + V''(\bar{\phi}) + \frac{2}{M_{\rm Pl}^2}\partial_t\left(\frac{V(\bar{\phi})}{H}\right)\right]Q_q = 0. \tag{1.2.41}$$

If one neglects the third term in the bracket, the above equation is just reduced to the equation for $\delta\phi$ ignoring the metric perturbation. Therefore this term can be interpreted to represent the effect of the metric perturbations. However, if the universe is sufficiently close to the de Sitter spacetime, this time derivative term is indeed negligible. Thus in the slow-roll limit one can safely neglect the metric perturbation and simply regard Q as $\delta\phi$.

Now the EoM for $\delta\phi$ reduces to

$$\delta\ddot{\phi} + 3H\delta\dot{\phi} + \left[\frac{k^2}{a^2} + V''\right]\delta\phi = 0. \tag{1.2.42}$$

If one assumes that V'' is almost constant as $V'' \simeq m^2$, it is useful to rewrite this equation by changing the variable to $u = a\delta\phi$ and using the conformal time $a\mathrm{d}\eta = \mathrm{d}t$. Then the equation reads

$$u'' + \left(k^2 - \frac{a''}{a} + a^2m^2\right)u = 0, \tag{1.2.43}$$

where prime denotes the η-derivative. In the de Sitter limit, it is

$$u'' + \left[k^2 - \left(2 - \frac{m^2}{H^2}\right)\frac{1}{\eta^2}\right]u = 0. \tag{1.2.44}$$

The solution of this equation is given by the Hankel function, and considering the initial condition (1.2.35), the resultant expression is

$$u_k(\eta) = \mathrm{e}^{i\frac{2\nu+1}{4}\pi}\sqrt{\frac{\pi}{4k}}\sqrt{-k\eta}H_\nu^{(1)}(-k\eta), \tag{1.2.45}$$

where $H_\nu^{(1)}(x)$ is the Hankel function of the first kind and

$$\nu = \sqrt{\frac{9}{4} - \frac{m^2}{H^2}} \simeq \frac{3}{2} - \frac{m^2}{3H^2}. \tag{1.2.46}$$

Therefore the power spectrum of the original variable $\delta\phi$ is given by

$$\mathcal{P}_{\delta\phi}(k) = \frac{k^3}{2\pi^2}|\delta\phi_k|^2 = \frac{H^2}{8\pi}\left(\frac{k}{aH}\right)^3\left|H_\nu^{(1)}\left(\frac{k}{aH}\right)\right|^2, \tag{1.2.47}$$

in the de Sitter limit $\eta = -(aH)^{-1}$. With use of the asymptotic form of the Hankel function:

$$H_\nu^{(1)}(x) \to -\frac{i\Gamma(\nu)}{\pi}\left(\frac{2}{x}\right)^\nu, \qquad \text{for } x \to 0, \tag{1.2.48}$$

one can obtain the superhorizon asymptotic value of $\mathcal{P}_{\delta\phi}$ as

$$\mathcal{P}_{\delta\phi}(k) \to \frac{H^2}{2\pi^3}\Gamma^2(\nu)\left(\frac{k}{aH}\right)^{3-2\nu} \simeq \left(\frac{H}{2\pi}\right)^2\left(\frac{k}{aH}\right)^{\frac{2m^2}{3H^2}}, \qquad \text{for } k \ll aH. \tag{1.2.49}$$

Here we used $\Gamma(\nu) \simeq \Gamma(3/2) = \sqrt{\pi}/2$. Therefore in the massless limit, the amplitude of the perturbation $\delta\phi$ asymptotes to the constant $(H/(2\pi))^2$ on the superhorizon, and moreover, the asymptotic form of the Hankel function (1.2.48) indicates that $\delta\phi$ itself ceases to oscillation. This phenomenon is called *freeze-out of perturbations*.

The power spectrum of the curvature perturbations can be derived easily as

$$\mathcal{P}_{\mathcal{R}} = \left(\frac{H}{\dot{\phi}}\right)^2 \mathcal{P}_{\delta\phi} = \frac{1}{2\epsilon_H M_{\rm Pl}^2}\left(\frac{H}{2\pi}\right)^2, \tag{1.2.50}$$

where $\epsilon_H = -\dot{H}/H^2$ is the slow-roll parameter. This is the standard result in the linear perturbation theory.

Finally let us briefly mention the classicalization of the perturbation. As we have seen, the perturbations are assumed to be quantum field operators during inflation. However generally the cosmological perturbations are treated as classical fields after inflation. This is justified by the so-called classicalization of the perturbation. The commutation relation

$$[\delta\phi(\mathbf{x}, t), \delta\dot{\phi}(\mathbf{y}, t)] = ia^{-3}\delta^{(3)}(\mathbf{x} - \mathbf{y}). \tag{1.2.51}$$

is equivalent to the normalization of the mode function

$$u_k^* u_k' - u_k u_k^{*\prime} = 2i\mathrm{Im}u_k^* u_k' = -i\hbar. \tag{1.2.52}$$

Here we explicitly write $\hbar$. Since the classical limit corresponds with the $\hbar \to 0$ limit, the perturbations can be interpreted to be classical if $\mathrm{Im}u_k^* u_k'$ becomes negligible. Therefore the quantity $F(k) = \mathrm{Re}u_k^* u_k'$ would be the indicator [19], that is, $F \gg 1$ becomes a criterion of the classicalization in the $\hbar = 1$ unit. In the subhorizon limit, Eq. (1.2.35) shows $F(k)$ is quite smaller than unity and indeed the quantum property cannot be neglected. However in the superhorizon limit $F(k)$ grows as a^3 and therefore the perturbations are considered to be classicalized on the superhorizon scale.

Chapter 2

Stochastic-δN Formalism

To go beyond the perturbation theory, the superhorizon dynamics has several useful properties. One is that it allows the wavenumber expansions. The other is that the superhorizon perturbations can be treated as classical quantities. In this chapter, taking advantage of these things, we introduce stochastic-δN formalism, *in which the power spectrum of the curvature perturbations can be calculated without the perturbative expansion w.r.t. the inflaton fields. This chapter is partially based on Refs. [20, 21].*

2.1 δN formalism

In the previous chapter, we show the gauge-invariant curvature perturbation is conserved on the superhorizon scale in the adiabatic solution at least to linear order. Lyth, Malik, and Sasaki [22] further proved that the superhorizon curvature perturbation is conserved in all orders. Moreover they found that this quantity is simply given by the fluctuation of the e-folding number δN, and therefore calculating the curvature perturbation in their formulation is called *δN formalism*.

At first we use the standard $(3+1)$-decomposition of the metric, which applies to any smooth spacetime [23]:

$$\mathrm{d}s^2 = -\mathcal{N}^2\mathrm{d}t^2 + \gamma_{ij}(\mathrm{d}x^i + \beta^i\mathrm{d}t)(\mathrm{d}x^j + \beta^j\mathrm{d}t), \tag{2.1.1}$$

where $\mathcal{N}$ is the lapse function, β^i is the shift vector, and γ_{ij} is the spatial three metric. Let us renormalize the spatial three metric as

$$\gamma_{ij} = \tilde{a}^2(t,\mathbf{x})\tilde{\gamma}_{ij}, \qquad \det\tilde{\gamma}_{ij} = 1. \tag{2.1.2}$$

Here $\tilde{a}(t,\mathbf{x})$ represents the local scale factor. Further we define the curvature perturbation $\psi(t,\mathbf{x})$ by

$$\tilde{a}(t,\mathbf{x}) = a(t)\exp(\psi(t,\mathbf{x})), \tag{2.1.3}$$

with the global scale factor $a(t)$.

We consider only the long wavelength modes as $k \ll aH$, and in this case, the universe should seem to be locally homogeneous and isotropic from the separate universe assumption [24]. However the metric (2.1.1):

$$\mathrm{d}s^2 = -(\mathcal{N}^2 - \beta^i\beta_i)\mathrm{d}t^2 + 2\beta_i \mathrm{d}t\mathrm{d}x^i + \gamma_{ij}\mathrm{d}x^i\mathrm{d}x^j, \tag{2.1.4}$$

includes the anisotropic component $2\beta_i \mathrm{d}t\mathrm{d}x^i$. Here spatial indices are raised and lowered by γ_{ij}. Therefore at least β^i should be negligible in the long wavelength limit and it can be written as $\beta^i = \mathcal{O}(\epsilon)$ where[1]

$$\epsilon = \frac{k}{aH} \ll 1. \tag{2.1.5}$$

These expansions w.r.t. $\epsilon = k/(aH)$ is called *gradient expansion*. We will use this gradient expansion in the followings, but note that the expansion w.r.t. the perturbation itself is not used.

By virtue of the separate universe assumption, the energy-momentum tensor will have the perfect fluid form

$$T_{\mu\nu} = pg_{\mu\nu} + (\rho + p)u_\mu u_\nu. \tag{2.1.6}$$

Then let us take the comoving gauge where the spatial coordinate comoves with the fluid, that is,

$$0 = v^i = \frac{\mathrm{d}x^i}{\mathrm{d}t} = \frac{\mathrm{d}x^i}{\mathrm{d}\tau}\Big/\frac{\mathrm{d}t}{\mathrm{d}\tau} = \frac{u^i}{u^0}. \tag{2.1.7}$$

Here τ is the proper time. Recall that the four-velocity is normalized by $u^\mu u_\mu = -1$ and therefore

$$u^\mu = \left[\frac{1}{\sqrt{\mathcal{N}^2 - \beta^i\beta_i}}, 0, 0, 0\right] \sim \left[\frac{1}{\mathcal{N}}, 0, 0, 0\right], \tag{2.1.8}$$

at the leading order in ϵ. Now let us define the expansion θ as

$$\begin{aligned}\theta = \nabla_\mu u^\mu &= \frac{1}{\sqrt{-g}}\partial_\mu(\sqrt{-g}u^\mu) = \frac{1}{\mathcal{N}\mathrm{e}^{3\psi}a^3}\partial_\mu(\mathcal{N}\mathrm{e}^{3\psi}a^3u^\mu) \\ &\sim \frac{1}{\mathcal{N}\mathrm{e}^{3\psi}a^3}\partial_0\left(\mathcal{N}\mathrm{e}^{3\psi}a^3\frac{1}{\mathcal{N}}\right) = \frac{3}{\mathcal{N}}\left(\frac{\dot{a}}{a} + \dot{\psi}\right).\end{aligned} \tag{2.1.9}$$

It is convenient to introduce the local Hubble parameter by $3\tilde{H} = \theta$.

To relate the local Hubble parameter with the energy density of the universe, we now consider the conservation of the energy density $\nabla_\mu T^{\mu\nu}$. From this, one can obtain

$$0 = u_\mu \nabla_\nu T^{\mu\nu} = -u^\nu \nabla_\nu \rho - (\rho + p)\theta. \tag{2.1.10}$$

The first term is

$$u^\nu \nabla_\nu \rho = \frac{\mathrm{d}x^\nu}{\mathrm{d}\tau}\frac{\mathrm{d}\rho}{\mathrm{d}x^\nu} = \frac{\mathrm{d}\rho}{\mathrm{d}\tau}, \tag{2.1.11}$$

[1] Note that this ϵ parameter is irrelevant to the gauge transformation $\epsilon(t)$ (1.1.63).

and therefore

$$\frac{\mathrm{d}\rho}{\mathrm{d}\tau} = -(\rho + p)\theta. \tag{2.1.12}$$

Since now the spatial coordinates are comoving with the fluid, the proper time is given by $\mathrm{d}\tau = \mathcal{N}\mathrm{d}t$. Thus

$$\dot{\rho} = -(\rho + p)\mathcal{N}\theta \sim -3\left(\frac{\dot{a}}{a} + \dot{\psi}\right)(\rho + p). \tag{2.1.13}$$

Therefore the generalized continuity equation is given by

$$\frac{\dot{a}}{a} + \dot{\psi} = -\frac{1}{3}\frac{\dot{\rho}}{\rho + p}, \tag{2.1.14}$$

at the leading order in ϵ.

The e-folding number of the expansion from the time t_i to t_f can be defined as

$$\begin{aligned} N(t_\mathrm{f}, t_\mathrm{i}; \mathbf{x}) &= \frac{1}{3}\int_{t_\mathrm{i}}^{t_\mathrm{f}} \theta\mathcal{N}\mathrm{d}t = -\frac{1}{3}\int_{t_\mathrm{i}}^{t_\mathrm{f}} \frac{\dot{\rho}}{\rho + p}\mathrm{d}t = \int_{t_\mathrm{i}}^{t_\mathrm{f}}\left(\frac{\dot{a}}{a} + \dot{\psi}\right)\mathrm{d}t \\ &= \log\left[\frac{a(t_\mathrm{f})}{a(t_\mathrm{i})}\right] + \psi(t_\mathrm{f}, \mathbf{x}) - \psi(t_\mathrm{i}, \mathbf{x}). \end{aligned} \tag{2.1.15}$$

On the other hand the global e-foldings is

$$N_0(t_\mathrm{f}, t_\mathrm{i}) = \log\left[\frac{a(t_\mathrm{f})}{a(t_\mathrm{i})}\right]. \tag{2.1.16}$$

Therefore its perturbation is given by

$$\delta N(t_\mathrm{f}, t_\mathrm{i}; \mathbf{x}) = N(t_\mathrm{f}, t_\mathrm{i}; \mathbf{x}) - N_0(t_\mathrm{f}, t_\mathrm{i}) = \psi(t_\mathrm{f}, \mathbf{x}) - \psi(t_\mathrm{i}, \mathbf{x}). \tag{2.1.17}$$

If one takes the flat time slice ($\psi = 0$) at t_i and the uniform density slice ($\delta\rho = 0$) at t_f, the fluctuation of the e-foldings is

$$\delta N(t_\mathrm{f}, t_\mathrm{i}; \mathbf{x}) = \psi(t_\mathrm{f})|_{\psi(t_\mathrm{i})=0,\, \delta\rho(t_\mathrm{f})=0}, \tag{2.1.18}$$

and let the symbol ζ denote this quantity:

$$\zeta = \delta N(t_\mathrm{f}, t_\mathrm{i}; \mathbf{x})|_{\psi(t_\mathrm{i})=0,\, \delta\rho(t_\mathrm{f})=0}. \tag{2.1.19}$$

On the other hand, if the universe is adiabatic and the pressure is a function only of the energy density $p = p(\rho)$, the global continuity equation gives

$$N_0 = \int_{t_\mathrm{i}}^{t_\mathrm{f}} \frac{\dot{a}}{a}\mathrm{d}t = -\frac{1}{3}\int_{\bar{\rho}(t_\mathrm{i})}^{\bar{\rho}(t_\mathrm{f})} \frac{\mathrm{d}\rho}{\rho + p}. \tag{2.1.20}$$

Therefore Eq. (2.1.17) reads

$$\begin{aligned} \psi(t_\mathrm{f}, \mathbf{x}) - \psi(t_\mathrm{i}, \mathbf{x}) &= -\frac{1}{3}\int_{\rho(t_\mathrm{i}, \mathbf{x})}^{\rho(t_\mathrm{f}, \mathbf{x})} \frac{\mathrm{d}\rho}{\rho + p} + \frac{1}{3}\int_{\bar{\rho}(t_\mathrm{i})}^{\bar{\rho}(t_\mathrm{f})} \frac{\mathrm{d}\rho}{\rho + p} \\ &= \frac{1}{3}\left(-\int_{\bar{\rho}(t_\mathrm{f})}^{\rho(t_\mathrm{f}, \mathbf{x})} \frac{\mathrm{d}\rho}{\rho + p} + \int_{\bar{\rho}(t_\mathrm{i})}^{\rho(t_\mathrm{i}, \mathbf{x})} \frac{\mathrm{d}\rho}{\rho + p}\right). \end{aligned} \tag{2.1.21}$$

Hence the quantity $\zeta(\mathbf{x})$ defined by

$$\zeta(t,\mathbf{x}) = \psi(t,\mathbf{x}) + \frac{1}{3}\int_{\bar{\rho}(t)}^{\rho(t,\mathbf{x})} \frac{\mathrm{d}\rho}{\rho+p}, \tag{2.1.22}$$

is time-independent, and indeed it is equivalent δN (2.1.19) if one takes the flat slice at t_i and the uniform density slice at t_f. That is the proof of the conservation of the curvature perturbations.

Finally let us mention the correspondence with the Newtonian gauge. In the Newtonian gauge, the metric is given by

$$\mathrm{d}s^2 = -(1+2\Phi)\mathrm{d}t^2 + a^2\left[\delta_{ij}(1-2\Psi) + D_{ij}\right]\mathrm{d}x^i\mathrm{d}x^j, \tag{2.1.23}$$

while the current notation gives

$$\mathrm{d}s^2 = -\mathcal{N}^2\mathrm{d}t^2 + a^2\mathrm{e}^{2\psi}\tilde{\gamma}_{ij}\mathrm{d}x^i\mathrm{d}x^j. \tag{2.1.24}$$

This spatial part can be written as, with use of the traceless tensor χ_{ij},

$$a^2(t)[(1+2\psi)\delta_{ij} + 2\chi_{ij}], \tag{2.1.25}$$

in the small perturbation case. Therefore there is a correspondence as $\psi \leftrightarrow -\Psi$, and with use of

$$\int_{\bar{\rho}}^{\rho(\mathbf{x})} \frac{\mathrm{d}\rho}{\rho+p} \sim \frac{\delta\rho(\mathbf{x})}{\bar{\rho}+\bar{p}}, \tag{2.1.26}$$

at the linear order, one can see that $\zeta(\mathbf{x})$ defined in this section is equivalent to the quantity described in the previous chapter (1.1.59).

2.1.1 Application to the perturbation theory

Here let us briefly see that the δN formalism consistently reproduces the result of the linear perturbation theory in the single-field case. We consider the slow-roll EoM (0.2.21) for the background inflaton field

$$3H\dot{\bar{\phi}} = -V', \quad \Leftrightarrow \quad \frac{\mathrm{d}\bar{\phi}}{\mathrm{d}N} = -M_\mathrm{Pl}^2\frac{V'}{V} = -\sqrt{2\epsilon_V}M_\mathrm{Pl}, \tag{2.1.27}$$

where $\epsilon_V = \frac{M_\mathrm{Pl}^2}{2}\left(\frac{V'}{V}\right)^2$ is the slow-roll parameter (0.2.23) (here we assume $V' > 0$). Also here we introduce the e-foldings as a time variable such that $\mathrm{d}N = H\mathrm{d}t$. Due to the separate universe assumption, Each Hubble patch evolves as a locally homogeneous FLRW universe, following the same above EoM for the background field. Therefore the elapsed e-folding number from ϕ_i to ϕ_f in each Hubble patch $\mathbf{x}$ is (note again that $\phi_\mathrm{f} < \phi_\mathrm{i}$ since we assume $V' > 0$)[2]

$$N(t_\mathrm{f}, t_\mathrm{i}; \mathbf{x}) = \int_{\phi_\mathrm{f}}^{\phi_\mathrm{i}(\mathbf{x})} \frac{\mathrm{d}\phi}{\sqrt{2\epsilon_V}M_\mathrm{Pl}}. \tag{2.1.28}$$

[2]The e-folding number with such a definition is often called *backward e-folds*, since it is counted backwardly from the end surface. In the δN formalism, the curvature perturbation is given by the fluctuation of this backward e-folds, strictly speaking.

Here we take the uniform ϕ slice at t_f, which is equivalent to the uniform density slice in the slow-roll single-field case, while the initial field value $\phi_\mathrm{i}(\mathbf{x})$ is fluctuated and causes the difference in the elapsed e-foldings $N(t_\mathrm{f}, t_\mathrm{i}; \mathbf{x})$. At the linear order, its fluctuation is given by

$$\delta N(t_\mathrm{f}, t_\mathrm{i}; \mathbf{x}) = \frac{1}{\sqrt{2\epsilon_V} M_\mathrm{Pl}} \delta\phi(\mathbf{x}), \tag{2.1.29}$$

and its power spectrum reads

$$\mathcal{P}_{\delta N} = \frac{1}{2\epsilon_V M_\mathrm{Pl}^2} \mathcal{P}_{\delta\phi} = \frac{1}{2\epsilon_V M_\mathrm{Pl}^2} \left(\frac{H}{2\pi}\right)^2, \tag{2.1.30}$$

consistently with the result of the linear perturbation theory (1.2.50). Since the inflaton's perturbation is assumed to be classicalized soon after its horizon exit, the right-hand side of this equation is evaluated at the horizon exit of the considered scale $k = aH$.

The scale dependence of the power spectrum $\partial \log \mathcal{P}_\zeta / \partial \log k$ can be also calculated easily. In the slow-roll limit, the horizon scale $k = aH$ and the backward e-folds N at that time are related with $k = aH \sim k_\mathrm{f} \mathrm{e}^{-N}$ where k_f is the horizon scale at the end of inflation $k_\mathrm{f} = (aH)_\mathrm{f}$. Then the considered scale and the evaluation time are connected by $\mathrm{d} \log k = -\mathrm{d}N$. Therefore the the spectral index n_s defined by

$$n_\mathrm{s} - 1 = \frac{\partial \log \mathcal{P}_\zeta}{\partial \log k}, \tag{2.1.31}$$

is given by

$$n_\mathrm{s} - 1 = -\frac{\partial \log V}{\partial N} + \frac{\partial \log \epsilon_V}{\partial N} = -6\epsilon_V + 2\eta_V, \tag{2.1.32}$$

which can be checked with use of the definition of the slow-roll parameters (0.2.23) and (0.2.27) and the slow-roll EoM (2.1.27).

Note that in the δN formalism we only need the background EoM as long as the amplitude of the scalar perturbation is well approximated by $H/(2\pi)$. Therefore even in the multi-field case, fluctuating the initial field value by $H/(2\pi)$ and solving the background EoM, obtained fluctuations of the elapsed e-folds to the end surface is nothing but the curvature perturbation. This simplicity is the strong point of the δN formalism.

2.2 Stochastic formalism

To treat the superhorizon scalar perturbations more explicitly and intuitively, the stochastic formalism is quite strong tool, which was proposed by Starobinsky [25]. In this formalism, the background field is not assumed to be homogeneous any longer, but instead all superhorizon perturbations are directly treated as the classical background field. In this section, let us derive the EoM for this perturbed background field, following Ref. [26–28].

We begin by the standard scalar action:

$$S[\phi] = \int \mathrm{d}^4x \sqrt{-g} \left[-\frac{1}{2} g^{\mu\nu} \partial_\mu \phi \partial_\nu \phi - V(\phi) \right]. \tag{2.2.1}$$

For the inflaton potential, we assume that it is sufficiently flat to support the slow-roll inflation and its mass term $m^2 = V''(\bar{\phi})$ can be approximated to be almost constant. In the slow-roll limit, one can neglect the metric perturbation as we mentioned in Sec. 1.2.2, therefore the background metric is given by the flat FLRW as

$$ds^2 = a^2(\eta)(-d\eta^2 + d\mathbf{x}^2), \tag{2.2.2}$$

where η is the conformal time.

Then let us decompose the scalar field into the super- and subhorizon modes as

$$\phi(x) = \phi_{\rm IR}(x) + \phi_{\rm UV}(x), \tag{2.2.3}$$

where $\phi_{\rm IR}$ and $\phi_{\rm UV}$ denote the super- and subhorizon modes respectively. Concretely speaking, it is achieved with use of some window function $W(\mathbf{k}, t)$ as

$$\phi_{\rm UV}(x) = \int \frac{d^3k}{(2\pi)^3} W(\mathbf{k}, t)\phi_{\mathbf{k}} e^{i\mathbf{k}\cdot\mathbf{x}}, \tag{2.2.4}$$

where the window function $W(\mathbf{k}, t)$ cuts off the superhorizon modes. We also decompose the action itself into the part depending only on the IR field $S_{\rm IR}[\phi_{\rm IR}] = S[\phi_{\rm IR}]$, only on the UV field $S_{\rm UV}[\phi_{\rm UV}] = S[\phi_{\rm UV}]$, and depending on both the IR and UV field $S_{\rm int}[\phi_{\rm IR}, \phi_{\rm UV}]$:

$$S[\phi] = S_{\rm IR}[\phi_{\rm IR}] + S_{\rm UV}[\phi_{\rm UV}] + S_{\rm int}[\phi_{\rm IR}, \phi_{\rm UV}]. \tag{2.2.5}$$

To obtain the vacuum expectation value of several operators for this action, one can use the closed time path formulation (see e.g. the textbook [29]). In this formulation, the vacuum expectation value can be calculated in the same manner of the scattering process along both the forward and backward time paths. The partition function is expressed as follows in the path integral formalism.

$$\begin{aligned} Z[J] = \mathcal{N} \int \mathcal{D}\phi^+_{\rm IR}\mathcal{D}\phi^-_{\rm IR}\mathcal{D}\phi^+_{\rm UV}\mathcal{D}\phi^-_{\rm UV} \exp[i(S[\phi^+] - S[\phi^-])] \\ \times \exp\left[i\int d^4x (J^+(x)\phi^+(x) - J^-(x)\phi^-(x))\right]. \end{aligned} \tag{2.2.6}$$

The superscripts $+$ and $-$ stand for the field on the forward and backward time path respectively. Note that $\mathcal{N}$ formally represents the normalization factor and they do not necessarily take the same value in different equations. Let us introduce the doublet expression to avoid a heavy notation as

$$J^a = \begin{pmatrix} J^+ \\ J^- \end{pmatrix}, \qquad \phi^a = \begin{pmatrix} \phi^+ \\ \phi^- \end{pmatrix}, \tag{2.2.7}$$

and we express the spacetime integral as the inner product in the 2D space whose metric is $(1, -1)$:

$$\int d^4x (J^+(x)\phi^+(x) - J^-(x)\phi^-(x)) = J^a\phi_a = J\cdot\phi. \tag{2.2.8}$$

The partition function can be also decomposed into the IR and UV part as

$$Z[J_{\rm IR}, J_{\rm UV}] = \mathcal{N} \int \mathcal{D}\phi^\pm_{\rm IR} e^{i(S^+_{\rm IR} - S^-_{\rm IR} + J_{\rm IR}\cdot\phi_{\rm IR})} \int \mathcal{D}\phi^\pm_{\rm UV} \exp\left[i(S^+_{\rm UV} - S^-_{\rm UV} + S^+_{\rm int} - S^-_{\rm int} + J_{\rm UV}\cdot\phi_{\rm UV})\right], \tag{2.2.9}$$

and the latter part:

$$F[\phi_{\rm IR};J_{\rm UV}]=\int\mathscr{D}\phi^{\pm}_{\rm UV}\exp\left[i(S^{+}_{\rm UV}-S^{-}_{\rm UV}+S^{+}_{\rm int}-S^{-}_{\rm int}+J_{\rm UV}\cdot\phi_{\rm UV})\right], \tag{2.2.10}$$

is referred to as *influence functional*, and the *influence action* $S_{\rm IA}[\phi_{\rm IR};J_{\rm UV}]$ is defined by $F[\phi_{\rm IR};J_{\rm UV}]=\mathscr{N}\mathrm{e}^{iS_{\rm IA}[\phi_{\rm IR};J_{\rm UV}]}$.

These expressions are still mere identical transformations. But here we impose two assumptions. One is that the UV field can be treated perturbatively as we did so far. That is, the influence functional $F[\phi_{\rm IR};J_{\rm UV}]$ is assumed to be solved in the perturbative expansion. The other one is that the IR field can be regarded as a classical field. Therefore the integral w.r.t. the IR field just gives the stationary value around the vev $\varphi=\langle\phi_{\rm IR}\rangle$. As a result, one can expect the following form of the partition function.

$$Z[J_{\rm IR},J_{\rm UV}]=\mathscr{N}\mathrm{e}^{i(S[\varphi^{+}]-S[\varphi^{-}]+S_{\rm IA}[\varphi,J_{\rm UV}]+J_{\rm IR}\cdot\varphi)}. \tag{2.2.11}$$

Writing it as $\mathrm{e}^{iW[J]}$, the Legendre transformation of $W[J]$ is the effective action for φ:

$$\Gamma[\langle\phi\rangle]=W[J]-J\cdot\langle\phi\rangle, \tag{2.2.12}$$

where $\langle\phi\rangle=(\delta/\delta J)W[J]$. The UV modes are almost free fields and we do not assume that they have non-zero vev. Also for IR modes, $J_{\rm IR}\cdot\varphi$ obviously cancel each other. Therefore the effective action for the IR field is given by taking $J=0$ in $W[J]$:

$$\Gamma_{\rm IR}[\varphi]=S[\varphi^{+}]-S[\varphi^{-}]+S_{\rm IA}[\varphi;J=0]. \tag{2.2.13}$$

If one takes account only of the mass term for the UV integral as a leading order calculation, one can obtain the following result whose detailed derivation is described in Appendix B.

$$S^{(1)}_{\rm IA}=\frac{i}{2}\int\mathrm{d}^4x\mathrm{d}^4x'\varphi_{\rm q}(x)\mathrm{Re}[\Pi(x,x')]\varphi_{\rm q}(x')-2\int\mathrm{d}^4x\mathrm{d}^4x'\theta(t-t')\varphi_{\rm q}(x)\mathrm{Im}[\Pi(x,x')]\varphi_{\rm c}(x'), \tag{2.2.14}$$

where

$$\Pi(x,x')=\int\frac{\mathrm{d}^3k}{(2\pi)^3}a^3(t)[P_t\phi_{\mathbf{k}}(t)]\mathrm{e}^{i\mathbf{k}\cdot\mathbf{x}}a^3(t')[P_{t'}\phi^{*}_{\mathbf{k}}(t')]\mathrm{e}^{-i\mathbf{k}\cdot\mathbf{x}'}, \tag{2.2.15}$$

with the following derivative operator

$$P_t=[\ddot{W}(\mathbf{k},t)+3H\dot{W}(\mathbf{k},t)+2\dot{W}(\mathbf{k},t)\partial_t]. \tag{2.2.16}$$

Also $\varphi_{\rm c}$ and $\varphi_{\rm q}$ are the Keldysh basis defined by

$$\begin{pmatrix}\varphi_{\rm c}\\ \varphi_{\rm q}\end{pmatrix}=\begin{pmatrix}\frac{\varphi^{+}+\varphi^{-}}{2}\\ \varphi^{+}-\varphi^{-}\end{pmatrix}. \tag{2.2.17}$$

$\phi_{\mathbf{k}}(t)$ is the mode function of ϕ.

The second term of this influence action is actually negligible. To proceed further calculations, let us take a concrete window function as $W(\mathbf{k},t) = \theta(k-\epsilon aH) = \theta_t$ where ϵ would be a small positive parameter. Then the influence action reads

$$S_{\rm IA}^{(1)} \simeq \frac{i}{2}\int \mathrm{d}^4x\mathrm{d}^4x' \int \frac{\mathrm{d}^3k}{(2\pi)^3}a^3(t)\varphi_{\rm q}(x)\mathrm{Re}[(3H\dot\theta_t+\ddot\theta_t+2\dot\theta_t\partial_t)\phi_{\mathbf{k}}(t)\mathrm{e}^{i\mathbf{k}\cdot\mathbf{x}} \\ \times(3H\dot\theta_{t'}+\ddot\theta_{t'}+2\dot\theta_{t'}\partial_{t'})\phi_{\mathbf{k}}(t')\mathrm{e}^{i\mathbf{k}\cdot\mathbf{x}'}]a^3(t')\varphi_{\rm q}(x'). \tag{2.2.18}$$

For the mode function, we adopt the free field solution (1.2.45):

$$\phi_{\mathbf{k}} = \frac{\sqrt{\pi}}{2}H|\eta|^{3/2}H_\nu^{(1)}\left(\frac{k}{aH}\right), \qquad \nu = \sqrt{\frac{9}{4}-\frac{m^2}{H^2}}, \tag{2.2.19}$$

neglecting the interaction terms as a leading order calculation. Here we omit the irrelevant constant phase. For this mode function, the following relation is satisfied on the cut-off scale $k=\epsilon aH$:

$$\dot\phi_{\mathbf{k}}(t)|_{k=\epsilon aH} = q_\nu(\epsilon)\phi_{\mathbf{k}}(t)|_{k=\epsilon aH}, \tag{2.2.20}$$

where

$$q_\nu(\epsilon) = -H\left(\left(\frac{3}{2}-\nu\right)+\epsilon\frac{H_{\nu-1}^{(1)}(\epsilon)}{H_\nu^{(1)}(\epsilon)}\right). \tag{2.2.21}$$

With these results, integrating by parts, one can obtain

$$S_{\rm IA}^{(1)} \simeq \frac{i}{2}\int \mathrm{d}^4x\mathrm{d}^4x'\mathrm{Re}[Q(x)A(x,x')Q^*((x')], \tag{2.2.22}$$

where

$$Q(x) = (\varphi_{\rm q}(x)q_\nu(\epsilon)-\dot\varphi_{\rm q}(x))a^3(t), \tag{2.2.23}$$

and

$$A(x,x') = \int\frac{\mathrm{d}^3k}{(2\pi)^3}\dot\theta_t\phi_{\mathbf{k}}(t)\dot\theta_{t'}\phi_{\mathbf{k}}^*(t')\mathrm{e}^{i\mathbf{k}\cdot(\mathbf{x}-\mathbf{x}')} \\ = \frac{H^3}{8\pi}\epsilon^3|H_\nu^{(1)}(\epsilon)|^2\frac{\sin(\epsilon aHr)}{\epsilon aHr}\delta(t-t'), \qquad r=|\mathbf{x}-\mathbf{x}'|. \tag{2.2.24}$$

Here note that the influence action is pure imaginary, while we would like a real contribution for a real scalar φ. Indeed the contribution of this term to the EoM for the IR mode vanishes at this stage, which can be described as follows. First, originally $+/-$ basis is just copied d.o.f. and classical solution for them should be the same $\varphi^+=\varphi^-$. Therefore $\varphi_{\rm c}=(\varphi^++\varphi^-)/2$ represents the true solution for the IR field and its EoM can be obtained by $\delta S/\delta\varphi_{\rm q}|_{\varphi_{\rm q}=0}$. However, since the obtained influence action is the quadratic order of $\varphi_{\rm q}$, its contribution to EoM vanishes. To take account of its true effect, one has to rewrite this term by the Gaussian integral. That is, the effective action can be rewritten as

$$\exp(i\Gamma_{\rm IR}[\varphi]) = \int\mathscr{D}\xi_{\rm R}\mathscr{D}\xi_{\rm I}P[\xi_{\rm R}]P[\xi_{\rm I}]\exp(iS_{\rm eff}[\varphi]), \tag{2.2.25}$$

with the auxiliary fields $\xi_{\mathrm{R,I}}$. Here $P[\xi]$ is the Gaussian weight:

$$P[\xi] = (2\pi\sqrt{\det A})^{-1} \exp\left(-\frac{1}{2}\int \mathrm{d}^4x\mathrm{d}^4x'\xi(x)A^{-1}(x,x')\xi(x')\right), \tag{2.2.26}$$

and the real effective action S_{eff} is

$$S_{\mathrm{eff}}[\varphi] = S[\varphi^+] - S[\varphi^-] + \int \mathrm{d}^4x[\xi_{\mathrm{R}}(x)\mathrm{Re}Q(x) + \xi_{\mathrm{I}}\mathrm{Im}Q(x)]. \tag{2.2.27}$$

So finally one obtains the following EoM for $\varphi = \varphi_{\mathrm{c}}$.

$$0 = \left.\frac{\delta S_{\mathrm{eff}}}{\delta\varphi_{\mathrm{q}}}\right|_{\varphi_{\mathrm{q}}=0} = \ddot{\varphi} + 3H\dot{\varphi} - a^{-2}\nabla^2\varphi + V'(\varphi) - (q_{\mathrm{R}} + 3H)\xi_{\mathrm{R}} - \dot{\xi}_{\mathrm{R}} - q_{\mathrm{I}}\xi_{\mathrm{I}}, \tag{2.2.28}$$

where $q_{\mathrm{R,I}}$ represent $\mathrm{Re}q_\nu$ and $\mathrm{Im}q_\nu$ respectively. Also it can be rewritten as

$$\begin{cases} \dot{\varphi} = \pi + \xi_{\mathrm{R}}, \\ \dot{\pi} = -3H\pi + a^{-2}\nabla^2\varphi - V' + q_{\mathrm{R}}\xi_{\mathrm{R}} + q_{\mathrm{I}}\xi_{\mathrm{I}}, \end{cases} \tag{2.2.29}$$

$\xi_{\mathrm{R,I}}$ can be treated as Gaussian noise, whose correlations are given by

$$\langle\xi_{\mathrm{R}}(x)\xi_{\mathrm{R}}(x')\rangle = \int \mathscr{D}\xi_{\mathrm{R}}P[\xi_{\mathrm{R}}]\xi_{\mathrm{R}}(x)\xi_{\mathrm{R}}(x') = A(x,x'), \tag{2.2.30}$$

$$\langle\xi_{\mathrm{I}}(x)\xi_{\mathrm{I}}(x')\rangle = \int \mathscr{D}\xi_{\mathrm{I}}P[\xi_{\mathrm{I}}]\xi_{\mathrm{I}}(x)\xi_{\mathrm{I}}(x') = A(x,x'), \tag{2.2.31}$$

$$\langle\xi_{\mathrm{R}}(x)\xi_{\mathrm{I}}(x')\rangle = \int \mathscr{D}\xi_{\mathrm{R}}\mathscr{D}\xi_{\mathrm{I}}P[\xi_{\mathrm{R}}]P[\xi_{\mathrm{I}}]\xi_{\mathrm{R}}(x)\xi_{\mathrm{I}}(x') = 0. \tag{2.2.32}$$

Note that $q_\nu(\epsilon) = \mathcal{O}(\epsilon^2)$ and the gradient term also gives only the contribution of $\mathcal{O}(\epsilon)$. Therefore for sufficiently small ϵ, the EoM can be much simplified as

$$\begin{cases} \dot{\varphi} = \pi + \xi, \\ \dot{\pi} = -3H\pi - V'. \end{cases} \tag{2.2.33}$$

Also, since the correlation amplitude $A(x,x')$ can be written in terms of the power spectrum of ϕ (1.2.47) as

$$A(x,x') = \mathcal{P}_\phi(k=\epsilon aH)\frac{\sin(\epsilon aHr)}{\epsilon aHr}H\delta(t-t') = \mathcal{P}_\phi(k=\epsilon aH)\frac{\sin(\epsilon aHr)}{\epsilon aHr}H^2\delta(N-N'), \tag{2.2.34}$$

and $\sin(\epsilon aHr)/(\epsilon aHr)$ can be approximated by the step function $\theta(1-\epsilon aHr)$ for a coarse-grained field, the EoM can be rewritten as follows where we take the e-folds as a time variable $\mathrm{d}N = H\mathrm{d}t$ and renormalize the noise term to unity:

$$\begin{cases} \dfrac{\mathrm{d}\phi}{\mathrm{d}N} = \dfrac{\pi}{H} + \mathcal{P}_\phi^{1/2}(k=\epsilon aH)\xi, \\ \dfrac{\mathrm{d}\pi}{\mathrm{d}N} = -3\pi - \dfrac{V'}{H}, \\ \langle\xi(N,\mathbf{x})\xi(N',\mathbf{x}')\rangle = \theta(1-\epsilon aHr)\delta(N-N'). \end{cases} \tag{2.2.35}$$

By considering the field coarse-grained on the superhorizon scale as the classical background, we obtained the additional noise term, which is independent for each Hubble patch ($\propto \theta(1-\epsilon aHr)$) and has a white spectrum ($\propto \delta(N-N')$), and whose amplitude is given by the scalar power spectrum. That is, the stochastic formalism can take account of the Hubble fluctuation into the EoM for the background field as this noise term. Due to this noise, each Hubble patch behaves as a Brownian motion drifted by the potential force.

2.3 Stochastic-δN formalism

So far we have seen the δN formalism and the stochastic formalism. According to the δN formalism, the gauge-invariant curvature perturbations can be obtained as the fluctuations of the elapsed e-foldings due to the scalar field fluctuation. On the other hand, the stochastic formalism reveals that each Hubble patch receives the independent Brownian noise as the Hubble fluctuation. This Hubble noise automatically generates the e-folds fluctuation, and therefore combining it with the δN formalism, the curvature perturbations can be calculated without any perturbative expansion w.r.t. the inflaton fields. We call this formulation *stochastic-δN formalism* and in Refs. [20, 21] we proposed the concrete algorithm to calculate the power spectrum of the curvature perturbation in this formalism.

The key obstacle is that it is quite difficult to solve the Langevin equation (2.2.35) (EoM with noise term) for all spatial points simultaneously. On the other hand the one point dynamics (or one Hubble patch dynamics) can be easily calculated at least numerically since it is nothing but the simple drifted Brownian motion. Of course the information of the correlation function cannot be obtained at this stage, but here let us recall that the original δN formalism also does not require the equations for the perturbation which involve the information of the scale. Instead the corresponding scale is assumed to be given by the horizon scale $k = aH$ at the initial surface. That is, in the δN formalism, the scale is related with the cosmic time N of the initial slice. This concept can be extended to the stochastic-δN formalism.

Let us consider the single-field case for simplicity at first. If one takes the initial condition at some field value ϕ_1, by solving the one Hubble patch dynamics many times, one can obtain the data set of the elapsed e-folding numbers, and of course its mean value, variance, and so on, ($\langle N_1\rangle$, $\langle \delta N_1^2\rangle = \langle N_1^2\rangle - \langle N_1\rangle^2$, $\cdots$). The mean e-folds indicates that the Hubble patch at the initial time is expanded to $\epsilon^{-1}H_{\rm f}^{-1}\mathrm{e}^{\langle N\rangle}$ at the end surface, where $\epsilon^{-1}H_{\rm f}^{-1}$ is the Hubble scale at that time (we include ϵ parameter since the Hubble scale is determined in this way in the stochastic formalism). Therefore the variance $\langle \delta N^2\rangle$ only involves the perturbations whose scales are between them $k_{\rm i} = \epsilon(aH)_{\rm f}\,\mathrm{e}^{-\langle N\rangle} < k < k_{\rm f} = \epsilon(aH)_{\rm f}$ as

$$\langle \delta N^2\rangle = \int_{k_{\rm i}}^{k_{\rm f}} \frac{\mathrm{d}k}{k}\mathcal{P}_{\delta N} \simeq \int_{\log k_{\rm f}-\langle N\rangle}^{\log k_{\rm f}} \mathcal{P}_\zeta \mathrm{d}N. \tag{2.3.1}$$

Inversely the power spectrum of the curvature perturbation can be obtained by differentiating them as

$$\mathcal{P}_\zeta(k) = \frac{\mathrm{d}}{\mathrm{d}\langle N\rangle}\langle \delta N^2\rangle\Big|_{k=k_{\rm f}\mathrm{e}^{-\langle N\rangle}}. \tag{2.3.2}$$

Practically it is calculated by slightly shifting the initial condition to ϕ_2 and then

$$\mathcal{P}_\zeta\left(k = k_\mathrm{f} \mathrm{e}^{-(\langle N_1\rangle + \langle N_2\rangle)/2}\right) \simeq \frac{\langle \delta N_1^2\rangle - \langle \delta N_2^2\rangle}{\langle N_1\rangle - \langle N_2\rangle}. \tag{2.3.3}$$

This is the rough sketch of the algorithm to calculate the power spectrum in the stochastic-δN formalism. Below let us summarize this algorithm in detail.

1. Choose "initial" value ϕ_i for the inflaton field, from which the Langevin equation is solved.[3]

2. By solving the Langevin equations (2.2.35) for one Hubble patch:

$$\begin{cases} \dfrac{\mathrm{d}\phi}{\mathrm{d}N} = \dfrac{\pi}{H} + \mathcal{P}_\phi^{1/2}(k = \epsilon a H)\xi, \\ \dfrac{\mathrm{d}\pi}{\mathrm{d}N} = -3\pi - \dfrac{V'}{H}, \\ \langle \xi(N)\xi(N')\rangle = \delta(N - N'), \end{cases} \tag{2.3.4}$$

   from this "initial" value, one can obtain the elapsed e-folds N to some end uniform density slice. Since the Langevin equations include random noise, this e-folds varies in each calculation. Therefore, by reiterating the calculations, one can have a data set of N, or equivalently its statistics like $\langle N\rangle$, $\langle \delta N^2\rangle = \langle N^2\rangle - \langle N\rangle^2$, and so on.

3. Then repeat the above procedure with different "initial" values, and it gives other data sets, $\langle N\rangle$ and $\langle \delta N^2\rangle$. With sufficient iteration, the variance $\langle \delta N^2\rangle$ can be written as a function of $\langle N\rangle$.

4. Finally, differentiating the variance w.r.t. the mean e-folds, one can obtain the power spectrum of the curvature perturbation.

$$\mathcal{P}_\zeta = \frac{\mathrm{d}}{\mathrm{d}\langle N\rangle}\langle \delta N^2\rangle . \tag{2.3.5}$$

   The scale of the perturbations is related with the mean e-folds by

$$k = k_\mathrm{f} \mathrm{e}^{-\langle N\rangle}, \tag{2.3.6}$$

   where k_f is the horizon scale on the end surface.

This procedure is enough to obtain the power spectrum in the single-field case, but one should be careful when this algorithm is extended to the multi-field case. That is because in the multi-field case neither $\langle N\rangle$ nor $\langle \delta N^2\rangle$ has the one-to-one correspondence with the initial field value. It means that $\langle \delta N^2\rangle$ is not a single-valued function w.r.t. $\langle N\rangle$. To avoid this problem, each initial field value should be properly weighted. It can be achieved by making sample paths so that they reproduce the Hubble patch dynamics in our observable universe because what we observe practically is the fluctuation amplitude averaged over the observable universe. The concrete algorithm as follows.

[3] Note that this "initial" value is set artificially to obtain the correspondence between $\langle N\rangle$ and $\langle \delta N^2\rangle$ and does not mean the true initial condition of inflation.

i. Set the initial condition so that the mean e-folds from this point is around 60 e-folds. This field value represents that of our observable universe around 60 e-folds before the end of inflation (note that at that time the observable universe is within one Hubble patch).[4]

ii. Solve the Langevin equations for multi-inflatons:

$$\begin{cases} \dfrac{\mathrm{d}\phi^I}{\mathrm{d}N} = \dfrac{\pi^I}{H} + \mathcal{P}_{\phi^I}^{1/2}(k=\epsilon aH)\xi^I, \\ \dfrac{\mathrm{d}\pi^I}{\mathrm{d}N} = -3\pi^I - \dfrac{V_I}{H}, \\ \langle \xi^I(N)\xi^J(N')\rangle = \delta^{IJ}\delta(N-N'), \end{cases} \tag{2.3.7}$$

from this initial condition many times, and then obtained solutions are called as sample paths. Here the superscripts I and J stands for the flavors of inflatons and $V_I = \partial V/\partial\phi^I$. They represent the dynamics of the Hubble patches in our universe.

iii. Take the "initial" field value on these sample paths and proceed the algorithm 1–4. The true variance or power spectrum is given by those averaged over these sample paths:

$$\overline{\mathcal{P}}_\zeta = \frac{\mathrm{d}}{\mathrm{d}\langle N\rangle}\overline{\langle \delta N^2\rangle}, \tag{2.3.8}$$

where overlines stand for the average over the sample paths. It is properly weighted as the observable in our universe.

In Chapter 6, we apply this algorithm to hybrid inflation and calculate the power spectrum around its critical point where the perturbative expansion w.r.t. inflaton fields is broken down.

2.3.1 Analytic expression

After our proposal of the stochastic-δN formalism, several authors [30–32] proceeded the analytic studies for this algorithm. Particularly Vennin and Starobinsky [30] found the recursive partial differential equation (2.3.31) which the nth moment of the backward e-folds should satisfy. Therefore, if one can solve this partial differential equation, all information of the curvature perturbation can be obtained beyond the perturbative expansion technique. Let us review them in this subsection.

In the slow-roll limit ($\mathrm{d}\pi^I/\mathrm{d}N = 0$ and $\mathcal{P}_{\phi^I} = (H/2\pi)^2$), the Langevin equation (2.3.7) reads

$$\frac{\mathrm{d}\phi^I}{\mathrm{d}N} = -\frac{V_I}{3H^2} + \frac{H}{2\pi}\xi^I, \tag{2.3.9}$$

[4] Of course we do not know the true initial condition of our universe, and generally the resultant power spectrum depends on this initial condition. However it is not the problem only for our formalism, but common in the multi-field case. In general, the predictability of the inflationary models gets lost if the inflaton trajectory does not converge well at least at the horizon exit of our universe.

which is mathematically written as

$$\mathrm{d}\phi^I = -\frac{V_I}{3H^2}\mathrm{d}N + \frac{H}{2\pi}\mathrm{d}W^I, \tag{2.3.10}$$

where W^I is the independent Brownian motion. The Hubble parameter is given by the slow-roll Friedmann equation:

$$3M_{\rm Pl}^2 H^2 = V. \tag{2.3.11}$$

Below we consider the first passage time from some initial point ϕ_* to some end surface. For the hilltop type models, the initial point is inside the end surface around the end of inflation and therefore the considered field space region Ω is compact. On the other hand, for the chaotic type models, the initial point is outside the end surface. So we set another boundary $\partial\Omega^+$ so that this and the end surface $\partial\Omega^-$ enclose the initial point just for mathematical reasons. In this case we consider the first passage time to $\partial\Omega^+$ or $\partial\Omega^-$. Practically $\partial\Omega^+$ is taken to infinity.

Let us consider some function of ϕ, $f(\phi)$. According to the Ito-Doeblin formula (see e.g. the textbook [33]), the differential form of f is not given by the simple chain rule but written as

$$\mathrm{d}f(\phi) = f_I \mathrm{d}\phi^I + \frac{1}{2} f_{IJ}\mathrm{d}\phi^I \mathrm{d}\phi^J. \tag{2.3.12}$$

Also the differential of the Brownian motion shows following properties:

$$\mathrm{d}W^I(N)\mathrm{d}W^J(N) = \delta^{IJ}\mathrm{d}N, \qquad \mathrm{d}N\mathrm{d}N = \mathrm{d}N\mathrm{d}W^I(N) = 0. \tag{2.3.13}$$

Substituting these properties into Eq. (2.3.12), one obtains,

$$\mathrm{d}f(\phi) = \left(-f_I \frac{v_I}{v} M_{\rm Pl}^2 + f_{II} v M_{\rm Pl}^2\right)\mathrm{d}N + f_I\sqrt{2v}M_{\rm Pl}\mathrm{d}W^I. \tag{2.3.14}$$

Here we used the useful dimensionless potential:

$$v = \frac{V}{24\pi^2 M_{\rm Pl}^4} = \frac{H^2}{8\pi^2 M_{\rm Pl}^2}. \tag{2.3.15}$$

Integrating it from ϕ_* at $N = 0$ until it reaches the boundary $\partial\Omega^+$ or $\partial\Omega^-$ for the first time with the first passage time $\mathcal{N}$, one obtains

$$f(\partial\Omega^+ \text{ or } \partial\Omega^-) - f(\phi_*) = \int_0^{\mathcal{N}} f_I\sqrt{2v}M_{\rm Pl}\mathrm{d}W^I + \int_0^{\mathcal{N}} \left[f_{II} v M_{\rm Pl}^2 - f_I \frac{v_I}{v} M_{\rm Pl}^2\right]\mathrm{d}N. \tag{2.3.16}$$

Note that the first passage time $\mathcal{N}$ itself is a random variable due to the Hubble noise. Regarding the first term in the righthand side, let us define the following function:

$$I(N) = \int_0^N f_I\sqrt{2v}M_{\rm Pl}\mathrm{d}W^I \tag{2.3.17}$$

Here N is not a random variable but an ordinary time variable. This function is martingale since it is known that any integral of a stochastic process w.r.t. a Brownian motion called *Ito integral* is martingale. That is, its expectation value is given by its initial value.

$$\langle I(N)\rangle = I(0) = 0. \tag{2.3.18}$$

Then we define $\tilde{I}(N)$ as $I(N)$ stopped at the boundary $\partial\Omega^+$ or $\partial\Omega^-$ after its first reach:

$$\tilde{I}(N) = \begin{cases} I(N), & N < \mathcal{N}, \\ I(\mathcal{N}), & N \geq \mathcal{N}. \end{cases} \tag{2.3.19}$$

Therefore the first term in the righthand side of Eq. (2.3.16) is given by $\lim_{N\to\infty} \tilde{I}(N)$. Here according to the optional sampling theorem, it is known that any stopped martingale is also martingale. Thus the expectation value of this term is actually zero.

Now these facts lead an interesting relation. If one imposes the following differential equation on f,

$$f_{II}v - f_I\frac{v_I}{v} = -\frac{1}{M_{\rm Pl}^2}, \tag{2.3.20}$$

with the boundary condition $f(\partial\Omega^+) = f(\partial\Omega^-) = 0$, Eq. (2.3.16) reads

$$\mathcal{N} = f(\phi^*) + \int_0^{\mathcal{N}} f_I\sqrt{2v}M_{\rm Pl}{\rm d}W^I, \tag{2.3.21}$$

and its expectation value gives

$$f(\phi^*) = \langle\mathcal{N}\rangle\,. \tag{2.3.22}$$

Therefore this function f gives the mean e-folds from ϕ_* to the boundary $\partial\Omega^+$ or $\partial\Omega^-$.

The higher moments can be also obtained in a similar way. The square of Eq. (2.3.21) is

$$\mathcal{N}^2 = f^2(\phi_*) + 2f(\phi_*)\int_0^{\mathcal{N}} f_I\sqrt{2v}M_{\rm Pl}{\rm d}W^I + \left(\int_0^{\mathcal{N}} f_I\sqrt{2v}M_{\rm Pl}{\rm d}W^I\right)^2, \tag{2.3.23}$$

and according to the isometry of the Ito integral:

$$\left\langle\left(\int \Delta_I{\rm d}W^I\right)^2\right\rangle = \left\langle\int \Delta_I\Delta_I{\rm d}N\right\rangle, \tag{2.3.24}$$

its expectation value reads

$$\langle\mathcal{N}^2\rangle = f^2(\phi_*) + \left\langle\int_0^{\mathcal{N}} 2vf_If_IM_{\rm Pl}^2{\rm d}N\right\rangle. \tag{2.3.25}$$

Then, by letting $g(\phi)$ be a function satisfying

$$g_{II}v - g_I\frac{v_I}{v} = -2vf_If_I, \tag{2.3.26}$$

and the boundary condition $g(\partial\Omega^+) = g(\partial\Omega^-) = 0$, one obtains

$$\langle\mathcal{N}^2\rangle = f^2(\phi_*) + g(\phi_*). \tag{2.3.27}$$

Therefore $g(\phi_*)$ is a function giving the variance:

$$g(\phi_*) = \langle\mathcal{N}^2\rangle - \langle\mathcal{N}\rangle^2 = \langle\delta\mathcal{N}^2\rangle\,. \tag{2.3.28}$$

Also, if one defines the function $\tilde{f}(\phi)$ by $\tilde{f}(\phi) = f^2(\phi) + g(\phi)$ so that $\tilde{f}$ gives the quadratic moment $\langle \mathcal{N}^2 \rangle$, this function satisfies the following differential equation.

$$\left(v\partial_I^2 - \frac{v_I}{v}\partial_I \right) \tilde{f} = -2\frac{f}{M_{\rm Pl}^2}. \tag{2.3.29}$$

Similarly the function f_n giving the nth moment $\langle \mathcal{N}^n \rangle$:

$$f_n(\phi_*) = \langle \mathcal{N}^n \rangle (\phi_*), \tag{2.3.30}$$

can be obtained by solving the following recursive partial differential equation

$$\left(v\partial_I^2 - \frac{v_I}{v}\partial_I \right) f_n = -n\frac{f_{n-1}}{M_{\rm Pl}^2}, \tag{2.3.31}$$

with $f_0 = 1$ and the boundary condition $f_n(\partial\Omega^+) = f_n(\partial\Omega^-) = 0$. Unfortunately it is difficult to solve partial differential equations generally, but several authors keep tackling this equation [31, 32].

Single-field case

In the single-field case, the problem reduces to ordinary differential equations and can be solved formally. First, taking the boundary $\partial\Omega^- = \phi_1$ and $\partial\Omega^+ = \phi_2$, the solution for f (2.3.20) is

$$\langle \mathcal{N} \rangle = f(\varphi) = \int_{\phi_1}^{\varphi} \frac{\mathrm{d}x}{M_{\rm Pl}} \int_x^{\bar{\phi}(\phi_1,\phi_2)} \frac{\mathrm{d}y}{M_{\rm Pl}} \frac{1}{v(y)} \exp\left[\frac{1}{v(y)} - \frac{1}{v(x)} \right], \tag{2.3.32}$$

where $\bar{\phi}$ is an integration constant set to satisfy the boundary condition $f(\phi_2) = 0$. There is no generic expression for it, but since the integrand is positive, for $f(\phi_2)$ to be zero x has to be able to be larger than $\bar{\phi}$ so that y-integral gives negative contributions. It means $\bar{\phi}$ must lie between ϕ_1 and ϕ_2.

Let us evaluate this $\langle \mathcal{N} \rangle$ with several assumptions. First we take ϕ_2 so that the potential is monotonic between ϕ_1 and ϕ_2. Also φ is assumed to be sufficiently near to ϕ_1 so that $V(\phi_1) < V(\varphi) < V(\bar{\phi}) < V(\phi_2)$. Therefore the maximal contribution to the y-integral comes from $y \sim x$.Then Taylor expanding $1/v$ at first order around x, $1/v(y) \simeq 1/v(x) - v'(x)/v^2(x)(y-x)$, one obtains, after integrating by parts,

$$\int_x^{\bar{\phi}} \frac{\mathrm{d}y}{v(y)} \exp\left(\frac{1}{v(y)} \right) \simeq \frac{v(x)}{v'(x)} \exp\left(\frac{1}{v(x)} \right). \tag{2.3.33}$$

Plugging back this expression into Eq. (2.3.32), one finally obtains

$$\langle \mathcal{N} \rangle = f(\varphi) \simeq \int_{\phi_1}^{\varphi} \frac{\mathrm{d}x}{M_{\rm Pl}^2} \frac{v(x)}{v'(x)}. \tag{2.3.34}$$

It is nothing but the classical result (2.1.28) without the stochastic effect. Therefore the classical trajectory appears as a saddle-point limit of the mean stochastic trajectory.

This calculation also allows us to identify the conditions under which the classical limit is recovered. A priori, the Taylor expansion of $1/v$ can be trustable as long as the difference

between $1/v(x)$ and $1/v(y)$ is not too large, say $|1/v(y) - 1/v(x)| < \alpha$, where α is some small number. If one uses the Taylor expansion of at the first order, this means that $|y - x| < \alpha v^2/v'$. Requiring that the second order term of the Taylor expansion is sufficiently small at the boundary of this domain not sensitively to α, one obtains the condition $|2v - v''v^2/v'^2| \ll 1$. Therefore one can define the classicality criterion

$$\eta_{\rm cl} = \left| 2v - \frac{v''v^2}{v'^2} \right|. \tag{2.3.35}$$

When this quantity is small enough, the stochastic effect will be negligible. In this case, the next order correction for the mean e-folds can be written as

$$\langle \mathcal{N} \rangle |_{\eta_{\rm cl} \ll 1} \simeq \int_{\phi_1}^{\varphi} \frac{{\rm d}x}{M_{\rm Pl}^2} \frac{v(x)}{v'(x)} \left[1 + v(x) - \frac{v''(x)v^2(x)}{v'^2(x)} + \cdots \right]. \tag{2.3.36}$$

The variance is also solvable. The formal solution of Eq. (2.3.26) is given by

$$\langle \delta\mathcal{N}^2 \rangle = g(\varphi) = 2 \int_{\phi_1}^{\varphi} {\rm d}x \int_{x}^{\bar{\phi}_2(\phi_1,\phi_2)} {\rm d}y f'^2(y) \exp\left[\frac{1}{v(y)} - \frac{1}{v(x)} \right], \tag{2.3.37}$$

where $\bar{\phi}_2(\phi_1, \phi_2)$ is an integration constant set to satisfy the boundary condition $g(\phi_2) = 0$. From Eq. (2.3.2), the power spectrum is given by

$$\begin{aligned} \mathcal{P}_\zeta(\varphi) = \frac{g'(\varphi)}{f'(\varphi)} =& 2 \left\{ \int_{\varphi}^{\bar{\phi}} \frac{{\rm d}x}{M_{\rm Pl}} \frac{1}{v(x)} \exp\left[\frac{1}{v(x)} - \frac{1}{v(\varphi)} \right] \right\}^{-1} \\ & \times \int_{\varphi}^{\bar{\phi}_2} \frac{{\rm d}x}{M_{\rm Pl}} \left\{ \int_{x}^{\bar{\phi}} \frac{{\rm d}y}{M_{\rm Pl}} \frac{1}{v(y)} \exp\left[\frac{1}{v(y)} - \frac{1}{v(x)} \right] \right\}^2 \exp\left[\frac{1}{v(x)} - \frac{1}{v(\varphi)} \right]. \end{aligned} \tag{2.3.38}$$

Also the spectral index can be given, with use of $\partial/\partial \log(k) \simeq -\partial\phi/\partial \langle \mathcal{N} \rangle \times \partial/\partial\phi$ at the leading order, by

$$n_{\rm s} - 1 = -\frac{g''}{f'g'} + \frac{f''}{f'^2}. \tag{2.3.39}$$

Let us consider the classical limit of the power spectrum, too. Similarly to $\langle \mathcal{N} \rangle$, with use of a saddle-point approximation to Eq. (2.3.37), one can obtain

$$\langle \delta\mathcal{N}^2 \rangle = g(\varphi) \simeq \frac{2}{M_{\rm Pl}^4} \int_{\phi_1}^{\varphi} {\rm d}x \frac{v^4(x)}{v'^3(x)}. \tag{2.3.40}$$

Then, by using this and Eq. (2.3.34), the classical result can be recovered as

$$\mathcal{P}_\zeta(\varphi) = \frac{g'(\varphi)}{f'(\varphi)} \simeq \frac{2}{M_{\rm Pl}^2} \frac{v^3(\varphi)}{v'^2(\varphi)} = \mathcal{P}_\zeta|_{\rm cl}(\varphi). \tag{2.3.41}$$

The next order correction is given by

$$\mathcal{P}_\zeta|_{\eta_{\rm cl} \ll 1}(\varphi) \simeq \mathcal{P}_\zeta|_{\rm cl}(\varphi) \left[1 + 5v(\varphi) - 4\frac{v^2(\varphi)v''(\varphi)}{v'^2(\varphi)} + \cdots \right]. \tag{2.3.42}$$

These reproductions of the classical results are not so surprising. In the classicality criterion, $v \ll 1$ is naturally satisfied. The second term comes from the classical power spectrum times the slow-roll parameter $\eta_V = M_{\rm Pl}^2 v''/v$. Therefore the classical condition can be interpreted as the condition that the slow-roll approximation is good and the classical power spectrum is not large. It is known that the non-Gaussianity of the curvature perturbations is suppressed by the slow-roll parameters in the single-field case, and therefore, if the leading order power spectrum is small enough, the non-perturbative corrections due to the stochastic effect can be thought to be small.

Chapter 3

Squeezed Bispectrum

As the lowest order observables beyond the linear perturbation, the three point function or its Fourier mode bispectrum *is an important indicator of the physics of the early universe. Particularly, its squeezed limit, where one scale is much larger than the other two scales, corresponds with the soft particle exchange, and its non-zero value will indicate the existence of the extra d.o.f. during inflation. However the previous perturbative approach to bispectrum can calculate the squeezed limit only where the hierarchy of the scales is not so large. Also it has been suggested recently that the squeezed bispectrum includes the non-physical mode. In this chapter, we go beyond the small hierarchy limit and suggest the interpretation of such a non-physical mode in the δN formalism. In this chapter, we adopt the Planck unit $M_{Pl} = 1$ and this chapter is based on Ref. [34].*

3.1 Standard approach

In this chapter, we consider the canonical multi-field action:

$$S = \int \mathrm{d}^4x \left[\frac{1}{2}R - \frac{1}{2}g^{\mu\nu}\delta_{IJ}\partial_\mu\phi^I\partial_\nu\phi^J - V(\phi)\right]. \tag{3.1.1}$$

If the field space metric is sufficiently flat, it can be reduced to this trivial case by the field redefinition. Along the slow-roll attractors, the fields evolve according to the slow-roll EoM (2.1.27):

$$\frac{\mathrm{d}\phi^I}{\mathrm{d}N} = -\frac{V_I}{V}. \tag{3.1.2}$$

As mentioned previously, in the δN formalism, the superhorizon curvature perturbations are given by the spatial differences in the number of e-folds realized between an initial flat hypersurface and a final uniform density slice. Such fluctuations of the e-folding number δN are usually approximated by a perturbative expansion around the background field

values as

$$\zeta(\mathbf{x}) = \delta N(\mathbf{x}) = N_I(\bar{\phi}_*)\delta\phi^I(\mathbf{x}) + \frac{1}{2}N_{IJ}(\bar{\phi}_*)\delta\phi^I(\mathbf{x})\delta\phi^J(\mathbf{x}) + \cdots . \tag{3.1.3}$$

In this expression, $N(\bar{\phi}_*)$ denotes the backward e-foldings realized from the initial field value $\bar{\phi}_*$ and until a given final uniform density slice is reached, and $N_I = \partial N/\partial\bar{\phi}_*^I$ and $N_{IJ} = \partial^2 N/(\partial\bar{\phi}_*^I\partial\bar{\phi}_*^J)$ are its derivatives w.r.t. the field values $\bar{\phi}_*$. From here, at the leading order of the perturbation $\delta\phi$, the power spectrum of the curvature perturbations is given by, as seen previously in Sec. 2.1.1,

$$\mathcal{P}_\zeta(k) = N_I N_J \delta^{IJ}\mathcal{P}_\phi, \tag{3.1.4}$$

where we assume that the power spectrum of each scalar is equally given by $\mathcal{P}_\phi = (H/(2\pi))^2$.

A similar expression can be obtained for the bispectrum of the curvature perturbations. Let us define the bispectrum by

$$\langle\zeta_{\mathbf{k}_1}\zeta_{\mathbf{k}_2}\zeta_{\mathbf{k}_3}\rangle = (2\pi)^3\delta^{(3)}(\mathbf{k}_1+\mathbf{k}_2+\mathbf{k}_3)B_\zeta(k_1,k_2,k_3). \tag{3.1.5}$$

Then the lowest order expression for the bispectrum is given by

$$B_\zeta(k_1,k_2,k_3) = N_I N_J N_K B_{\phi^I\phi^J\phi^K}(k_1,k_2,k_3) + \left[N_I N_J N_{IJ}P_\phi(k_1)P_\phi(k_2) + 2\text{ perms.}\right], \tag{3.1.6}$$

where $P_\phi(k) = \frac{2\pi^2}{k^3}\mathcal{P}_\phi(k)$ is the dimensionful scalar power spectrum. In this expression, the first term comes from the NG of the scalar field fluctuations themselves and is called *intrinsic NG*, while the second term is due to the higher order expansion in δN which is called δN *component* of the bispectrum. It is useful to use the dimensionless non-linearity parameter defined by

$$\frac{3}{5}f_{\rm NL}(k_1,k_2,k_3) = \frac{B_\zeta(k_1,k_2,k_3)}{2\left[P_\zeta(k_1)P_\zeta(k_2)+P_\zeta(k_2)P_\zeta(k_3)+P_\zeta(k_3)P_\zeta(k_1)\right]}, \tag{3.1.7}$$

instead of the bispectrum itself for a clear expression. In the squeezed limit like $k_{\rm L} = k_1 \ll k_2 \simeq k_3 = k_{\rm S}$, it can be found that the term $P_\zeta(k_2)P_\zeta(k_3)$ is sub-dominant in the denominator if ζ has an almost scale-invariant power spectrum $P_\zeta(k) \sim k^{-3}$. Therefore the squeezed one can be given by

$$\frac{3}{5}f_{\rm NL}(k_{\rm L},k_{\rm S}) = \frac{B_\zeta(k_{\rm L},k_{\rm S},k_{\rm S})}{4P_\zeta(k_{\rm L})P_\zeta(k_{\rm S})}. \tag{3.1.8}$$

Parametrizing the intrinsic NG as

$$B_{\phi^I\phi^J\phi^K} = \frac{(2\pi^2\mathcal{P}_\phi)^2}{(k_1k_2k_3)^3}\mathcal{A}^{IJK}(k_1,k_2,k_3), \tag{3.1.9}$$

the non-linearity parameters corresponding to the intrinsic and δN components are respectively given by

$$\frac{3}{5}f_{\rm NL}^{\rm int} = \frac{\mathcal{A}^{IJK}(k_1,k_2,k_3)N_IN_JN_K}{2(N_LN_L)^2(k_1^3+k_2^3+k_3^3)}, \qquad \frac{3}{5}f_{\rm NL}^{\delta N} = \frac{N_IN_JN_{IJ}}{2(N_KN_K)^2}, \tag{3.1.10}$$

where $f_{\rm NL} = f_{\rm NL}^{\rm int} + f_{\rm NL}^{\delta N}$. To obtain the explicit form of $\mathcal{A}^{IJK}$, one has to consider the at least cubic order action. Seery and Lidsey [35] have done such calculations and obtained the following result.

$$\begin{aligned}\mathcal{A}^{IJK}(k_1,k_2,k_3) &= -\sum_{6\text{ perms.}} \frac{\dot\phi^I}{4H}\delta^{JK}\left(3\frac{k_2^2k_3^2}{k_{\rm t}} + \frac{k_2^2k_3^2}{k_{\rm t}}(k_1+2k_3) - \frac{1}{2}k_1^3 + k_1k_2^2\right)\\ &= \sum_{6\text{ perms.}} \frac{V_I}{4V}\delta^{JK}\left(3\frac{k_2^2k_3^2}{k_{\rm t}} + \frac{k_2^2k_3^2}{k_{\rm t}}(k_1+2k_3) - \frac{1}{2}k_1^3 + k_1k_2^2\right). \end{aligned} \tag{3.1.11}$$

In the second line, we used the slow-roll EoM (3.1.2). In the squeezed limit, taking e.g. $k_{\rm L} = k_1 \ll k_2 \simeq k_3 = k_{\rm S}$, this expression boils down to

$$\mathcal{A}^{IJK} = k_{\rm S}^3 \frac{V_I}{V}\delta^{JK}, \tag{3.1.12}$$

and the non-linearity parameter reads

$$\frac{3}{5}f_{\rm NL} = \frac{3}{5}f_{\rm NL}^{\rm int} + \frac{3}{5}f_{\rm NL}^{\delta N} = \frac{N_I\frac{V_I}{V}}{4N_JN_J} + \frac{N_IN_JN_{IJ}}{2(N_KN_K)^2}. \tag{3.1.13}$$

Particularly, in the single-field case, with use of $N_\phi = 1/(\sqrt{2\epsilon_V})$, $V_\phi/V = \sqrt{2\epsilon_V}$, and $N_{\phi\phi} = 1 - \eta_V/(2\epsilon_V)$, one can obtain

$$\frac{3}{5}f_{\rm NL} = \frac{3}{2}\epsilon_V - \frac{1}{2}\eta_V = \frac{1-n_{\rm s}}{4}, \tag{3.1.14}$$

from Eq. (2.1.32). This relation is know as *Maldacena's consistency relation* [36]. For the expressions in this section, one should note that the all quantities are evaluated at the same time, assuming that the horizon crosses of k_1, k_2, and k_3 are sufficiently close. Therefore they are valid only in the near equilateral limit $k_1 \lesssim k_2 \sim k_3$.[1]

3.2 Local observer effect on the squeezed bispectrum

Let us now consider the role of the squeezed bispectrum and the meaning of Maldacena's consistency relation. At first, as a simple ansatz which cause a non-zero squeezed bispectrum, the following local type NG is often used:

$$\zeta(\mathbf{x}) = g(\mathbf{x}) + \frac{3}{5}f_{\rm NL}^{\rm local}(g^2(\mathbf{x}) - \langle g^2\rangle), \tag{3.2.1}$$

where $g(\mathbf{x})$ is a Gaussian field. With this assumption, making use of Wick's theorem, the bispectrum is simply given by

$$B_\zeta(k_1,k_2,k_3) = \frac{6}{5}f_{\rm NL}^{\rm local}[P_\zeta(k_1)P_\zeta(k_2) + P_\zeta(k_2)P_\zeta(k_3) + P_\zeta(k_3)P_\zeta(k_1)], \tag{3.2.2}$$

[1] Note that here, the near-equilateral limit does not refer to the non-linearity parameter in the equilateral configuration $f_{\rm NL}^{\rm equil}$, but to the squeezed non-linearity parameter in the limit where the hierarchy between the two scales $k_{\rm L}$ and $k_{\rm S}$ can be neglected.

at the lowest order. Then in the squeezed limit, if ζ has an almost scale-invariant power spectrum as $P_\zeta(k) \sim k^{-3}$, the second term in the bracket is sub-dominant compared to the other two terms, and therefore

$$B_\zeta(k_\mathrm{L}, k_\mathrm{S}, k_\mathrm{S}) \simeq \frac{12}{5} f_\mathrm{NL}^\mathrm{local} P_\zeta(k_\mathrm{L}) P_\zeta(k_\mathrm{S}), \qquad \text{for } k_\mathrm{L} \ll k_\mathrm{S}. \tag{3.2.3}$$

Then the corresponding non-linearity parameter is nothing but the coefficient $f_\mathrm{NL}^\mathrm{local}$.

This squeezed bispectrum shows that the local-type NG represents a non-vanishing correlation between long and short wavelength fluctuations. This can be understood as follows. Let us consider a long and a short wavelength modes k_L and k_S in a given patch whose size R satisfies $k_\mathrm{L}^{-1} \gg R \gg k_\mathrm{S}^{-1}$. In the local model (3.2.1), one can expand $g(\mathbf{x})$ into a long wavelength part g_L and a short wavelength part $g_\mathrm{S}(\mathbf{x})$, yielding

$$\begin{aligned}\zeta(\mathbf{x}) =& g_\mathrm{L} + \frac{3}{5} f_\mathrm{NL}^\mathrm{local} (g_\mathrm{L}^2 - \langle g^2 \rangle) \\ &+ g_\mathrm{S}(\mathbf{x}) + \frac{3}{5} f_\mathrm{NL}^\mathrm{local} [g_\mathrm{S}^2(\mathbf{x}) + 2 g_\mathrm{L} g_\mathrm{S}(\mathbf{x})].\end{aligned} \tag{3.2.4}$$

Here the $\mathbf{x}$-dependence of g_L is omitted since the long-wavelength mode is almost constant within the considered patch. Therefore its second line terms represent the non-constant short-wavelength mode of ζ, and at linear order in g_S, it reads

$$\zeta_\mathrm{S}(\mathbf{x}) \sim \left(1 + \frac{6}{5} f_\mathrm{NL}^\mathrm{local} g_\mathrm{L}\right) g_\mathrm{S}(\mathbf{x}). \tag{3.2.5}$$

This expression indicates that the local-type NG yields a modulation of the amplitude of the short-wavelength mode by the long-wavelength mode.

Now let us try to similarly interpret the CR:

$$\frac{3}{5} f_\mathrm{NL} = \frac{1 - n_\mathrm{s}}{4}, \tag{3.2.6}$$

as a modulation of the amplitude of the short-wavelength mode due to the long-wavelength mode. Substituting this CR into Eq. (3.2.5) suggests that the CR would cause the modulation of ζ_S as $\zeta_\mathrm{S} \to [1 + (1 - n_\mathrm{s})\zeta_\mathrm{L}/2]\zeta_\mathrm{S}$. Schematically taking $\zeta_\mathrm{S} \sim \sqrt{\mathcal{P}_\zeta(k_\mathrm{S})}$, this modulation reads

$$\Delta\zeta_\mathrm{S} \sim \frac{1 - n_\mathrm{s}}{2} \zeta_\mathrm{L} \zeta_\mathrm{S} \sim -\frac{\mathrm{d}\log\zeta_\mathrm{S}}{\mathrm{d}\log k_\mathrm{S}} \zeta_\mathrm{L} \zeta_\mathrm{S} \sim -\frac{\mathrm{d}\zeta_\mathrm{S}}{\mathrm{d}\log k_\mathrm{S}} \zeta_\mathrm{L}. \tag{3.2.7}$$

Interpreted as the chain rule of differentiation, this expression suggests that the effect of the long-wavelength modulation is the same as a simple scale shift:

$$\log k_\mathrm{S} \to \log k_\mathrm{S} - \zeta_\mathrm{L}. \tag{3.2.8}$$

Indeed, in the uniform density slice, the local scale factor is given by

$$a(t, \mathbf{x}) = a_0(t) \mathrm{e}^{\zeta(t, \mathbf{x})}. \tag{3.2.9}$$

For a fixed comoving wavenumber k, the physical wavenumbers $k_\mathrm{ph} = k/a$ inside and outside the considered patch thus differ by $\Delta \log k_\mathrm{ph} = -\zeta_\mathrm{L}$, which exactly matches the scale

shift (3.2.8). Inversely speaking, if the scales are defined w.r.t. their physical wavenumbers, the correlations between long- and short-wavelengths given by the CR (3.2.6) are thought to vanish.

These are intuitive understanding of the so-called *local observer effect*. For precise discussion, Tanaka and Urakawa [37, 38] pointed out that the squeezed bispectrum given by the CR can be removed by using the additional gauge d.o.f. associated to the finiteness of the observable universe (see also the discussion about the adiabatic perturbation in Sec. 1.1.3). The same conclusion was reached in Ref. [39] by introducing locally homogeneous isotropic coordinates called *conformal Fermi normal coordinates*, denoted by $\overline{\mathrm{FNC}}$. Let us briefly review their argument by considering again a patch of size R satisfying $k_{\mathrm{L}}^{-1} \gg R \gg k_{\mathrm{S}}^{-1}$, at a time when the long-wavelength mode is superhorizon, $k_{\mathrm{L}} \ll aH$, and the short-wavelength mode is subhorizon or of the order of the horizon scale, $k_{\mathrm{S}} \gtrsim aH$. Including only the long-wavelength scalar perturbations, the metric is given, in the uniform density slice, by

$$\mathrm{d}s^2 = -\mathrm{d}t^2 + a^2(t)[1+2\zeta_{\mathrm{L}}(\mathbf{x})]\mathrm{d}\mathbf{x}^2 + \mathcal{O}\left(\frac{k_{\mathrm{L}}^2}{a^2H^2}\right). \tag{3.2.10}$$

The $\overline{\mathrm{FNC}}$ are then defined according to

$$\overline{\mathbf{x}}_{\mathrm{F}} = [1+\zeta_{\mathrm{L}}(\mathbf{x}=0)]\mathbf{x}. \tag{3.2.11}$$

Since the long-wavelength mode is almost constant in the considered patch, the metric can be expanded as

$$\mathrm{d}s^2 = -\mathrm{d}t^2 + a^2(t)\mathrm{d}\overline{\mathbf{x}}_{\mathrm{F}}^2 + \mathcal{O}(k_{\mathrm{L}}^2\overline{x}_{\mathrm{F}}^2) + \mathcal{O}\left(\frac{k_{\mathrm{L}}^2}{a^2H^2}\right), \tag{3.2.12}$$

where $\overline{x}_{\mathrm{F}} \ll k_{\mathrm{L}}^{-1}$ inside the patch. Then the long-wavelength metric perturbation disappears in the $\overline{\mathrm{FNC}}$. Note that this does not mean that the gauge-invariant curvature perturbation ζ vanishes, since it simply transforms as a scalar, $\overline{\zeta}[\overline{\mathbf{x}}_{\mathrm{F}}(\mathbf{x})] = \zeta(\mathbf{x})$. This is why, at linear order, the two-point function of ζ_{S} transforms according to

$$\langle\overline{\zeta}_{\mathrm{S}}(\overline{\mathbf{x}}_{\mathrm{F}})\overline{\zeta}_{\mathrm{S}}(0)\rangle = \langle\zeta_{\mathrm{S}}[\mathbf{x}(\overline{\mathbf{x}}_{\mathrm{F}})]\zeta_{\mathrm{S}}(0)\rangle \simeq \left[1-\zeta_{\mathrm{L}}(0)\overline{x}_{\mathrm{F}i}\frac{\partial}{\partial\overline{x}_{\mathrm{F}i}}\right]\langle\zeta_{\mathrm{S}}(\overline{\mathbf{x}}_{\mathrm{F}})\zeta_{\mathrm{S}}(0)\rangle. \tag{3.2.13}$$

Configurations mostly contributing to the squeezed bispectrum are such that $|\mathbf{x}_1-\mathbf{x}_2| \gg |\mathbf{x}_2-\mathbf{x}_3|$, where only the long-wavelength mode can contribute to $\zeta(\mathbf{x}_1)$. Therefore the squeezed three point function $\langle\zeta(\mathbf{x}_1)\zeta(\mathbf{x}_2)\zeta(\mathbf{x}_3)\rangle$ can be understood as the modulation of the small scale two point correlator under the long-wavelength mode, $\langle\zeta_{\mathrm{L}}(\mathbf{x}_1)\langle\zeta_{\mathrm{S}}(\mathbf{x}_2)\zeta_{\mathrm{S}}(\mathbf{x}_3)\rangle\rangle$. With use of the transformation rule (3.2.13), the squeezed bispectrum then transforms as

$$\begin{aligned} B_{\overline{\zeta}}(k_{\mathrm{L}},k_{\mathrm{S}},k_{\mathrm{S}}) &= B_{\zeta}(k_{\mathrm{L}},k_{\mathrm{S}},k_{\mathrm{S}}) + P_{\zeta}(k_{\mathrm{L}})\partial_{k_{\mathrm{S},i}}[k_{\mathrm{S},i}P_{\zeta}(k_{\mathrm{S}})] \\ &= B_{\zeta}(k_{\mathrm{L}},k_{\mathrm{S}},k_{\mathrm{S}}) + \left[3+\frac{\mathrm{d}\log P_{\zeta}(k_{\mathrm{S}})}{\mathrm{d}\log k_{\mathrm{S}}}\right]P_{\zeta}(k_{\mathrm{L}})P_{\zeta}(k_{\mathrm{S}}), \end{aligned} \tag{3.2.14}$$

where we performed the integration by parts and used the relation $\partial_i(x_i\mathrm{e}^{-i\mathbf{k}\cdot\mathbf{x}}) = \partial_{k_i}(k_i\mathrm{e}^{-i\mathbf{k}\cdot\mathbf{x}})$. The terms inside the brackets of the second line reduce to $n_{\mathrm{s}}(k_{\mathrm{S}})-1$, and therefore, if the original bispectrum is given by the CR (3.2.6), the bispectrum vanishes in the $\overline{\mathrm{FNC}}$ where the scale is normalized in terms of the physical scale.

Here note that, in practice, an apparent bispectrum reappears in concrete observables, such as the CMB angular correlations due to projection effects [39, 40]. These are related with the fact that, since the long-wavelength mode is observed inside our horizon, it affects the mapping of the actual positions of the light sources on the celestial sphere. However, these projection effects can be evaluated separately, once the local bispectrum is calculated in terms of physical scales.

In the following, we present a new approach to the calculation of the squeezed bispectrum in the δN formalism. This allows us to reformulate the difference between the squeezed bispectrum of ζ (*forward formulation*, see Sec. 3.3.1), given by the CR in the single-field case, and the one of $\overline{\zeta}$ (*backward formulation*, see Sec. 3.3.2), which vanishes in single-field inflation.

3.3 New approach

Let us now see how the standard approach can be extended to arbitrary separations between the scales $k_{\rm L}$ and $k_{\rm S}$. As discussed in the previous section, the squeezed bispectrum is related to the correlation between the long-wavelength perturbation and the short-wavelength two point function. We consider the patch of comoving size $k_{\rm L}^{-1}$, where $\zeta_{\rm L}$ is the coarse-grained curvature perturbation on this scale defined through the window function $W_R(x)$. If the power spectrum $\mathcal{P}_\zeta(k_{\rm S})$ is evaluated within this local patch, one has

$$\begin{aligned}\langle\zeta_{\rm L}\mathcal{P}_\zeta(k_{\rm S})\rangle =&\frac{k_{\rm S}^3}{2\pi^2}\int {\rm d}^3x{\rm d}^3y\,{\rm e}^{-i\mathbf{k}_{\rm S}\cdot\mathbf{y}}W_{k_{\rm L}^{-1}}(x)\left\langle\zeta(\mathbf{x})\zeta\left(-\frac{\mathbf{y}}{2}\right)\zeta\left(\frac{\mathbf{y}}{2}\right)\right\rangle\\ =&\frac{k_{\rm S}^3}{2\pi^2}\int {\rm d}^3x{\rm d}^3y\int\frac{{\rm d}^3p{\rm d}^3q}{(2\pi)^6}\exp\left(i\left[\mathbf{p}\cdot\left(\mathbf{x}+\frac{\mathbf{y}}{2}\right)+\mathbf{q}\cdot\mathbf{y}-\mathbf{k}_{\rm S}\cdot\mathbf{y}\right]\right)\\ &\times W_{k_{\rm L}^{-1}}(x)B_\zeta(p,q,|\mathbf{p}+\mathbf{q}|)\\ =&\frac{k_{\rm S}^3}{2\pi^2}\int\frac{{\rm d}^3p{\rm d}^3q}{(2\pi)^3}\delta^{(3)}\left(\frac{\mathbf{p}}{2}+\mathbf{q}-\mathbf{k}_{\rm S}\right)\tilde{W}\left(\frac{p}{k_{\rm L}}\right)B_\zeta(p,q,|\mathbf{p}+\mathbf{q}|).\end{aligned}\tag{3.3.1}$$

In this expression, since the Fourier transform of the window function $\tilde{W}(p/k_{\rm L})$ selects out the modes such that $p\lesssim k_{\rm L}$, the delta function and the bispectrum can be approximated by $\delta^{(3)}(\mathbf{p}/2+\mathbf{q}-\mathbf{k}_{\rm S})\simeq\delta^{(3)}(\mathbf{q}-\mathbf{k}_{\rm S})$ and $B_\zeta(p,q,|\mathbf{p}+\mathbf{q}|)\simeq B_\zeta(p,k_{\rm S},k_{\rm S})$. Therefore one obtains

$$\langle\zeta_{\rm L}\mathcal{P}_\zeta(k_{\rm S})\rangle\simeq\frac{k_{\rm S}^3}{2\pi^2}\int^{\log k_{\rm L}}\frac{p^3}{2\pi^2}B_\zeta(p,k_{\rm S},k_{\rm S}){\rm d}\log p.\tag{3.3.2}$$

The squeezed non-linearity parameter (3.1.8) is then given by

$$\frac{3}{5}f_{\rm NL}(k_{\rm L},k_{\rm S})=\frac{1}{4\mathcal{P}_\zeta(k_{\rm L})\mathcal{P}_\zeta(k_{\rm S})}\frac{{\rm d}\langle\zeta_{\rm L}\mathcal{P}_\zeta(k_{\rm S})\rangle}{{\rm d}\log k_{\rm L}}.\tag{3.3.3}$$

In this expression, since $\zeta_{\rm L}$ includes all fluctuations with wavelengths larger than $k_{\rm L}^{-1}$, evaluating the bispectrum when its first argument is $k_{\rm L}$ requires to differentiate the integral in Eq. (3.3.2) w.r.t. $\log k_{\rm L}$. In the δN formalism, a different method is commonly used, which relies on the introduction of a single-mode impulsive field fluctuation

$$\delta\phi_{\rm L}(\mathbf{x})=\int_{\log p=\log k_{\rm L}}\frac{{\rm d}^3p}{(2\pi)^3}{\rm e}^{i\mathbf{p}\cdot\mathbf{x}}\delta\phi_{\mathbf{p}},\tag{3.3.4}$$

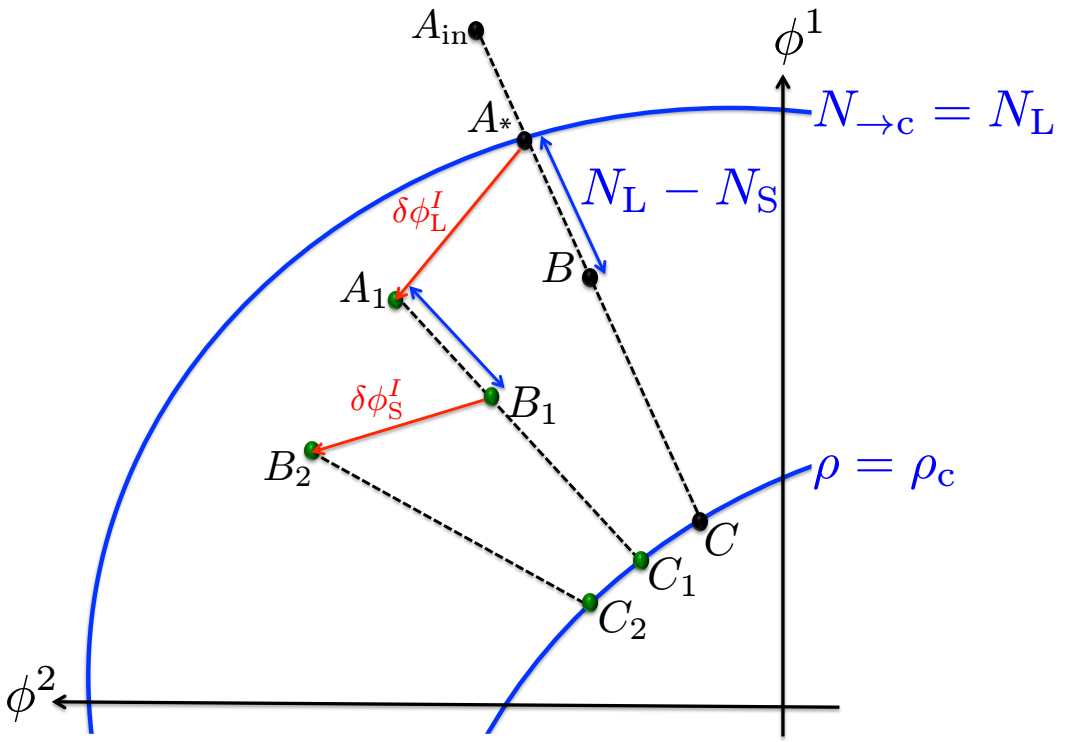

Figure 3.1. Schematic representation of the forward procedure for the calculation of the squeezed bispectrum in the δN formalism, which is also shown in Ref. [34]. In this formulation, the forward e-folds realized between A_1 and B_1 is fixed as $N_{A_1B_1} = N_{\rm L} - N_{\rm S}$.

yielding a single-mode number of e-folds fluctuation

$$\delta N_{\rm L}(\mathbf{x}) = \int_{\log p = \log k_{\rm L}} \frac{{\rm d}^3 p}{(2\pi)^3} {\rm e}^{i\mathbf{p}\cdot\mathbf{x}} \zeta_{\mathbf{p}}. \tag{3.3.5}$$

The correlation $\langle \delta N_{\rm L} \mathcal{P}_\zeta(k_{\rm S}) \rangle$ thus includes only the modes $k_{\rm L}$ and $k_{\rm S}$ and allows one to avoid differentiation w.r.t. $\log k_{\rm L}$,[2]

$$\frac{3}{5} f_{\rm NL}(k_{\rm L}, k_{\rm S}) = \frac{\langle \delta N_{\rm L} \mathcal{P}_\zeta(k_{\rm S}) \rangle}{4 \mathcal{P}_\zeta(k_{\rm L}) \mathcal{P}_\zeta(k_{\rm S})}. \tag{3.3.6}$$

3.3.1 Forward formulation

Now let us discuss how Eq. (3.3.6) can be evaluated in practice in the δN formalism. In Fig. 3.1, we describe how this is done in the forward formulation. The black dotted lines represent slow-roll attractor trajectories, $[A_{\rm in}C]$ being the unperturbed trajectory. The point A_* is where the long-wavelength mode exits the horizon. At this point, the field fluctuations $\delta\phi^I_{\rm L}$ leads to the variation $\delta N_{\rm L} = N(A_1) - N(A_*)$ in the e-folding number, that can be identified with the long-wavelength curvature perturbation $\zeta_{\rm L}$. This fluctuation also shifts the field

[2]This situation corresponds with the replacement of the window function $\tilde{W}$ in Eq. (3.3.1) by a delta function $\delta(\log p - \log k_{\rm L})$.

space trajectory to a different slow-roll solution, $[A_1C_1]$, along which the short-wavelength perturbation emerges at B_1. Since the location of B_1 depends on $\delta\phi^I_{\rm L}$, the long-wavelength curvature perturbation $\zeta_{\rm L}$ and the short-wavelength power spectrum $\mathcal{P}_\zeta(B_1)$ can be correlated as

$$\langle \delta N_{\rm L} \mathcal{P}_\zeta(k_{\rm S})\rangle \simeq N_I(A_*)\left.\frac{\partial \mathcal{P}_\zeta}{\partial \phi^J}\right|_B \langle \delta\phi^I_{\rm L}\delta\tilde{\phi}^J_{\rm L}\rangle\,, \tag{3.3.7}$$

where $\delta\tilde{\phi}^I_{\rm L}$ denotes the evolved value of $\delta\phi^I_{\rm L}$ after $N_{\rm L}-N_{\rm S}$ e-folds, that is, $\delta\tilde{\phi}^I_{\rm L}=\phi^I(B_1)-\phi^I(B)$. At the leading order, it can be expressed as $\delta\tilde{\phi}^I_{\rm L}=\partial\phi^J_B/\partial\phi^K|_*\delta\phi^K_{\rm L}$ where $\partial\phi^J_B/\partial\phi^K|_*$ encodes the variation of the coordinates of B due to the field fluctuations $\delta\phi_{\rm L}$ at A_*.Then, with use of the field fluctuations power spectrum $\langle\delta\phi^I_{\rm L}\delta\phi^J_{\rm L}\rangle=\delta^{IJ}\mathcal{P}_\phi$, one obtains

$$\frac{3}{5}f_{\rm NL}=\frac{\langle\delta N_{\rm L}\mathcal{P}(k_{\rm S})\rangle}{4\mathcal{P}_\zeta|_*\mathcal{P}_\zeta|_B}=\frac{N_I|_*\left.\frac{\partial\mathcal{P}_\zeta}{\partial\phi^J}\right|_B\left.\frac{\partial\phi^J_B}{\partial\phi^I}\right|_*\mathcal{P}_\phi|_*}{4\mathcal{P}_\zeta|_*\mathcal{P}_\zeta|_B}. \tag{3.3.8}$$

In order to calculate the power spectrum at small scales, one should add an impulsive field fluctuation $\delta\phi^I_{\rm S}$ on B_1 and then the difference in the e-foldings $\delta N_{\rm S}=N(B_1)-N(B_2)$ yields the small-scale power spectrum. Let us also note that, in this framework, the *forward*[3] e-folding number $N_{\rm L}-N_{\rm S}$ is used to determine the location of the point B_1 where the small-scale fluctuations emerge, hence the name of the formulation. Actually one can check that this formulation is consistent with those by the recent works [41–43].

This indeed seems natural in the context of the δN formalism since it implies that, if large-scale fluctuations $\delta\phi^I_{\rm L}$ are defined on a spatially flat slice, evolving this hypersurface by a uniform $N_{\rm L}-N_{\rm S}$ e-folds conserves its flatness. This is why in the forward formulation, scales can be uniformly defined in comoving coordinates, which however doe not imply that they lead to the same physical scales on the uniform density slice. If one would like to use the physical scales on the uniform density slice, the backward formulation which will be discussed in Sec. 3.3.2 should be derived.

single-field case

Before moving to the backward formulation, now let us show that the CR can properly be recovered in single-field inflation. In this case, the background field value ϕ and the backward e-folding number N have a one-to-one correspondence which is why one can label field space with N instead of ϕ. Here note that the fluctuation δN does not depend on the time of the initial flat slice which can be seen by Eq. (2.1.17) and $\psi(t_{\rm i},\mathbf{x})=0$. Therefore it can be evaluated at any time after the horizon exit of the considered perturbations and the relation $\delta N_{\rm L}=N_\phi(A_*)\delta\phi_{\rm L}=N_\phi(B)\delta\tilde{\phi}_{\rm L}$ is satisfied. With use of this relation, Eq. (3.3.7) then gives rise to

$$\langle\delta N_{\rm L}\mathcal{P}_\zeta(k_{\rm S})\rangle\simeq\left.\frac{\partial\mathcal{P}_\zeta}{\partial N}\right|_B\langle\delta N^2_{\rm L}\rangle\,. \tag{3.3.9}$$

[3]Note that, to calculate δN itself, the backward e-foldings is employed, but the forward e-folding number is used when relating a perturbation scale with the location in the field space where it exits the horizon.

In this expression, $\langle \delta N_{\rm L}^2 \rangle$ should be interpreted as $\mathcal{P}_\zeta(k_{\rm L})$ (see Eq. (3.3.5) and footnote 2), and the derivative of the power spectrum w.r.t. N reads the spectral index as

$$\left.\frac{\partial \mathcal{P}_\zeta}{\partial N}\right|_B = -\mathcal{P}_\zeta \left.\frac{\partial \log \mathcal{P}_\zeta}{\partial \log k}\right|_B = (1-n_{\rm S})\mathcal{P}_\zeta|_B. \tag{3.3.10}$$

Therefore the non-linearity parameter (3.3.6) indeed leads the CR:

$$\frac{3}{5} f_{\rm NL}(k_{\rm L}, k_{\rm S}) = \frac{1-n_{\rm S}(k_{\rm S})}{4}. \tag{3.3.11}$$

Near-equilateral limit

The result of the standard approach (3.1.13) can be also reproduced in the near-equilateral limit $N_{\rm S} \to N_{\rm L}$. In this regime indeed, $B \to A_*$ and Eq. (3.3.8) directly gives rise to the standard result. However note that, in the alternative approach presented here, there is no need to calculate $f_{\rm NL}^{\rm int}$ separately from the cubic action and that this term is already incorporated in the δN formalism. The interpretation of the two contributions $f_{\rm NL}^{\rm int}$ and $f_{\rm NL}^{\delta N}$ also become clearer. Since $\mathcal{P}_\zeta = N_I N_I \mathcal{P}_\phi$, the derivatives of the power spectrum w.r.t. the field values appearing in Eq. (3.3.7) contain two terms: one proportional to the derivative of N_I which yields $f_{\rm NL}^{\delta N}$, and the other one proportional to the derivative of $\mathcal{P}_\phi$ which yields $f_{\rm NL}^{\rm int}$. Therefore the so-called *intrinsic NG* is nothing but the effect of the field dependence of the amplitude of the field fluctuations.

Non-canonical kinetic term case

Finally let us briefly see how the forward formulation can be extended to the case of the non-canonical kinetic terms. We consider the single-field k-inflation [44], whose action is written as

$$S = \int \mathrm{d}^4x\sqrt{-g}\left[\frac{1}{2}R + P(X,\phi)\right], \tag{3.3.12}$$

where $X = -g^{\mu\nu}\partial_\mu\phi\partial_\nu\phi/2$. Here we assume that the system has reached the phase-space attractor, along which the scalar field ϕ is not necessarily slowly rolling in k-inflation. In Refs. [45, 46], the δN and intrinsic components of the non-linearity parameter are calculated as

$$\frac{3}{5} f_{\rm NL}^{\delta N} = \frac{1}{2}(\epsilon_H + \delta), \qquad \frac{3}{5} f_{\rm NL}^{\rm int} = \frac{1}{4}(\eta + s - 2\delta), \tag{3.3.13}$$

where $\eta = \dot{\epsilon}_H/(H\epsilon_H)$, $s = \dot{c}_{\rm S}/(Hc_{\rm S})$, and $\delta = \ddot{\phi}/(H\dot{\phi})$. The sound speed $c_{\rm S}$ is given by $c_{\rm S}^{-2} = 1 + 2XP_{XX}/P_X$, where $P_X = \partial P(X,\phi)/\partial X$ and $P_{XX} = \partial^2 P(X,\phi)/\partial X^2$. By summing up these two components, one obtains the CR as

$$\frac{3}{5} f_{\rm NL} = \frac{3}{5} f_{\rm NL}^{\delta N} + \frac{3}{5} f_{\rm NL}^{\rm int} = \frac{1}{4}(2\epsilon_H + \eta + s) = \frac{1-n_{\rm S}}{4}. \tag{3.3.14}$$

These formulae can be recovered as follows. The δN component of the non-linearity parameter is simply given by the $N_{\phi\phi}$ term with use of $N_\phi = -H/\dot{\phi}$. The intrinsic component is

related with the field derivative of $\mathcal{P}_\phi$, which in the near-equilateral limit $N_S \to N_L$ is given by

$$\frac{3}{5} f_{NL}^{int} = \frac{N_\phi N_{\phi}^2 \partial_\phi(\mathcal{P}_\phi)\mathcal{P}_\phi}{4\mathcal{P}_\zeta^2} = \frac{\partial_\phi \log \mathcal{P}_\phi}{4N_\phi}. \tag{3.3.15}$$

In k-inflation, the power spectrum of $\delta\phi$ reads [47]

$$\mathcal{P}_\phi = \frac{\dot\phi^2}{H^2}\mathcal{P}_\zeta = \frac{\dot\phi^2}{H^2}\frac{1}{2\epsilon_H c_s}\left(\frac{H}{2\pi}\right)^2 = \frac{1}{8\pi^2}\frac{\dot\phi^2}{\epsilon_H c_s}. \tag{3.3.16}$$

Therefore one obtains

$$\partial_\phi \log \mathcal{P}_\phi = N_\phi(\eta - 2\delta + s), \tag{3.3.17}$$

and Eq. (3.3.13) is recovered. In fact, the result (3.3.14) should not come as a surprise since, when dealing with the single-field case in Eqs. (3.3.9)–(3.3.11), no assumption was made regarding $\mathcal{P}_\phi$ and the CR was therefore also valid in the case of the non-canonical kinetic terms.

3.3.2 Backward formulation

The forward formulation developed in Sec. 3.3.1 gives the bispectrum B_ζ in terms of comoving scales. Let us now derive the bispectrum $B_{\tilde\zeta}$ in terms of the physical scales that would be seen by a local observer. The idea is to define all perturbation scales using the *backward* e-foldings realized until the final uniform density slice is reached. This procedure is thus called *backward formulation* and is summarized in Fig. 3.2. Since the physical horizon scale H on the final uniform density slice is constant, the horizon crossing physical scale k_c^{phys} is constant on this hypersurface as well, which implies that the physical scales $k_L^{phys} = e^{-N_L} k_c^{phys}$ and $k_S^{phys} = e^{-N_S} k_c^{phys}$ are also unperturbed quantities on the final uniform density slice.

From Figs. 3.1 and 3.2, one can see that the only difference between the forward and backward formulations is the definition of the point B. Therefore the formal expression of f_{NL} (3.3.8) still applies here. Before explaining how it can be evaluated in general, let us see how it compares with the forward formulation in the single-field case and in the near-equilateral limit respectively.

Single-field case

In single-field inflation, one can readily see that the backward formulation always yields a vanishing squeezed bispectrum. In this case, the hypersurfaces of constant backward e-foldings (the blue lines in Fig. 3.2) are single points, and the point B_1 always coincides with B irrespectively of the long-wavelength perturbation $\delta\phi_L$. There is therefore no correlation between the long-wavelength perturbation at A_* and the power spectrum at B_1, and then the squeezed bispectrum vanishes. In this picture, the fact that the squeezed non-linearity parameter vanishes in single-field inflation has a clear geometrical interpretation in the field space.

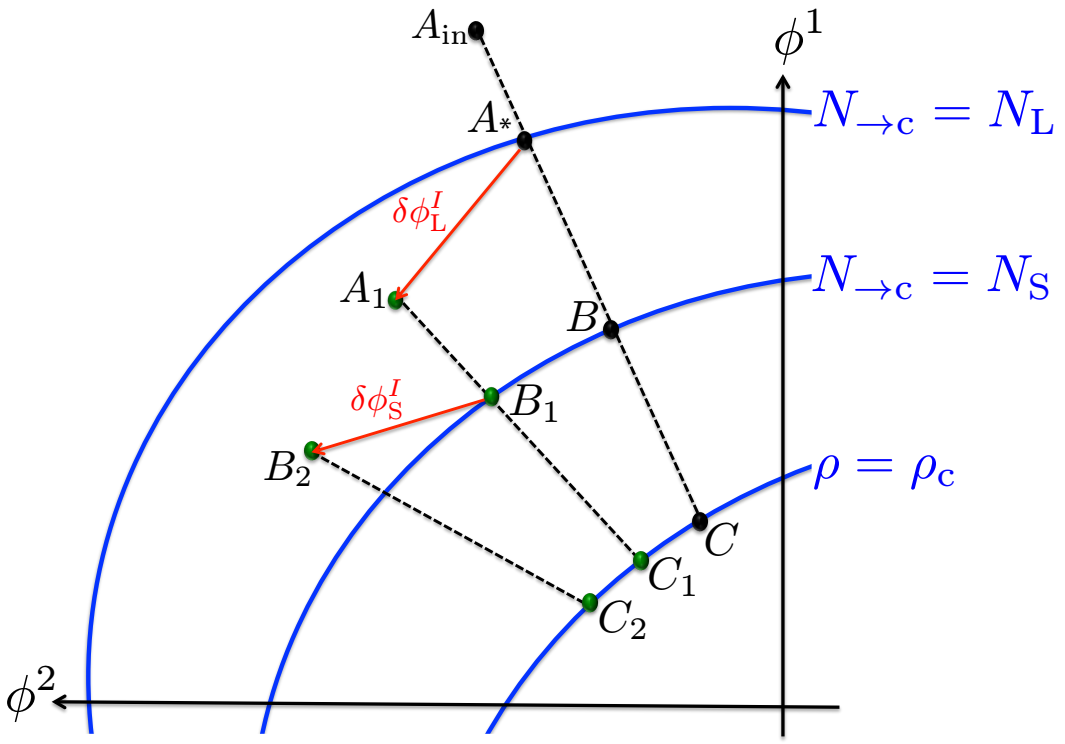

Figure 3.2. Schematic representation of the backward procedure for the calculation of the squeezed bispectrum in the δN formalism, which is also shown in Ref. [34]. In this formulation, the backward e-foldings $N_{\to c}$ determines the location of B_1, $N_{B_1C_1} = N_{\rm S}$. This condition yields unperturbed physical scales on the uniform density slice $\rho = \rho_c$.

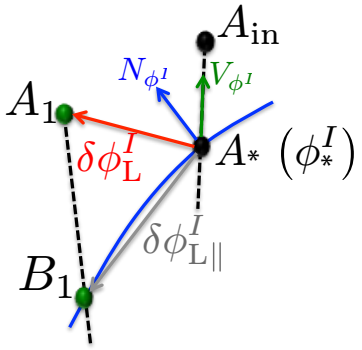

Figure 3.3. Schematic representation of the backward formulation for the calculation of the squeezed bispectrum in the near-equilateral limit. In this regime, the constant backward e-folding hypersurfaces $N_{\to c} = N_{\rm L}$ and $N_{\to c} = N_{\rm S}$ coincide (blue line). The slow-roll trajectories $[A_{\rm in}A_*]$ and $[A_1B_1]$ are aligned with the gradient of the potential V_I. The gradients of the backward e-folding function $N(\phi)$ and of the potential $V(\phi)$ are misaligned in general, but if they are parallel (as in single-field inflation), the squeezed bispectrum vanishes.

Near-equilateral limit

Let us now work out the near-equilateral limit $N_{\rm S} \to N_{\rm L}$, illustrated in Fig. 3.3. It corresponds with the limit $B \to A_*$ but note that the point A_1 does not coincide with B_1 in contrast

to the forward formulation. The difference in the field values between A_* and B_1 is denoted as $\delta\phi^I_{\mathrm{L}||}$. In the limit $N_{\mathrm{S}} \to N_{\mathrm{L}}$, the e-folding number realized until the final uniform density slice is reached are the same from A_* and from B_1, therefore

$$0 = N\left(\phi^J_* + \delta\phi^J_{\mathrm{L}||}\right) - N(\phi^J_*) \simeq N_I(\phi_*)\delta\phi^I_{\mathrm{L}||}. \tag{3.3.18}$$

Another condition to write down is that the points A_1 and B_1 lie on the same slow-roll trajectory, which implies that $[A_1B_1]$ is parallel to the gradient of the potential, giving rise to

$$\delta\phi^I_{\mathrm{L}} - \delta\phi^I_{\mathrm{L}||} = \lambda V_I, \tag{3.3.19}$$

with some constant λ. Combining them, one can find the solutions as

$$\lambda = \frac{N_I\delta\phi^I_{\mathrm{L}}}{N_J V_J}, \qquad \delta\phi^I_{\mathrm{L}||} = \delta\phi^I_{\mathrm{L}} - \frac{N_J\delta\phi^J_{\mathrm{L}}}{N_K V_K}V_I. \tag{3.3.20}$$

The power spectrum at B_1 can then be evaluated as

$$\begin{aligned}\mathcal{P}_\zeta|_{B_1} &\simeq \mathcal{P}_\zeta(\phi_*) + \frac{\partial\mathcal{P}_\zeta}{\partial\phi^J}\delta\phi^J_{\mathrm{L}||} \\ &\simeq \mathcal{P}_\zeta(\phi_*) + 2\left(\frac{H}{2\pi}\right)^2\left(N_IN_{IJ} + N_IN_I\frac{H_J}{H}\right)\left(\delta\phi^J_{\mathrm{L}} - \frac{N_K\delta\phi^K_{\mathrm{L}}}{N_MV_M}V_J\right),\end{aligned} \tag{3.3.21}$$

and its correlation with $\delta N_{\mathrm{L}} \simeq N_I\delta\phi^I_{\mathrm{L}}$ is given by

$$\begin{aligned}\langle\delta N_{\mathrm{L}}\mathcal{P}_\zeta(k_{\mathrm{S}})\rangle &= 2\left(\frac{H}{2\pi}\right)^2 N_I\left(N_JN_{JK} + N_JN_J\frac{V_K}{2V}\right)\left(\langle\delta\phi^I_{\mathrm{L}}\delta\phi^K_{\mathrm{L}}\rangle - \frac{N_N\langle\delta\phi^I_{\mathrm{L}}\delta\phi^N_{\mathrm{L}}\rangle}{N_MV_M}V_K\right) \\ &= 2\left(\frac{H}{2\pi}\right)^4 N_I\left(N_JN_{JK} + N_JN_J\frac{V_K}{2V}\right)\left(\delta_{IK} - \frac{N_N\delta_{IN}}{N_MV_M}V_K\right).\end{aligned} \tag{3.3.22}$$

Plugging this expression into Eq. (3.3.6), one obtains for the squeezed non-linearity parameter

$$\frac{3}{5}f_{\mathrm{NL}} = \frac{1}{2(N_MN_M)^2}\left(N_JN_{IJ} + N_JN_J\frac{V_I}{2V}\right)\left(N_I - \frac{N_NN_N}{N_KV_K}V_I\right). \tag{3.3.23}$$

This formula is one of the main results of this chapter since it allows one to directly calculate the squeezed f_{NL} parameter (in the near-equilateral limit) in terms of physical scales and as seen by a local observer.

Note that this expression is similar to the forward formulation's one (3.1.13), except that N_I is now replaced by $N_I - \frac{N_NN_N}{N_KV_K}V_I$. Therefore f_{NL} in the backward formalism is proportional to the projection of the gradient of V on the hypersurface of the constant backward e-foldings. In other words, if the gradients of $V(\phi)$ and $N(\phi)$ in field space are parallel, then the squeezed bispectrum vanishes. This is obviously the case in single-field inflation, but can also happen in some multi-field models. Let us also mention that the difference between the forward and backward formulae is actually given by $\frac{3}{5}f^{\mathrm{CR}}_{\mathrm{NL}} = \frac{1-n_{\mathrm{S}}}{4}$, in agreement with Eq. (3.2.14):

$$\frac{5}{3}f^{\mathrm{forward}}_{\mathrm{NL}} - \frac{5}{3}f^{\mathrm{back}}_{\mathrm{NL}} = \frac{1-n_{\mathrm{S}}}{4}. \tag{3.3.24}$$

It can be shown as follows. First, the scalar spectral index is given by

$$1-n_{\rm S}=\frac{{\rm d}\log\mathcal{P}_\zeta}{{\rm d}N}=\frac{1}{\mathcal{P}_\zeta}\frac{{\rm d}\phi^I}{{\rm d}N}\partial_I\mathcal{P}_\zeta=\frac{1}{N_KN_K}\frac{V_I}{V}\left(2N_JN_{IJ}+N_JN_J\frac{V_I}{V}\right), \tag{3.3.25}$$

where the slow-roll EoM (3.1.2) has been used. Let us consider two near constant backward e-folds hypersurfaces N and $N+\delta N$ and let $\delta\bar{\phi}^I$ denote the field variation between these two slices along the unperturbed attractor trajectory. By definition of N_I, one has $\delta N=N_I\delta\bar{\phi}^I$. On the other hand, the slow-roll EoM (3.1.2) for ϕ^I yields $\delta\bar{\phi}^I=\frac{V_I}{V}\delta N$. Combining these two relations, one obtains

$$N_IV_I=V, \tag{3.3.26}$$

which allows one to show that the difference between the result of the forward formulation (3.1.13) and the one of the backward formulation (3.3.23) is indeed given by $(1-n_{\rm S})/4$. In Sec. 3.4, this consistency check will be extended beyond the near-equilateral limit.

Computational program

Let us now explain how the proposed approach can be implemented in practice. The formula (3.3.6) allows one to calculate the squeezed $f_{\rm NL}(k_{\rm L},k_{\rm S})$ both in the forward and backward formulation for any multi-field models. In the limit where $k_{\rm S}\to k_{\rm L}$, this gives rise to analytical expressions such as Eqs. (3.1.13) or (3.3.23) which can be easily evaluated. In general however, the quantities appearing in Eq. (3.3.8) cannot be calculated analytically and one has to evaluate them numerically, according to the following procedure:

1. Starting from $A_{\rm in}(\phi^I_{\rm in})$, integrate the background EoM for the fields and find the coordinates in the field space of A_*, B, and C defined in Figs. 3.1 (forward) or 3.2 (backward).

2. Starting from $\phi^I_*+\epsilon\delta^I_I$, integrate the background EoM until the condition $\rho=\rho_{\rm c}$ is met. If N^I_ϵ denotes the realized e-folding number, assess $N_I|_*=(N^I_\epsilon-N_{\rm L})/\epsilon$. Repeat this step for $I=1,\cdots,D$, where D is the number of fields.

3. Reproduce step 2 but starting from B instead of A_* to compute $N_I|_B$.

4. Compute the power spectrum amplitude $\mathcal{P}_\zeta=N_IN_J\langle\delta\phi^I\delta\phi^J\rangle$ at A_* and B. In this expression, the derivatives N_I have been computed in step 2 for A_* and in step 4 for B, but $\langle\delta\phi^I\delta\phi^J\rangle$ depends on the model one considers. In standard slow-roll inflation for instance, it is simply given by $\langle\delta\phi^I\delta\phi^J\rangle=\mathcal{P}_\phi\delta_{IJ}=[H/(2\pi)]^2\delta_{IJ}$ and is straightforward to compute.

5. Using the trajectories integrated in step 2, find the coordinates of B^I_ϵ defined w.r.t. the shifted starting points $\phi^J_*+\epsilon\delta^J_I$. Using the same technique as in step 4, compute $\mathcal{P}_\zeta(B^I_\epsilon)$, the power spectrum amplitude at B^I_ϵ. Assess $\partial\mathcal{P}_\zeta(B)/\partial\phi^I_*=[\mathcal{P}_\zeta(B^I_\epsilon)-\mathcal{P}_\zeta(B)]/\epsilon$, where $\mathcal{P}_\zeta(B)$ has been computed in step 4. Repeat this step for $i=1,\cdots,D$.

6. Evaluate

$$\frac{3}{5}f_{\rm NL}=\frac{N_I|_*\frac{\partial\mathcal{P}_\zeta(B)}{\partial\phi^I_*}\mathcal{P}_\phi|_*}{4\mathcal{P}_\zeta(A_*)\mathcal{P}_\zeta(B)}, \tag{3.3.27}$$

where $N_{\phi^I_*}$ has been computed in step 2, $\partial\mathcal{P}_\zeta(B)/\partial\phi^I_*$ in step 5, and $\mathcal{P}_\zeta(A_*)$ and $\mathcal{P}_\zeta(B)$ in step 4.

This makes the implementation of our proposal straightforward as soon as one knows how to solve the background EoM. In the next section, we discuss the results which it gives in the concrete examples.

3.4 Example

In the previous section, we have explained how to calculate the squeezed $f_{\rm NL}(k_{\rm L}, k_{\rm S})$ in a generic multi-field models, in the forward and backward formulation, allowing for an arbitrary separation between the two scales $k_{\rm L}$ and $k_{\rm S}$, and automatically taking the intrinsic NG into account. Let us now illustrate our approach on the concrete two-field model, where the two fields have a simple quadratic potential. This shows how the method which we propose works in practice, and provides a few interesting results for the value taken by the squeezed non-linearity parameter. We focus on the backward formulation since it yields the result a local observer would see, and given that, as shown in Eq. (3.3.24), both formulations only differ by $(1 - n_{\rm s}(k_{\rm S}))/4$.

Let us consider the case where inflation is driven by two scalar fields ϕ and ψ, slowly rolling down the potential

$$V(\phi, \psi) = \frac{m_\phi^2}{2}\phi^2 + \frac{m_\psi^2}{2}\psi^2. \tag{3.4.1}$$

In the following, without loss of generality, we assume that $m_\phi \geq m_\psi$. In this case inflation is first mainly driven by ϕ, before a turning point occurs in the field space and ψ takes over. The ending hypersurface is determined by $\rho = \rho_{\rm c}$, where $\rho_{\rm c}$ is the energy density when $\epsilon_H = 1$ on the unperturbed trajectory.

In Sec. 3.3.2, we have sketched the computational program which allows one to numerically evaluate $f_{\rm NL}$. For the model (3.4.1), there exists an analytical integral of motion $K = m_\psi^2 \log\phi - m_\phi^2 \log\psi$ which is constant along slow-roll trajectories and can label them [48]. Moreover the e-folding number realized between two points $M_1(\phi_1, \psi_1)$ and $M_2(\phi_2, \psi_2)$ in the field space which belong to the same slow-roll trajectory is given by $N_{12} = (\phi_1^2 + \psi_1^2 - \phi_2^2 - \psi_2^2)/4$ [49]. These relations provide analytical results for all steps of the procedure described in Sec. 3.3.2. This is in fact the case for all separable potentials, for which we provide all relevant formulae in Appendix C.

In Fig. 3.4, different values of $N_{\rm L} - N_{\rm S}$ are displayed and a few remarks are in order. First, one can see that $|f_{\rm NL}|$ reaches a maximum, corresponding to when the scales one considers exit the horizon at the time when the turn in the field space is maximal (which happens about 40 e-folds before the end of inflation for the parameters used in Fig. 3.4). Away from this point, the model effectively describes a single-field system (driven by ϕ much before the turning point and by ψ soon after the turning point) and $f_{\rm NL}$ vanishes. Second the value of $N_{\rm L}$ at which $|f_{\rm NL}|$ is maximal is shifted by $N_{\rm L} - N_{\rm S}$ from one curve to the other. This indicates that $|f_{\rm NL}|$ is maximal if $k_{\rm S}$ exits the horizon at the time of the maximal turn in the field space. Third, when $N_{\rm L} - N_{\rm S}$ increases, the maximal value of $f_{\rm NL}$ decreases. This can be understood noticing that fixing $N_{\rm S}$ to the time of maximal turn in the field space, the large wavelength fluctuation exits the horizon away from the turning point if $N_{\rm L} - N_{\rm S}$ is large, that is to say when the system is near to the single-field case. It confirms that it is important to account for the actual values of the scales $k_{\rm L}$ and $k_{\rm S}$ to properly compute $f_{\rm NL}$, and that the near-equilateral limit $k_{\rm L} \to k_{\rm S}$ does not always provide a reliable estimate when the two scales differ.

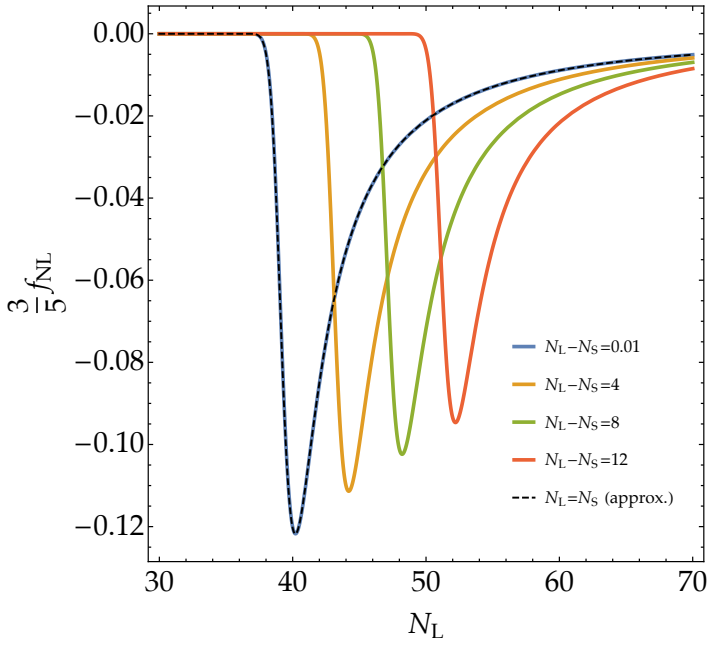

Figure 3.4. Squeezed backward $f_{\rm NL}$ computed in the double massive potential (3.4.1), as a function of $N_{\rm L}$, with $\phi_{\rm in} = \psi_{\rm in} = 13$, $m_\psi = m_\phi/9$, and $\rho_{\rm c} = m_\psi^2$. The result is shown for a few values of $N_{\rm L} - N_{\rm S}$ (labeled by different colors). The black dashed line stands for the limit $N_{\rm S} \to N_{\rm L}$ given by Eq. (3.4.2) where the contributions from the end of inflation are neglected. One can check that, when $N_{\rm L} - N_{\rm S} \ll 1$, this provides a good approximation indeed.

In this model, $f_{\rm NL}$ is therefore maximal when the two scales $k_{\rm L}$ and $k_{\rm S}$ are close. In this limit, if one ignores the contribution from the end of inflation and simply plugs $N = (\phi^2 + \psi^2)/4 + \text{const.}$ into Eq. (3.3.23), one obtains

$$\frac{3}{5} f_{\rm NL}(k_{\rm S} \to k_{\rm L}) \simeq \frac{1}{\phi^2 + \psi^2} \left[1 - \frac{(\phi^2 + \psi^2)(m_\phi^4 \phi^2 + m_\psi^4 \psi^2)}{(m_\phi^2 \phi^2 + m_\psi^2 \psi^2)^2} \right] . \tag{3.4.2}$$

In this expression, one can check that $m_\phi = m_\psi$ leads to $f_{\rm NL} = 0$, which is consistent with the fact that, when the two masses are equal, the model is effectively equivalent to a single-field setup and $f_{\rm NL}$ vanishes. This expression is displayed in Fig. 3.4 as the black dashed line. One can check that, when $N_{\rm L} - N_{\rm S} \ll 1$, it porvides a good approximation to the exact result. The reason is that, if the turn in field space occurs much before the end of inflation, inflation is effectively driven by one of the fields only when it ends and the vev of the other field almost vanishes. In this limit, it is safe to neglect the dependence of the end of inflation field space coordinates on small changes in the initial conditions.

Finally let us see how this result compares to the forward formulation. In Fig. 3.5, the non-linearity parameter $f_{\rm NL}$ is displayed in each formulation for $N_{\rm L} - N_{\rm S} = 7$. It is interesting to notice that opposite signs are obtained with the two formulations. Moreover one can check that $\frac{3}{5} f_{\rm NL}^{\rm forward} - \frac{1 - n_{\rm S}(k_{\rm S})}{4}$ represented by the black dotted line matches $\frac{3}{5} f_{\rm NL}^{\rm back}$. This is in agreement with Eq. (3.3.24) and confirms that the backward formulation yields the squeezed bispectrum in terms of physical scales as seen by a local observer.

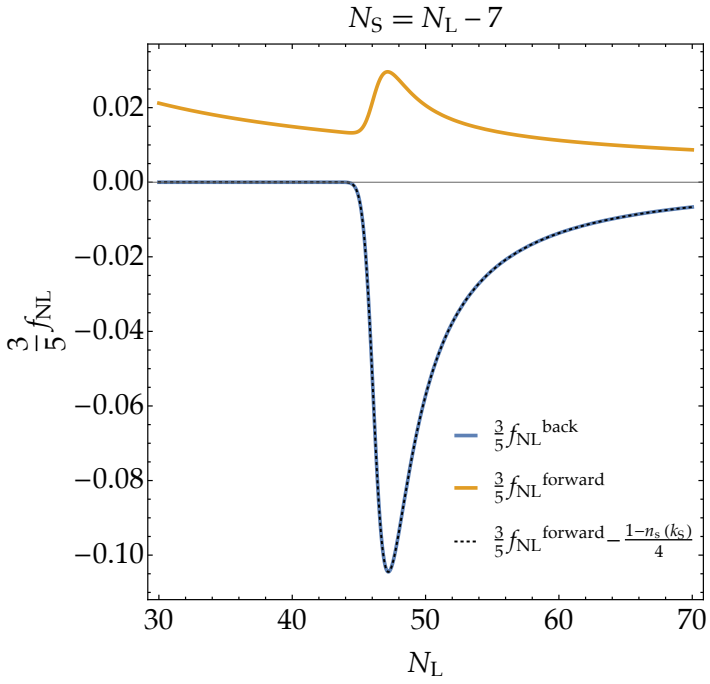

Figure 3.5. Forward and backward formulations' results for squeezed $f_{\rm NL}$ as a function of $N_{\rm L}$, where $N_{\rm L} - N_{\rm S}$ is fixed to 7. The black dotted line shows $\frac{3}{5} f_{\rm NL}^{\rm forward} - \frac{1-n_{\rm S}(k_{\rm S})}{4}$ where the spectral index is given by Eq. (3.3.25). It matches $\frac{3}{5} f_{\rm NL}^{\rm back}$ and confirms that even beyond the near-equilateral limit, the backward formulation yields the squeezed bispectrum in terms of physical scales as seen by a local observer.

3.5 Extension to the stochastic formalism

The key idea of the procedure in this chapter does not basically depend on the perturbative expansion, except for the impulsive field fluctuations. Therefore the extension to the stochastic-δN formalism is straightforward though it is quite difficult to solve practically. The schematic image to calculate the squeezed bispectrum in the stochastic formalism is shown in Fig. 3.6. The concrete algorithm as follows. First, take the initial field value $\phi_{\rm i}$ from which the mean e-folds $\langle N_{\rm T} \rangle$ becomes almost 60 e-folds. Then let us assume that some sample path reaches the field space point $\phi_{\rm L}$ with $N_{\rm TL}$ e-folds from this initial point. If one makes many sample paths from $\phi_{\rm L}$ and the mean e-folds realized until the end of inflation is given by $\langle N_{\rm L} \rangle$, the mean curvature perturbation of the corresponding local patch is nothing but $\zeta_{\rm L} = N_{\rm TL} + \langle N_{\rm L} \rangle - \langle N_{\rm T} \rangle$. The scale of the local patch or the coarse-graining scale of $\zeta_{\rm L}$ is related with $\langle N_{\rm L} \rangle$ here. Moreover, calculating the power spectrum in the stochastic-δN formalism by taking the "initial" point on the subbranches after $\phi_{\rm L}$, one can obtain the power spectrum averaged in that local patch. Thus the correlation between the long-wavelength mode $\zeta_{\rm L}$ and the short-wavelength power $\mathcal{P}_\zeta k_{\rm S}$ can be calculated in this way. Finally, differentiating it w.r.t. $\langle N_{\rm L} \rangle$, the squeezed non-linearity parameter is obtained:

$$\frac{3}{5} f_{\rm NL}(k_{\rm L}, k_{\rm S}) = -\frac{1}{4\mathcal{P}_\zeta(k_{\rm L})\mathcal{P}_\zeta(k_{\rm S})} \frac{{\rm d}\,\langle \zeta_{\rm L} \mathcal{P}_\zeta(k_{\rm S}) \rangle}{{\rm d}\,\langle N_{\rm L} \rangle}. \tag{3.5.1}$$

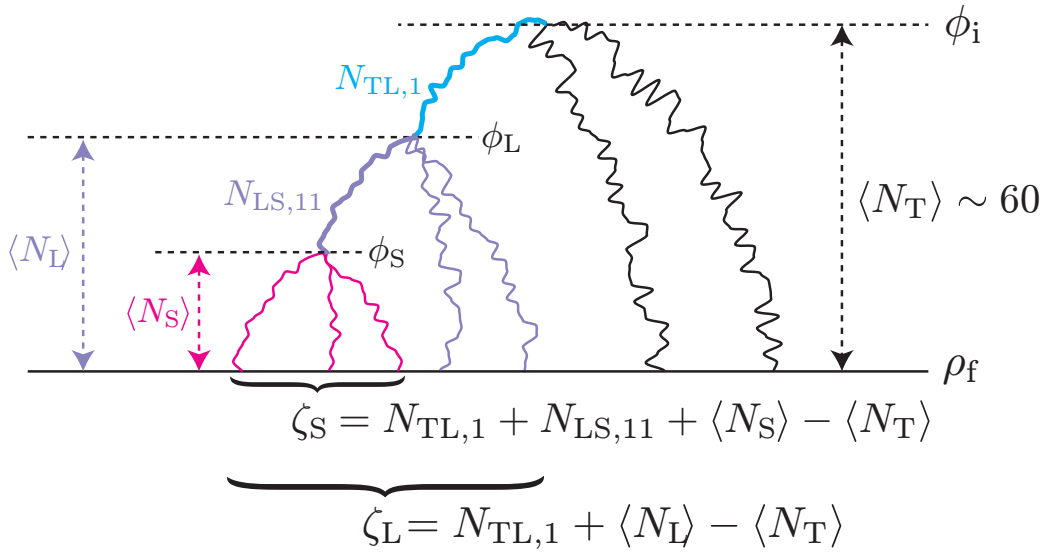

Figure 3.6. Schematic image to calculate the squeezed bispectrum in the stochastic formalism. In the stochastic formalism, the coarse-grained curvature perturbation can be obtained by branching the trajectories. Further, by branching the trajectories again from their subbranches, the obtained fluctuations of e-folds are those in the local patch corresponding with the large-scale coarse-grained field.

However practical calculations are quite difficult even numerically, and we are in progress now for this topic. Note that, even if one includes the stochastic effect, the backward squeezed bispectrum does vanish in single-field inflation since the discussion done in Sec. 3.3.2 does not change.

Part II

Primordial Black Holes

Chapter 4

Overview of Primordial Black Holes

The primordial black hole has attracted a lot of cosmologists for more than 40 years after its first proposal by Hawking and Carr [50–52] even though it has not been detected yet. That is because PBH can give us many implications both for the theory of the early universe and the astrophysical phenomenology. Recently its possibility has been refocused on more and more. In this chapter, let us review its basics as well as the current situation including the motivation of PBH and the observational constraints. This chapter is partially based on Ref. [53].

4.1 Basics

From the first exact solution of general relativity by Schwarzschild in 1916 [54], the astrophysical object called *black hole* has been a key topic for various fields beyond astronomy. Though its standard origin is gravitational collapse of dying massive stars, Hawking and Carr proposed a completely novel formation scenario of black holes [50–52], that is, the sufficiently overdense Hubble patch can collapse directly into black holes in the radiation-dominated era. It is called *primordial black hole*. Now several other formation mechanisms have been proposed, e.g. bubble collisions [55–61] or the collapse of cosmic strings [62–70], nacklaces [71, 72], or domain walls [73–78], but we concentrate on the gravitational collapse of overdense Hubble patches in this thesis. Then let us begin by the brief review of this formation mechanism.

4.1.1 Formation of primordial black hole

Before discussing the PBH formation, we have to introduce the Jeans instability [79], which is described in Newtonian gravity. The fundamental equations for the non-relativistic fluid in Newtonian gravity are the equation of continuity:

$$\frac{\partial \rho}{\partial t} + \nabla \cdot (\mathbf{v}\rho) = 0, \tag{4.1.1}$$

the Euler equation:

$$\frac{\partial \mathbf{v}}{\partial t} + (\mathbf{v}\cdot\nabla)\mathbf{v} = -\frac{\nabla p}{\rho} - \nabla\phi, \tag{4.1.2}$$

and the Poisson equation:

$$\nabla^2\phi = \frac{1}{2M_{\rm Pl}^2}\rho, \tag{4.1.3}$$

with mass density ρ, pressure p, velocity $\mathbf{v}$,and gravitational potential ϕ. Neglecting pressure, one can find the unperturbed solution for these equations as

$$\bar{\rho} = \rho_0\left(\frac{a_0}{a}\right)^3, \qquad \bar{\mathbf{v}} = H\mathbf{X}, \qquad \bar{\phi} = \frac{1}{12M_{\rm Pl}^2}\bar{\rho}\mathbf{X}^2, \tag{4.1.4}$$

where $H = \dot{a}/a$. Also a_0 and ρ_0 are constant, and $a(t)$ satisfies the condition:

$$\dot{a}^2 + K = \frac{1}{3M_{\rm Pl}^2}\bar{\rho}a^2, \tag{4.1.5}$$

with some constant K. Here $\mathbf{X}$ denotes the Euclidean coordinate vector which is related with the comoving coordinate $\mathbf{x}$ by $\mathbf{X} = a\mathbf{x}$.[1] Indeed the solution of the equation $\mathrm{d}\mathbf{X}/\mathrm{d}t = \bar{\mathbf{v}} = H\mathbf{X}$ for a comoving object is consistently given by $\mathbf{X}(t) = \frac{a(t)}{a(t_0)}\mathbf{X}(t_0)$.

Then let us perturb these equation at the linear order as

$$\begin{cases} \dfrac{\partial\delta\rho}{\partial t} + 3H\delta\rho + H\mathbf{X}\cdot\nabla\delta\rho + \bar{\rho}\nabla\cdot\delta\mathbf{v} = 0, \\ \dfrac{\partial\delta\mathbf{v}}{\partial t} + H\mathbf{X}\cdot\nabla\delta\mathbf{v} + H\delta\mathbf{v} = -\dfrac{\nabla\cdot\delta p}{\bar{\rho}} - \nabla\cdot\delta\phi, \\ \nabla^2\delta\phi = \dfrac{1}{2M_{\rm Pl}^2}\delta\rho. \end{cases} \tag{4.1.6}$$

These equations do not appear traslational invariance, but actually it can be restored by writing them in a comoving way. Namely the Fourier modes of the perturbations should be defined as

$$\delta\rho(\mathbf{X},t) = \int\frac{\mathrm{d}^3k}{(2\pi)^3}\exp\left(\frac{i\mathbf{k}\cdot\mathbf{X}}{a(t)}\right)\delta\rho_{\mathbf{k}}(t), \tag{4.1.7}$$

and likewise for $\delta\mathbf{v}$ and $\delta\phi$. Then the equations for these Fourier modes are given by

$$\begin{cases} \dfrac{\mathrm{d}\delta\rho_{\mathbf{k}}}{\mathrm{d}t} + 3H\delta\rho_{\mathbf{k}} + i\bar{\rho}\dfrac{\mathbf{k}\cdot\delta\mathbf{v}_{\mathbf{k}}}{a} = 0, \\ \dfrac{\mathrm{d}\delta\mathbf{v}_{\mathbf{k}}}{\mathrm{d}t} + H\delta\mathbf{v}_{\mathbf{k}} = -i\dfrac{\mathbf{k}}{a}\dfrac{\delta p}{\bar{\rho}} - i\dfrac{\mathbf{k}}{a}\delta\phi, \\ -\dfrac{k^2}{a^2}\delta\phi_{\mathbf{k}} = \dfrac{1}{2M_{\rm Pl}^2}\delta\rho_{\mathbf{k}}. \end{cases} \tag{4.1.8}$$

[1] Note that nablas here indicate the derivatives w.r.t. this Euclidean coordinate $\mathbf{X}$.

In general, pressure p is a function of mass density ρ and entropy density s, and therefore its linear perturbation is

$$\delta p = \left(\frac{\partial p}{\partial \rho}\right)_s \delta\rho + \left(\frac{\partial p}{\partial S}\right)_\rho \delta s. \tag{4.1.9}$$

Here the first coefficient gives the square of the sound speed $c_{\rm s}^2 = (\partial p/\partial\rho)_s$. Assuming the adiabatic perturbations (i.e. $\delta s = 0$) for simplicity, finally one can obtain the EoM for $\delta_{\mathbf{k}} = \delta\rho_{\mathbf{k}}/\bar{\rho}$ as

$$\ddot{\delta}_{\mathbf{k}} + 2H\dot{\delta}_{\mathbf{k}} + \left(c_{\rm s}^2\frac{k^2}{a^2} - \frac{\bar{\rho}}{2M_{\rm Pl}^2}\right)\delta_{\mathbf{k}} = 0, \tag{4.1.10}$$

from Eqs. (4.1.8) where dots denote time derivatives.

This equation indicates that the perturbation on the larger scale than $k_{\rm J} = a\sqrt{\bar{\rho}}/(\sqrt{2}M_{\rm Pl}c_{\rm s})$ shows tachyonic instability. The criterion scale $k_{\rm J}$ is called *Jeans scale* and it shows the smallest scale which can gravitationally grow against the pressure. Smaller scale perturbations than the Jeans scale cannot grow due to pressure and simply show the oscillation called *acoustic oscillation*.

In the radiation-dominated universe, the sound speed is given by $c_{\rm s}^2 = p/\rho = w = 1/3$. Then, if one simply applies the above expression to the radiation-dominated era, the Jeans scale is as large as the horizon scale:

$$\left(\frac{k_{\rm J}}{a}\right)^{-1} = c_{\rm s}\sqrt{\frac{\bar{\rho}}{2M_{\rm Pl}^2}}^{-1} \sim c_{\rm s}H^{-1}, \tag{4.1.11}$$

due to non-negligible radiational pressure. On the other hand, the Schwarzschild radius of the horizon mass itself is formally equal to the horizon scale as

$$r_{\rm Sch} = \frac{1}{4\pi M_{\rm Pl}^2}M_{\rm H} = \frac{1}{4\pi M_{\rm Pl}^2}\frac{4\pi}{3}\bar{\rho}H^{-3} = H^{-1}. \tag{4.1.12}$$

Therefore, if the scale of some overdensity is as large as the horizon, that overdensity is assumed to gravitationally collapse into a black hole. In the following, let us evaluate the PBH formation criterion, following Ref. [52].

Now we consider the constant (top-hat type) overdensity $\rho = \bar{\rho} + \delta\rho$ in a flat FLRW universe. Namely the background metric is given by

$$ds^2 = -dt^2 + a^2(t)(dr^2 + r^2 d\Omega^2). \tag{4.1.13}$$

Also we assume that the overdensity size is initially larger than the Hubble scale and then the inner metric of the overdense region is given by another FLRW metric as

$$ds^2 = -dt^2 + b^2(t)\left(\frac{dr^2}{1-kr^2} + r^2 d\Omega^2\right). \tag{4.1.14}$$

As initial conditions, let us impose $a_{\rm i} = b_{\rm i}$ and $\dot{a}_{\rm i} = \dot{b}_{\rm i}$. From the Friedmann equation, they give the condition for the curvature k as

$$H^2 = \frac{\bar{\rho}_{\rm i}}{3M_{\rm Pl}^2} = \frac{\bar{\rho}_{\rm i} + \delta\rho_{\rm i}}{3M_{\rm Pl}^2} - \frac{k}{a_{\rm i}^2}, \quad \Leftrightarrow \quad \frac{k}{a_{\rm i}^2} = \frac{\delta\rho_{\rm i}}{3M_{\rm Pl}^2}. \tag{4.1.15}$$

Then the Friedmann equation in the overdense region reads, with use of the dilution law $\rho \propto b^{-4}$,

$$\dot{b}^2 = \frac{\rho}{3M_{\rm Pl}^2} b^2 - k = \frac{\bar{\rho}_{\rm i} a_{\rm i}^4}{3M_{\rm Pl}^2} \left(\frac{1+\delta_{\rm i}}{b^2} - \frac{\delta_{\rm i}}{a_{\rm i}^2} \right), \tag{4.1.16}$$

where $\delta_{\rm i}$ is the initial density contrast $\delta\rho_{\rm i}/\bar{\rho}_{\rm i}$. Therefore the time of the beginning of collapse at which $\dot{b} = 0$ is given by,

$$\begin{cases} b_{\rm c} = a_{\rm i} \left(\dfrac{1+\delta_{\rm i}}{\delta_{\rm i}} \right)^{1/2} \sim a_{\rm i} \delta_{\rm i}^{-1/2}, \\ t_{\rm c} \sim t_{\rm i} \delta_{\rm i}^{-1}, \end{cases} \tag{4.1.17}$$

with use of the approximation $b \propto t^{1/2}$. Then the criterion of PBH formation is whether the overdensity size is larger than the Jeans scale at that time, namely, letting R be the comoving scale of the overdensity,

$$b_{\rm c} R > c_{\rm s} H_{\rm c}^{-1} = 2 c_{\rm s} t_{\rm c}, \quad \Leftrightarrow \quad \delta_{\rm i} > c_{\rm s}^2 \left(\frac{H_{\rm i}^{-1}}{a_{\rm i} R} \right)^2. \tag{4.1.18}$$

Therefore the threshold value for the density perturbation at the horizon crossing is roughly given by the square of the sound speed $\delta_{\rm th} = c_{\rm s}^2 = w = 1/3$. The resultant PBH mass is given by the Jeans mass $M_{\rm PBH} \sim c_{\rm s}^3 M_{\rm H}$ where $M_{\rm H}$ is the horizon mass at the horizon reenter of the overdensity.

The above discussion is just a simple estimation and includes many subtleties. Many authors have tackled the PBH formation mechanism beyond this simple discussion both numerically and analytically. Nadazhin et al. [80] carried out the first detailed numerical study with use of a hydrodynamical code and gave the resultant PBH mass relatively smaller than the Jeans mass. Bicknell and Henrikse [81] followed this with different initial conditions and found PBH formation with masses of the same order as the horizon mass.

Regarding the threshold value, further numerical studies by Niemeyer and Jedamzik [82, 83] and Musco et al. [84–86] found a relatively large threshold $\delta_{\rm th} \simeq 0.7$ on the comoving slice for Gaussian, Mexican-hat, and polynomial initial shapes of the overdensity, while the result by Hawke and Stewart [87] is $\delta_{\rm th} \simeq 0.4$ for the Gaussian shape. Recently Harada et al. [88] studied the top-hat shape and found the analytical formula $\delta_{\rm th} = \sin^2[\pi\sqrt{w}/(1+3w)] \simeq 0.62$. Nakama et al. [89] numerically studied the generalized initial shape and found the two key parameters which determine the PBH formation beyond the simple $\delta_{\rm th}$ discussion.

Shibata and Sasaki [90] numerically studied the PBH formation in terms of the curvature perturbation instead of the density perturbation from the view point of the connection with inflation. Green et al. [91] addressed it and found the threshold value for the gauge invariant curvature perturbation on the uniform density slice as $\zeta_{\rm th} \sim 0.7$–1.2, assuming the threshold for the comoving density perturbation is $\delta_{\rm th} \sim 0.3$–0.5. It is reasonable since the comoving density perturbation is related with the curvature perturbation $\mathcal{R}$ on the comoving slice, which reads equal to ζ in the superhorizon limit, by (1.1.79)

$$\delta = \frac{2(1+w)}{5+3w} \left(\frac{k}{aH} \right)^2 \mathcal{R}, \tag{4.1.19}$$

and therefore $\delta \simeq \frac{4}{9}\mathcal{R}$ at the horizon crossing in the radiation-dominated era.

Kopp et al. [92] also claimed the merit of the metric perturbation from another view point, addressing the separate universe problem. Previously it was thought that there was an upper bound $\delta_{\rm max}$ for the density perturbation above which the overdensity would form a separate closed universe rather than a PBH (see e.g. Ref. [93]). However Kopp et al. showed that the density perturbation never exceeds $\delta_{\rm max}$ even for the large metric perturbation due to the enhancement of the physical volume of the overdense region. The density perturbation rather decreases for an increasing curvature perturbation after reaching $\delta_{\rm max}$. They further numerically examined that the large curvature perturbation (and the decreased small density perturbation) in fact produces the separate closed universe but leaves a PBH for the mother universe, too. Since now the density perturbation is not a monotonically increasing function of the curvature perturbation, they claimed that the curvature perturbation should be used for the criterion of the PBH formation.

On the other hand, recently Young et al. [94] pointed out the demerit of the curvature perturbation. That is, since the curvature perturbation is constant on the superhorizon scale, the much superhorizon modes can apparently affect the PBH formation if one uses the curvature perturbation as a criterion, while such superhorizon modes should not have effects on the dynamics of the horizon patch. The density perturbation on the comoving slice safely damps on the superhorizon scale as shown in Eq. (4.1.19), and therefore they claimed that the density perturbation should be used as a criterion.

Finally let us mention the critical collapse phenomenon. It has been reported that the mass of the gravitational collapsed object is given by the power law in $(\delta - \delta_{\rm th})$ by Choptuik [95] and many subsequent authors (see e.g. Ref. [96] and the recent review article [97]). Several numerical studies mentioned above [82–87] confirmed this phenomenon also for PBH, namely the PBH mass is not simply given by the Hubble mass but depends also on the amplitude of the density perturbation. Recently several authors have worked on its application to the PBH mass function [98, 99].

The above rich phenomena of the PBH formation make the simple analysis difficult. In this thesis, we only consider a naive evaluation, not considering the critical collapse for simplicity, and keep the threshold value and the mass ratio to the horizon mass as free parameters.

4.1.2 Mass function

Now let us discuss the evaluation of the current abundance and mass of PBH. At first we briefly mention the mass evolution of PBH after its formation. It is known that black holes can evaporate due to the Hawking radiation [100, 101] whose temperature is given by $T_{\rm BH} = M_{\rm Pl}^2/M_{\rm BH}$. Since it is inversely proportional to the black hole mass, the black hole explosively evaporates away at its last phase. On the other hand, the evaporation effect is almost negligible for sufficiently massive black holes. The energy flux due to this temperature is given by the Stefan-Boltzmann law $I = \frac{\pi^2}{120} g T^4$ where g is the total effective degrees of freedom, and therefore the black hole mass loss per unit time is

$$-\frac{{\rm d}M}{{\rm d}t} = 4\pi r_{\rm Sch} \times I = \frac{\pi}{480} g \frac{M_{\rm Pl}^4}{M^2}. \tag{4.1.20}$$

Accordingly the black hole lifetime is given by,

$$\tau_{\rm BH} \sim \frac{160}{\pi g}\frac{M^3}{M_{\rm Pl}^4} \sim 13.8\,{\rm Gyr}\left(\frac{M}{5\times 10^{14}\,{\rm g}}\right)^3, \tag{4.1.21}$$

where we approximated g as a constant and neglected a numerical factor $160/(\pi g)$. Therefore PBHs of less than around 10^{15} g should have evaporated away by now.

On the other hand, PBH may be able to grow by accretion. Though the accretion process strongly depends on the circumstances around PBH, here let us briefly estimate the growth rate to show that it will not increase the PBH mass by orders of magnitude. Since accreted material will be crossing the Schwarzschild radius at about the speed of light, the PBH growth rate will be

$$\frac{{\rm d}M}{{\rm d}t} \sim \bar{\rho} r_{\rm Sch}^2 \sim \bar{\rho}\frac{M^2}{M_{\rm Pl}^4} \sim t^{-2}\frac{M^2}{M_{\rm Pl}^2}. \tag{4.1.22}$$

Integrating this equation gives,

$$M \sim \left(\frac{1}{M_{\rm Pl}^2}\left(\frac{1}{t}-\frac{1}{t_1}\right)+\frac{1}{M_1}\right)^{-1}, \tag{4.1.23}$$

where M_1 is the mass of PBH at any time t_1 as long as PBH is well inside the horizon. Namely the fraction of M_1 to the horizon mass $M_{\rm H1} \sim t_1 M_{\rm Pl}^2$ is less than unity, $f = M_1/M_{\rm H1} < 1$. Thus M tends to $M_1/(1-f)$ in the limit of $t \to \infty$ and the PBH cannot increase its mass by orders of magnitude since f cannot be too close to unity. In summary, the current PBH mass is almost given by the mass at its formation, except for the PBH of less than 10^{15} g which has evaporated away by now.

Hereafter we focus on the PBH formation by the large density perturbation. If one assumes that the perturbation of the comoving scale k produces a PBH at its horizon crossing at temperature T, the corresponding PBH mass is given by

$$\begin{aligned} M_{\rm PBH} &= \gamma M_{\rm H}|_{k=aH} = \sqrt{2}\gamma M_{\rm eq}\left(\frac{g_{*\rm eq}}{g_*}\right)^{1/2}\left(\frac{T_{\rm eq}}{T}\right)^2 \\ &= \frac{\gamma M_{\rm eq}}{\sqrt{2}}\left(\frac{g_{*\rm eq}}{g_*}\right)^{1/6}\left(\frac{k_{\rm eq}}{k}\right)^2, \end{aligned} \tag{4.1.24}$$

where γ is a ratio of the PBH mass to the horizon mass and we used the entropy conservation $g_{*s}a^3T^3 = $ const. with an approximation that the effective degrees of freedom for energy density g_* is almost equal to that for entropy density g_{*s}. $M_{\rm eq}$ denotes the horizon mass at the matter-radiation equality:

$$M_{\rm eq} = \frac{4\pi}{3}\rho_{\rm eq}H_{\rm eq}^{-3} = \frac{8\pi}{3}\frac{\rho_{\rm r}^0}{a_{\rm eq}k_{\rm eq}^3}, \tag{4.1.25}$$

with the current radiation density $\rho_{\rm r}^0 = 7.84\times 10^{-34}\,{\rm g\,cm^{-3}}$, and the comoving horizon scale $k_{\rm eq} = 0.07\Omega_{\rm m}h^2\,{\rm Mpc}^{-1}$ and and the scale factor $a_{\rm eq}^{-1} = 24000\Omega_{\rm m}h^2$ at the equality which are

normalized for the current scale factor to be unity [102]. With use of $g_{*\mathrm{eq}} = 3.36$, one can obtain

$$\begin{aligned} M_{\mathrm{PBH}} &= 18.8\gamma M_\odot \left(\frac{g_*}{10.75}\right)^{-1/2} \left(\frac{T}{100\,\mathrm{MeV}}\right)^{-2} \\ &= 19.3\gamma M_\odot \left(\frac{g_*}{10.75}\right)^{-1/6} \left(\frac{k}{10^6\,\mathrm{Mpc}^{-1}}\right)^{-2}. \end{aligned} \tag{4.1.26}$$

In the standard model of particle physics, $g_* \sim 106.75$ before the QCD scale $T \gtrsim 200\,\mathrm{MeV}$, $g_* \sim 10.75$ until the electron-positron annihilation $200\,\mathrm{MeV} \gtrsim T \gtrsim 0.1\,\mathrm{MeV}$, and $g_* \sim 3.36$ after that $T \lesssim 0.1\,\mathrm{MeV}$.

To evaluate the formation rate of PBH, we consider the coarse-grained density perturbation, following the Press-Schechter approach [103], as

$$\delta_R(\mathbf{x}) = \int \mathrm{d}^3 y W_R(|\mathbf{x}-\mathbf{y}|)\delta(\mathbf{y}), \tag{4.1.27}$$

where $W_R(x)$ is some window function on the coarse-graining scale R. The corresponding PBH mass is given by Eq. (4.1.26) by letting k be R^{-1}. Then the formation rate of the PBH of that mass is nothing but the probability at which the coarse-grained perturbation exceeds the threshold δ_{th}. That is, assuming the density perturbation follows the Gaussian distribution, the energy fraction at the formation time $\beta(M) = \rho_{\mathrm{PBH}}/\bar{\rho}|_{k=aH}$ is given by

$$\beta(M) = \gamma \int_{\delta_{\mathrm{th}}} \frac{\mathrm{d}\delta}{\sqrt{2\pi\sigma_R^2}} \mathrm{e}^{-\frac{\delta^2}{2\sigma_R^2}} = \frac{\gamma}{2}\mathrm{Erfc}\left(\frac{\delta_{\mathrm{th}}}{\sqrt{2}\sigma_R}\right) \simeq \frac{\gamma}{\sqrt{2\pi}}\frac{\sigma_R}{\delta_{\mathrm{th}}}\mathrm{e}^{-\frac{\delta_{\mathrm{th}}^2}{2\sigma_R^2}}, \tag{4.1.28}$$

where σ_R is the standard deviation of the coarse-grained density perturbation:

$$\sigma_R^2 = \langle \delta_R^2 \rangle = \int \mathrm{d}^3x \mathrm{d}^3y\, W_R(x) W_R(y) \langle \delta(\mathbf{x})\delta(\mathbf{y})\rangle = \int \mathrm{d}\log k\, \tilde{W}^2(kR)\mathcal{P}_\delta(k). \tag{4.1.29}$$

with the Fourier mode of the window function $\tilde{W}$:

$$\tilde{W}(kR) = \int \mathrm{d}^3x\, W_R(x)\mathrm{e}^{-i\mathbf{k}\cdot\mathbf{x}}. \tag{4.1.30}$$

Note that the power spectrum of the comoving density perturbation $\mathcal{P}_\delta$ is related with that of the primordial curvature perturbation $\mathcal{P}_\zeta$ by

$$\mathcal{P}_\delta(k) = \frac{16}{81}\left(\frac{k}{aH}\right)^4 \mathcal{P}_\zeta(k), \tag{4.1.31}$$

in the radiation-dominated era as shown in Eq. (4.1.19), and the coarse-graining scale should be taken to the horizon scale at the formation time for the PBH formation, therefore the variance is given by

$$\sigma_R^2 = \frac{16}{81}\int \mathrm{d}\log k\, (kR)^4 \tilde{W}^2(kR)\mathcal{P}_\zeta(k), \tag{4.1.32}$$

from the information of the primordial perturbation.

For PBHs of more than 10^{15} g, their current abundance can be evaluated with use of $\beta(M)$. Since the PBH energy density at the formation time is given by $\beta(M)\bar{\rho}|_{k=aH}$, the current abundance of PBHs with in M–$M + \mathrm{d}\log M$ can be calculated as

$$\begin{aligned}\frac{\Omega_{\rm PBH}(M)h^2}{\Omega_{\rm c}h^2} &= \frac{\Omega_{\rm m}h^2}{\Omega_{\rm c}h^2}\left.\frac{\rho_{\rm PBH}}{\rho_{\rm m}}\right|_{\rm eq} = \frac{\Omega_{\rm m}h^2}{\Omega_{\rm c}h^2}\frac{1}{\rho_{\rm r,eq}}\left(\frac{a_{\rm f}}{a_{\rm eq}}\right)^{-3}\rho_{\rm PBH,f} = \frac{\Omega_{\rm m}h^2}{\Omega_{\rm c}h^2}\frac{T_{\rm f}}{T_{\rm eq}}\beta(M) \\ &= 6.09\times10^8\gamma^{1/2}\beta(M)\left(\frac{0.12}{\Omega_{\rm c}h^2}\right)\left(\frac{10.75}{g_{*\rm f}}\right)^{1/4}\left(\frac{M_\odot}{M}\right)^{1/2}, \end{aligned} \tag{4.1.33}$$

where the subscript f denotes the PBH formation time and $\Omega_{\rm m}$ ($\Omega_{\rm c}$) is the current density parameter of matter (DM). We used the recent value for the DM density $\Omega_{\rm c}h^2 = 0.12$ [7]. The total PBH abundance is given by its integration as

$$\Omega_{\rm PBH,tot}h^2 = \int \mathrm{d}\log M\,\Omega_{\rm PBH}(M)h^2. \tag{4.1.34}$$

For PBHs of less than 10^{15} g, the energy fraction $\beta(M)$ is generally used to be constrained. The current number density of PBHs can be also easily calculated as

$$n_{\rm PBH}(t_0) = \frac{\beta}{\gamma\frac{4\pi}{3}k^{-3}} = 33\,{\rm kpc}^{-3}\gamma^{1/2}(6.09\times10^8\beta)\left(\frac{M_\odot}{M}\right)^{3/2}\left(\frac{g_*}{10.75}\right)^{-1/4}, \tag{4.1.35}$$

where the comoving wavenumber k is normalized for the current scale factor a_0 to be unity. With use of this number density, $\rho_{\rm PBH}(t_0) = Mn_{\rm PBH}(t_0)$ should also reproduce the current PBH abundance (4.1.33).

The large coefficient in Eq. (4.1.33) obviously shows that PBHs should be quite rare objects at their formation time not to overclose the universe. That is because PBH is produced as a matter component during the radiation-dominated era and its relative abundance grows linearly in the scale factor. As a result, current PBH non-detection can constrain the amplitude of the primordial curvature perturbation as $\mathcal{P}_\zeta < \mathcal{O}(0.01)$ even for very small scales as we mention in detail in the next section.

4.2 Phenomenology

Despite its non-detection, so far many authors have been working on primordial black holes. That is why PBH can give a lot of suggestions for the physics of the early universe (even by its non-detection), or can be used as possible solutions of various astrophysical open questions. In this section, let us briefly introduce the phenomenology of PBH and the current situation of the PBH research.

4.2.1 Constraints on evaporating PBH

So far various observational constraints have been imposed on the abundance of PBH both of less and more than 10^{15} g. In this subsection, we review the constraints on the light and evaporating PBHs at first. The high energy particles emitted by PBH evaporation can affect the physics in the early universe or be directly detected today. From these predictions, the

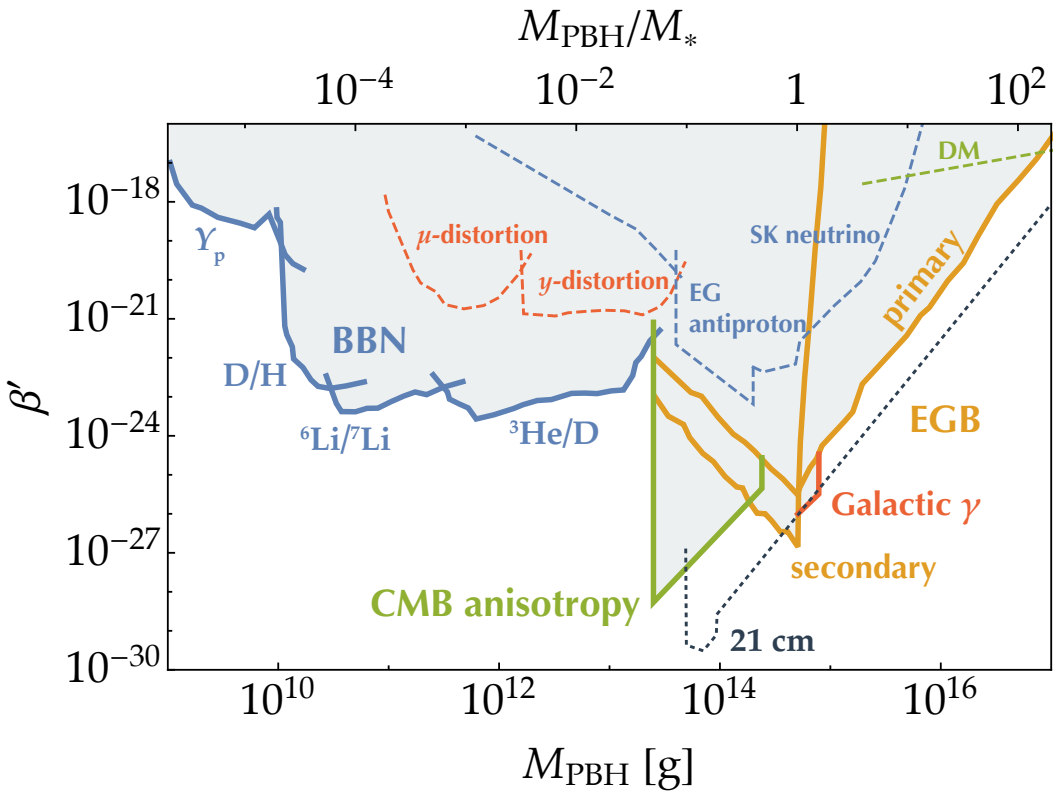

Figure 4.1. Several constraints on the energy fraction of evaporating PBHs summarized in Ref. [104]. The gray region shows the excluded parameters. PBHs with the initial mass $M_* \simeq 5 \times 10^{14}$ g evaporate away just now.

energy fraction $\beta(M)$ can be constrained. Conventionally, to remove the dependence of the uncertain parameters, the new parameter

$$\beta'(M) = \gamma^{1/2} \left(\frac{g_*}{106.75}\right)^{-1/4} \beta(M), \tag{4.2.1}$$

is used instead of $\beta(M)$ itself. All constraints described in this subsection are summarized in Fig. 4.1. We review Ref. [104] in this subsection.

Big-bang nucleosynthesis

PBHs evaporating away around the big-bang nucleosynthesis phase $t \sim 10^{-2}$–10^{12} s, corresponding to the PBH mass of $M \sim 10^9$–10^{13} g, can leave effects on the abundance of synthesized light elements. This has been a subject of long-standing interest and recently Carr et al. [104] updated the constraints with the detailed analysis particularly of the secondary long-lived hadrons such as pions, kaons, and nucleons.

Though we do not describe in detail here, let us briefly summarize their results. First the abundance of PBHs with mass $M \sim 19^9$–10^{10} g or lifetime $\tau \sim 10^{-2}$–10^2 s are constrained by the extra interconversion between protons and neutrons due to emitted mesons and antinucleons, which increases the neutron-proton freeze-out ratio as well as the final ^{4}He abundance. For PBHs of $M \sim 10^{10}$–10^{12} g, corresponding with $\tau \sim 10^2$–10^7 s, hadrodissociation

processes are important and they increase the fragments deuterons and ^{6}Li, which would be strongly constrained. Finally, for $M \sim 10^{12}$–10^{13} g and $\tau \sim 10^7$–10^{12} s, the hadrodissociation is already insignificant since the energetic neutrons decay before inducing it. Instead, photodissociation processes are efficient, which cause the overproduction of ^{3}He or D.

As observational constraints on the light elements abundance, they used $Y_{\rm p} = 0.2516 \pm 0.0080$ [105–110], $\mathrm{D/H} < 5.16 \times 10^{-5}$ [111, 112], $^3\mathrm{He/D} < 1.37$ [113], and $^6\mathrm{Li}/^7\mathrm{Li} < 0.302$ [114, 115]. By comparing them with the prediction under the existence of PBHs, they obtained the constraints on the PBH formation rate, which are summarized in Fig. 4.1 as thick blue lines.

Cosmic microwave background and 21 cm signature

The evaporated high energy particles can also affect the spectrum of the cosmic microwave background. First, for PBHs evaporating after the recombination, the emitted particles contribute to the reionization of matter and decrease the small scale power spectrum of CMB due to the Thomson scattering by the free electrons. Originally Zhang et al. [116] considered these effects to constrain the decaying DM, and Carr et al. [104] modified their analysis to the PBH case. The resultant constraints are given by

$$\beta' < 3 \times 10^{-30} \left(\frac{f_{\rm H}}{0.1}\right)^{-1} \left(\frac{M}{10^{13}\,\mathrm{g}}\right)^{3.1}, \qquad (2.5 \times 10^{13}\,\mathrm{g} \lesssim M \lesssim 2.4 \times 10^{14}\,\mathrm{g}), \tag{4.2.2}$$

where $f_{\rm H} \simeq 0.1$ is the fraction of emission which comes out in electrons and positrons. Here the lower mass limit corresponds to black holes evaporating at recombination and the upper one to those evaporating at a redshift 6 [117], after which the reionization is almost completed and the opacity is too low for the emitted electrons and positrons to heat the matter much. This constraint is shown as a thick green line in Fig. 4.1.

The reionization history will be also severely constrained by future 21 cm observations. Mack and Wesley [118] have shown that PBHs in the range $5 \times 10^{13}\,\mathrm{g} < M < 10^{17}\,\mathrm{g}$ can be constrained in this way, and their concrete results are shown as a navy blue dotted line in Fig. 4.1.

Slightly before the recombination, the evaporation makes the CMB spectrum deviate from the Planck distribution since the heated photon cannot be perfectly rethermalized near the recombination. Those spectral distortions are parametrized as μ and y-distortions, which are observationally constrained as $|\mu| < 9 \times 10^{-5}$ and $y < 1.5 \times 10^{-5}$ [119]. They were first considered in the context of decaying particle models [120], and Tashiro and Sugiyama [121] applied them to PBH constraints. The concrete constraints are shown as red dashed lines in Fig. 4.1. They are not significant currently, but the future space mission like PIXIE [122] and PRISM [123], which will improve the constraints on μ and y down to $\mathcal{O}(10^{-8}$–$10^{-9})$, will make them considerable.

Extragalactic and galactic photon background

As a direct observation of the Hawking radiation by PBHs, one can consider the extragalactic diffuse γ-ray background. The origin of the diffuse photon has not been clarified yet, but at least the predicted photon flux emitted by PBHs must not exceed the observed value. Here let us show the analytic estimation of such constraints with use of the fitting formula of the

observed flux [124]:

$$I(E_\gamma) = 2.743 \times 10^{-3}\,\mathrm{cm}^{-2}\mathrm{s}^{-1}\mathrm{sr}^{-1}\left(\frac{E_\gamma}{1\,\mathrm{MeV}}\right)^{-1.1}. \tag{4.2.3}$$

The treatment is different for PBHs with initial masses below and above $M_* \simeq 5 \times 10^{14}$ g with which the lifetime of the PBH is just the current age of the universe. For $M > M_*$, the temperature of PBH $T_{\rm BH} = M_{\rm Pl}^2/M$ is almost constant and the peak energy of emitted photons is given by this temperature. With its lifetime τ, the number of total emitted photons is roughly $M/T_{\rm BH} = M^2/M_{\rm Pl}^2$. Therefore the current number density of the total photons emitted by now can be estimated by

$$n_{\gamma 0} \sim n_{\rm PBH}(t_0)\left(\frac{M}{T_{\rm BH}}\right)\left(\frac{t_0}{\tau}\right). \tag{4.2.4}$$

With this photon number density, the photon flux is then $I = \frac{c}{4\pi} n_{\gamma 0}$ in units of $\mathrm{cm}^{-2}\mathrm{s}^{-1}\mathrm{sr}^{-1}$. This flux should not exceed the observed one (4.2.3) at the peak energy $E_{\gamma 0}^{\rm pri} \sim T_{\rm BH}$, and then the constraints on the PBH abundance is

$$I(E_{\gamma 0}^{\rm pri}) > \frac{c}{4\pi} n_{\rm PBH}(t_0)\left(\frac{M}{T_{\rm BH}}\right)\left(\frac{t_0}{\tau}\right), \quad \Leftrightarrow \quad \beta' \lesssim 10^{-26}\left(\frac{M}{M_*}\right)^{3.6}, \quad (\text{for } M > M_*). \tag{4.2.5}$$

On the other hand, the light PBHs of $M < M_*$ emit the strongest radiations at their last phase, at which the Hawking temperature will exceed the QCD scale. In this case, the flux of the secondary photons from the decay of the hadrons produced by fragmentation of emitted quarks and gluons and by the decay of gauge bosons dominates that of the directly emitted primary photons. The spectrum of secondary photons was first analyzed by MacGibbon and Webber [125], and they showed that the spectrum has its peak around $E_\gamma \simeq m_{\pi^0}/2 \simeq 68\,\mathrm{MeV}$ independent of the Hawking temperature because the secondary photons are dominated by the 2γ-decay of soft neutral pions which are practically at rest. Then the secondary photon number at the peak scale per unit time and unit energy is given by

$$\frac{\mathrm{d}\dot{N}_\gamma^{\rm sec}}{\mathrm{d}E_\gamma}(E_\gamma = m_{\pi^0}/2) \sim \frac{T_{\rm BH}}{m_{\pi^0}/2}, \tag{4.2.6}$$

and the corresponding current flux is

$$I^{\rm sec} = \frac{c}{4\pi} n_{\rm PBH}(t_0)\frac{m_{\pi^0}}{2}\frac{\mathrm{d}\dot{N}_\gamma^{\rm sec}}{\mathrm{d}E_\gamma}(E_\gamma = m_{\pi^0}/2)\tau. \tag{4.2.7}$$

Note that the flux is defined as the photon number for each logarithmic energy bin. The current peak energy has been redshifted from the PBH evaporation time as

$$E_{\gamma 0} = \frac{m_{\pi^0}}{2}\frac{a(\tau)}{a_0} = \frac{m_{\pi^0}}{2}\left(\frac{\tau}{t_0}\right)^{2/3} = \frac{m_{\pi^0}}{2}\left(\frac{M}{M_*}\right)^2, \tag{4.2.8}$$

supposing the evaporation time τ is in the matter-dominated era. Finally one can obtain the constraints as

$$I(E_{\gamma 0}) > I^{\rm sec}, \quad \Leftrightarrow \quad \beta' \lesssim 5 \times 10^{-27} \left(\frac{M}{M_*}\right)^{-2.7}, \quad (\text{for } M < M_*). \tag{4.2.9}$$

Carr et al. [104] calculated the current diffuse photon flux more precisely and obtained the constraints with use of the observed flux by HEAO 1 and other balloon experiments in the 3–500 keV range [126], COMPTEL in the 0.8–30 MeV range [127], EGRET in the 30–200 MeV range [128], and Fermi LAT in 200 MeV–102 GeV range [129]. They are summarized in Fig. 4.1 as thick orange lines. PBHs of $M \sim M_*$ in our galaxy can also give the galactic γ-ray background. The corresponding constraints given by Carr et al. [104] are shown by a thick red line.

Extragalactic antiproton and neutrino

As other cosmic ray components, extragalactic antiprotons and neutrinos can be considered. The constraints by extragalactic antiprotons given by Carr et al. [104] are shown by a blue dashed line. They first adopted the upper mass limit $M \lesssim 2 \times 10^{14}$ g, corresponding with the PBHs evaporating before the galaxy formation. That is because more massive PBHs will be clustered in galaxies and the leakage time for emitted antiproton to escape galaxies has a lot of uncertainties. On the other hand, the emitted antiprotons have to survive by now against the $p\bar{p}$ annihilation in the cosmological background. The mean rate of this annihilation is given by $\Gamma_{p\bar{p}}(t) \sim 2 \times 10^{-22} (t/t_0)^{-2}\,{\rm s}^{-1}$, and therefore the surviving condition after the evaporation time τ reads

$$\int_\tau^{t_0} \Gamma_{p\bar{p}}(t')\mathrm{d}t' < 1, \quad \Leftrightarrow \quad \tau \gtrsim 1.3\,{\rm Myr}. \tag{4.2.10}$$

It gives the lower limit of mass as $M \gtrsim 4 \times 10^{13}$ g for the extragalactic antiproton constraints.

Relic neutrinos can also give constraints and the results by Carr et al. [104] are shown by blue dashed lines. Potentially they can constrain PBHs whose lifetime is more than the time of neutrino decoupling ($\tau \gtrsim 1\,{\rm s}$), corresponding with the lower mass limit of $M \gtrsim 10^9$ g. However Super-Kamiokande has its sensitivity only for high energy neutrinos $E_{\bar{\nu}_e 0} > 19.3$ MeV [130], and therefore the constraints for light PBHs are quite limitted.

Other constraints

For $M \gtrsim M_*$, PBHs have not been evaporated away yet, so at least their current abundance must not exceed the observed DM abundance. The constraints from this condition are directly given by Eq. (4.1.33) and shown by a green dashed line in Fig. 4.1.

Basically PBHs evaporating before the BBN phase cannot be constrained since the emitted radiations are completely rethermalized and therefore they merely change the baryon-to-photon ratio $\eta_{\rm B}$. If one assumes that the original $\eta_{\rm B}$ is at most unity, the constraints can be given so that the baryon should not be diluted further than the observed value $\eta_{\rm B} \sim 10^{-9}$. Noting that the PBH energy density grows as linearly in the scale factor compared to the radiation, and the PBH formation and evaporation time are given by $t_{\rm f} \sim M/M_{\rm Pl}^2$ and

$\tau \sim M^3/M_{\rm Pl}^4$, the corresponding constraints are [131]

$$\beta' < 10^9 \left(\frac{\tau}{t_{\rm f}}\right)^{-1/2} \sim 10^9 \left(\frac{M}{M_{\rm Pl}}\right)^{-1} \sim 10^{-5} \left(\frac{M}{10^9\,{\rm g}}\right)^{-1}, \quad (M < 10^9\,{\rm g}). \tag{4.2.11}$$

The evaporating PBH can produce any other particles predicted in theories beyond the standard model. For example, in supersymmetry or supergravity, the lightest supersymmetric particle (LSP) can be stable and become a candidate for DM. If such a particle exists, the condition that the current abundance of emitted LSPs do not exceed the DM abundance can give constraints as [132]

$$\beta' \lesssim 10^{-18} \left(\frac{M}{10^{11}\,{\rm g}}\right)^{-1/2} \left(\frac{m_{\rm LSP}}{100\,{\rm GeV}}\right)^{-1}, \quad (M < 10^{11}\,{\rm g}(m_{\rm LSP}/100\,{\rm GeV})^{-1}). \tag{4.2.12}$$

Also PBHs may not be evaporated completely but leave stable Planck-mass relics as pointed out by MacGibbon [133]. In this case, the Planck-mass relics must not exceed the DM abundance and this condition implies [134]

$$\beta' < 2 \times 10^{-28} \kappa^{-1} \left(\frac{M}{M_{\rm Pl}}\right)^{3/2}, \tag{4.2.13}$$

for the mass range

$$\left(\frac{T_{\rm R}}{M_{\rm Pl}}\right)^{-2} < \frac{M}{M_{\rm Pl}} < 10^{11} \kappa^{2/5}, \tag{4.2.14}$$

where the relic mass is parametrized as $m_{\rm relic} = \kappa M_{\rm Pl}$ and $T_{\rm R}$ denotes the reheating temperature. The upper mass limit arises because PBHs larger than this dominate the total density before they evaporate.

We did not show these constraints (4.2.11), (4.2.12), and (4.2.13) since they depends on several model assumptions.

4.2.2 Non-evaporating PBH and dark matter

PBHs of more than about 10^{15} g can survive until now and they can ba a candidate of DM. Therefore the observational constraints on the abundance of such PBHs are so important. Compared with evaporating PBHs, the constraints on non-evaporating PBHs are often shown in terms of the fraction to DM, $f(M) = \Omega_{\rm PBH}(M)/\Omega_{\rm DM}$. In Fig. 4.2, we summarized the existing constraints, which are described in detail below. This figure shows the DM window is sill opened in the mass range of $\sim 10^{21}$–10^{24} g. Basically we review Ref. [99] in this subsection.

Evaporation constraints

The constraint shown by a purple line is the same as that from the extragalactic γ-ray background, which was described in the previous subsection and shown by thick orange lines in Fig. 4.1. But here we used the simple analytic expression:

$$\text{EG}\gamma\text{:} \qquad f(M) \lesssim 2 \times 10^{-8} \left(\frac{M}{M_*}\right)^{3+\epsilon}, \qquad (M > M_* = 5 \times 10^{14}\,{\rm g}), \tag{4.2.15}$$

following Ref. [99], where ϵ is a fitting parameter of the observed extragalactic intensity $I^{\rm obs} \propto E^{-(1+\epsilon)} \propto M^{1+\epsilon}$. ϵ lies between 0.1 (favored in Ref. [124]) and 0.4 (favored in Ref. [128]) and we adopt $\epsilon = 0.2$ in Fig. 4.2.

Lensing constraints

To observe the point-like objects such as BHs, the gravitational lensing is a strong tool. The constraints using the lensing are indicated by blue lines in Fig. 4.2.[2]

First, the constraints on very low mass objects come from the femtolensing of γ-ray bursts. The recent work by Barnacka et al. [137] shows the constraints which can be approximated as

$$\text{Femto:} \qquad f(M) < 0.1, \qquad (5 \times 10^{16}\,{\rm g} < M < 10^{19}\,{\rm g}). \tag{4.2.16}$$

The precise form is shown in Fig. 4.2.

MACHO and EROS collaborations proceed microlensing observations of stars in the Large and Small Magellanic Clouds. First MACHO observed 17 events and claimed that these were consistent with compact objects of $\sim 0.5 M_\odot$ contributing 20% of the halo mass [138]. However the later studies suggested that the halo contribution of $\sim 0.5 M_\odot$ PBHs could be at most 10% [139]. The EROS experiment obtained more stringent constraints by arguing that some of the MACHO events were due to self-lensing or halo clumpiness [140], and excluded $6 \times 10^{-8} M_\odot < M < 15 M_\odot$ compact objects from dominating the halo. Combining the earlier MACHO results [141] with the EROS-I and EROS-II results extended the upper bound to $30 M_\odot$ [140]. The constraints can be roughly expressed as

$$\text{EROS/MACHO:} \qquad f(M) < \begin{cases} 1, & (6 \times 10^{-8} M_\odot < M < 30 M_\odot), \\ 0.1, & (10^{-6} M_\odot < M < M_\odot), \\ 0.04, & (10^{-3} M_\odot < M < 0.1 M_\odot). \end{cases} \tag{4.2.17}$$

Recent Kepler data considerably improved the limits in the low-mass range as [142]

$$\text{Kepler:} \qquad f(M) < 0.3, \qquad (2 \times 10^{-9} M_\odot < M < 10^{-7} M_\odot). \tag{4.2.18}$$

Millilensing of compact radio sources [143] gives a limit which can be approximated as

$$\text{mLQ:} \qquad f(M) < \begin{cases} \left(\dfrac{M}{2 \times 10^4 M_\odot} \right)^{-2}, & (M < 10^5 M_\odot), \\ 0.06, & (10^5 M_\odot < M < 10^8 M_\odot), \\ \left(\dfrac{M}{4 \times 10^8 M_\odot} \right)^{2}, & (M > 10^8 M_\odot). \end{cases} \tag{4.2.19}$$

[2] In the process of finalizing this thesis, Niikura et al. [135] put a new stringent constraint in the mass range $10^{20}\,{\rm g} < M < 10^{28}\,{\rm g}$, making use of the Subaru Hyper Suprime-Cam(HSC) dense cadence data. When one combines it with other observational constraints summarized in this section, only the mass region $\simeq 10^{20}\,{\rm g}$ remains for PBHs as all DM. In Ref. [136], we showed that the PBHs, which have an inflationary origin, can still be a dominant component of DM of mass $\simeq 10^{20}\,{\rm g}$, taking the model which we describe in the next chapter.

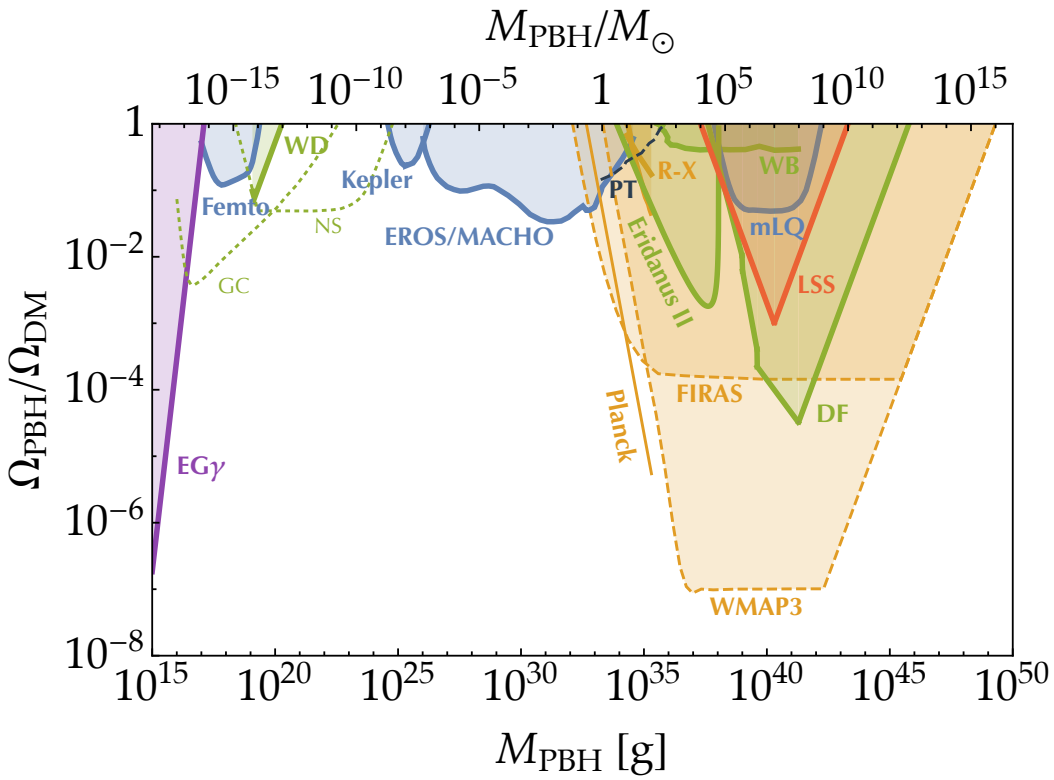

Figure 4.2. Constraints on the current abundance of the non-evaporating PBHs. The shaded regions are excluded. The effects are extragalactic γ-rays from evaporation (EGγ) [104], femtolensing of γ-ray bursts (Femto) [137], white-dwarf explosions (WD) [144], survival of star compact remnants in globular clusters (GC) [145], neutron-star capture constraints (NS) [146], Kepler microlensing of stars (Kepler) [142], accretion radio and X-ray (R-X) [147], pulsar timing (PT) [148], EROS/MACHO microlensing of stars (EROS/MACHO) [140], survival of star cluster in Eridanus II (Eridanus II) [149], wide binary disruption (WB) [150], dynamical friction on halo objects (DF) [151], millilensing of quasars (mLQ) [143], large scale Poisson noise (LSS) [104, 152], and accretion effects on CMB (WMAP3 and FIRAS [153], and Planck [154]). The color of lines indicates the observation methods: extragalactic γ-ray (purple), gravitational lensing (blue), dynamical constraints (green), large scale structure (red), pulsar timing (navy blue), and accretion effects on CMB (orange). GC and NS are plotted by dotted lines since they assume the significant DM density in globular clusters though there is no observational evidence [155, 156] and they seem to be questionable. FIRAS and WMAP3 (Planck) are shown by dashed (thin) lines because they are not the direct observations of the current BHs and involve several uncertainties of the accretion physics [99, 157, 158]. Finally PT are shown by the dashed line because it requires the further 30-year observing.

Dynamical constraints

The existence of PBHs or their movement in galaxies will affect the evolution of stars or the property of interstellar media. These dynamical constraints are shown by green lines in Fig. 4.2.

For low-mass range $\sim 10^{19}$–10^{20} g, Graham et al. [144] claimed that the transition of PBHs through a white dwarf causes localized heating due to dynamical friction and induce its supernova explosion. The abundance of these PBHs is constrained by the observation of the white dwarf population near the galactic center and also the observed supernova rate.

The constraints can be written as

$$\text{WD:} \qquad f(M) < \left(\frac{0.4\,\mathrm{GeV/cm^3}}{\rho_{\mathrm{DM}}}\right)\left(\frac{M}{2\times10^{20}\,\mathrm{g}}\right), \qquad (M < 10^{20}\,\mathrm{g}), \tag{4.2.20}$$

where ρ_{DM} is the local dark matter density. We plot the precise constraints in the case of $\rho_{\mathrm{DM}} = 0.4\,\mathrm{GeV/cm^3}$.

Binary star systems with wide separation are vulnerable to disruption from encounters with compact objects. Observations of wide binaries in our galaxy thus constrain the abundance of PBHs. According to Quinn et al. [150], the constraint became

$$\text{WB:} \qquad f(M) < \begin{cases} \left(\dfrac{M}{500M_\odot}\right)^{-1}, & (500M_\odot < M \lesssim 10^3 M_\odot), \\ 0.4, & (10^3 M_\odot \lesssim M < 10^8 M_\odot). \end{cases} \tag{4.2.21}$$

Carr and Sakellariadou [151] pointed out that massive PBHs will be dragged into the nucleus of our galaxy by the dynamical friction of the spheroid stars and PBHs themselves, which leads to excessive nuclear mass unless

$$\text{DF:} \quad f(M) < \begin{cases} \left(\dfrac{M}{2\times10^4 M_\odot}\right)^{-10/7}\left(\dfrac{r_{\mathrm{c}}}{2\,\mathrm{kpc}}\right)^2, & (M < 5\times10^5 M_\odot), \\ \left(\dfrac{M}{4\times10^4 M_\odot}\right)^{-2}\left(\dfrac{r_{\mathrm{c}}}{2\,\mathrm{kpc}}\right)^2, & \left(5\times10^5 M_\odot \ll M < 2\times10^6 M_\odot\left(\frac{r_{\mathrm{c}}}{2\,\mathrm{kpc}}\right)\right), \\ \left(\dfrac{M}{0.1M_\odot}\right)^{-1/2}, & \left(2\times10^6 M_\odot\left(\frac{r_{\mathrm{c}}}{2\,\mathrm{kpc}}\right) < M < 10^7 M_\odot\right), \\ \dfrac{M}{M_{\mathrm{halo}}}, & (M > 10^7 M_\odot), \end{cases} \tag{4.2.22}$$

where $r_{\mathrm{c}} \sim 2\,\mathrm{kpc}$ and $M_{\mathrm{halo}} \sim 3\times10^{12} M_\odot$ represent the core radius and mass of our galactic halo. The last constraint comes from the requirement that at least one PBH should be in the galactic halo to be constrained.

Recently Brandt [149] claims that a mass above $5M_\odot$ is excluded by the fact that a star cluster near the center of the dwarf galaxy Eridanus II has not been disrupted by PBHs. His constraint can be written as

$$\text{Eridanus II:} \qquad f(M) \lesssim \frac{0.5\left(1+\frac{0.046M_\odot\,\mathrm{pc^{-3}}}{\rho}\right)\left(\frac{10M_\odot}{M}\right)\left(\frac{\sigma}{10\,\mathrm{km\,s^{-2}}}\right)}{1+0.1\log\left[\frac{10M_\odot}{M}\left(\frac{\sigma}{10\,\mathrm{km\,s^{-1}}}\right)^2\right]}, \tag{4.2.23}$$

where ρ and σ are the density and velocity dispersion of the dark matter at the center of the galaxy Eridanus II. In Fig. 4.2, we take $\rho = 0.1M_\odot\,\mathrm{pc^{-3}}$ and $\sigma = 5\,\mathrm{km\,s^{-1}}$.

Capela et al. claimed that white dwarfs and neutron stars would be destroyed by PBHs absorbed into their progenitor stars at their formation (GC) [145], or by PBH capture due to dynamical friction (NS) [146] in globular clusters. Thus the observation of white dwarfs or neutron stars in globular clusters can constrain the PBH abundance. However their constraints assume so high dark matter density in globular clusters as $\rho_{\mathrm{DM}} \sim 2\times10^3\,\mathrm{GeV/cm^3}$

though observations of globular clusters show no evidence of significant dark matter content in such systems [155, 156]. As a related limit, it was suggested that tidal deformation of a neutron star could lead to an efficient energy dissipation and capture of a black hole, leading to stronger constraints [159], but such energy losses are uncertain and they are likely to be suppressed for realistic parameters and velocities in excess of the speed of sound [160, 161]. So these constraints seem to be questionable and then we plotted them by dotted lines.

Large scale structure

For large mass region, the number density of PBHs should be small and they get to show the point-like property even on the large scale, deviating from the fluid picture. That is, the two point function of the PBH density perturbation includes the delta function component:

$$\langle \delta_{\rm PBH}(\mathbf{x})\delta_{\rm PBH}(\mathbf{y})\rangle \supset A\delta^{(3)}(\mathbf{x}-\mathbf{y}), \tag{4.2.24}$$

which yields the constant offset to the matter power spectrum. Afshordi et al. [152] used observations of the Lyman-α forest to obtain an upper limit of about $10^4 M_\odot$ on the mass of any PBHs which provide the dark matter. Carr et al. [104] analytically extended it to the case where the PBHs only provide a fraction of the dark matter. Their constraints can be written as

$$\text{LSS:} \qquad f(M) < \begin{cases} \left(\dfrac{M}{10^4 M_\odot}\right)^{-1}\left(\dfrac{M_{\rm Ly\alpha}}{10^{10}M_\odot}\right), & (M < 10^7 M_\odot), \\ \left(\dfrac{M}{10^{10}M_\odot}\right)\left(\dfrac{M_{\rm Ly\alpha}}{10^{10}M_\odot}\right)^{-1}, & (M > 10^7 M_\odot). \end{cases} \tag{4.2.25}$$

The lower expression corresponds to having at least one PBH per the mass of the Lyman-α scale $M_{\rm Ly\alpha} \sim 10^{10} M_\odot$.

Pulsar timing

Schutz and Liu [148] suggested the constraints by the pulsar timing. The transit of BHs induces the increase of optical path length due to the deep gravitational potential. Therefore it can be detected by the modulation of the pulse period. With future 30-year observations of the currently known pulsars, the expected constraints can be written as

$$\text{PT:} \qquad f(M) < 0.1\left(\frac{M}{M_\odot}\right)^{1/3}, \qquad (M_\odot < M \lesssim 1000 M_\odot). \tag{4.2.26}$$

We plot the precise constraints by the navy blue dashed line.

Accretion effects

Though the Hawking radiation itself of PBHs with the initial mass $M > M_* \simeq 5\times 10^{14}\,\mathrm{g}$ is neglegible, they can emit the high energy radiation through the accretion process, which might affect the thermal history of the universe. Ricotti et al. [153] studied such accretion

effects on the optical depth or CMB spectral distortion in detail, which can be respectively constrained by WMAP3 as

$$\text{WMAP3:} \qquad f(M) < \begin{cases} \left(\dfrac{M}{30M_\odot}\right)^{-2}, & (30M_\odot < M \lesssim 10^4 M_\odot), \\ 10^{-5}, & (10^4 M_\odot \lesssim M < 10^{11} M_\odot), \\ \dfrac{M}{M_{\ell=100}}, & (M > 10^{11} M_\odot), \end{cases} \tag{4.2.27}$$

and by FIRAS as

$$\text{FIRAS:} \qquad f(M) < \begin{cases} \left(\dfrac{M}{M_\odot}\right)^{-1}, & (M_\odot < M \lesssim 10^3 M_\odot), \\ 0.015, & (10^3 M_\odot \lesssim M < 10^{14} M_\odot), \\ \dfrac{M}{M_{\ell=100}}, & (M > 10^{14} M_\odot). \end{cases} \tag{4.2.28}$$

The last expressions of both of them were not included in original Ref. [153] but are required to have at least one PBH on the scale associated with the CMB anisotropies for $\ell = 100$ mode, $M_{\ell=100} \sim 10^{16} M_\odot$ [104]. Recently Chen et al. [154] updated the WMAP constraints with use of the Planck data (Planck). These constraints are shown just by dashed or thin lines in Fig. 4.2 since they are not direct constraints on the current PBH abundance and potentially involve several uncertainties of the accretion dynamics as pointed in Ref. [99, 157, 158].[3]

Gaggero et al. [147] model the accretion of gas on to massive PBHs in our Milky Way and predict the radio and X-ray emissions. Comparing them with the VLA radio catalog and the NuSTAR X-ray catalog, they show the constraints on $10 M_\odot \lesssim M \lesssim 100 M_\odot$ (R-X).

4.2.3 Constraints on primordial perturbations

So far we reviewed several constraints on PBH abundance. From them, the first merit of considering PBHs arises; the PBH abundance is related with the amplitude of the primordial perturbations even on much small scale than the CMB scale and so on. Namely the limit on the PBH abundance can be extended to the constraints on the amplitude of the primordial perturbations because too large primordial perturbations inevitably overproduce PBHs basically. In this section, let us summarize the constraints on the primordial curvature perturbations, inspired by e.g. Ref. [102].

To obtain the conservative constraints, we assume the delta-function-like peak on the power spectrum of the curvature perturbations on some scale $k_{\rm PBH}$ as

$$\mathcal{P}_\zeta(k) = \mathcal{P}_\zeta(k_{\rm PBH}) \delta(\log k - \log k_{\rm PBH}). \tag{4.2.29}$$

Here the PBH mass is associated with the scale $k_{\rm PBH}$ by Eq. (4.1.26). In this section, we fix the parameters γ and $g_{*\rm f}$ to $\gamma = 1$ and $g_{*\rm f} = 106.75$ for simplicity. Then the PBH mass and

[3] While preparing this thesis, Ali-Haïmoud and Kamionkowski [162] reanalyzed the accretion constraints with the Planck data and conclude that updated constraints are weaker by at least two orders of magnitude than those by Ricotti et al. [153].

the current abundance can be approximated by

$$M_{\rm PBH} \sim 13 M_\odot \left(\frac{k}{10^6\,{\rm Mpc}^{-1}} \right)^{-2}, \tag{4.2.30}$$

and

$$f(M) \sim 3.4 \times 10^8 \beta(M) \left(\frac{M_\odot}{M} \right)^{1/2}. \tag{4.2.31}$$

$\beta(M)$ is given by

$$\beta(M) = \frac{1}{2} {\rm Erfc} \left(\frac{\delta_{\rm th}}{\sqrt{2}\sigma_R} \right), \tag{4.2.32}$$

where

$$\sigma_R^2 = \frac{16}{81} \int {\rm d}\log k \left(\frac{k}{k_{\rm PBH}} \right)^4 \tilde{W}^2 \left(\frac{k}{k_{\rm PBH}} \right) \mathcal{P}_\zeta(k) = \frac{16}{81{\rm e}} \mathcal{P}_\zeta(k_{\rm PBH}). \tag{4.2.33}$$

Here we adopt the Gaussian window $\tilde{W}(x) = {\rm e}^{-x^2/2}$. The threshold value $\delta_{\rm th}$ will be fixed to the analytic prediction $\delta_{\rm th} = w = 1/3$. Note that $\beta(M)$ is now equal to $\beta'(M)$ with the current parameter fixing.

Now the PBH abundance is completely related with the primordial curvature perturbations and the amplitude $\mathcal{P}_\zeta(k_{\rm PBH})$ can be constrained with use of the limits previously shown. In Fig. 4.3, we plot the corresponding upper bound of the amplitude $\mathcal{P}_\zeta(k_{\rm PBH})$. Navy blue lines are given by the observational constraints shown in Fig. 4.1 and 4.2. The blue line corresponds with the DM constraint $f(M) \leq 1$. The limits corresponding with the accretion effects on CMB (WMAP3 and FIRAS) are shown by green dotted lines. We also include the constraints by the μ-distortion due to the Silk damping and secondary gravitational waves, which are represented by red plain and dot-dashed lines respectively. We describe them in the rest of this section.

Note that the PBH constraints are not so strong but can be imposed even on very small scale $10\,{\rm Mpc} > k^{-1} > 10^{-19}\,{\rm Mpc}$. That is one of the advantages of PBH. The PBH constraints are almost scale-invariant and can be approximated as $\mathcal{P}_\zeta \lesssim \mathcal{O}(0.01)$. It can be easily understood. The constraints on the PBH energy fraction are around $10^{-18} < \beta' < 10^{-28}$, which corresponds with 9–11σ rarity. Namely the PBH formation threshold $\zeta_{\rm th}$ should be 9–11 times larger than the square root of the variance of the curvature perturbations, which can be approximated by $\mathcal{P}_\zeta^{1/2}(k_{\rm PBH})$. Therefore one can obtain rough PBH constraints as

$$\zeta_{\rm th} \gtrsim (9\text{–}11) \times \mathcal{P}_\zeta^{1/2}(k_{\rm PBH}), \quad \Leftrightarrow \quad \mathcal{P}_\zeta(k_{\rm PBH}) \lesssim \mathcal{O}(0.01), \tag{4.2.34}$$

almost scale independently. Here we used $\zeta_{\rm th} \sim \mathcal{O}(1)$.

4.2.4 LIGO event and secondary gravitational wave

In the beginning of 2016, the report by LIGO/Virgo collaboration excited the world; they succeeded the direct detection of gravitational waves for the first time [163]. The signal comes from the merger of a binary black hole whose masses are estimated as $36^{+5}_{-4} M_\odot$ and

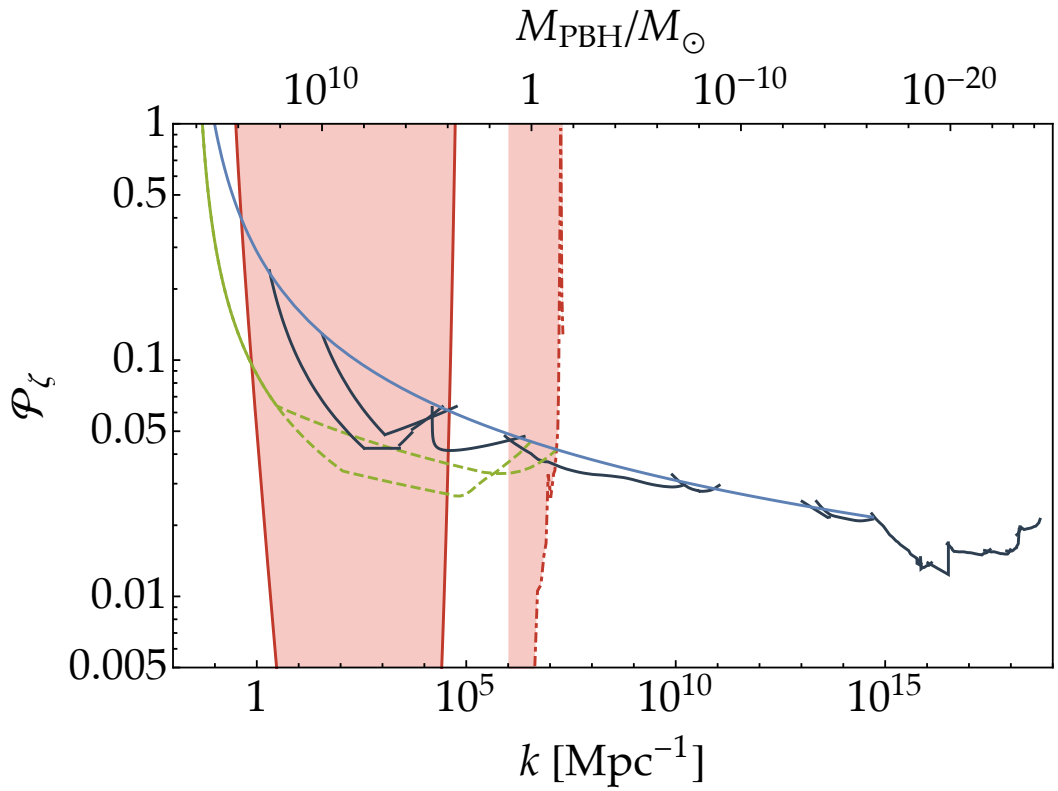

Figure 4.3. The upper bound on the power spectrum of the primordial curvature perturbations from the non-detection of PBH. Navy blue lines are given by the observational PBH constraints shown previously. The blue line corresponds with $f(M) \leq 1$. Green dotted lines come from the accretion constraints (WMAP3 and FIRAS). We also include the constraints by μ-distortion (red plain) and the secondary gravitational waves (red dot-dashed).

$29^{+4}_{-4} M_\odot$. The suggestive thing is these black holes are relatively massive and indeed they are the most massive stellar black holes which human beings have detected. Following this, the three groups (Bird et al. [157], Clesse and García-Bellido [158], and Sasaki et al. [164]) independently proposed the possibility that those black holes might be PBHs.

Bird et al. and Clesse and García-Bellido basically concentrated on the binary PBH formation from the pass and capture of each other in the DM halos. Then they found that $30 M_\odot$ PBHs should dominate the DM component to explain the merger rate inferred by LIGO, 9–240 Gpc^{-3} yr^{-1} [165]. On the other hand Sasaki et al. discussed another binary formation mechanism; they considered the free fall of PBHs toward each other in the radiation-dominated era. This mechanism is much more efficient and the resultant orbit of binary PBH tends to be eccentric. Then the merger rate can be significantly enhanced and the required fraction of $30 M_\odot$ PBH is around $f \sim 5 \times 10^{-4}$–5×10^{-3}, being marginally consistent with the accretion constraints at that time. After that, Eroshenko [166] claimed that the merger rate would be worse if one takes account of the effect of the matter perturbation, resulting in the slightly higher fraction requirement as $f \sim 2 \times 10^{-3}$–2×10^{-2}. Also Chen et al. [154] reported that the accretion constraints would be stronger by around two orders of magnitude with use of the recent Planck data. However both of the binary PBH formation rate and the accretion constraints involve several uncertainties and therefore the possibility of $30 M_\odot$

PBHs for LIGO events is still worth considering.

In these circumstances, recently another constraint on $30M_\odot$ PBHs is refocused on. That is secondary gravitational waves. At the linear order, the scalar perturbations are separated from the metric tensor perturbations (i.e. gravitational wave), but beyond the linear order, the scalar modes can source the tensor perturbations. If one considers the PBH formation from the large density perturbations, this effect cannot be negligible. Eq. (4.1.26) indicates that $O(10)M_\odot$ PBHs correspond with parsec scale perturbations, where the pulsar timing array observations have their sensitivities. Therefore the secondary gravitational waves accompanied by $30M_\odot$ PBH formation would be detected or excluded by PTA as first pointed out by Saito and Yokoyama [167, 168]. However there exist several notation confusions in the literature, so let us resummarize the secondary GW constraints in this subsection, following Ref. [53].

Here let us review the energy of the gravitational wave at first. The metric with the linear tensor perturbation can be written as,

$$g_{00} = -a^2, \qquad g_{ij} = a^2\left(\delta_{ij} + \frac{1}{2}h_{ij}\right), \tag{4.2.35}$$

and its inverse is,

$$g^{00} = -a^{-2}, \qquad g^{ij} = a^{-2}\left(\delta^{ij} - \frac{1}{2}h^{ij}\right), \tag{4.2.36}$$

at the leading order. h_{ij} is a transverse-traceless tensor perturbation, $\partial_i h^i{}_j = h^i{}_i = 0$, and its upper indices are defined by $h^{ij} = \delta^{ik}\delta^{jl}\delta_{kl}$. In this normalization, the second order action for the tensor perturbation reads

$$S_h = \frac{M_{\rm Pl}^2}{32}\int \mathrm{d}\eta \mathrm{d}^3x\, a^2\left(\left(h'_{ij}\right)^2 - \left(\nabla h_{ij}\right)^2\right), \tag{4.2.37}$$

where η is the conformal time and prime denotes a derivative with respect to η. Therefore, in the subhorizon limit where the time derivative of the scale factor is negligible, the energy density of graviton would be given by

$$\rho_{\rm GW} = \frac{M_{\rm Pl}^2}{32}a^{-2}\left\langle h'_{ij}h'_{ij} + h_{ij,k}h_{ij,k}\right\rangle \simeq \frac{M_{\rm Pl}^2}{16}a^{-2}\overline{\langle h_{ij,k}h_{ij,k}\rangle}. \tag{4.2.38}$$

The overline stands for the oscillation average to fulfill $\overline{\langle h'^2\rangle} \simeq \overline{\langle(\nabla h)^2\rangle}$. Then it can be related with the amplitude of the Fourier mode of h.

It is useful to decompose the tensor perturbation into two polarizations as

$$h_{ij}(\eta, \mathbf{x}) = \int \frac{\mathrm{d}^3k}{(2\pi)^3}\left[e_{ij}(\mathbf{k})h_{\mathbf{k}}(\eta) + \bar{e}_{ij}(\mathbf{k})\bar{h}_{\mathbf{k}}(\eta)\right]\mathrm{e}^{i\mathbf{k}\cdot\mathbf{x}}. \tag{4.2.39}$$

The traceless-transverse polarization tensors are defined by

$$\begin{cases} e_{ij}(\mathbf{k}) = \dfrac{1}{\sqrt{2}}\left[e_i(\mathbf{k})e_j(\mathbf{k}) - \bar{e}_i(\mathbf{k})\bar{e}_j(\mathbf{k})\right], \\ \bar{e}_{ij}(\mathbf{k}) = \dfrac{1}{\sqrt{2}}\left[e_i(\mathbf{k})\bar{e}_j(\mathbf{k}) + \bar{e}_i(\mathbf{k})e_j(\mathbf{k})\right], \end{cases} \tag{4.2.40}$$

where $\mathbf{e}(\mathbf{k})$ and $\bar{\mathbf{e}}(\mathbf{k})$ are two independent unit vectors orthogonal to $\mathbf{k}$, satisfying $\mathbf{e}\cdot\bar{\mathbf{e}}=0$. Thus the polarization tensors satisfy the canonical normalization conditions $e_{ij}e_{ij}=\bar{e}_{ij}\bar{e}_{ij}=1$ and $e_{ij}\bar{e}_{ij}=0$. With use of this Fourier decomposition, the spectrum of the energy density defined by

$$\rho_{\rm GW}(\eta)=\int \mathrm{d}\log k\,\rho_{\rm GW}(\eta,k), \tag{4.2.41}$$

can be written by the oscillation average of the power spectrum of h as

$$\rho_{\rm GW}=\frac{M_{\rm Pl}^2}{16}\left(\frac{k}{a}\right)^2\overline{(\mathcal{P}_h(k)+\mathcal{P}_{\bar{h}}(k))}=\frac{M_{\rm Pl}^2}{8}\left(\frac{k}{a}\right)^2\overline{\mathcal{P}_h(k)}. \tag{4.2.42}$$

In the second equality, we expect $\mathcal{P}_h=\mathcal{P}_{\bar{h}}$ for CP conserving background. It is useful to define the density parameter of GWs normalized by the critical density of the universe as

$$\Omega_{\rm GW}(\eta,k)=\frac{\rho_{\rm GW}(\eta,k)}{\rho_{\rm crit}}=\frac{1}{24}\left(\frac{k}{aH}\right)^2\overline{\mathcal{P}_h(\eta,k)}. \tag{4.2.43}$$

Now let us include the scalar perturbations into the metric to see the excitation of GW from the scalar perturbations. We consider the following metric

$$g_{00}=-a^2(1+2\Phi),\qquad g_{ij}=a^2\left[(1-2\Psi)\delta_{ij}+\frac{1}{2}h_{ij}\right], \tag{4.2.44}$$

in the Newtonian gauge. Hereafter we assume that the anisotropic inertia term is negligible, i.e., $\Phi=\Psi$ for simplicity. Also, to see the excited GW, we neglect the first order tensor perturbation and expect $h\sim\Phi^2\sim\Psi^2$ for order counting. The spatial component of the relevant lowest order Einstein tensor in these assumptions (i.e. at the second order w.r.t. Ψ and the linear order w.r.t. h) is given by

$$\hat{\mathcal{T}}_{ij;kl}\,\delta_{kk'}G^{(2)k'}{}_{l}=-\frac{1}{a^2}\left[\frac{1}{4}\left(h_{ij}''+2\mathcal{H}-\nabla^2h_{ij}\right)+\hat{\mathcal{T}}_{ij;kl}\,\tilde{S}_{kl}\right], \tag{4.2.45}$$

where

$$\tilde{S}_{ij}=4\Psi\partial_i\partial_j\Psi+2\partial_i\Psi\partial_j\Psi, \tag{4.2.46}$$

and $\mathcal{H}=a'/a=aH$ is the Hubble parameter in the conformal time. The second order energy-momentum tensor is

$$\hat{\mathcal{T}}_{ij;kl}\,\delta_{kk'}T^{(2)k'}{}_{l}=\hat{\mathcal{T}}_{ij;kl}\,\frac{M_{\rm Pl}^2}{a^2}\left[\frac{4}{3(1+w)}\partial_k\left(\frac{\Psi'}{\mathcal{H}}+\Psi\right)\partial_l\left(\frac{\Psi'}{\mathcal{H}}+\Psi\right)\right]. \tag{4.2.47}$$

To extract the transverse-traceless component, we used the projection operator $\hat{\mathcal{T}}_{ij;kl}$, which has the following properties:

$$\hat{\mathcal{T}}_{ij;kl}\,\hat{\mathcal{T}}_{kl;mn}=\hat{\mathcal{T}}_{ij;mn},\qquad \partial_i\hat{\mathcal{T}}_{ij;kl}\,\mathcal{O}_{kl}=\hat{\mathcal{T}}_{ii;kl}\,\mathcal{O}_{kl}=0, \tag{4.2.48}$$

for an arbitrary tensor $\mathcal{O}_{ij}$. From the transverse-traceless component of the second order Einstein equation:

$$\hat{\mathcal{T}}_{ij;kl}\,\delta_{kk'}G^{(2)k'}{}_{l}=-\frac{1}{M_{\rm Pl}^2}\hat{\mathcal{T}}_{ij;kl}\,\delta_{kk'}T^{(2)k'}{}_{l}, \tag{4.2.49}$$

one can obtain EoM for excited GWs as

$$h_{ij}'' + 2\mathcal{H}h_{ij}' - \nabla^2 h_{ij} = -4\hat{\mathcal{T}}_{ij;kl}S_{kl}, \tag{4.2.50}$$

where the source term is given by

$$S_{ij} = 4\Psi\partial_i\partial_j\Psi + 2\partial_i\Psi\partial_j\Psi - \frac{4}{3(1+w)}\partial_i\left(\frac{\Psi'}{\mathcal{H}} + \Psi\right)\partial_j\left(\frac{\Psi'}{\mathcal{H}} + \Psi\right). \tag{4.2.51}$$

Here we have used $\hat{\mathcal{T}}_{ij;kl}h_{kl} = h_{ij}$. In terms of polarization tensors, the source term can be expressed as

$$\hat{\mathcal{T}}_{ij;kl}S_{kl} = \int \frac{\mathrm{d}^3k}{(2\pi)^3}\mathrm{e}^{i\mathbf{k}\cdot\mathbf{x}}\hat{\mathcal{T}}_{ij;kl}(\mathbf{k})S_{kl}(\mathbf{k}), \tag{4.2.52}$$

where

$$\hat{\mathcal{T}}_{ij;kl}(\mathbf{k}) = e_{ij}(\mathbf{k})e_{kl}(\mathbf{k}) + \bar{e}_{ij}(\mathbf{k})\bar{e}_{kl}(\mathbf{k}). \tag{4.2.53}$$

Performing the Fourier transformation, one obtains EoM for $h_{\mathbf{k}}$ as

$$h_{\mathbf{k}}''(\eta) + 2\mathcal{H}h_{\mathbf{k}}'(\eta) + k^2 h_{\mathbf{k}}(\eta) = 4S_{\mathbf{k}}(\eta), \tag{4.2.54}$$

where

$$S_{\mathbf{k}}(\eta) = \int \frac{\mathrm{d}^3q}{(2\pi)^3}e_{ij}(\mathbf{k})q_iq_j\left[2\Psi_{\mathbf{q}}(\eta)\Psi_{\mathbf{k}-\mathbf{q}}(\eta) + \left(\frac{\Psi_{\mathbf{q}}'(\eta)}{\mathcal{H}} + \Psi_{\mathbf{q}}(\eta)\right)\left(\frac{\Psi_{\mathbf{k}-\mathbf{q}}'(\eta)}{\mathcal{H}} + \Psi_{\mathbf{k}-\mathbf{q}}(\eta)\right)\right]. \tag{4.2.55}$$

The EoM for $\bar{h}_{\mathbf{k}}$ can be obtained simply by replacing the polarization tensor $e_{ij}(\mathbf{k})$ with $\bar{e}_{ij}(\mathbf{k})$ in Eq. (4.2.55).

This EoM can be formally solved by the Green function method as

$$h_{\mathbf{k}}(\eta) = \frac{4}{a(\eta)}\int^{\eta}\mathrm{d}\tilde{\eta}G_{\mathbf{k}}^{(h)}(\eta,\tilde{\eta})a(\tilde{\eta})S_{\mathbf{k}}(\tilde{\eta}), \tag{4.2.56}$$

where $G_{\mathbf{k}}^{h}$ is the Green function for $ah_{\mathbf{k}}$:

$$G_{\mathbf{k}}^{(h)\prime\prime}(\eta,\tilde{\eta}) + \left(k^2 - \frac{a''}{a}\right)G_{\mathbf{k}}^{(h)}(\eta,\tilde{\eta}) = \delta(\eta-\tilde{\eta}). \tag{4.2.57}$$

During the radiation-dominated era $a \propto \eta$, the explicit form of this Green function can be easily found as

$$G_{\mathbf{k}}^{(h)}(\eta,\tilde{\eta}) = \theta(\eta-\tilde{\eta})\frac{\sin[k(\eta-\tilde{\eta})]}{k}, \tag{4.2.58}$$

with use of the step function $\theta(\eta-\tilde{\eta})$. On the other hand, the linear order scalar perturbation can be expressed by the transfer function $D(x)$ and the initial amplitude $\psi_{\mathbf{k}}$ as [169]

$$\Psi_{\mathbf{k}}(\eta) = D(k\eta)\psi_{\mathbf{k}}. \tag{4.2.59}$$

The explicit form of the transfer function during the radiation-dominated era is

$$D(x) = \frac{9}{x^2}\left[\frac{\sin(x/\sqrt{3})}{x/\sqrt{3}} - \cos(x/\sqrt{3})\right]. \tag{4.2.60}$$

The initial amplitude $\psi_{\mathbf{k}}$ is related with the primordial curvature perturbation by $\psi_{\mathbf{k}} = -2\zeta/3$ (1.1.78) in the Newtonian gauge. With use of this expression of the scalar perturbation, the two point function of the source term is given by

$$\begin{aligned}\langle S_{\mathbf{k}}(\eta_1) S_{\mathbf{k}'}(\eta_2)\rangle = &\int \frac{\mathrm{d}^3\tilde{k}\mathrm{d}^3\tilde{k}'}{(2\pi)^6} e_{ij}(\mathbf{k})\tilde{k}_i\tilde{k}_j\, e_{kl}(\mathbf{k}')\tilde{k}'_k\tilde{k}'_l \\ &\times f(\tilde{\mathbf{k}}, \mathbf{k}-\tilde{\mathbf{k}}, \eta_1) f(\tilde{\mathbf{k}}', \mathbf{k}'-\tilde{\mathbf{k}}', \eta_2)\left\langle \psi_{\mathbf{k}-\tilde{\mathbf{k}}}\psi_{\tilde{\mathbf{k}}}\psi_{\mathbf{k}'-\tilde{\mathbf{k}}'}\psi_{\tilde{\mathbf{k}}'}\right\rangle,\end{aligned} \tag{4.2.61}$$

where

$$f(\mathbf{k}_1, \mathbf{k}_2, \eta) = 2D(x_1)D(x_2) + \left(\frac{k_1}{\mathcal{H}}D'(x_1) + D(x_1)\right)\left(\frac{k_2}{\mathcal{H}}D'(x_2) + D(x_2)\right), \quad x_i = k_i\eta. \tag{4.2.62}$$

Note that here prime does not denote the η-derivative but instead x-derivative. One can clearly see that $f(\mathbf{k}_1, \mathbf{k}_2, \eta)$ is symmetric under $\mathbf{k}_1 \leftrightarrow \mathbf{k}_2$, and invariant under $\mathbf{k}_i \to -\mathbf{k}_i$. The projection of $\tilde{k}$ reads $e_{ij}(\mathbf{k})\tilde{k}_i\tilde{k}_j = \tilde{k}^2\sin^2\theta\cos 2\varphi/\sqrt{2}$ for our normalization of the polarization tensors, where θ and φ are the zenith and azimuthal angle of $\tilde{\mathbf{k}}$ w.r.t. $\mathbf{k}$. Non-vanishing contributions of $\langle\psi_{\mathbf{k}-\tilde{\mathbf{k}}}\psi_{\tilde{\mathbf{k}}}\psi_{\mathbf{k}'-\tilde{\mathbf{k}}'}\psi_{\tilde{\mathbf{k}}'}\rangle$ come from two connected parts which are proportional to $\delta^{(3)}(\mathbf{k}+\mathbf{k}')\delta^{(3)}(\tilde{\mathbf{k}}+\tilde{\mathbf{k}}')\mathcal{P}_\psi(\tilde{k})\mathcal{P}_\psi(|\mathbf{k}-\tilde{\mathbf{k}}|)$ or $\delta^{(3)}(\mathbf{k}+\mathbf{k}')\delta^{(3)}(\mathbf{k}-\tilde{\mathbf{k}}+\tilde{\mathbf{k}}')\mathcal{P}_\psi(\tilde{k})\mathcal{P}_\psi(|\mathbf{k}-\tilde{\mathbf{k}}|)$. Noting that $f(\mathbf{k}_1, \mathbf{k}_2, \eta)$ is invariant under $\mathbf{k}_1 \leftrightarrow \mathbf{k}_2$ or $\mathbf{k}_i \to -\mathbf{k}_i$, and that the projection $e_{ij}(\mathbf{k})\tilde{k}_i\tilde{k}_j$ is invariant under $\mathbf{k} \to -\mathbf{k}$ or $\tilde{\mathbf{k}} \to -\tilde{\mathbf{k}}$, one can see that these two contributions are the same after the integration of $\tilde{\mathbf{k}}'$. Thus, Eq. (4.2.61) reads

$$\begin{aligned}\langle S_{\mathbf{k}}(\eta_1) S_{\mathbf{k}'}(\eta_2)\rangle = &\frac{2\pi^2}{k^3}\delta^{(3)}(\mathbf{k}+\mathbf{k}')\frac{4}{81}\int_0^\infty \mathrm{d}\tilde{k}\int_{-1}^1 \mathrm{d}\mu \frac{k^3\tilde{k}^3}{|\mathbf{k}-\tilde{\mathbf{k}}|^3}(1-\mu^2)^2 \\ &\times f(\tilde{\mathbf{k}}, \mathbf{k}-\tilde{\mathbf{k}}, \eta_1) f(\tilde{\mathbf{k}}, \mathbf{k}-\tilde{\mathbf{k}}, \eta_2)\mathcal{P}_\zeta(\tilde{k})\mathcal{P}_\zeta(|\mathbf{k}-\tilde{\mathbf{k}}|).\end{aligned} \tag{4.2.63}$$

Now we are already armed with all weapons. Changing the integration variables to $k_1 = \tilde{k}$ and $k_2 = |\mathbf{k}-\tilde{\mathbf{k}}|$ and substituting this into Eq. (4.2.56) and (4.2.43), one can finally obtain,

$$\Omega_{\mathrm{GW}}(\eta, k) = \frac{8}{243}\int\int_{|\mu_{12}|\le 1} \mathrm{d}\log k_1 \mathrm{d}\log k_2\, \mathcal{P}_\zeta(k_1)\mathcal{P}_\zeta(k_2)(1-\mu_{12}^2)^2\left(\frac{k_1k_2}{k^2}\right)^3 \overline{I^2(k_1/k, k_2/k, k\eta)}, \tag{4.2.64}$$

where $\mu_{12} = (k_1^2 + k_2^2 - k^2)/(2k_1k_2)$ and

$$\begin{aligned}I(u, v, x) = &\int^x \mathrm{d}\tilde{x}\,\tilde{x}\sin(x-\tilde{x})\left[3D(u\tilde{x})D(v\tilde{x})\right. \\ &\left.+\tilde{x}\left(uD'(u\tilde{x})D(v\tilde{x}) + vD(u\tilde{x})D'(v\tilde{x})\right) + \tilde{x}^2 uvD'(u\tilde{x})D'(v\tilde{x})\right].\end{aligned} \tag{4.2.65}$$

To obtain this expression, we have used the relations $a \propto \eta$ and $\mathcal{H} = aH = \eta^{-1}$ in the radiation-dominated era. Instead of taking the oscillation average of I^2, one can use the

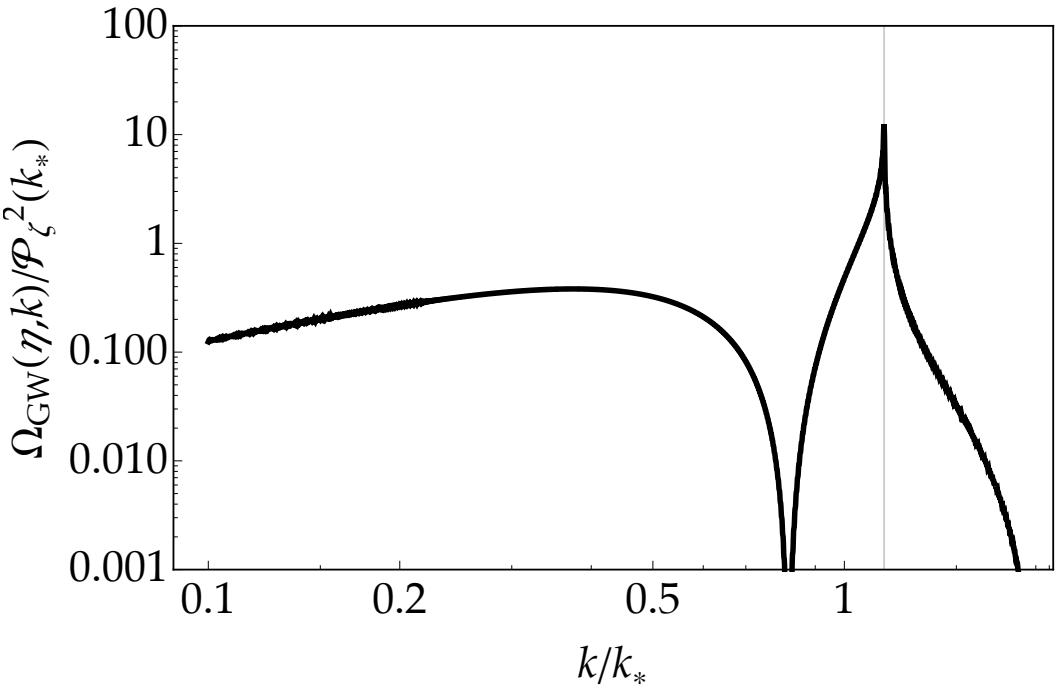

Figure 4.4. The numerical result of $\Omega_{\rm GW}$ for the delta-function-type curvature perturbation $\mathcal{P}_\zeta(k) = \mathcal{P}_\zeta(k_*)\delta(\log k - \log k_*)$ at $k\eta = 10^4$. The GW spectrum has a sharp peak on $k_{\rm p} = 2k_*/\sqrt{3}$ (gray line) and its amplitude is evaluated as $\Omega_{\rm GW}(\eta, 2k_*/\sqrt{3}) \sim 12.3\mathcal{P}_\zeta^2(k_*)$.

other transfer function given by replacing $\sin(x-\tilde{x})$ with $\cos(x-\tilde{x})$ in I as

$$J(u,v,x) = \int^x \mathrm{d}\tilde{x}\,\tilde{x}\cos(x-\tilde{x})\,[3D(u\tilde{x})D(v\tilde{x}) + \tilde{x}\left(uD'(u\tilde{x})D(v\tilde{x}) + vD(u\tilde{x})D'(v\tilde{x})\right) + \tilde{x}^2 uvD'(u\tilde{x})D'(v\tilde{x})\big]\,, \tag{4.2.66}$$

which corresponds with the kinetic energy of h well inside the horizon, and the oscillation average of I^2 can be well approximated by

$$\overline{I^2(u,v,x)} = \frac{I^2(u,v,x) + J^2(u,v,x)}{2}. \tag{4.2.67}$$

The oscillation average of I^2 becomes almost constant for sufficiently large η because the dominant mode of the integrand of I (J) decays as $\sin(x)/x$ ($\cos(x)/x$), whose integration asymptotes to a constant. Therefore the density parameter of GWs is also constant until the matter-radiation equality. After the matter-radiation equality, GWs decay as the radiation and therefore the fraction of GWs to the total radiation does not change. Hence the current density parameter of GWs is given by

$$\Omega_{\rm GW}(\eta_0,k)h^2 = \Omega_{r0}h^2\Omega_{\rm GW}(\eta_{\rm c},k) \simeq 4\times10^{-5}\Omega_{\rm GW}(\eta_{\rm c},k), \tag{4.2.68}$$

where $\eta_{\rm c}$ denotes some time when $\Omega_{\rm GW}$ well settles down to a constant in the radiation-dominated era.

Though the exact value of $\Omega_{\rm GW}(k)$ depends on the shape of $\mathcal{P}_\zeta(k)$ since it includes the convolution, let us evaluate the current GW spectrum for the delta-function-type primordial

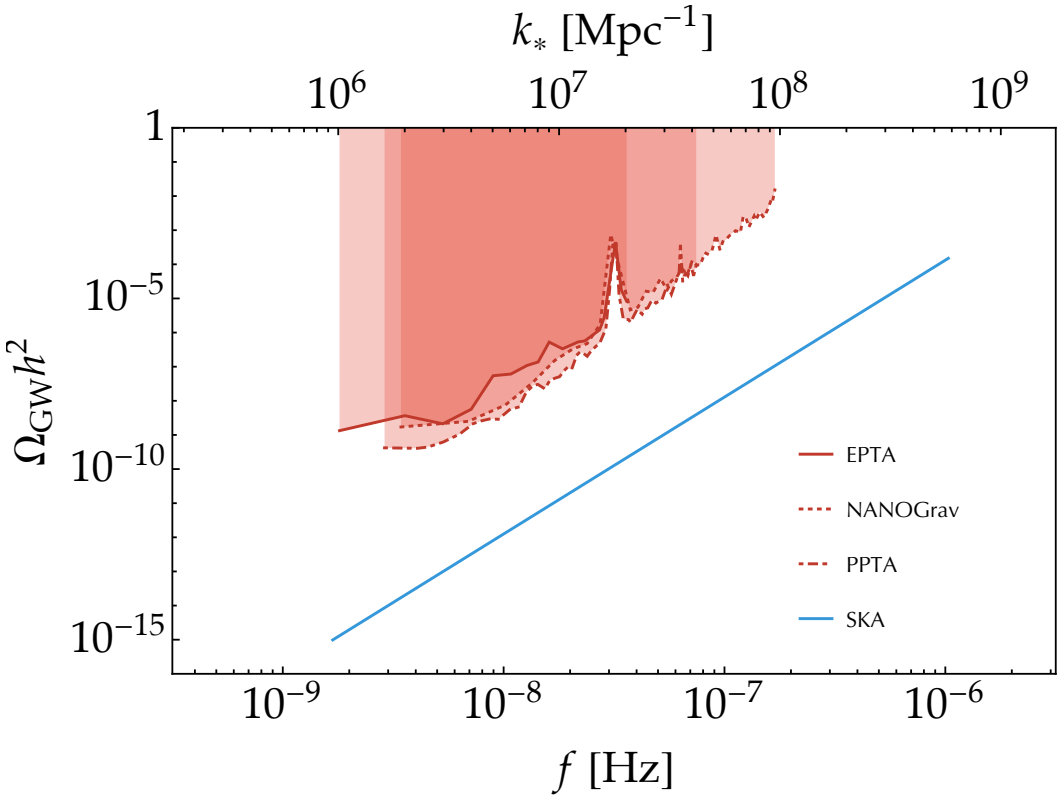

Figure 4.5. Red lines represent the several current PTA constraints: European Pulser Timing Array (plane) [170], NANOGrav (dotted) [171], and Parkes Pulsar Timing Array (dot-dashed) [172], and the sensitivity of the future SKA experiments is shown by the blue line [173, 174]. The frequency of GW and the wavelength of the scalar perturbation are related by $f = k_{\rm p}/(2\pi) = k_*/(\sqrt{3}\pi)$.

curvature perturbation $\mathcal{P}_\zeta(k) = \mathcal{P}_\zeta(k_*)\delta(\log k - \log k_*)$ to estimate the constraints on the amplitude of the primordial perturbation from the secondary GW. For this power spectrum, the density parameter of GWs reads

$$\Omega_{\rm GW}(\eta, k) = \frac{8}{243}\mathcal{P}_\zeta^2(k_*)\left(1-\left(1-\frac{k^2}{2k_*^2}\right)^2\right)^2\left(\frac{k_*}{k}\right)^6 \overline{I^2(k_*/k, k_*/k, k\eta)}, \qquad k \leq 2k_*. \tag{4.2.69}$$

In Fig. 4.4, we plotted the result of the numerical integration of this for $k\eta = 10^4$. The resultant GW spectrum has a sharp peak on $k_{\rm p} = 2k_*/\sqrt{3}$ [168] represented by the gray line in this figure. The peak amplitude is evaluated as $\Omega_{\rm GW}(\eta, 2k_*/\sqrt{3}) \sim 12.3\mathcal{P}_\zeta^2(k_*)$. Therefore the current GW abundance is given by

$$\Omega_{\rm GW}\left(\eta_0, \frac{2k_*}{\sqrt{3}}\right)h^2 \sim 5\times 10^{-8}\left(\frac{\mathcal{P}_\zeta(k_*)}{0.01}\right)^2. \tag{4.2.70}$$

On the other hand, the parsec scale GW is severely constrained by the pulsar timing array experiments. In Fig. 4.5, we show the several current PTA constraints as well as the future SKA experiments. Note that the GW frequency and the wavelength of the scalar

perturbation are related by $f = k_{\rm p}/(2\pi) = k_*/(\sqrt{3}\pi)$. Eq. (4.1.26) shows the relevant scale corresponds with $\sim$ 0.1–$10M_\odot$, and with use of Eq. (4.2.70), it can be seen that the PBH formation at this range is severely constrained by PTA constraints. In Fig. 4.3, we plot the amplitude constraints corresponding with EPTA by the red dot-dashed line as an example. Though these PTA constraints are quite strong, we show a concrete model which can explain $30M_\odot$ PBHs, being marginally consistent with these constraints in the next chapter.

4.2.5 Supermassive black hole

Finally let us discuss the supermassive black holes in this subsection. Most galaxies including our Milky Way are thought to possess one or a few SMBHs whose masses reach to 10^6–$10^{9.5}M_\odot$ in their centers (see e.g. the recent review [175]), and moreover, such massive black holes have been found even at high redshifts as $z \sim 6$–7 [176, 177]. It is difficult to astrophysically explain the formation of such SMBHs in the early phase, and it has been still an open question. Bean and Magueijo [178] suggested that PBHs as initially massive as $10^5 M_\odot$ could be the seeds of SMBHs. Though their analysis in fact assumed an optimistic growth rate for massive PBHs, the precise growth process of massive PBHs is still unknown and various authors are working on this possibility.

On the other hand, the massive PBH formation in inflation is known to be a difficult problem due to the μ-distortion [134, 179–181]. μ-distortion is one type of the CMB spectral distortion as mentioned previously, and in the standard cosmology, it is caused by the entropy release due to the Silk damping of the subhorizon density perturbations. If the density perturbations are large enough to produce non-negligible PBHs, their decays due to the Silk damping would yield too large μ-distortion and be excluded by CMB observations. The expected μ-distortion with a single k-mode can be approximated by [180, 181]

$$\mu \sim 2.2\mathcal{P}_\zeta(k)\left[\exp\left[-\frac{k}{5400\,\mathrm{Mpc}^{-1}}\right] - \exp\left[-\left(\frac{k}{31.6\,\mathrm{Mpc}^{-1}}\right)^2\right]\right], \tag{4.2.71}$$

which should be smaller than the current upper bound $\mu < 9 \times 10^{-5}$ [119]. We plot the corresponding constraints in Fig. 4.3 by the red plain line, which strongly constrain the formation of $\sim 10^5 M_\odot$ PBHs. Several future experiments such as PIXIE [122] or PRISM [123] could update the μ constraints to $\mu \lesssim 10^{-9}$.

Recently Nakama et al. proposed a novel massive PBH formation scenario in inflation, avoiding this constraint [182]. They prepared the multi-field inflation potential, in which the inflatons roll along a special trajectory different from the unperturbed one with a quite low probability. If this trajectory corresponds with the $\mathcal{O}(1)$ large e-foldings, the corresponding regions are assumed to be PBHs. However the other regions evolve around the unperturbed trajectory, which is assumed to give a standard small perturbation as $\sim 10^{-5}$, and therefore the predicted mean μ-distortion remains small enough. Although their potential is too artificial in fact, massive PBHs might be produced in such a way.

Chapter 5

Case 1: Separated Double Inflation

In general, it is difficult to realize sharp variation on the scalar power spectrum in the simplest single-field slow-roll inflation since the change ratio of the power spectrum is suppressed by the slow-roll parameters. Here let us consider a double inflation model whose energy scales are separated as a first example. Separating the source for the small scale perturbations from that for the CMB scale perturbations, this model can easily realize the PBH formation in any mass region and in any abundance. Furthermore, in some parameter region, a second sharp peak which is available for explaining LIGO's events can be produced, corresponding with the modes which cross the horizon around the beginning of the second inflation. In this chapter, we adopt the Planck unit $M_{Pl} = 1$ and this chapter is based on Refs. [53, 183].

5.1 New inflation in supergravity

First let us introduce a realization of new inflation in the SUGRA framework, which naturally imply the existence of the preinflation phase before the new inflation. In the following sections, we assume that the preinflation is responsible for the CMB scale perturbations, while the new inflation generates the small scale perturbations so that sufficient PBHs are produced.

In this section, we follow the model proposed in Refs. [184, 185]. This model is based on a discrete R symmetry Z_{2nR} which is broken down to a discrete Z_{2R} during and after the new inflation. The inflaton superfield Φ is supposed to have an R charge 2, which leads the following effective superpotential at the leading order,

$$W(\Phi) = v^2\Phi - \frac{g}{n+1}\Phi^{n+1}. \tag{5.1.1}$$

The R-invariant effective Kähler potential can be written as

$$K(\Phi) = |\Phi|^2 + \frac{\kappa}{4}|\Phi|^4 + \cdots . \tag{5.1.2}$$

For these super- and Kähler potentials, the scalar potential is given by

$$V(\Phi) = \mathrm{e}^K (K^{\bar{\Phi}\Phi} D_\Phi W D_{\bar{\Phi}} W^* - 3|W|^2), \tag{5.1.3}$$

where bars denote complex conjugation, $K^{\bar{\Phi}\Phi}$ is the inverse of the Kähler metric $K_{\Phi\bar{\Phi}} = \partial^2 K / \partial\Phi\partial\bar{\Phi}$, and D_Φ is a covariant derivative $D_\Phi W = W_\Phi + K_\Phi W$. Then, defining the inflaton by $\varphi = \sqrt{2}\mathrm{Re}\Phi$,[1] the leading terms of the potential are shown as

$$V \simeq v^4 - \frac{\kappa}{2} v^4 \varphi^2 - \frac{g}{2^{\frac{n}{2}-1}} v^2 \varphi^n + \frac{g^2}{2^n} \varphi^{2n}, \tag{5.1.4}$$

and the slow-roll inflation can be driven either by the quadratic or nth moment term.

This potential has a negative minimum at $\varphi_{\min} \simeq \sqrt{2}\left(v^2/g\right)^{1/n}$ as

$$\langle V \rangle \simeq -3 \langle \mathrm{e}^K |W|^2 \rangle \simeq -3 \left(\frac{n}{n+1}\right)^2 v^4 \left(\frac{v^2}{g}\right)^{2/n}, \tag{5.1.5}$$

due to the SUGRA effect. If one assumes that this negative energy is canceled out after inflation with a positive contribution μ_{SUSY}^4 due to the SUSY-breaking effect, the SUSY-breaking scale (or the gravitino mass $m_{3/2}$) can be related with the new inflation scale by

$$m_{3/2} \simeq \frac{\mu_{\mathrm{SUSY}}^2}{\sqrt{3}} \simeq \frac{n}{n+1} v^2 \left(\frac{v^2}{g}\right)^{1/n}. \tag{5.1.6}$$

After inflation, φ oscillates around its potential minimum with a mass scale of $m_\varphi \simeq n v^2 \left(v^2/g\right)^{-1/n}$, and therefore, assuming that φ decays via a dimension-five Planck-suppressed operator, the reheating temperature can be evaluated as

$$T_{\mathrm{R}} \simeq 0.1 m_\varphi^{3/2} \simeq 0.1 n^{\frac{3}{2}} g^{\frac{3}{2n}} v^{3-\frac{3}{n}}. \tag{5.1.7}$$

The reheating temperature is necessary for the normalization of the perturbation scale as

$$\log\left(\frac{k}{0.002\,\mathrm{Mpc}^{-1}}\right) = -N + 56 + \frac{2}{3}\log\left(\frac{\rho_{\mathrm{f}}^{1/4}}{10^{16}\,\mathrm{GeV}}\right) + \frac{1}{3}\log\left(\frac{T_{\mathrm{R}}}{10^9\,\mathrm{GeV}}\right), \tag{5.1.8}$$

where N denotes the backward e-folds at the horizon exit of the considered mode, and ρ_{f} is the energy density at the end of new inflation.

Now let us consider the initial condition for this inflation. Small field new inflation generally suffers from a severe initial condition problem. That is, both the inflaton's initial field value and its time derivative should be extremely small to have a sufficiently long inflation, but originally there is no reason to stabilize the inflaton field to the potential origin since the inflaton potential should be flat enough to satisfy the slow-roll conditions. Moreover, even if one can introduce some stabilizing term in the potential, new inflaton realizes eternal inflation if the inflaton's initial field value is much smaller than the Hubble fluctuation $H/(2\pi)$, and the curvature perturbations generated around the beginning of new inflation should exceed unity. Because we want new inflation to contribute only to small

[1] Φ has n potential minima and the positive direction of $\varphi = \mathrm{Re}\Phi$ is always toward one of them. Furthermore, due to the linear potential term which we will introduce later, indeed this direction is chosen as a true trajectory.

scale perturbations as mentioned below, we have to avoid the eternal inflation condition for our observable universe not to be eaten by PBHs due to large curvature perturbations.

As proposed in Ref. [185], these problems can be naturally solved in SUGRA frameworks by introducing a preinflation phase before the new inflation and adding a constant term to superpotential $W_{\rm const} = C$.[2] During the preinflation, the inflaton of the new inflation can have a Hubble induced mass term $\frac{1}{2}V_{\rm pre}\varphi^2 \simeq \frac{3}{2}H^2\varphi^2$ through the coefficient e^K of the potential. Moreover the constant superpotential term yields the linear term $2\sqrt{2}Cv^2\varphi$ in the potential, which shifts the potential minimum from 0 to $2\sqrt{2}\frac{Cv^2}{V_{\rm pre}}$. The Hubble induced mass keeps stabilizing the inflaton even after the preinflation until the beginning of the new inflation $V_{\rm pre} \simeq v^4$, and therefore the initial field value of φ is given by

$$\varphi_{\rm i} \simeq 2\sqrt{2}\frac{C}{v^2}. \tag{5.1.9}$$

The new inflation can avoid eternal inflation as long as $\varphi_{\rm i}$ is sufficiently larger than the Hubble fluctuation $H/(2\pi)$ at the beginning of the new inflation.

For concrete discussion, let us assume chaotic inflation as a preinflation here and hereafter since large field inflation is favored from the view point of the initial condition problem.[3] Following Ref. [186], we consider the following super- and Kähler potential:

$$\begin{cases} W = v^2\Phi - \dfrac{g}{n+1}\Phi^{n+1} + mSX + C, \\ K = |\Phi|^2 + \dfrac{1}{2}(X+X^*)^2 + |S|^2 + \dfrac{\kappa}{4}|\Phi|^4 + \lambda|\Phi|^2|S|^2 + \dfrac{\xi}{2}|\Phi|^2(X+X^*)^2. \end{cases} \tag{5.1.10}$$

Here X and Φ include the inflatons χ and φ for chaotic and new inflation respectively as their scalar components, and S is called *stabilizer*. Φ and S have R charge 2 and X and S additionally have Z_2 charge 1. The Kähler potential is written by invariant terms under these symmetries, including relevant higher order terms. In addition, we suppose a shift symmetry for X so that the Kähler potential is invariant under the shift $\mathrm{Im}X \to \mathrm{Im}X + \alpha$ for an arbitrary α. For these super- and Kähler potentials, the scalar potential is given by

$$\begin{aligned} V &= e^K(K^{\bar{J}I}D_I W D_{\bar{J}} W^* - 3|W|^2) \\ &\simeq v^4 - 2\sqrt{2}Cv^2\varphi - \frac{\kappa}{2}v^4\varphi^2 - \frac{g}{2^{\frac{n}{2}-1}}v^2\varphi^n + \frac{g}{2^n}\varphi^{2n} + \frac{1}{2}m^2\chi^2\left(1 + \frac{c_{\rm pot}}{2}\varphi^2\right), \end{aligned} \tag{5.1.11}$$

where $\chi = \sqrt{2}\mathrm{Im}X$, $\varphi = \sqrt{2}\mathrm{Re}\Phi$, and $c_{\rm pot} = 1 - \lambda$. Also the kinetic terms are given by

$$\mathcal{L}_{\rm kin} = -K_{I\bar{J}}\partial_\mu\bar{\phi}^{\bar{J}}\partial^\mu\phi^I \supset -\frac{1}{2}\left(1 - \frac{c_{\rm kin}}{2}\varphi^2\right)(\partial\chi)^2 - \frac{1}{2}\left(1 + \frac{\kappa}{2}\varphi^2\right)(\partial\varphi)^2, \tag{5.1.12}$$

[2] Note that, in the original model [185], hybrid inflation is assumed as a preinflation, which automatically gives a nonzero constant superpotential during preinflation. However, since we have already introduced the constant superpotential term by hand (though its possible origin is described later), the inflation models which do not give a nonzero superpotential can be also adopted as a preinflation in our model.

[3] Note here that this simple choice is not consistent with Planck's results. This is because the e-folding number of the preinflation for the observable universe gets smaller than 60, for the following new inflation continues ~ 30 e-folds here. As a result, the predicted $n_{\rm s}$ and r are shifted. However, for small scale perturbations, almost only the oscillatory behavior of the inflaton for preinflation is relevant and it can be approximated by a quadratic potential force at the leading order. Therefore we assume that our discussions for PBH formation are valid also for other large field inflation than a quadratic potential.

for relevant fields χ and φ, where $c_{\rm kin} = -\xi$. Thanks to higher order terms in the Kähler potential, now we can vary the coefficient of the Hubble induced mass during the preinflation and the χ-oscillation phase. During preinflation, the total energy is only given by the χ's potential energy, $\rho = 3H^2 = \frac{1}{2}m^2\chi^2$, therefore the Hubble induced mass term for φ can be written as $\frac{3}{2}c_{\rm pot}H^2\varphi^2$. On the other hand, during the χ-oscillation phase, the total energy is equally given by χ's kinetic and potential energy, $\frac{1}{2}\overline{\dot{\chi}^2} = \frac{1}{2}m^2\overline{\chi^2} = \frac{1}{2}\overline{\rho}$ if the χ's oscillation is driven by the quadratic potential force, where overlines indicate the time average. Therefore the coefficient of the Hubble induced mass is roughly given by $c_{\rm eff} = \frac{1}{2}(c_{\rm pot} + c_{\rm kin})$. Hereafter we study this model (5.1.11) and (5.1.12) phenomenologically.

5.2 Inflection point and SUSY-breaking sector

Let us move to the amplification mechanism of the curvature perturbations in this model. There are two ways to amplify the curvature perturbations, one of which we focus on in this section.

As can be easily seen from the potential form (5.1.11), the linear, quadratic, and nth moment terms can have an inflection point for $\varphi > 0$ if $\kappa < 0$. Since V_φ is locally maximized at that inflection point, if the maximum of V_φ is still negative but quite close to zero, the slow-roll inflation is not spoiled and moreover very large curvature perturbations can be produced at this point. The inflection point φ_* can be obtained as

$$V_{\varphi\varphi}(\varphi_*) \simeq |\kappa|v^4 - \frac{n(n-1)}{2^{\frac{n}{2}-1}}gv^2\varphi_*^{n-2} = 0, \quad \Rightarrow \quad \varphi_* = \left(\frac{2^{\frac{n}{2}-1}}{n(n-1)}\frac{|\kappa|v^2}{g}\right)^{\frac{1}{n-2}}. \tag{5.2.1}$$

Then if one requires the flat inflection condition as

$$\begin{aligned} V_\varphi(\varphi_*) &\simeq -2\sqrt{2}Cv^2 + \frac{n-2}{n-1}\left(\frac{2^{\frac{n}{2}-1}}{n(n-1)}\right)^{\frac{1}{n-1}}\frac{|\kappa|^{\frac{n-1}{n-2}}v^{\frac{4n-6}{n-2}}}{g^{\frac{1}{n-2}}} \sim 0, \\ \Rightarrow \quad g &\sim \frac{1}{n(n-2)}\left(\frac{n-2}{2(n-1)}\right)^{n-2}\frac{|\kappa|^{n-1}v^{2(n-1)}}{C^{n-2}}, \end{aligned} \tag{5.2.2}$$

The curvature perturbations generated around φ_* can be large enough to produce abundant PBHs.

If one assumes that the new inflation realizes both small perturbations like those on the CMB scale and large perturbations which would cause the formation of PBHs, it generally takes too many e-folds in the transition from small to large perturbations since the time derivative of the slow-roll parameter itself is suppressed by the slow-roll parameters, $\frac{\mathrm{d}}{\mathrm{d}N}\log\epsilon_V \sim \mathcal{O}(\epsilon_V, \eta_V)$, where N denotes the e-folding number and ϵ_V and η_V represent the slow-roll parameters $\frac{1}{2}\left(\frac{V_\varphi}{V}\right)^2$ and $\frac{V_{\varphi\varphi}}{V}$ respectively. However, since we have already introduced double inflation, the new inflation can be free from the COBE normalization simply by assuming that the preinflation is responsible for the CMB scale perturbations, and then the new inflation can end in sufficiently short time in that case. In this case, the curvature perturbations generated by new inflation should be large even apart from the inflection point, and then the linear term itself is required to be small enough. By letting $A_{\rm lin}$ denote the amplitude of the power spectrum of the curvature perturbations during the linear term in

the potential dominantly contributes to the perturbations, the constant superpotential C is determined through the following relation:

$$A_{\rm lin} = \frac{1}{12\pi^2}\frac{V^3}{V_\varphi^2} \simeq \frac{1}{96\pi^2}\frac{v^8}{C^2}, \quad \Leftrightarrow \quad C \simeq \frac{1}{\sqrt{96\pi^2 A_{\rm lin}}}v^4. \tag{5.2.3}$$

Therefore, for $A_{\rm lin} \sim 10^{-3}$, C is required to be as small as v^4.

The above two conditions (5.2.2) and (5.2.3) are required for PBH formation by the flat inflection point. Now, by combining them, the v-dependence of g can be clarified as $g \sim |\kappa|^{n-1}v^{6-2n}$. Therefore, in the case of $n = 3$, $g \sim |\kappa|^2$ does not depend on the new inflation scale v and could be smaller than unity. On the other hand, for $n \geq 4$, g becomes much larger than unity for $v \ll 1$ and such a large g would spoil unitarity of the theory [187]. Moreover $n = 3$ is uniquely favored by the anomaly free conditions for supersymmetric standard gauge groups with the discrete R symmetry Z_{2nR} [188]. For those reasons, we concentrate on the case of $n = 3$ hereafter.

Before closing this section, let us mention the origin of the constant superpotential term. Actually the required small constant term C in the superpotential can be interpreted to come from the SUSY-breaking sector in the case of $n = 3$ [189].[4] The SUSY-breaking F-term order $\mu_{\rm SUSY}^2$ naively arises from the term like

$$W_{\not{\rm SUSY}} = \mu_{\rm SUSY}^2 Z. \tag{5.2.4}$$

If Z obtains a vacuum expectation value $\langle Z\rangle \sim \mu_{\rm SUSY}$, this term can lead the constant superpotential $C \sim \mu_{\rm SUSY}^3$. Indeed it can be realized in the dynamical SUSY-breaking models proposed in Refs. [190, 191] if the origin of Z is destabilized due to a large Yukawa coupling ($\sim 4\pi$),[5] and the estimated constant term is given by $C \sim \Lambda^3/(4\pi)^2$ where the dynamical scale Λ is related with $\mu_{\rm SUSY}$ by $\mu_{\rm SUSY}^2 = \Lambda^2/(4\pi)$. On the other hand, under the flat inflection condition (5.2.2) and the large curvature perturbation condition (5.2.3), the vanishing cosmological constant condition (5.1.6) gives the parameter dependence of the SUSY-breaking scale as $\mu_{\rm SUSY} \sim |\kappa|^{\frac{1-n}{2n}}v^{2\frac{n-1}{n}}$, neglecting numerical factors. Therefore the scale dependence of the constant term C is consistent with the above assumption if and only if $n = 3$ as

$$C \sim v^4 \sim \mu_{\rm SUSY}^3. \tag{5.2.5}$$

It can be checked that this consistency is retained for the concrete parameter values which will be shown later even if numerical factors are included.

5.3 At the beginning of new inflation

Other than the inflection point, the model can make a peak on the scalar power spectrum around the beginning of new inflation. The simplest way is taking large positive κ and making the absolute value of the second slow-roll parameter $\eta_V = V_{\varphi\varphi}/V \simeq -\kappa$ large. In this case, from the naive estimation of the spectral index $n_{\rm s} - 1 = -6\epsilon_V + 2\eta_V \simeq -2\kappa$, the power spectrum is expected to be strongly red-tilted and show its maximum on around the

[4] Note that $n = 4$ is considered in Ref. [189] because the authors' motivation is not to produce PBHs but to modify the spectral index in new inflation and therefore the required condition is different.

[5] It has been shown that Z's origin is not destabilized at least perturbatively [192].

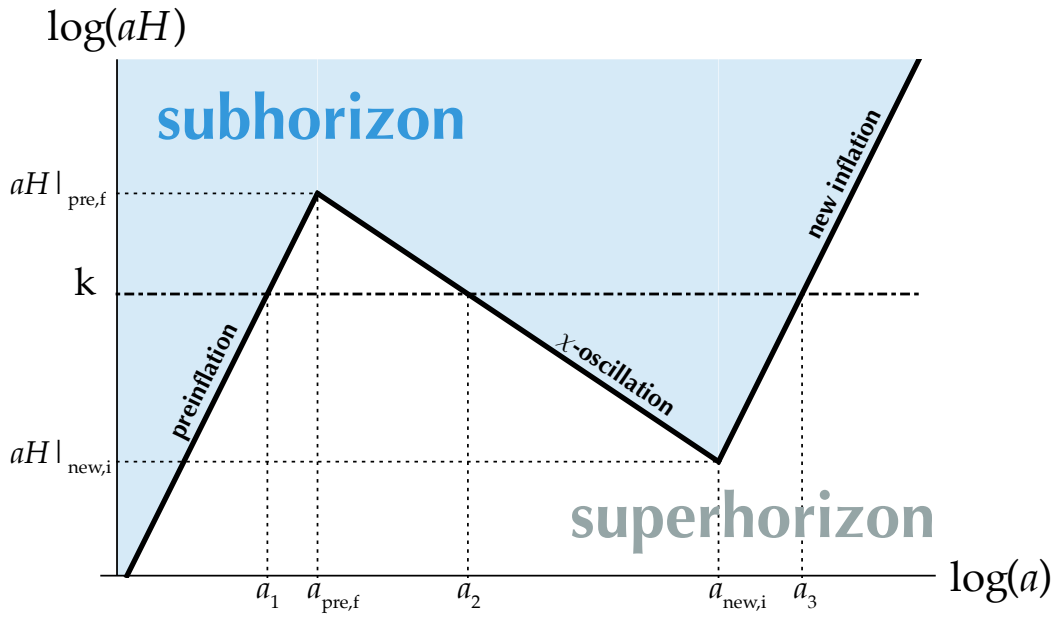

Figure 5.1. The schematic image of the horizon scale aH. $a_{\mathrm{pre,f}}$ and $a_{\mathrm{new,i}}$ represent the time of the end of preinflation and the beginning of new inflation. Between two inflations, the horizon scale generally decreases as $aH \propto a^{-\frac{1+3w}{2}}$ with $w = p/\rho$. Therefore the modes which saturate $aH|_{\mathrm{pre,f}} < k < aH|_{\mathrm{new,i}}$ can reenter the horizon during the χ-oscillation phase.

largest scale corresponding with the beginning of new inflation. However actually those modes experience the horizon crossing three times; they at first exit the horizon near the end of preinflation, then enter the horizon during the χ-oscillation phase between the pre- and new inflation, and finally reexit the horizon soon after the beginning of new inflation. Therefore let us briefly study the behavior of the mode function of $\delta\varphi$ first.

The linear EoM for perturbations which have a generic Hubble induced mass term $\frac{3}{2}cH^2\varphi^2$ is given by

$$0 \sim \begin{cases} \delta\ddot{\varphi} + 3H\delta\dot{\varphi} + 3cH^2\delta\varphi, & k \ll aH, \\ \delta\ddot{\varphi} + 3H\delta\dot{\varphi} + \dfrac{k^2}{a^2}\delta\varphi. & k \gg aH. \end{cases} \tag{5.3.1}$$

Here we neglected the effect of metric perturbations for simplicity though we include them in the later full numerical calculations. The subhorizon EoM can be rewritten as

$$\partial_\eta^2(a\delta\varphi) + \frac{k^2}{a^2}(a\delta\varphi) \simeq 0, \tag{5.3.2}$$

with use of the conformal time $a\mathrm{d}\eta = \mathrm{d}t$ and in the subhorizon limit. Therefore it only has oscillating solutions whose amplitudes decreases as a^{-1}. On the other hand, in the case where the background EoS is given by $w = p/\rho > -1$ ($a \propto t^{\frac{2}{3(1+w)}}$), the superhorizon EoM reads

$$\delta\ddot{\varphi} + \frac{2}{(1+w)t}\delta\dot{\varphi} + \frac{4c}{3(1+w)^2t^2}\delta\varphi = 0. \tag{5.3.3}$$

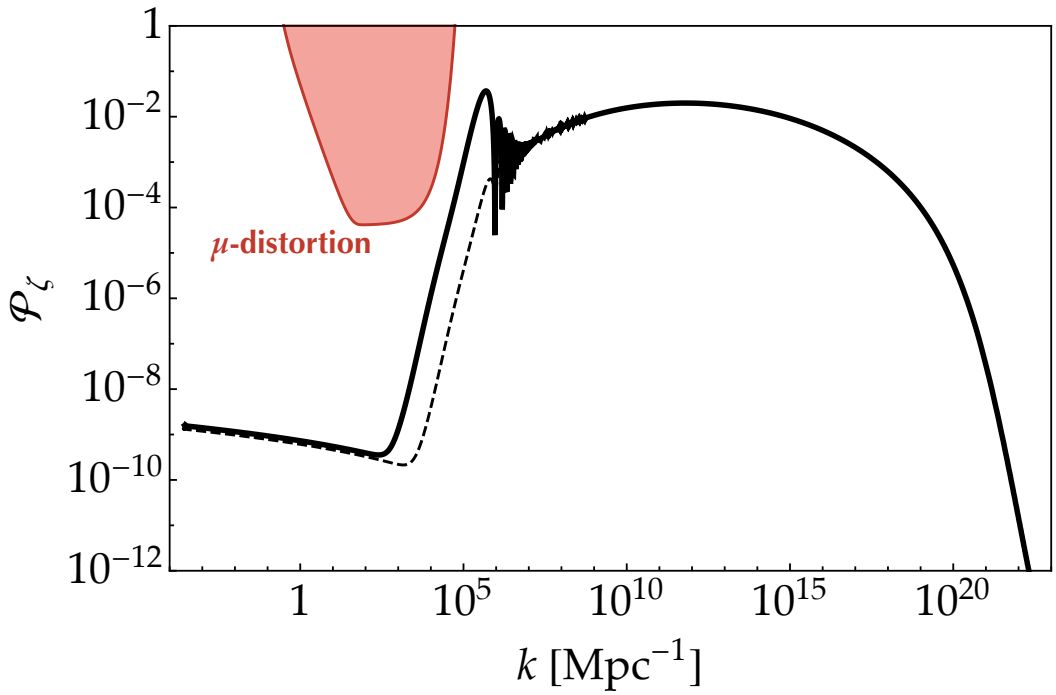

Figure 5.2. The scalar power spectrum for the parameters shown in Eq. (5.4.1) (black thick line) and that for the same parameters except that $c_{\rm kin} = 0$ (black dashed line). The red region represents the constraints from the CMB μ-distortion (5.4.2). The black thick line shows the extra peak around $10^5\,{\rm Mpc}^{-1}$ caused bye the amplification of the φ's power due to the cancellation of the Hubble induced mass during the oscillation phase as mentioned in the previous section.

Its dominant mode decays as $t^{-\frac{1-w}{2(1+w)}+\frac{2}{3(1+w)}{\rm Re}\nu}$, where $\nu = \sqrt{\left(\frac{3(1-w)}{4}\right)^2 - 3c}$. That is, the decay factor is $t^{-\frac{1-w}{2(1+w)}} \propto a^{-\frac{3(1-w)}{4}}$ if $c \geq \frac{3(1-w)^2}{16}$, and otherwise $t^{-\frac{1-w}{2(1+w)}+\frac{2}{3(1+w)}\nu} \propto a^{-\frac{3(1-w)}{4}+\nu}$. In particular, in the massless limit $c \to 0$, the amplitude of the dominant mode is indeed constant consistently with intuition. In the exact de Sitter background, the two solutions can be easily found as $\delta\varphi \propto \exp\left[-\frac{3}{2}Ht\left(1 \pm \sqrt{1-\frac{4}{9}c}\right)\right]$ since the Hubble parameter is constant. Therefore the dominant mode damps as $a^{-\frac{3}{2}+{\rm Re}\sqrt{\frac{9}{4}-3c}}$ and actually this damping factor is an extension of the above one for $w > -1$ to the de Sitter case $w = -1$.

In summary, the amplitude of the perturbations decreases as

$$\delta\varphi \propto \begin{cases} a^{-\frac{3(1-w)}{4}+{\rm Re}\nu}, & \text{superhorizon } (k \ll aH), \\ a^{-1}, & \text{subhorizon } (k \gg aH). \end{cases} \tag{5.3.4}$$

Here note that the coefficient of the Hubble induced mass c can be varied for the preinflation and χ-oscillation phase as mentioned in Sec. 5.1. In the parametrization of (5.1.11) and (5.1.12), $c_{\rm pre} = c_{\rm pot}$ during preinflation and $c_{\rm osc} = \frac{1}{2}(c_{\rm pot} + c_{\rm kin})$ during the oscillation phase.

Now let us evaluate the total damping factor. In Fig. 5.1, we show the schematic image of the horizon scale aH. $a_{\rm pre,f}$ and $a_{\rm new,i}$ represent the time of the end of preinflation and the beginning of new inflation respectively, and the mode k crosses the horizon three times, at

a_1, a_2, and a_3. Assuming that the amplitude of $\delta\varphi$ is given by the standard value $H_{\rm pre}/(2\pi)$ at the first horizon exit a_1, its amplitude at a_3 is estimated as,

$$\delta\varphi|_3 \sim \frac{H_{\rm pre}}{2\pi}\left(\frac{a_{\rm pre,f}}{a_1}\right)^{-\frac{3}{2}+{\rm Re}\nu_{\rm pre}}\left(\frac{a_2}{a_{\rm pre,f}}\right)^{-\frac{3(1-w)}{4}+{\rm Re}\nu_{\rm osc}}\left(\frac{a_{\rm new,i}}{a_2}\right)^{-1}\left(\frac{a_3}{a_{\rm new,i}}\right)^{-1}, \tag{5.3.5}$$

with use of the above decaying formula. Here $\nu_{\rm pre}$ and $\nu_{\rm osc}$ are the values of ν for $c_{\rm pre}$ and $c_{\rm osc}$ respectively. Noting that the horizon scale aH is proportional to $a^{-\frac{1+3w}{2}}$, this expression can be rewritten as

$$\begin{aligned}\delta\varphi|_3 &\sim \frac{H_{\rm pre}}{2\pi}\left(\frac{aH|_{\rm pre,f}}{k}\right)^{-\frac{3}{2}+{\rm Re}\nu_{\rm pre}}\left(\frac{k}{aH|_{\rm pre,f}}\right)^{\frac{3(1-w)}{2(1+3w)}-\frac{2}{1+3w}{\rm Re}\nu_{\rm osc}}\left(\frac{aH|_{\rm new,}}{k}\right)^{\frac{2}{1+3w}}\left(\frac{k}{aH|_{\rm new,i}}\right)^{-1}\\ &= \frac{H_{\rm pre}}{2\pi}\left(\frac{aH|_{\rm pre,f}}{aH|_{\rm new,i}}\right)^{-\frac{3(1+w)}{1+3w}}\left(\frac{k}{aH|_{\rm pre,f}}\right)^{-{\rm Re}\nu_{\rm pre}-\frac{2}{1+3w}{\rm Re}\nu_{\rm osc}}.\end{aligned} \tag{5.3.6}$$

Finally, with use of $aH \propto a^{-\frac{1+3w}{2}} \propto \rho^{\frac{1+3w}{6(1+w)}}$ for $a_{\rm pre,f} < a < a_{\rm new,i}$, one can obtain

$$\begin{aligned}\delta\varphi|_3 &\sim \frac{H_{\rm pre}}{2\pi}\left(\frac{\rho_{\rm pre}}{\rho_{\rm new}}\right)^{-1/2}\left(\frac{k}{aH|_{\rm pre,f}}\right)^{-{\rm Re}\nu_{\rm pre}-\frac{2}{1+3w}{\rm Re}\nu_{\rm osc}}\\ &\simeq \frac{H_{\rm new}}{2\pi}\left(\frac{k}{aH|_{\rm pre,f}}\right)^{-{\rm Re}\nu_{\rm pre}-\frac{2}{1+3w}{\rm Re}\nu_{\rm osc}}.\end{aligned} \tag{5.3.7}$$

Therefore, if φ is sufficiently massive both during preinflation and the oscillation phase as ${\rm Re}\nu_{\rm pre} = {\rm Re}\nu_{\rm osc} = 0$, the amplitude $\delta\varphi$ at the second horizon exit a_3 is amazingly evaluated by the simple $H_{\rm new}/(2\pi)$. In this case, the curvature perturbations can be also estimated in the standard way, and then the above expectation that the large κ leads a sharp peak on the scalar power spectrum around the beginning of new inflation can be validated.

Moreover this expression suggests another possibility for a peak of the power spectrum. That is, if the Hubble induced mass is so small during the oscillation phase as ${\rm Re}\nu_{\rm osc} > 0$ (the Hubble induced mass during preinflation should be sufficiently large to solve the initial condition problem of new inflation), the spectrum of $\delta\varphi|_3$ can be strongly red-tilted and the modes for $k < aH|_{\rm pre,f}$ can be much amplified. This situation can be realized because the Hubble induced mass during the oscillation phase can be canceled out by the negative $c_{\rm kin}$. Furthermore, in this case, κ should not be large any longer and even the flat inflection condition mentioned in the previous section can be satisfied simultaneously. Then this model can make two peaks on the power spectrum as shown in the next section.

Finally let us mention the large scale modes, $k < aH|_{\rm new,i}$. Those modes are already superhorizon at the beginning of new inflation and therefore the k-dependence of the scalar power spectrum for those modes are given by that of the $\mathcal{P}_\varphi$ at $a_{\rm new,i}$ with use of the δN formalism, taking the initial slice at $a_{\rm new,i}$. For those modes, the amplitude of $\delta\varphi$ at $a_{\rm new,i}$ can be evaluated as

$$\begin{aligned}\delta\varphi|_{\rm new,i} &\sim \frac{H_{\rm pre}}{2\pi}\left(\frac{a_{\rm pre,f}}{a_1}\right)^{-\frac{3}{2}+{\rm Re}\nu_{\rm pre}}\left(\frac{a_{\rm new,i}}{a_{\rm pre,f}}\right)^{-\frac{3(1-w)}{4}+{\rm Re}\nu_{\rm osc}}\\ &\simeq \frac{H_{\rm new}}{2\pi}\left(\frac{\rho_{\rm pre}}{\rho_{\rm new}}\right)^{\frac{1+3w}{6(1+w)}{\rm Re}\nu_{\rm pre}+\frac{1}{3(1+w)}{\rm Re}\nu_{\rm osc}}\left(\frac{k}{aH|_{\rm new,i}}\right)^{\frac{3}{2}-{\rm Re}\nu_{\rm pre}}.\end{aligned} \tag{5.3.8}$$

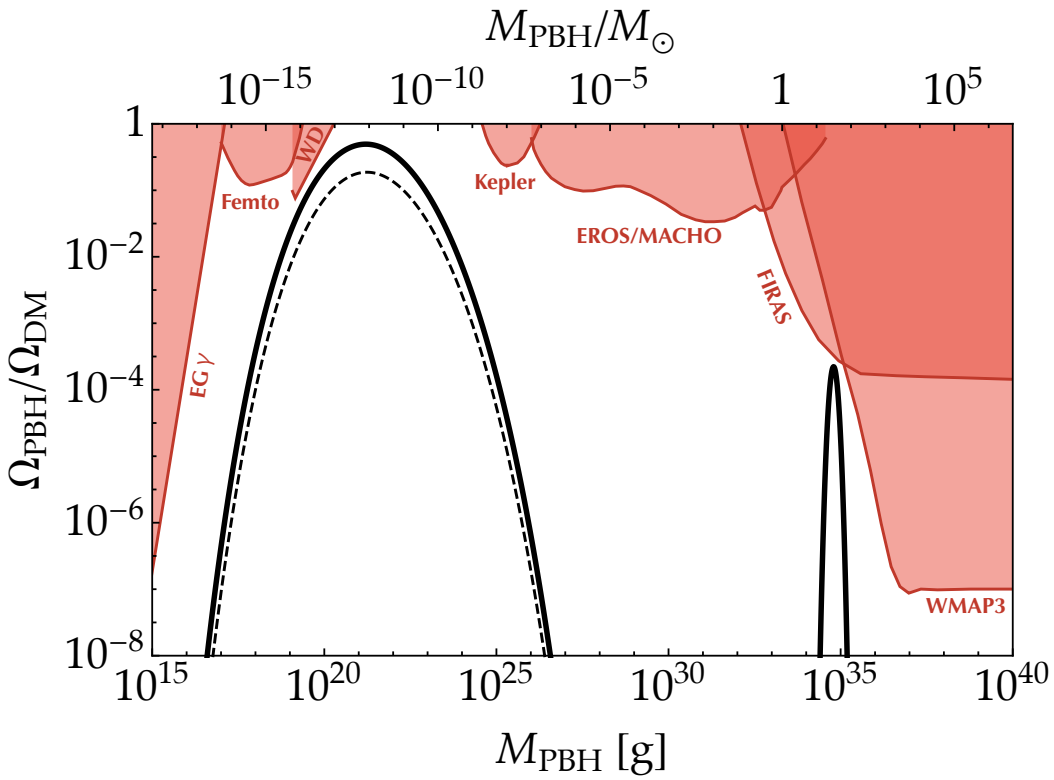

Figure 5.3. The PBH mass fraction to DM $\Omega_{\rm PBH}/\Omega_{\rm DM}$ calculated from the power spectrum shown in Fig. 5.2. The large bump around 10^{20} g corresponds with the flat inflection point, while the sharp peak on $\sim 6\times10^{34}\,\mathrm{g} \sim 30M_\odot$ is caused by a steep amplification on $k \sim 10^5\,\mathrm{Mpc}^{-1}$ due to the cancellation of the Hubble induce mass during the oscillation phase (note that the dashed power spectrum in Fig. 5.2 does not show this second peak). For this mass spectrum, the total PBH fraction reaches unity.

In the second line, the first parenthesis simply represents the amplification factor mentioned in the previous paragraph. The k-dependence is shown by the second parenthesis, and since the Hubble induced mass during preinflation is assumed to be large enough ($\mathrm{Re}\nu_{\rm pre} \sim 0$) as mentioned, finally it can be found that the scalar power spectrum is strongly blue-tilted for $k < aH|_{\rm new,i}$. Therefore the constraints on the large scale power spectrum could be safely satisfied.

5.4 Specific examples

Let us show some concrete examples where PBHs constitute the main component of DM. In Fig. 5.2, the resultant scalar power spectrum for parameters:

$$\begin{aligned} &m = 10^{-5}, \quad v = 10^{-4}, \quad C = 1.3\times10^{-16}, \quad \kappa = -0.338, \\ &g = 0.00456, \quad c_{\rm pot} = 1, \quad c_{\rm kin} = -0.92, \end{aligned} \tag{5.4.1}$$

is shown as a black thick line. To obtain this spectrum, we do not use the slow-roll approximation but numerically solve the full EoM in the linear perturbation theory described in Sec. 1.2.1. That is, we solve the EoM (1.2.14) and (1.2.15) with the initial conditions (1.2.26)

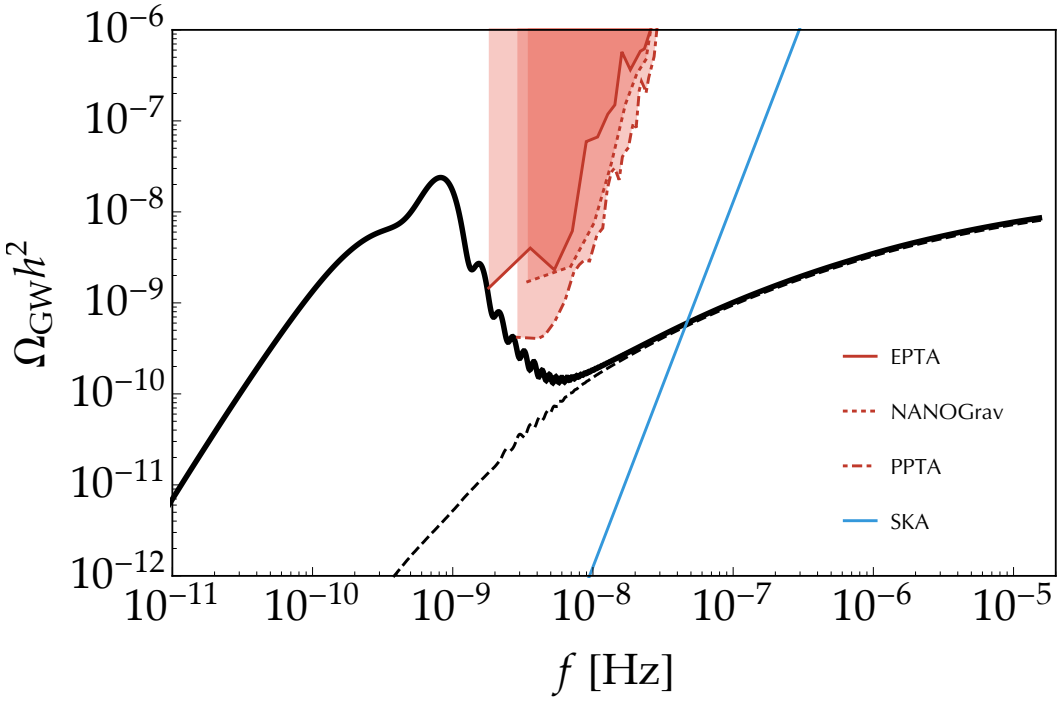

Figure 5.4. The black thick/dashed line represents the associated secondary GW spectrum caused by the scalar perturbations shown as the black thick/dashed line in Fig. 5.2. Red lines represent the several current PTA constraints: European Pulser Timing Array (plane) [170], NANOGrav (dotted) [171], and Parkes Pulsar Timing Array (dot-dashed) [172]. The black thick line marginally avoids them despite the formation of $30M_\odot$-PBH, thanks to the steep fall-off of the scalar power spectrum apart from the maximum point. The future SKA experiments whose sensitivity is shown by the blue line [173, 174] can detect both black thick and dashed signals.

and (1.2.27), and obtain the power spectrum of the curvature perturbation, following Eqs. (1.2.29) and (1.2.30). We also plot the result for the same parameters except that $c_{\rm kin}$ is zero as a black dashed line for comparison. The red region illustrates the constraints from the CMB spectral μ-distortion (4.2.71) described in Sec. 4.2.5 [119, 180, 181]

$$9\times10^{-5}\gtrsim\mu\sim2.2\mathcal{P}_\zeta(k)\left[\exp\left(-\frac{k}{5400\,\mathrm{Mpc}^{-1}}\right)-\exp\left(-\left(\frac{k}{31.6\,\mathrm{Mpc}^{-1}}\right)^2\right)\right]. \quad (5.4.2)$$

The broad bump both on the thick and dashed power spectrum corresponds with the flat inflection in new inflation, while the peak around $10^5\,\mathrm{Mpc}^{-1}$ on the thick one is caused by the amplification of the φ's power due to the cancellation of the Hubble induced mass during the oscillation phase ($c_{\rm osc}=\frac{1}{2}(c_{\rm pot}+c_{\rm kin})=0.04$) as mentioned in the previous section.

The corresponding PBH mass spectrum is shown in Fig. 5.3. To obtain this spectrum, we used the Gaussian window function $\tilde{W}(kR)=\mathrm{e}^{-k^2R^2/2}$, the original value for the PBH mass fraction to the horizon mass $\gamma=c_{\rm s}^3=3^{-3/2}$ and the threshold $\delta_{\rm th}=w=1/3$ [52]. The broad bump on the scalar power causes the large abundance of PBHs around $10^{20}\,\mathrm{g}$, while the steep amplification on $k\sim10^5\,\mathrm{Mpc}^{-1}$ yields a second peak on the PBH mass spectrum around $6\times10^{34}\,\mathrm{g}\sim30M_\odot$ which might be able to explain the LIGO's GW events (note that the dashed power spectrum does not show this second peak). For this mass spectrum,

the total PBH fraction to DM reaches unity, so this is a concrete example where the main component of DM consists of PBHs, while their small fraction is on $\sim 30M_\odot$ for LIGO's events simultaneously.

Also, following Sec. 4.2.4, we estimate the secondary GW spectrum and plot them in Fig. 5.4 with several current PTA (European Pulser Timing Array [170], NANOGrav [171], Parkes Pulsar Timing Array [172]) and future SKA constraints [173, 174]. In spite of the formation of PBHs $\sim 30M_\odot$, the resultant GW marginally avoids the current constraints, thanks to the steep fall-off of the scalar power spectrum apart from the maximum point. However it still depends on the precise value of γ, the fraction of the PBH mass to the horizon mass at the formation time. Slightly larger γ leads the smaller corresponding scale as Eq. (4.1.26) indicates, and the peak frequency of the secondary GW is shifted to higher values. Anyway the model cannot be excluded immediately currently. The blue line shows that the future SKA experiment can severely constrain the PBH scenario even if one gives up the $30M_\odot$-PBH (namely the black dashed line), or might detect GW signals associated with the PBH formation.

Chapter 6

Case 2: Continuous Double Inflation

In this chapter, we consider the PBH formation in the continuous double inflation models, whose energy scales are not separated and two inflation phases are connected smoothly. Particularly we focus on the hybrid-inflation-type potential as the simplest example. Around the critical point of hybrid inflation, the perturbative expansion w.r.t. inflaton fields is broken down, and therefore we use the non-perturbative method described in Sec. 2.3. After the numerical parameter searches, we conclude that detectably massive PBHs are inevitably overproduced in hybrid inflation. In this chapter, we adopt the Planck unit $M_{Pl} = 1$ and this chapter is based on Ref. [193].

6.1 Aspects of hybrid inflation

In this section, we would like to introduce hybrid inflation and its various aspects. Hybrid inflation was originally proposed by Linde [194], combining chaotic and hilltop inflation. The generic form of its potential is given by

$$V(\phi,\psi) = V(\phi) + \Lambda^4\left[\left(1-\frac{\psi^2}{M^2}\right)^2 + 2\frac{\phi^2\psi^2}{\phi_c^2 M^2}\right], \tag{6.1.1}$$

where ϕ and ψ are two real scalar fields and Λ, M, and ϕ_c are dimensionful model parameters. In this model, the inflationary universe is driven by the false vacuum energy Λ^4 of the so-called waterfall field represented by ψ here, which is stabilized by the coupling to the inflaton ϕ at first. Then, at the time when the ϕ's vev becomes smaller than ϕ_c due to its own potential $V(\phi)$, ψ's effective mass squared $m^2_{\psi,\mathrm{eff}}|_{\psi\sim 0} = \partial^2_\psi V|_{\psi\sim 0} = 2\frac{\Lambda^4}{M^2}\left(\frac{\phi^2}{\phi_c^2}-1\right)$ becomes negative and inflation will be terminated by the second order phase transition of ψ. Hybrid inflation is an attractive model in the point that the initial condition problem is much improved even though it is small field inflation (namely the scalar fields' vev do not exceed the Planck scale).

The stage before ϕ reaches ϕ_c is called *valley phase* and the stage after that is referred as *waterfall phase*. In the generic parameter regions, the waterfall phase basically ends instantaneously and the valley phase should continue more than 60 e-folds, being fully responsible for the observable universe. Among this type, the original model by Linde where the inflaton's potential is given by the simple mass term predicts blue-tilted curvature perturbations and is already excluded. The supersymmetric flat inflaton whose potential is raised up logarithmically due to the Coleman-Weiberg correction can give a red-tilted spectrum [195], and moreover, it has been suggested that the additional linear potential from the soft SUSY breaking can realize $n_s \sim 0.96$ [196–198], which is in the Planck's sweet spot [9]. On the other hand, the literatures [199–203] suggested the possibility of the long-lasting waterfall phase. In these models, ψ's potential is so flat that the waterfall phase continues more than 60 e-folds like hilltop inflation.

In this chapter we concentrate on the intermediate case, that is, the mild-waterfall models where the waterfall phase continues more than a few e-folds but less than 60 e-folds. The attractive point of the mild case is that very massive PBHs can be produced a lot. That is because the perturbations can grow much around the phase transition critical point due to the flatness of the (especially ψ's) potential and such perturbations will be inflated during the following mild-waterfall phase. The PBH mass, which can be approximated by the horizon mass at its formation time, is given by

$$M_{\rm PBH} \sim H^{-1} \sim H_{\rm inf}^{-1} e^{2N_{\rm water}} \simeq 1.0 \times 10^4\,{\rm g} \left(\frac{H_{\rm inf}}{10^9\,{\rm GeV}}\right)^{-1} e^{2N_{\rm water}}, \tag{6.1.2}$$

where $N_{\rm water}$ represents the e-folding numbers for the waterfall phase, and then the mode exiting the horizon around the critical point can be written as $k \sim e^{-N_{\rm water}} k_f$ with use of the horizon scale at the end of inflation $k_f = (aH)_f$. In the second approximation, we use the relation $H \propto (aH)^2$ in the radiation dominated era. If the waterfall phase continues sufficiently, the corresponding PBH mass can be detectably large due to the exponential boost.

To estimate the PBH abundance in such models, one has to calculate the curvature perturbations generated around the critical point. Historically García-Bellido et al. [204] gave a first rough estimation with use of δN formalism. Lyth [205, 206] analytically studied the growth of the perturbation of ψ and gave a more precise result, but his analysis can be applied only for a relatively fast waterfall transition. Bugaev and Klimai [207, 208] applied the Lyth's result to PBH formation. Sfakianakis et al. [209, 210] used the similar formulation and found the dependence of the curvature perturbation on the number of the waterfall fields. Recently Clesse et al. [203, 211] derived the semi-classical formula for the curvature perturbations in the mild-waterfall case, using the stochastic formalism for the initial condition of ψ at the critical point, and applied it to PBH formation. Their results were qualitatively correct but not completed yet quantitatively. Also their main conclusions about PBH formation seem to be wrong due to some simple mistakes. In this chapter, with use of the non-perturbative method described in Sec. 2.3 we proceed the calculation of PBH formation more precisely, but before that, let us briefly review the Clesse's works in the next section for analytic comprehension.

6.2 Analytic estimation of curvature perturbation in mild-waterfall case

Let us begin by the potential (6.1.1). Generically the inflaton's potential $V(\phi)$ is an arbitrary function. However in the case of the mild waterfall, ϕ's vev is almost constant around ϕ_c during the last 60 e-folds and therefore one can Taylor expand $V(\phi)$ around ϕ_c. Namely, adopting the notation of Ref. [211], we consider the following potential form hereafter:

$$V(\phi,\psi) = \Lambda^4\left[\left(1-\frac{\psi^2}{M^2}\right)^2 + 2\frac{\phi^2\psi^2}{\phi_c^2 M^2} + \frac{\phi-\phi_c}{\mu_1} - \frac{(\phi-\phi_c)^2}{\mu_2^2}\right]. \tag{6.2.1}$$

This is the most generic hybrid potential for the mild-waterfall case. It has five dimensionful parameters as Λ, M, ϕ_c, μ_1, and μ_2. Among them, two d.o.f. can be fixed by the information of the amplitude and tilt of the power spectrum of the curvature perturbations on the CMB scale. In the mild-waterfall case, the CMB scale corresponds with the point in the valley phase, where the waterfall field is still irrelevant due to its large effective mass. Therefore the perturbations can be analyzed linearly as the simple single-field slow-roll case. At first the slow-roll parameters are given by,

$$\epsilon_V = \frac{1}{2}\left(\frac{V_\phi}{V}\right)^2\Bigg|_{\phi\sim\phi_c,\psi\sim 0} \simeq \frac{1}{2\mu_1^2}, \qquad \eta_V = \frac{V_{\phi\phi}}{V}\Bigg|_{\phi\sim\phi_c,\psi\sim 0} \simeq -\frac{2}{\mu_2^2}. \tag{6.2.2}$$

The spectral index n_s is given by

$$n_s = 1 - 6\epsilon_V + 2\eta_V \simeq 1 - \frac{4}{\mu_2^2}, \tag{6.2.3}$$

where we assumed that η_V dominates ϵ_V (as can be checked easily for specific parameter regions shown in the following sections), which is the case for small field inflation. From this relation, with the Planck's best fit value $n_s \simeq 0.9655$ [9], μ_2 should be fixed to

$$\mu_2 = \frac{2}{\sqrt{1-n_s}} \simeq 11. \tag{6.2.4}$$

Also the amplitude of the power spectrum is given by

$$A_s = \frac{1}{24\pi^2}\frac{V}{\epsilon_V} \simeq \frac{\Lambda^4\mu_1^2}{12\pi^2}. \tag{6.2.5}$$

Again it should be fixed by the Planck's result $A_s \simeq 2.198\times 10^{-9}$ [9], which gives the following relation:

$$\Lambda^4 \simeq 2.198\times 10^{-9}\times 12\pi^2\mu_1^{-2}. \tag{6.2.6}$$

In the following sections, we will fix Λ with this constraint and take M, ϕ_c, and μ_1 as free parameters.

At the critical point, ψ can be assumed to have a non-zero vev due to the Hubble fluctuation. Though its expectation value will be given later, let us consider the classical dynamics

after the critical point from some initial field value $(\phi, \psi) = (\phi_c, \psi_0)$. The slow-roll EoM at the leading order is given by

$$\begin{cases} 3H^2 \dfrac{d\phi}{dN} = -V_\phi \simeq -\dfrac{\Lambda^4}{\mu_1} - \dfrac{4\Lambda^4\psi^2}{M^2\phi_c^2}\phi, & (6.2.7) \\ 3H^2 \dfrac{d\psi}{dN} = -V_\psi \simeq -\dfrac{4\Lambda^4}{M^2}\left(\dfrac{\phi^2}{\phi_c^2} - 1\right)\psi, & (6.2.8) \\ 3H^2 \simeq \Lambda^4. & (6.2.9) \end{cases}$$

Then let us divide the waterfall phase into two stages; in the first phase-1 the second term of the right side of Eq. (6.2.7) is negligible, while in the phase-2 that term dominates over the first term. Though we do not describe in detail here, Clesse and García-Bellido showed that the contributions of the phase-2 for the e-folding number and the curvature perturbation can be negligible.

In the phase-1, changing the variables as

$$\phi = \phi_c e^{\xi} \simeq \phi_c(1+\xi), \qquad \psi = \psi_0 e^{\chi}, \tag{6.2.10}$$

the EoM reads

$$\begin{cases} 3H^2 \dfrac{d\xi}{dN} \simeq -\dfrac{\Lambda^4}{\mu_1\phi_c}, & (6.2.11) \\ 3H^2 \dfrac{d\chi}{dN} \simeq -\dfrac{8\Lambda^4}{M^2}\xi. & (6.2.12) \end{cases}$$

Eq. (6.2.11) can be easily solve as

$$N = -\xi\mu_1\phi_c. \tag{6.2.13}$$

Substituting it to Eq. (6.2.12), one can obtain the classical trajectory as

$$\xi^2 = \frac{M^2}{4\mu_1\phi_c}\chi. \tag{6.2.14}$$

The end of the phase-1 is determined by

$$\frac{\Lambda^4}{\mu_1} = \frac{4\Lambda^4\psi^2}{M^2\phi_c^2}\phi, \tag{6.2.15}$$

and therefore, approximating ϕ by ϕ_c, the value of χ at the end of the phase-1 is given by

$$\chi_2 = \log\left(\frac{M\phi_c^{1/2}}{2\mu_1^{1/2}\psi_0}\right). \tag{6.2.16}$$

With use of this value, the total e-folds for the phase-1 can be written as

$$N_1 = \frac{\sqrt{\chi_2}}{2} M\phi_c^{1/2}\mu_1^{1/2}. \tag{6.2.17}$$

To obtain the curvature perturbation in the δN formalism, one has to calculate the e-folding number from the arbitrary initial field values (ξ_i, χ_i). It can be done as

$$N_1 = -\mu_1\phi_c(\xi_{2i} - \xi_i), \qquad \xi_{2i} = -\sqrt{-\xi_i^2 + \frac{M^2(\chi_2 - \chi_i)}{4\mu_1\phi_c}}. \tag{6.2.18}$$

Fluctuating the inflaton fields around the classical trajectory (6.2.14), the difference of the e-folding number is nothing but the curvature perturbations. The derivatives of N_1 w.r.t. ϕ and ψ can be obtained by the chain rule as

$$N_{1,\phi} = \frac{\partial N_1}{\partial \xi_i}\frac{\partial \xi_i}{\partial \phi}\bigg|_{\rm cl} \simeq \mu_1, \qquad N_{1,\psi} = \frac{\partial N_1}{\partial \chi_i}\frac{\partial \chi_i}{\partial \psi}\bigg|_{\rm cl} \simeq \frac{M^2}{8\xi_2\psi_k}, \tag{6.2.19}$$

where ψ_k is the ψ's value on the classical trajectory at N_k which is the backward e-folds corresponding with $k = aH$:

$$\psi_k = \psi_0 e^{\chi_k}, \qquad \chi_k = \frac{4\phi_c\mu_1\xi_k^2}{M^2}, \qquad \xi_k \simeq -\frac{(N_1 - N_k)}{\mu_1\phi_c}, \tag{6.2.20}$$

and ξ_2 is the ξ's value at the end of the phase-1: $\xi_2^2 = M^2\chi_2/(4\mu_1\phi_c)$. Therefore the power spectrum of the curvature perturbation can be evaluated as

$$\mathcal{P}_\zeta \simeq (N_{1,\phi}^2 + N_{1,\psi}^2)\left(\frac{H}{2\pi}\right)^2 \simeq \frac{\Lambda^4 M^2\mu_1\phi_c}{192\pi^2\chi_2\psi_k^2}, \tag{6.2.21}$$

where we assumed that $N_{1,\phi}^2 \ll N_{1,\psi}^2$ which can be checked for the concrete parameter sets. Note that this power spectrum has its maximum at the critical point as

$$\mathcal{P}_{\zeta,\max} = \frac{\Lambda^4 M^2\mu_1\phi_c}{192\pi^2\chi_2\psi_0^2}. \tag{6.2.22}$$

Now let us evaluate the initial condition ψ_0. It would be approximated by $\sigma_\psi = \sqrt{\langle\psi^2\rangle}$ at the critical point, which can be estimated in the stochastic formalism. That is, the differential equation for ψ^2 can be obtained in the stochastic formalism as follows. First the Langevin equation which ψ follows is mathematically written as (see also Sec. 2.3.1)

$$\mathrm{d}\psi = -\frac{V_\psi}{3H^2}\mathrm{d}N + \frac{H}{2\pi}\mathrm{d}W, \tag{6.2.23}$$

where W denotes the Brownian motion. In the stochastic calculus, the differential of a function f is not given by the simple chain rule but written as

$$\mathrm{d}f(N, X(N)) = f_N(N, X(N))\mathrm{d}N + f_X(N, X(N))\mathrm{d}X + \frac{1}{2}f_{XX}(N, X(N))\mathrm{d}X\mathrm{d}X, \tag{6.2.24}$$

which is called the Ito-Doeblin formula (see e.g. the textbook [33]). Also the differential of the Brownian motion satsfies

$$\mathrm{d}W(N)\mathrm{d}W(N) = dN, \qquad \mathrm{d}N\mathrm{d}N = \mathrm{d}N\mathrm{d}W(N) = 0. \tag{6.2.25}$$

With use of these formulae, one can obtain the stochastic differential equation for ψ^2 as

$$\mathrm{d}\left(\psi^2\right) = 2\psi\mathrm{d}\psi + \mathrm{d}\psi\mathrm{d}\psi = \left[\frac{16}{M^2\mu_1\phi_\mathrm{c}}\psi^2 N + \left(\frac{H}{2\pi}\right)^2\right]\mathrm{d}N + \frac{H}{\pi}\psi\mathrm{d}W, \tag{6.2.26}$$

or one can consider its formal solution:

$$\psi^2 = \psi_\mathrm{i}^2 + \int_{N_\mathrm{i}}^{N}\left[\frac{16}{M^2\mu_1\phi_\mathrm{c}}\psi^2(N')N' + \left(\frac{H}{2\pi}\right)^2\right]\mathrm{d}N' + \int_{N_\mathrm{i}}^{N}\frac{H}{\pi}\psi\mathrm{d}W. \tag{6.2.27}$$

The expectation value of the last term of the right side becomes zero as described in Sec. 2.3.1, and therefore one obtains the differential equation for $\langle\psi^2\rangle$ as follows.

$$\frac{\mathrm{d}\langle\psi^2\rangle}{\mathrm{d}N} = \frac{16}{M^2\mu_1\phi_\mathrm{c}}\langle\psi^2\rangle N + \left(\frac{H}{2\pi}\right)^2. \tag{6.2.28}$$

Its solution is given by

$$\langle\psi^2\rangle = \langle\psi^2\rangle(N=0)\exp\left(\frac{AN^2}{2}\right) + \frac{B}{\sqrt{A}}\exp\left(\frac{AN^2}{2}\right)\sqrt{\frac{\pi}{2}}\mathrm{erf}\left(\frac{\sqrt{A}N}{\sqrt{2}}\right), \tag{6.2.29}$$

where

$$A = \frac{16}{M^2\mu_1\phi_\mathrm{c}}, \qquad B = \left(\frac{H}{2\pi}\right)^2. \tag{6.2.30}$$

Then we take the origin of N at the critical point and impose the boundary condition as

$$\lim_{N\to-\infty}\langle\psi^2\rangle = 0. \tag{6.2.31}$$

Noting that

$$\mathrm{erf}(x) = \frac{2}{\sqrt{\pi}}\int_0^x \mathrm{e}^{-t^2}\mathrm{d}t \to -1, \qquad x\to-\infty, \tag{6.2.32}$$

One finally obtain the variance of ψ at the critical point as

$$\sigma_\psi^2 = \langle\psi^2\rangle(N=0) = \sqrt{\frac{\pi}{2}}\frac{B}{\sqrt{A}} = \frac{\Lambda^4\sqrt{2\phi_\mathrm{c}\mu_1}M}{96\pi^{3/2}}. \tag{6.2.33}$$

Therefore, from Eq. (6.2.22), the maximum amplitude of the power spectrum can be approximated by

$$\mathcal{P}_{\zeta,\max} \simeq \frac{\Lambda^4 M^2\phi_\mathrm{c}\mu_1}{192\pi^2\chi_2\sigma_\psi^2} = \frac{M\phi_\mathrm{c}^{1/2}\mu_1^{1/2}}{2\sqrt{2\pi}\chi_2}. \tag{6.2.34}$$

The key point is that both the e-folding numbers for the waterfall phase $N_\mathrm{water} \simeq N_1$ and the maximum of the power spectrum $\mathcal{P}_{\zeta,\max}$ depend almost only on the specific parameter combination $\Pi^2 = M^2\phi_\mathrm{c}\mu_1$, except for the small logarithmic dependence due to χ_2. Indeed, from Eqs. (6.2.17) and (6.2.34), one can find a one-to-one monotonic increase correspondence

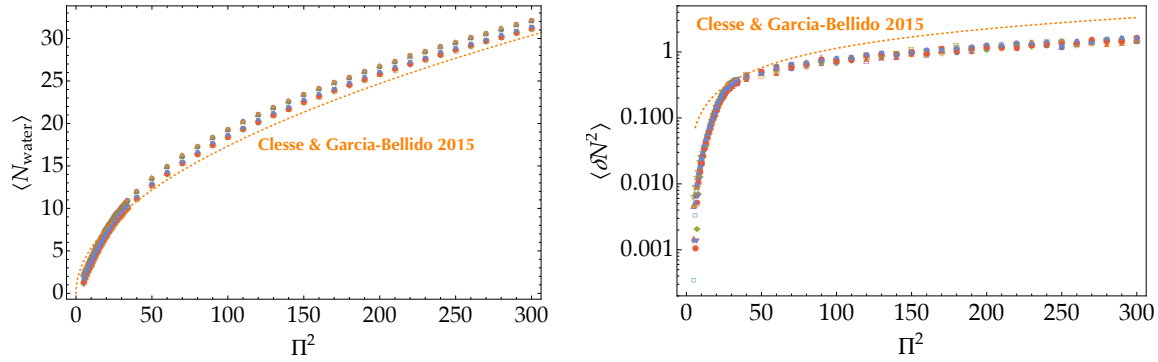

Figure 6.1. The mean e-folds of the waterfall phase (left panel) and the variance of their perturbations (right panel) vs. $\Pi^2 = M^2\phi_{\rm c}\mu_1$ for various parameter sets in the searching region (6.3.6). μ_1 is varied for each set of M and $\phi_{\rm c}$. There are 12 sets of $(M, \phi_{\rm c})$ represented by different markers although they cannot be distinguished in the figure. 2000 realizations are made for each data point. It is clearly seen that both $\langle N\rangle$ and $\langle \delta N^2\rangle$ depend almost only on Π^2 as the semi-classical result suggested. However, while the semi-classical results (orange dotted lines) are well consistent with the stochastic results for $\langle N\rangle$, there are factor differences in $\langle \delta N^2\rangle$. These plots indicate that Π^2 should be less than about 10 to satisfy the PBH constraint $\langle \delta N^2\rangle \lesssim 0.01$ and it means the waterfall phase cannot continue more than about 5 e-folds.

between $N_{\rm water}$ and $\mathcal{P}_{\zeta,\rm max}$. Also let us here estimate the typical value of χ_2. Substituting the initial condition $\psi_0 = \sigma_\psi$ (6.2.33) into Eq. (6.2.16) and using the CMB normalization (6.2.6),[1] χ_2 can be written as

$$\chi_2 = \log\left(\left(\frac{2}{\pi}\right)^{1/4} A_{\rm s}^{-1/2}\Pi^{1/2}\right), \qquad \Pi^2 = M^2\phi_{\rm c}\mu_1, \tag{6.2.35}$$

where $A_{\rm s} = 2.198\times 10^{-9}$. From this expression, it can be seen that χ_2 is around 10 for typical values $10 \lesssim \Pi^2 \lesssim 1000$ in the mild-waterfall cases. Therefore, from Eqs. (6.2.17) and (6.2.34), one obtains the following relation, which hardly depends on any detail parametrization.

$$\mathcal{P}_{\zeta,\rm max} \simeq \frac{1}{\sqrt{2\pi\chi_2^3}} N_{\rm water} \simeq 0.01 N_{\rm water}. \tag{6.2.36}$$

Since the PBH constraints on the curvature perturbations are $\mathcal{P}_\zeta \lesssim \mathcal{O}(0.01)$ as mentioned, it can be obviously seen that the PBH overproduction is inevitable in the mild-waterfall cases such that $N_{\rm water} \gtrsim \mathcal{O}(10)$. In the next section, we will check and clarify this estimation with use of the stochastic formalism.

6.3 Parameter search

Though we reviewed the semi-classical result in the previous section, the dynamics of the waterfall field around the critical point is dominated by the Hubble fluctuations. Therefore the perturbation theory w.r.t. ψ around the critical point essentially breaks down (cf. [28, 212]). Accordingly we calculate the curvature perturbation in the stochastic-δN formalism

[1] Even if one does not use the CMB normalization and deal with Λ as a free parameter, χ_2 depends on Λ only logarithmically.

described in Sec. 2.3 without the perturbative expansions w.r.t. ϕ and ψ. In this section we show the numerical results in the wide parameter region and conclude that PBHs are overproduced in the mild-waterfall cases which is the main claim of this chapter.

6.3.1 Mean and variance of e-folds

In the stochastic formalism, we concretely consider the following self-closed (except for $\mathcal{P}_{\phi^I}$) Langevin equations (2.3.7) with the Friedmann constraint.[2]

$$\begin{cases} \dfrac{\mathrm{d}\phi^I}{\mathrm{d}N}(N) = \dfrac{\pi^I}{H}(N) + \mathcal{P}_{\phi^I}^{1/2}(N)\xi^I(N), \\ \dfrac{\mathrm{d}\pi^I}{\mathrm{d}N}(N) = -3\pi^I(N) - \dfrac{V_I}{H}(N), \\ V_I(N) = V_I(\phi(N), \psi(N)), \\ 3H^2(N) = \displaystyle\sum_i \frac{\pi_i^2}{2} + V(\phi(N), \psi(N)), \\ \langle \xi^I(N) \rangle = 0, \\ \langle \xi^I(N)\xi^J(N') \rangle = \delta^{IJ}\delta(N - N'), \end{cases} \tag{6.3.1}$$

where the indices I and J denote 1 or 2 and $\phi^1 = \phi$ and $\phi^2 = \psi$. Regarding $\mathcal{P}_{\phi^I}$, the massless limit value $(H/(2\pi))^2$ is often used but here we try to take account of the mass effect. Concretely speaking, we approximate $\mathcal{P}_{\phi^I}$ by the constant mass solution (1.2.47) as

$$\mathcal{P}_{\phi^I}(N) = \mathcal{P}_{\phi^I}(k = \epsilon a H) = \frac{H^2}{8\pi}\epsilon^3 |H_{\nu_I}^{(1)}(\epsilon)|^2, \tag{6.3.2}$$

where $\epsilon \ll 1$ is the classicalization parameter which we will fix to 0.01 hereafter and $H_\nu^{(1)}(x)$ is the Hankel function of the first kind defined by

$$H_\nu^{(1)}(x) = J_\nu(x) + iY_\nu(x), \tag{6.3.3}$$

with the Bessel functions of the first and second kind, $J_\nu(x)$ and $Y_\nu(x)$. ν_I is given by

$$\nu_I = \sqrt{\frac{9}{4} - \frac{V_{II}}{H^2}}, \tag{6.3.4}$$

for $V_{ii}/H^2 \leq 9/4$. For massive fields satisfying $V_{ii}/H^2 > 9/4$, we simply assume that their Hubble noise vanishes. Since numerical calculations of the Bessel functions are time consuming, we use the asymptotic forms of them for small arguments as

$$J_\nu(x) \simeq \frac{1}{\Gamma(\nu+1)}\left(\frac{x}{2}\right)^\nu, \qquad Y_\nu(x) \simeq -\frac{\Gamma(\nu)}{\pi}\left(\frac{2}{x}\right)^\nu. \tag{6.3.5}$$

[2]Here we assume that there is no correlation between the different ξ^I. However the correlations between them due to the interactions well inside the horizon can be also included. In this chapter, we omit them for simplicity after easily checked that they do not affect the result so much.

Let us describe the method more concretely. At first, one must determine the initial flat slice in the valley phase and the final uniform density slice around the end of inflation. Here, regarding the initial flat slice, inflation at the valley phase can be approximated by the single-field case and moreover the curvature perturbations are much smaller than those expected in the waterfall phase. Therefore, neglecting the curvature perturbations, the initial flat slice can be approximated by the uniform ϕ slice and the ψ's field value is almost irrelevant. Next, making many realizations of the Langevin equations from the initial field values to the final energy density slice, one can obtain various realizations of the e-folding numbers. Their deviations from the mean value $\langle N \rangle$ are nothing but the data set of the curvature perturbations coarse-grained on the horizon scale at the end of inflation. Though the information of the correlation function like $\langle \zeta(\mathbf{x}_1)\zeta(\mathbf{x}_2)\rangle$ for $\mathbf{x}_1 \neq \mathbf{x}_2$ is not obtained at this stage, at least the probability distribution function of the coarse-grained curvature perturbations can be obtained up to the realization errors. With use of this PDF, one can calculate the formation rate of PBHs whose masses are larger than the horizon scale at the end of inflation. In this section, we briefly estimate the PBH abundance by this quantity and find the parameter constraints.

For parameter search, we consider the following three searching regions.

$$\begin{cases} \bullet \quad 10^{-4} \leq M \leq 10^{-1}, \quad \phi_c = \sqrt{2}M, \qquad \text{(SUSY like assumption)}, \\ \bullet \quad M = 0.1, \qquad\qquad 10^{-4} \leq \phi_c \leq 10^{-1}, \\ \bullet \quad 10^{-4} \leq M \leq 10^{-1}, \quad \phi_c = 0.1. \end{cases} \tag{6.3.6}$$

μ_1 is also varied so that $\Pi^2 = M^2\phi_c\mu_1$ takes the value up to 300. Λ is determined by Eq. (6.2.6) for each value of μ_1. In Fig. 6.1, we plot the mean e-folds for the waterfall phase $\langle N_{\rm water}\rangle$ and the variance of their perturbations $\langle \delta N^2\rangle = \langle N^2\rangle - \langle N\rangle^2$ vs. $\Pi^2 = M^2\phi_c\mu_1$ for various parameters in the above searching region. μ_1 is varied for each parameter set (M, ϕ_c). We also plot the semi-classical results (6.2.17) and (6.2.21) by orange dotted lines. Here note that the variance and the power spectrum are related by

$$\langle \delta N^2\rangle \simeq \int_0^{\langle N_{\rm water}\rangle} \mathcal{P}_\zeta(k) \mathrm{d}N_k. \tag{6.3.7}$$

From this figure, it is found that the mean e-folds $\langle N\rangle$ obtained in the stochastic formalism is well fitted by the semi-classical result, while there are factor differences in the variance $\langle \delta N^2\rangle$. It clearly shows the non-perturbative effects which the semi-classical result does not include. However at least it can be said that the full result of $\langle \delta N^2\rangle$ also depends only on the specific parameter combination $\Pi^2 = M^2\phi_c\mu_1$. Having in mind that the variance of the curvature perturbations should be roughly less than 10^{-2} at most not to overproduce PBHs, it can be seen that Π^2 should be less than around 10, which indicates the waterfall phase cannot continue more than about 5 e-folds.

Here let us mention the ϵ-dependence of the results. The stochastic formalism has an indeterminate parameter ϵ which fixes the separation between the classical superhorizon and the quantum subhorizon modes. Since this is just the uncertainty of the formalism, any result should have little ϵ-dependence for reliable calculations. To see the ϵ-dependence, we also show $\langle N\rangle$ and $\langle \delta N^2\rangle$ for $\epsilon = 0.1$ in Fig. 6.2, comparing them to those for $\epsilon = 0.01$. It shows that $\langle \delta N^2\rangle$ has relatively large differences in low Π^2, for which the waterfall phase does not continue so long. That is because, for small ϵ the modes shorter than the coarse-graining scale $k = \epsilon aH$ are erased in the stochastic formalism. Specifically, since $-\log 0.01 \simeq$

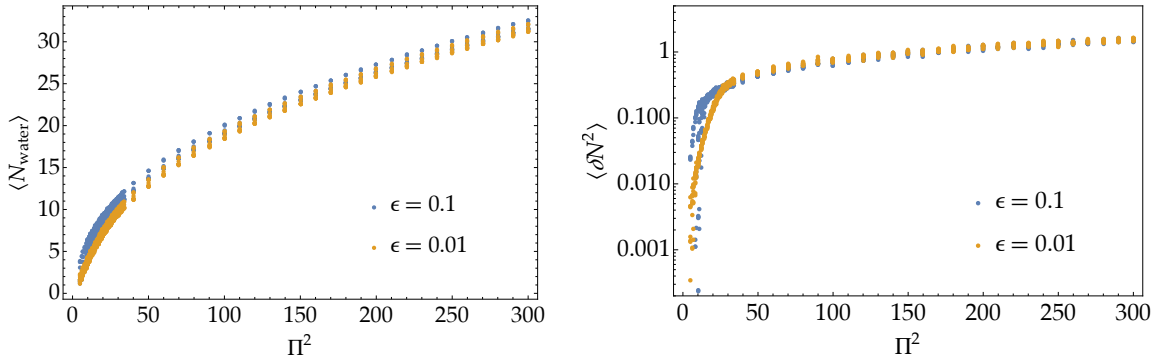

Figure 6.2. The same plots to Fig. 6.1 for $\epsilon = 0.1$ and 0.01. The orange data are the same ones of Fig. 6.1. While $\langle N_{\rm water}\rangle$ has good agreement between different ϵ, $\langle \delta N^2\rangle$ shows a large ϵ-dependence in low Π^2 which indicates that the results in the stochastic formalism for low Π^2 might be unreliable.

4.6, the perturbations generated in about last 4.6 e-folds cannot be treated in the calculations where $\epsilon = 0.01$. Therefore, for low Π^2, the contribution of the perturbations after the critical point cannot be taken into account well in the case of small ϵ, and that is the reason why $\langle \delta N^2\rangle$ for $\epsilon = 0.01$ is suppressed compared to that for $\epsilon = 0.1$. Anyway the case of low Π^2 is slightly out of the range of application of the stochastic formalism, but it does not change the results for large Π^2 and the main conclusion that massive PBHs are overproduced.

6.4 PBH abundance

In this subsection, we estimate the PBH abundance including the non-Gaussian effects. As described in Chapter 4, the PBH formation rate is given by

$$\beta = \int_{\zeta_{\rm th}} P(\zeta_R) {\rm d}\zeta_R, \tag{6.4.1}$$

where $P(\zeta_R)$ is the PDF of the coarse-grained curvature perturbation ζ_R.[3] If one assumes the curvature perturbations follow the Gaussian distribution, β can be easily estimated by

$$\beta_{\rm G} = \int_{\zeta_{\rm th}} \frac{1}{\sqrt{2\pi\sigma_R^2}} {\rm e}^{-\zeta_R^2/(2\sigma_R^2)} {\rm d}\zeta_R, \tag{6.4.2}$$

where σ_R^2 is the variance of the coarse-grained curvature perturbations.

On the left panel of Fig. 6.3, we plot the $\beta_{\rm G}$ with use of $\langle \delta N^2\rangle$ shown in Fig. 6.1 as σ_R^2 for different two threshold values. One is the simple assumption $\zeta_{\rm th} = 1$ and the other is the recent analytic prediction by Harada et al. [88] $\zeta_{\rm th} = \frac{1}{3}\log \frac{3(\chi_a - \sin\chi_a\cos\chi_a)}{2\sin^3\chi_a}\Big|_{\chi_a = \pi\sqrt{w}/(1+3w)} \simeq$

[3] As described in Chapter 4, Young et al. [94] claimed that the density perturbation should be used rather than the curvature perturbation, since the curvature perturbations are undamped quantities even on superhorizon scales and therefore their variance includes the much superhorizon modes, which should not affect the PBH formation. However now the power spectrum has a large peak as shown in the next section, and the larger scale modes than the peak scale are already suppressed. Therefore using the variance of the curvature perturbations will not overestimate the PBH abundance so much. Since we would like to include the NG effects by the form of the third and forth moment of the curvature perturbations, namely $\langle \delta N_R^3\rangle$ and $\langle \delta N_R^4\rangle$, we used the variance of the curvature perturbations here.

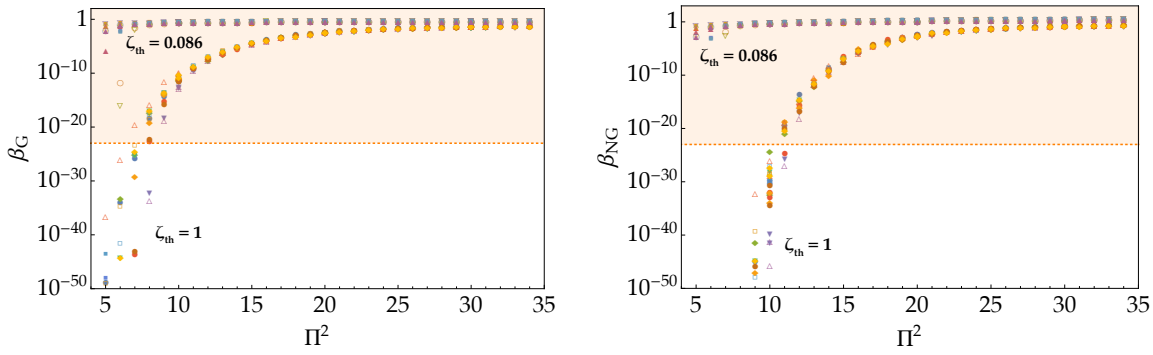

Figure 6.3. Left panel: the plot of the PBH abundance in the Gaussian assumption β_G (6.4.2) with use of the variance shown in Fig. 6.1. Namely it includes all contributions of PBHs more massive than the smallest mass scale $H_{\rm inf}^{-1}$ which corresponds with the horizon scale at the end of inflation. The bottom group is for $\zeta_{\rm th} = 1$, while the upper group is for $\zeta_{\rm th} = 0.086$ [88]. Also the orange dotted line represents the typical constraints for the light PBHs ($\lesssim 10^{15}$ g), namely $\beta \lesssim 10^{-23}$. If $\zeta_{\rm th} = 0.086$, there is no appropriate value of Π^2 with which PBHs are not overproduced. On the other hand, if $\zeta_{\rm th} = 1$, the PBH constraints indicate $\Pi^2 \lesssim 8$, which means the waterfall phase can continue few e-folds. Right panel: the same plot with NG corrections (6.4.3). Though the results for $\zeta_{\rm th} = 0.086$ are hardly different, the PBH abundance for $\zeta_{\rm th} = 1$ is suppressed for low Π^2 compared to the value without NG corrections. Then the constraints are lightly weakened to $\Pi^2 \lesssim 11$ but the duration of the waterfall phase is still as short as 4–5 e-folds.

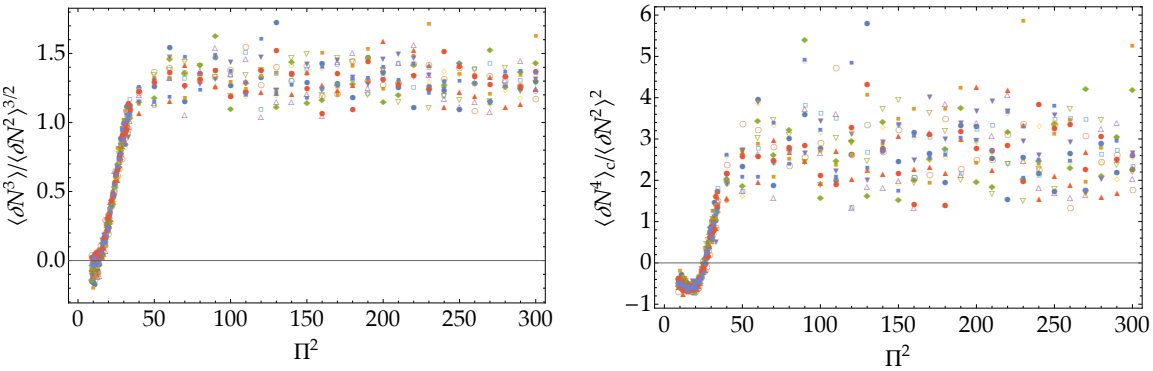

Figure 6.4. The skeness $S^{(3)} = \langle\delta N^3\rangle \,/\, \langle\delta N^2\rangle^{3/2}$ and kurtosis $S^{(4)} = \langle\delta N^4\rangle_{\rm c} \,/\, \langle\delta N^2\rangle^2$ where $\langle\delta N^4\rangle_{\rm c} = \langle\delta N^4\rangle - 3\langle\delta N^2\rangle^2$ is a connected part of the forth moment. It clearly indicates the non-negligible $\mathcal{O}(1)$ NG.

0.086. Also we show the typical constraints for light PBHs $\beta_G \sim 10^{-23}$ as an indicator.[4] The figure shows Π^2 should be less than around 8 for the case $\zeta_{\rm th} = 1$, which means the waterfall phase can continue few e-folds. Also there is almost no proper parameter set with which PBHs are not overproduced for $\zeta_{\rm th} = 0.086$.

However the curvature perturbations produced around the critical point are naively thought to have NG as indicated by its non-perturbativity. In Fig. 6.4, we show the skewness $S^{(3)} = \langle\delta N^3\rangle \,/\, \langle\delta N^2\rangle^{3/2}$ and kurtosis $S^{(4)} = \langle\delta N^4\rangle_{\rm c} \,/\, \langle\delta N^2\rangle^2$ where $\langle\delta N^4\rangle_{\rm c} = \langle\delta N^4\rangle - 3\langle\delta N^2\rangle^2$ is a connected part of the forth moment. These values vanish in a pure Gaussian

[4] Though we want massive PBHs $\gtrsim 10^{15}$ g, we will find such massive ones cannot be produced with proper abundance in hybrid inflation and then we used the constraints for light PBHs $\lesssim 10^{15}$ g.

case, therefore non-zero values of them directly indicate the NG of the curvature perturbations. Indeed these plots show non-negligible $\mathcal{O}(1)$ NG.

These NG modifies the PDF of the curvature perturbations and then β is given by

$$\begin{aligned}\beta_{\rm NG} &= \frac{1}{\sqrt{2\pi}}\int_\nu \mathrm{d}\alpha \exp\left[\sum_{n=3}\frac{(-1)^n}{n!}S^{(n)}\frac{\partial^n}{\partial\alpha^n}\right]\exp\left[-\frac{\alpha^2}{2}\right] \\ &\simeq \frac{1}{\sqrt{2\pi}}\frac{1}{\nu}\exp\left[\sum_{n=3}^{4}\frac{\nu^n}{n!}S^{(n)}\right]\mathrm{e}^{-\nu^2/2}, \end{aligned} \tag{6.4.3}$$

where $\nu = \zeta_{\rm th}/\sigma_R$ and we used the high peak limit $\nu \gg 1$ in the second line. Though we truncated them here, it is possible to include the higher order terms than forth order (see also Appendix K of Ref. [213]). This modified probability is plotted on the right panel of Fig. 6.3. Compared to the Gaussian case (left panel), it can be seen that the probability for small Π^2 is suppressed for $\zeta_{\rm c}$, while the result for $\zeta_{\rm th} = 0.086$ hardly changes. As a result, the constraint for Π^2 in the $\zeta_{\rm th} = 1$ case is weakened to $\Pi^2 \lesssim 11$, which corresponds with $\langle N_{\rm water}\rangle \lesssim 4$.

Let us briefly summarize the above results here. We calculated e-folds numerically in the stochastic formalism and checked that the mean e-folds for the waterfall phase and their variance depend almost only on some specific parameter combination $\Pi^2 = M^2\phi_{\rm c}\mu_1$. However simultaneously it was found that the variance of the perturbations becomes large for mild-waterfall hybrid inflation. In fact, if $\zeta_{\rm th} = 0.086$ [88], there is no parameter region where PBHs are not overproduced. Only if the PBH mass is lighter than 10^9 g, the constraint can be avoided because such PBHs are evaporated before the BBN phase. On the other hand, if the threshold is as high as $\zeta_{\rm th} = 1$, the PBH constraints are roughly given by $\Pi^2 \lesssim 8$ (or 11 with NG corrections), which means the waterfall phase can continue few e-folds. It is too short to produce PBHs massive enough to be DMs or seeds of SMBHs for example. This is the main result of this chapter.

Here note that the coarse-graining scale is the horizon scale at the end of inflation, which is the smallest one, and therefore β shown in this section includes all contributions of various mass PBHs. However, as we will show in the next section, the power spectrum has large and only one peak and the main contribution for β is given almost only by the PBHs whose mass corresponds with the peak scale. Hence the resulting β for peak scale can be approximated well by that obtained in this section.

6.5 Examples of power spectrum

In the previous section, we estimated the PBH abundances with use of the curvature perturbations coarse-grained on the horizon scale at the end of inflation. For them to be a good approximation, it is needed that the power spectrum has only one large peak. Moreover it is still unknown where the peak scale is. To clarify them, we show some examples of the power spectra with use of the stochastic-δN formalism described in Sec. 2.3.

Let us briefly review the algorithm here again.

1. Determine the initial field value from which the mean e-folds is about 60. It represents the field value of our observable universe at 60 e-folds before the end of inflation. In the mild-waterfall case we consider here, this initial field value corresponds with the point

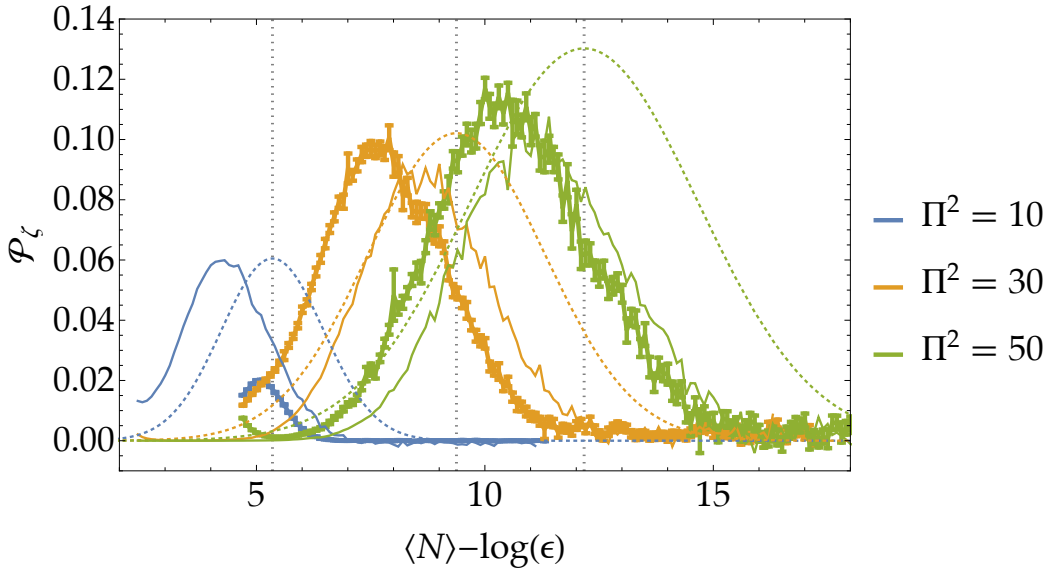

Figure 6.5. The power spectra calculated in the stochastic-δN formalism. The thick lines with error bars represent the results for $\epsilon = 0.01$, while the plane and dotted lines denote those for $\epsilon = 0.1$ and the semi-classical approximation respectively. For $\epsilon = 0.1$, we omit the error bars to avoid a busy figure. The color variation represents the difference of Π^2, but M and ϕ_c are fixed to 0.1 and $0.1\sqrt{2}$. Each power spectrum is averaged over 2500 sample paths and on each data point 1000 paths are made for each sample path. The error bars represent the standard errors. The horizontal axis shows the corresponding scale including $-\log\epsilon$ to cancel the scale shift due to the variation of ϵ. From left to right, the vertical gray dotted lines represent the times when the paths pass the critical point for $\Pi^2 = 10$, 30, and 50. It suggests that the power spectrum has a peak slightly after the critical point, which reflects that the ψ's noise itself becomes large after the critical point due to its tachyonic mass.

in the valley phase where the ψ's vev is almost irrelevant to the inflation dynamics and ϕ is the only relevant field. Therefore the initial condition can be determined almost uniquely, which assures the validity of the prediction of the curvature perturbations in this model.

2. Make one sample path (sample field trajectory including noise) by integrating the Langevin Eqs. (6.3.1) and (6.3.2) from the above initial field value. It represents the dynamics of some Hubble patch in our observable universe.

3. Produce various realizations (trajectories) branching from some point on the above sample path and calculate the e-folds for them to the final uniform density slice around the end of inflation. They give the mean and variance of the e-folds, referred as $\langle N_1\rangle$ and $\langle \delta N_1^2\rangle$ here. The produced realizations show the dynamics of various Hubble patches separated from the sample patch made in process 2 by about $\epsilon^{-1}H_f^{-1}e^{\langle N_1\rangle}$ at the end of inflation.

4. Repeat the procedure 3 with slightly different branching point on the same sample path to obtain another set of the mean and variance $\langle N_2\rangle$ and $\langle \delta N_2^2\rangle$. Then the difference between $\langle \delta N_1^2\rangle$ and $\langle \delta N_2^2\rangle$ indicates the perturbation on the scale $k \simeq k_f e^{-(\langle N_1\rangle + \langle N_2\rangle)/2}$,

that is,

$$\mathcal{P}_\zeta(k) \simeq \frac{\langle \delta N_1^2 \rangle - \langle \delta N_2^2 \rangle}{\langle N_1 \rangle - \langle N_2 \rangle}, \qquad \text{for } k \simeq k_\mathrm{f}\, \mathrm{e}^{-(\langle N_1 \rangle + \langle N_2 \rangle)/2}. \tag{6.5.1}$$

Note that this power spectrum is valid only in the local patch $\epsilon^{-1} H_\mathrm{f}^{-1} \mathrm{e}^{((\langle N_1 \rangle + \langle N_2 \rangle)/2}$ around the sample patch produced in process 2, while we want the power spectrum averaged over our observable universe.

5. To obtain such a power spectrum averaged over our universe, iterate the procedure 2–4 and average the obtained power spectra. This averaged one represents the true power spectrum obtained in our observable universe.

With use of the above algorithm, we calculate and plot the resultant power spectra for $\Pi^2 = 10$, 30, and 50 in Fig. 6.5, compared to those for $\epsilon = 0.1$ and the semi-classical results. While they are not so different for $\Pi^2 = 30$ or 50, the peak for $\epsilon = 0.01$ is much smaller than that for $\epsilon = 0.1$ or the semi-classical one for $\Pi^2 = 10$. This is because $-\log 0.01 \simeq 4.61$ is larger than the peak e-folds $N_\mathrm{peak} \sim 4$, and therefore the peak scale is smaller than $(\epsilon a H|_\mathrm{f})^{-1}$ for $\epsilon = 0.01$, which is the smallest scale the stochastic formalism can treat. Therefore the result for low Π^2 around 10 may be unreliable, but anyway the corresponding PBH mass $M_\mathrm{PBH} \sim H_\mathrm{inf}^{-1}\, \mathrm{e}^{2\times 4} = 3.0 \times 10^7\, \mathrm{g} \left(\frac{10^9\, \mathrm{GeV}}{H_\mathrm{inf}} \right)$ is still too small and our main conclusion that massive PBHs are overproduced in hybrid inflation is not changed.

Conclusions

In this thesis, we discuss the perturbation theory in inflation as well as the primordial black hole formation and its phenomenology. Part I is devoted to the inflationary perturbation theory, and we discuss the primordial black hole in Part II.

In Chapter 1, we review the linear perturbation theory of cosmology, particularly focusing on the perturbation in inflation. In particular, we summarize the most generic linear order formulation of the inflationary perturbations in Sec. 1.2.1, which we use for the calculation in Chapter 5. In Chapter 2, we discuss the formulation beyond the linear perturbation theory with use of the properties of the superhorizon modes. In Sec. 2.3, we derive the non-perturbative algorithm called *stochastic-δN formalism* for the power spectrum of the curvature perturbations. Also we introduce several analytic comprehensions for this algorithm in Sec. 2.3.1. In Chapter 3, we show the calculation algorithm of the squeezed bispectrum in the δN formalism, focusing on the so-called local observer effect. Our algorithm can directly give the bispectrum seen by a local observer.

In Chapter 4, we review the basics of the primordial black hole as well as the current situations of the research of PBH. The current PBH constraints are summarized in Figs. 4.1 and 4.2, and corresponding upper bounds on the power spectrum of the primordial curvature perturbations are shown in Fig. 4.3. Related with this, the constraints on the curvature perturbations by the pulsar timing arrays and CMB μ-distortion are discussed in Secs. 4.2.4 and 4.2.5. Particularly, the current constraints on the gravitational waves by PTA are summarized in Fig. 4.5. We further discuss the PBH formation in two classes of inflation in Chapters 5 and 6. In Chapter 5, we consider the chaotic-new double inflation model as an example of double inflation whose energy scales are separated. In this model, both the PBH-DM scenario and PBHs for LIGO-events can be realized simultaneously. The resultant power spectrum of the curvature perturbations and the mass spectrum of PBHs are shown in Figs. 5.2 and 5.3. The expected secondary GWs are marginally consistent with the current PTA constraints as shown in Fig. 5.4. On the other hand, we consider the hybrid-type inflation as an example of the continuous double inflation models whose energy scales are not separated. With use of the stochastic formalism, we conclude that detectably massive PBHs cannot be obtained in the proper abundance but rather they are inevitably overproduced in hybrid inflation. The specific examples of the power spectra of the curvature perturbations calculated in the stochastic-δN formalism are shown in Fig. 6.5.

Beyond the two point function, the development of robust techniques for computing e.g. the bispectrum is required, following the prospects of future galaxy surveys for non-Gaussianity measurements. We are now working on the extension of the stochastic-δN formalism to the squeezed bispectrum as briefly mentioned in Sec. 3.5. Also further research on the PBH formation in separated double inflation models are important as well as the more precise understanding of the observational PBH constraints since recent remarkable development on observational instruments allows us to significantly close in on the scenario of PBH-DM. We leave these topics for future works.

Acknowledgments

I gratefully thank my supervisor Masahiro Kawasaki. In the almost all of my works, we collaborated and he gave me crucial ideas and comments many times. Also he kindly supported my several research activities abroad. I also appreciate the help of my official supervisor Hitoshi Murayama for my student life. My works are also supported by all other collaborators: Tomohiro Fujita, Keisuke Inomata, Alexander Kusenko, Kyohei Mukaida, Tomohiro Takesako, Vincent Vennin, and Tsutomu T. Yanagida. This thesis is thankfully judged by Koichi Hamaguchi, Aya Bamba, Masahiro Ibe, Shinji Miyoki, and Jun'ichi Yokoyama. I would like to express my appreciation to them. Finally it is my great pleasure to acknowledge all help of the students and staffs of IPMU and ICRR, my parents, and particularly Hiroko Tamazawa, who always supports me both physically and mentally. My research is supported by Advanced Leading Graduate Course for Photon Science and JSPS Research Fellowship for Young Scientists.

Appendix A

Explicit Formulae for Linear Perturbation

In this section, we summarize several explicit formulae for the linear perturbations which are required to derive the field equations and so on. We basically follow Ref. [16].

Before the linear perturbations, let us list the background quantities. The background metric is given by the FLRW one as

$$\bar{g}_{00} = -1, \qquad \bar{g}_{0i} = \bar{g}_{i0} = 0, \qquad \bar{g}_{ij} = a^2(t)\delta_{ij}. \tag{A.0.1}$$

For this metric, the affine connection defined by

$$\Gamma^{\mu}_{\nu\kappa} = \frac{1}{2}g^{\mu\lambda}\left[\frac{\partial g_{\lambda\nu}}{\partial x^{\kappa}} + \frac{\partial g_{\lambda\kappa}}{\partial x^{\nu}} - \frac{\partial g_{\nu\kappa}}{\partial x^{\lambda}}\right], \tag{A.0.2}$$

reads

$$\bar{\Gamma}^{i}_{j0} = \bar{\Gamma}^{i}_{0j} = \frac{\dot{a}}{a}\delta_{ij}, \qquad \bar{\Gamma}^{0}_{ij} = a\dot{a}\delta_{ij}, \qquad \text{(otherwise)} = 0. \tag{A.0.3}$$

The Ricci tensor is defined by

$$R_{\mu\nu} = \frac{\partial\Gamma^{\lambda}_{\mu\lambda}}{\partial x^{\nu}} - \frac{\partial\Gamma^{\lambda}_{\mu\nu}}{\partial x^{\lambda}} + \Gamma^{\kappa}_{\mu\lambda}\Gamma^{\lambda}_{\nu\kappa} - \Gamma^{\kappa}_{\mu\nu}\Gamma^{\lambda}_{\lambda\kappa}, \tag{A.0.4}$$

and their background values are

$$\bar{R}_{00} = 3\frac{\ddot{a}}{a}, \qquad \bar{R}_{ij} = -(2\dot{a}^2 + a\ddot{a})\delta_{ij}, \qquad \text{(otherwise)} = 0. \tag{A.0.5}$$

The unperturbed energy-momentum tensor should be the form of the perfect fluid from the assumption of the rotational and translational invariance as

$$\bar{T}_{\mu\nu} = \bar{p}\bar{g}_{\mu\nu} + (\bar{p} + \bar{\rho})\bar{u}_{\mu}\bar{u}_{\nu}. \tag{A.0.6}$$

$\bar{\rho}(t)$, $\bar{p}(t)$, and $\bar{u}^\mu$ are the unperturbed energy density, pressure, and velocity four-vector respectively, with $\bar{u}^0 = 1$, and $\bar{u}^i = 0$. From the Friedmann equation (0.2.3) and the equation of acceleration (0.2.4), $\bar{\rho}$ and $\bar{p}$ satisfy

$$\bar{\rho} = 3M_{\rm Pl}^2 \frac{\dot{a}^2}{a^2}, \qquad \bar{p} = -M_{\rm Pl}^2 \left(\frac{2\ddot{a}}{a} + \frac{\dot{a}^2}{a^2} \right). \tag{A.0.7}$$

Therefore the trace of the unperturbed energy-momentum tensor is given by

$$\bar{T}^\lambda{}_\lambda = 3\bar{p} - \bar{\rho} = -6M_{\rm Pl}^2 \left(\frac{\ddot{a}}{a} + \frac{\dot{a}^2}{a^2} \right). \tag{A.0.8}$$

Then let us consider the linear perturbations of the metric and energy-momentum tensor:

$$h_{\mu\nu} = g_{\mu\nu} - \bar{g}_{\mu\nu}, \qquad \delta T_{\mu\nu} = T_{\mu\nu} - \bar{T}_{\mu\nu}. \tag{A.0.9}$$

First, at the leading order of them, the perturbation of the inverse metric is given by

$$h^{\mu\nu} = g^{\mu\nu} - \bar{g}^{\mu\nu} = -\bar{g}^{\mu\rho}\bar{g}^{\nu\sigma}h_{\rho\sigma}, \tag{A.0.10}$$

contrary to the standard raising and lowering of indices. The liner perturbations of the affine connection are given by

$$\delta\Gamma^\mu_{\nu\lambda} = \frac{1}{2}\bar{g}^{\mu\rho}[-2h_{\rho\sigma}\bar{\Gamma}^\sigma_{\nu\lambda} + \partial_\lambda h_{\rho\nu} + \partial_\nu h_{\rho\lambda} - \partial_\rho h_{\lambda\nu}], \tag{A.0.11}$$

whose explicit expressions read

$$\delta\Gamma^i_{jk} = \frac{1}{2a^2}(-2a\dot{a}h_{i0}\delta_{jk} + \partial_k h_{ij} + \partial_j h_{ik} - \partial_i h_{jk}), \tag{A.0.12}$$

$$\delta\Gamma^i_{j0} = \frac{1}{2a^2}\left(-\frac{2\dot{a}}{a}h_{ij} + \dot{h}_{ij} + \partial_j h_{i0} - \partial_i h_{j0} \right), \tag{A.0.13}$$

$$\delta\Gamma^0_{ij} = \frac{1}{2}(2a\dot{a}\delta_{ij}h_{00} - \partial_j h_{i0} - \partial_i h_{j0} + \dot{h}_{ij}), \tag{A.0.14}$$

$$\delta\Gamma^i_{00} = \frac{1}{2a^2}(2\dot{h}_{i0} - \partial_i h_{00}), \tag{A.0.15}$$

$$\delta\Gamma^0_{i0} = \frac{\dot{a}}{a}h_{i0} - \frac{1}{2}\partial_i h_{00}, \tag{A.0.16}$$

$$\delta\Gamma^0_{00} = -\frac{1}{2}\dot{h}_{00}. \tag{A.0.17}$$

In particular, we will need

$$\delta\Gamma^\lambda_{\lambda\mu} = \partial_\mu \left[\frac{1}{2a^2}h_{ii} - \frac{1}{2}h_{00} \right], \tag{A.0.18}$$

for the calculation of the Ricci tensor. The perturbations of the Ricci tensor is expressed as

$$\delta R_{\mu\kappa} = \frac{\partial\delta\Gamma^\lambda_{\mu\lambda}}{\partial x^\kappa} - \frac{\partial\delta\Gamma^\lambda_{\mu\kappa}}{\partial x^\lambda} + \delta\Gamma^\eta_{\mu\nu}\bar{\Gamma}^\nu_{\kappa\eta} + \delta\Gamma^\nu_{\kappa\eta}\bar{\Gamma}^\eta_{\mu\nu} - \delta\Gamma^\eta_{\mu\kappa}\bar{\Gamma}^\nu_{\nu\eta} - \delta\Gamma^\nu_{\nu\eta}\bar{\Gamma}^\eta_{\mu\kappa}, \tag{A.0.19}$$

or in more detail,

$$\begin{aligned}
\delta R_{jk} =& -\frac{1}{2}\partial_j\partial_k h_{00} - (2\dot{a}^2 + a\ddot{a})\delta_{jk}h_{00} - \frac{1}{2}a\dot{a}\delta_{jk}\dot{h}_{00} \\
&+ \frac{1}{2a^2}(\nabla^2 h_{jk} - \partial_i\partial_j h_{ik} - \partial_i\partial_k h_{ij} + \partial_j\partial_k h_{ii}) \\
&- \frac{1}{2}\ddot{h}_{jk} + \frac{\dot{a}}{2a}(\dot{h}_{jk} - \delta_{jk}\dot{h}_{ii}) + \frac{\dot{a}^2}{a^2}(-2h_{jk} + \delta_{jk}h_{ii}) + \frac{\dot{a}}{a}\delta_{jk}\partial_i h_{i0} \\
&+ \frac{1}{2}(\partial_j\dot{h}_{k0} + \partial_k\dot{h}_{j0}) + \frac{\dot{a}}{2a}(\partial_j h_{k0} + \partial_k h_{j0}), \qquad \text{(A.0.20)} \\
\delta R_{0j} =& \delta R_{j0} = \frac{\dot{a}}{a}\partial_j h_{00} + \frac{1}{2a^2}(\nabla^2 h_{j0} - \partial_j\partial_i h_{i0}) - \left(\frac{\ddot{a}}{a} + \frac{2\dot{a}^2}{a^2}\right)h_{j0} \\
&+ \frac{1}{2}\frac{\partial}{\partial t}\left[\frac{1}{a^2}(\partial_j h_{kk} - \partial_k h_{kj})\right], \\
\delta R_{00} =& \frac{1}{2a^2}\nabla^2 h_{00} + \frac{3\dot{a}}{2a}\dot{h}_{00} - \frac{1}{a^2}\partial_i\dot{h}_{i0} \\
&+ \frac{1}{2a^2}\left[\ddot{h}_{ii} - \frac{2\dot{a}}{a}\dot{h}_{ii} + 2\left(\frac{\dot{a}^2}{a^2} - \frac{\ddot{a}}{a}\right)h_{ii}\right]. \qquad \text{(A.0.21)}
\end{aligned}$$

To obtain the linear perturbations of the Einstein equations, we need the perturbation of the source tensor

$$S_{\mu\nu} = T_{\mu\nu} - \frac{1}{2}g_{\mu\nu}T^{\lambda}{}_{\lambda}. \qquad \text{(A.0.22)}$$

Its perturbation is formally given by

$$\delta S_{\mu\nu} = \delta T_{\mu\nu} - \frac{1}{2}\bar{g}_{\mu\nu}\delta T^{\lambda}{}_{\lambda} - \frac{1}{2}h_{\mu\nu}\bar{T}^{\lambda}{}_{\lambda}. \qquad \text{(A.0.23)}$$

With use of the trace of the background energy-momentum tensor (A.0.8), one obtains the explicit components of them as

$$\delta S_{jk} = \delta T_{jk} - \frac{a^2}{2}\delta_{jk}\delta T^{\lambda}{}_{\lambda} + 3M_{\rm Pl}^2\left(\frac{\ddot{a}}{a} + \frac{\dot{a}^2}{a^2}\right)h_{jk}, \qquad \text{(A.0.24)}$$

$$\delta S_{j0} = \delta T_{j0} + 3M_{\rm Pl}^2\left(\frac{\ddot{a}}{a} + \frac{\dot{a}^2}{a^2}\right)h_{j0}, \qquad \text{(A.0.25)}$$

$$\delta S_{00} = \delta T_{00} + \frac{1}{2}\delta T^{\lambda}{}_{\lambda} + 3M_{\rm Pl}^2\left(\frac{\ddot{a}}{a} + \frac{\dot{a}^2}{a^2}\right)h_{00}. \qquad \text{(A.0.26)}$$

Then, substituting these expressions into the perturbed Einstein equation

$$\delta R_{\mu\nu} = -M_{\rm Pl}^{-2}\delta S_{\mu\nu}, \qquad \text{(A.0.27)}$$

the explicit linear EoM (1.1.11)–(1.1.13) are obtained.

The conservation law is derived by

$$0 = T^{\mu}{}_{\nu;\mu} = \partial_\mu T^{\mu}{}_{\nu} + \Gamma^{\mu}_{\mu\lambda}T^{\lambda}{}_{\nu} - \Gamma^{\lambda}_{\mu\nu}T^{\mu}{}_{\lambda}. \qquad \text{(A.0.28)}$$

At the zeroth order, only the temporal component $\nu = 0$ is non-trivial and it gives the continuity equation:

$$\dot{\bar{\rho}} + 3\frac{\dot{a}}{a}(\bar{\rho} + \bar{p}) = 0. \tag{A.0.29}$$

The linear perturbation of the conservation law reads

$$\partial_\mu \delta T^\mu{}_\nu + \bar{\Gamma}^\mu_{\mu\lambda}\delta T^\lambda{}_\nu - \bar{\Gamma}^\lambda_{\mu\nu}\delta T^\mu{}_\lambda + \delta\Gamma^\mu_{\mu\lambda}\bar{T}^\lambda{}_\nu - \delta\Gamma^\lambda_{\mu\nu}\bar{T}^\mu{}_\lambda = 0. \tag{A.0.30}$$

Its temporal and spatial components give the energy and momentum conservations (1.1.14) and (1.1.15).

Finally, after the decomposition of $\delta T_{\mu\nu}$ (1.1.24)–(1.1.26), their mixed indices version will be useful to obtain the conservation laws (1.1.32), (1.1.33), and (1.1.36).

$$\delta T^i{}_j = \delta_{ij}\delta p + \partial_i\partial_j\pi^{\mathrm{S}} + \partial_i\pi^{\mathrm{V}}_j + \partial_j\pi^{\mathrm{V}}_i + \pi^{\mathrm{T}}_{ij}, \tag{A.0.31}$$

$$\delta T^i{}_0 = a^{-2}(\bar{\rho} + \bar{p})(a\partial_i F + aG_i - \partial_i\delta u - \delta u^{\mathrm{V}}_i), \tag{A.0.32}$$

$$\delta T^0{}_i = (\bar{\rho} + \bar{p})(\partial_i\delta u + \delta u^{\mathrm{V}}_i), \tag{A.0.33}$$

$$\delta T^0{}_0 = -\delta\rho, \tag{A.0.34}$$

$$\delta T^\lambda{}_\lambda = 3\delta p - \delta\rho + \nabla^2\pi^{\mathrm{S}}. \tag{A.0.35}$$

Let us also show the concrete expressions of their gauge transformation (1.1.41) and (1.1.42):

$$\Delta h_{ij} = -\frac{\partial\epsilon_i}{\partial x^j} - \frac{\partial\epsilon_j}{\partial x^i} + 2a\dot{a}\delta_{ij}\epsilon_0, \tag{A.0.36}$$

$$\Delta h_{i0} = -\frac{\partial\epsilon_i}{\partial t} - \frac{\partial\epsilon_0}{\partial x^i} + 2\frac{\dot{a}}{a}\epsilon_i, \tag{A.0.37}$$

$$\Delta h_{00} = -2\frac{\partial\epsilon_0}{\partial t} \tag{A.0.38}$$

$$\Delta\delta T_{ij} = -\bar{p}\left(\frac{\partial\epsilon_i}{\partial x^j} + \frac{\partial\epsilon_j}{\partial x^i}\right) + \frac{\partial}{\partial t}(a^2\bar{p})\delta_{ij}\epsilon_0, \tag{A.0.39}$$

$$\Delta\delta T_{i0} = -\bar{p}\frac{\partial\epsilon_i}{\partial t} + \bar{\rho}\frac{\partial\epsilon_0}{\partial x^i} + 2\bar{p}\frac{\dot{a}}{a}\epsilon_i, \tag{A.0.40}$$

$$\Delta\delta T_{00} = 2\bar{\rho}\frac{\partial\epsilon_0}{\partial t} + \dot{\bar{\rho}}\epsilon_0. \tag{A.0.41}$$

Note that indices are raised or lowered by the unperturbed metric $\bar{g}_{\mu\nu}$ at the linear order, and therefore $\epsilon_0 = -\epsilon^0$ and $\epsilon_i = a^2\epsilon^i$ for example.

A.1 Scalar theory

Here let us show the concrete expressions of the components of the energy-momentum tensor for the generic scalar-field theory:

$$S = \int \mathrm{d}^4x\sqrt{-g}\left[-\frac{1}{2}g^{\mu\nu}\gamma_{nm}(\phi)\partial_\mu\phi^n\partial_\nu\phi^m - V(\phi)\right]. \tag{A.1.1}$$

The energy-momentum tensor for this action can be calculated from

$$T_{\mu\nu} = -\frac{2}{\sqrt{-g}}\frac{\delta S}{\delta g^{\mu\nu}} = g_{\mu\nu}\left[-\frac{1}{2}g^{\rho\sigma}\gamma_{nm}(\phi)\partial_\rho\phi^n\partial_\sigma\phi^m - V(\phi)\right] + \gamma_{nm}(\phi)\partial_\mu\phi^n\partial_\nu\phi^m, \quad \text{(A.1.2)}$$

The unperturbed energy-momentum tensor takes the perfect fluid form with unperturbed energy density, pressure, and velocity as

$$\bar{\rho} = \frac{1}{2}\gamma_{nm}(\bar{\phi})\dot{\bar{\phi}}^n\dot{\bar{\phi}}^m + V(\bar{\phi}), \quad \text{(A.1.3)}$$

$$\bar{p} = \frac{1}{2}\gamma_{nm}(\bar{\phi})\dot{\bar{\phi}}^n\dot{\bar{\phi}}^m - V(\bar{\phi}), \quad \text{(A.1.4)}$$

$$\bar{u}^0 = 1, \qquad \bar{u}^i = 0. \quad \text{(A.1.5)}$$

On the other hand, comparing the first order terms in Eq. (A.1.2) with the definition of the perturbations to the energy-momentum tensor (1.1.24)–(1.1.26), one can see that the perturbations to the energy density, pressure, and velocity potential are

$$\delta\rho = \gamma_{nm}(\bar{\phi})\dot{\bar{\phi}}^n\delta\dot{\phi}^m + \frac{1}{2}\dot{\bar{\phi}}^n\dot{\bar{\phi}}^m\frac{\partial\gamma_{nm}(\bar{\phi})}{\partial\bar{\phi}^k}\delta\phi^k + V_n(\bar{\phi})\delta\phi^n + \frac{1}{2}h_{00}\gamma_{nm}(\bar{\phi})\dot{\bar{\phi}}^n\dot{\bar{\phi}}^m, \quad \text{(A.1.6)}$$

$$\delta p = \gamma_{nm}(\bar{\phi})\dot{\bar{\phi}}^n\delta\dot{\phi}^m + \frac{1}{2}\dot{\bar{\phi}}^n\dot{\bar{\phi}}^m\frac{\partial\gamma_{nm}(\bar{\phi})}{\partial\bar{\phi}^k}\delta\phi^k - V_n(\bar{\phi})\delta\phi^n + \frac{1}{2}h_{00}\gamma_{nm}(\bar{\phi})\dot{\bar{\phi}}^n\dot{\bar{\phi}}^m, \quad \text{(A.1.7)}$$

$$\delta u = -\frac{\gamma_{mn}(\bar{\phi})\dot{\bar{\phi}}^n\delta\phi^m}{\gamma_{kl}(\bar{\phi})\dot{\bar{\phi}}^k\dot{\bar{\phi}}^l}, \quad \text{(A.1.8)}$$

and the anisotropic inertia vanishes.

Appendix B

Influence Action

In Sec. 2.2, we briefly describe the derivation of the EoM in the stochastic formalism with use of the closed time path formulation. There, the white noise term of the EoM for the inflaton's superhorizon modes comes from the effective action after integrating out the subhorizon modes. In this section, let us show a more detailed derivation of the influence action (2.2.14) which gives the noise term, following Ref. [27].

First, the second order action for the inflaton field up to the mass term can be simply written as

$$S[\phi] = \int \mathrm{d}^4x \frac{1}{2}\phi\tilde{\Lambda}\phi, \tag{B.0.1}$$

where $\tilde{\Lambda}$ stands for the following derivative operator

$$\tilde{\Lambda} = -a^3(t)\left[\partial_t^2 + 3H\partial_t - \frac{\nabla^2}{a^2(t)} + m^2\right]. \tag{B.0.2}$$

Therefore the influence functional (2.2.10) is, up to the mass term,

$$\begin{aligned} &F[\phi_{\mathrm{IR}}; J_{\mathrm{UV}}] \\ &= \int \mathscr{D}\phi^{\pm}_{\mathrm{UV}} \exp\left[i\int \mathrm{d}^4x\mathrm{d}^4y \left(\frac{1}{2}\phi^a_{\mathrm{UV}}(x)\Lambda_{ab}(x,y)\phi^b_{\mathrm{UV}}(y) + \varphi^a(x)\Lambda_{ab}(x,y)\phi^b_{\mathrm{UV}}(y) + J_{\mathrm{UV},a}\phi^a_{\mathrm{UV}}\right)\right] \\ &= \int \mathscr{D}\phi^{\pm}_{\mathrm{UV}} \exp\left[i\left(\frac{1}{2}\phi_{\mathrm{UV}}\Lambda\phi_{\mathrm{UV}} + \varphi\Lambda\phi_{\mathrm{UV}} + J_{\mathrm{UV}}\cdot\phi_{\mathrm{UV}}\right)\right], \end{aligned} \tag{B.0.3}$$

where the indices a and b denote the time path label $+$ or $-$, and $\Lambda_{ab}(x,y)$ is defined by

$$\Lambda_{ab}(x,y) = \begin{pmatrix} \tilde{\Lambda}_x & 0 \\ 0 & -\tilde{\Lambda}_x \end{pmatrix} \delta^{(4)}(x-y). \tag{B.0.4}$$

The subscript x of $\tilde{\Lambda}_x$ represents that its derivatives are done w.r.t. x. We simplify the expression of the second line of Eq. (B.0.3) as its third line in the matrix form.

Then, substituting $1 = \Lambda\Lambda^{-1}$ and integrating by parts, one obtains

$$F[\varphi; J_{\rm UV}] = \int \mathcal{D}\phi^{\pm}_{\rm UV} \exp\left[i \left(\frac{1}{2}\phi_{\rm UV} \overrightarrow{\Lambda} \Lambda^{-1} \overleftarrow{\Lambda} \phi_{\rm UV} + \varphi \overrightarrow{\Lambda} \Lambda^{-1} \overleftarrow{\Lambda} \phi_{\rm UV} + J_{\rm UV} \cdot \phi_{\rm UV} \right) \right], \quad \text{(B.0.5)}$$

where over-arrows indicate the directions of derivative operations. Here let us explicitly show the spacetime arguments. For example, the first term can be written as

$$\phi_{\rm UV}(x_1) \overrightarrow{\Lambda}(x_1, x_2) \Lambda^{-1}(x_2, x_3) \overleftarrow{\Lambda}(x_3, x_4) \phi_{\rm UV}(x_4). \quad \text{(B.0.6)}$$

The derivatives in Λ are w.r.t. its first argument, and therefore neither $\phi_{\rm UV}(x_1)$ nor $\phi_{\rm UV}(x_4)$ is differentiated. Namely, $\overrightarrow{\Lambda} \Lambda^{-1} \overleftarrow{\Lambda}$ is simply c-number. Then the integration of Eq. (B.0.5) can be done as the Gaussian integration and one obtains

$$F[\varphi; J_{\rm UV}] = \mathcal{N} \exp\left[-i\frac{1}{2} \varphi \overrightarrow{\Lambda} \Lambda^{-1} \overleftarrow{\Lambda} \varphi - \varphi \cdot J_{\rm UV} - \frac{1}{2} J_{\rm UV} \left(\overrightarrow{\Lambda} \Lambda^{-1} \overleftarrow{\Lambda} \right)^{-1} J_{\rm UV} \right], \quad \text{(B.0.7)}$$

where $\mathcal{N}$ is the normalization factor independent of φ. Here, since $J_{\rm UV}$ is defined to be orthogonal to the IR mode φ, the second term vanishes. The third term simply gives the effective action for $\langle \phi_{\rm UV} \rangle$ after the Legendre transformation, which does not affect the IR part. Therefore the influence action can be given by

$$S^{(1)}_{\rm IA} = -\frac{1}{2} \varphi \overrightarrow{\Lambda} \Lambda^{-1} \overleftarrow{\Lambda} \varphi. \quad \text{(B.0.8)}$$

Now let us note that the inverse of the derivative operator can be given by the ϕ's propagator, that is, the time-ordered two point function:

$$\begin{aligned} i\tilde{\Lambda}^{-1}(x, y) &= \langle T(\phi_{\rm UV}(x)\phi_{\rm UV}(y)) \rangle \\ &= \theta(x^0 - y^0) \langle \phi_{\rm UV}(x)\phi_{\rm UV}(y) \rangle + \theta(y^0 - x^0) \langle \phi_{\rm UV}(y)\phi_{\rm UV}(x) \rangle . \end{aligned} \quad \text{(B.0.9)}$$

Since we consider the closed time path here, the inverse of the matrix derivative operator also can be obtained as its extension if one takes the time ordering along with the closed time path, that is, such time ordering $T_{\rm C}$ is defined by

$$\begin{cases} T_{\rm C}(\phi^+(x)\phi^+(y)) = T(\phi(x)\phi(y)), \\ T_{\rm C}(\phi^-(x)\phi^-(y)) = \bar{T}(\phi(x)\phi(y)), \\ T_{\rm C}(\phi^+(x)\phi^-(y)) = \phi(y)\phi(x), \\ T_{\rm C}(\phi^-(x)\phi^+(y)) = \phi(x)\phi(y), \end{cases} \quad \text{(B.0.10)}$$

where $\bar{T}$ is the inverse time ordering. Inspired by these expressions, one can find

$$i(\Lambda^{-1})^{ab}(x, y) = \begin{pmatrix} \langle T(\phi_{\rm UV}(x)\phi_{\rm UV}(t)) \rangle & \langle \phi_{\rm UV}(y)\phi_{\rm UV}(x) \rangle \\ \langle \phi_{\rm UV}(x)\phi_{\rm UV}(y) \rangle & \langle \bar{T}(\phi_{\rm UV}(x)\phi_{\rm UV}(y)) \rangle \end{pmatrix}. \quad \text{(B.0.11)}$$

Then with use of the definition of the UV mode:

$$\phi_{\rm UV}(x) = \int \frac{{\rm d}^3 k}{(2\pi)^3} W(\mathbf{k}, t) \phi_{\mathbf{k}} {\rm e}^{i\mathbf{k}\cdot\mathbf{x}}, \quad \text{(B.0.12)}$$

where $W(\mathbf{k},t)$ is some window function, the Fourier expression of the influence action reads

$$S^{(1)}_{\rm IA} = \frac{i}{2}\int {\rm d}t{\rm d}t' \int \frac{{\rm d}^3k}{(2\pi)^3}\frac{{\rm d}^3q}{(2\pi)^3}\varphi_{-\mathbf{k}}(t)\overrightarrow{\Lambda}_{\mathbf{k}}(t)W(\mathbf{k},t) \\ \times \begin{pmatrix} \langle T(\hat{\phi}_{\mathbf{k}}(t)\hat{\phi}_{\mathbf{q}}(t'))\rangle & \langle \hat{\phi}_{\mathbf{q}}(t')\hat{\phi}_{\mathbf{k}}(t)\rangle \\ \langle \hat{\phi}_{\mathbf{k}}(t)\hat{\phi}_{\mathbf{q}}(t')\rangle & \langle \bar{T}(\hat{\phi}_{\mathbf{k}}(t)\hat{\phi}_{\mathbf{q}}(t'))\rangle \end{pmatrix} W(\mathbf{q},t')\overleftarrow{\Lambda}_{\mathbf{q}}(t')\varphi_{-\mathbf{q}}(t'). \tag{B.0.13}$$

Note that the IR mode φ and the window W are orthogonal in the limit of $W \to \theta(k-\epsilon aH)$. Therefore the time derivative of Λ should be operated to W at least once, and otherwise it vanishes. Hence the non-zero contributions can be written as

$$S^{(1)}_{\rm IA} = \frac{i}{2}\int {\rm d}t{\rm d}t' \int \frac{{\rm d}^3k}{(2\pi)^3}\frac{{\rm d}^3q}{(2\pi)^3}a^3(t)\varphi_{-\mathbf{k}}(t)\overrightarrow{P}_t\sigma_3 \\ \times \begin{pmatrix} \langle T(\hat{\phi}_{\mathbf{k}}(t)\hat{\phi}_{\mathbf{q}}(t'))\rangle & \langle \hat{\phi}_{\mathbf{q}}(t')\hat{\phi}_{\mathbf{k}}(t)\rangle \\ \langle \hat{\phi}_{\mathbf{k}}(t)\hat{\phi}_{\mathbf{q}}(t')\rangle & \langle \bar{T}(\hat{\phi}_{\mathbf{k}}(t)\hat{\phi}_{\mathbf{q}}(t'))\rangle \end{pmatrix} \sigma_3\overleftarrow{P}_{t'}a^3(t')\varphi_{-\mathbf{q}}(t'), \tag{B.0.14}$$

where σ_3 is the third Pauli matrix:

$$\sigma_3 = \begin{pmatrix} 1 & 0 \\ 0 & 1 \end{pmatrix}, \tag{B.0.15}$$

and P_t is a derivative operator defined by

$$P_t = \left[\ddot{W}(\mathbf{k},t) + 3H\dot{W}(\mathbf{k},t) + 2\dot{W}(\mathbf{k},t)\partial_t\right]. \tag{B.0.16}$$

Finally, after a short calculation with the definition of the mode function

$$\hat{\phi}_{\mathbf{k}} = \phi_k(t)\hat{a}_{\mathbf{k}} + \phi^*_k(t)\hat{a}^\dagger_{-\mathbf{k}}, \tag{B.0.17}$$

one obtains the expression (2.2.14):

$$S^{(1)}_{\rm IA} = \frac{i}{2}\int {\rm d}^4x{\rm d}^4x'\varphi_{\rm q}(x){\rm Re}[\Pi(x,x')]\varphi_{\rm q}(x') \\ - 2\int {\rm d}^4x{\rm d}^4x'\theta(t-t')\varphi_{\rm q}(x){\rm Im}[\Pi(x,x')]\varphi_{\rm c}(x'), \tag{B.0.18}$$

$$\Pi(x,x') = \int \frac{{\rm d}^3k}{(2\pi)^3}a^3(t)[P_t\phi_{\mathbf{k}}(t)]{\rm e}^{i\mathbf{k}\cdot\mathbf{x}}a^3(t')[P_{t'}\phi^*_{\mathbf{k}}(t')]{\rm e}^{-i\mathbf{k}\cdot\mathbf{x}'}. \tag{B.0.19}$$

Appendix C

Additive Separable Potential

In Sec. 3.3.2, we have explained how the squeezed $f_{\rm NL}(k_{\rm L}, k_{\rm S})$ can be computed in generic multi-field models of inflation. In the limit where the two scales are equal, $k_{\rm L} = k_{\rm S}$, analytic formulae were provided. For the generic case $k_{\rm L} < k_{\rm S}$ however, one has to resort to numerical techniques in order to compute the correlators $\langle \delta N_{\rm L} \mathcal{P}_\zeta(k_{\rm S}) \rangle$. In this appendix, we detail the computational program one has to follow for a concrete class of models. Generalization to other models than that presented here can be done along the same lines. We focus on the backward formulation, while the calculations in the forward formulation are briefly mentioned in a footnote. Here we adopt the Planck unit $M_{\rm Pl} = 1$ and this appendix is based on Ref. [34].

Let us consider the case of a two-field additive separable potential

$$V(\phi, \psi) = U(\phi) + W(\psi). \tag{C.0.1}$$

The two fields ϕ and ψ are assumed to be slowly rolling during inflation, and evolve according to

$$\frac{{\rm d}\phi}{{\rm d}N} = -\frac{U'}{V}, \qquad \frac{{\rm d}\psi}{{\rm d}N} = -\frac{W'}{V}. \tag{C.0.2}$$

Additive separable potentials are convenient to work with since the following two formula can be derived. First, there is an integral of motion [48]

$$K(\phi, \psi) = \int^{\phi} \frac{{\rm d}\tilde{\phi}}{U'(\tilde{\phi})} - \int^{\psi} \frac{{\rm d}\tilde{\psi}}{W'(\tilde{\psi})}, \tag{C.0.3}$$

which allows us to label different slow-roll trajectories. Indeed, if one differentiates K w.r.t. N and making use of Eq. (C.0.2), one can readily show that K is a constant. Second, if two points $M_1(\phi_1, \psi_1)$ and $M_2(\phi_2, \psi_2)$ are on the same attractor trajectory (that is to say, $K(\phi_1, \psi_1) = K(\phi_2, \psi_2)$), the e-folding number realized between M_1 and M_2 is given by [49]

$$N_{M_1 M_2} = -\int_{\phi_1}^{\phi_2} \frac{U}{U'} {\rm d}\phi - \int_{\psi_1}^{\psi_2} \frac{W}{W'} {\rm d}\psi. \tag{C.0.4}$$

Let us now fix the three label lines $\rho = \rho_c$, $N_{\to c} = N_S$, and $N_{\to c} = N_L$ as in Fig. 3.2. Let $A_{in}(\phi, \psi)$ be a free point in the field space, and B and C the points associated to A_{in} according to Fig. 3.2. Let us calculate the derivatives of the coordinates of B and C and of $N = N_{AC}$ w.r.t. ϕ and ψ. These will be useful to calculate f_{NL}.

The values of ϕ_C and ψ_C are the same for all the points belonging to the same slow-roll trajectory, hence they depend only on K. One then has

$$\begin{cases} \dfrac{\partial \phi_C}{\partial \phi} = \dfrac{\partial K}{\partial \phi}\dfrac{\mathrm{d}\phi_C}{\mathrm{d}K}, & \dfrac{\partial \phi_C}{\partial \psi} = \dfrac{\partial K}{\partial \psi}\dfrac{\mathrm{d}\phi_C}{\mathrm{d}K}, \\ \dfrac{\partial \psi_C}{\partial \phi} = \dfrac{\partial K}{\partial \phi}\dfrac{\mathrm{d}\psi_C}{\mathrm{d}K}, & \dfrac{\partial \psi_C}{\partial \psi} = \dfrac{\partial K}{\partial \psi}\dfrac{\mathrm{d}\psi_C}{\mathrm{d}K}, \end{cases} \tag{C.0.5}$$

where, differentiating Eq. (C.0.3), one has $\partial K/\partial\phi = 1/U'(\phi)$ and $\partial K/\partial\psi = -1/W'(\psi)$. Differentiating the condition $U(\phi_C) + W(\psi_C) = \rho_c$, one also has $U'_C \mathrm{d}\phi_C/\mathrm{d}K + W'_C \mathrm{d}\psi_C/\mathrm{d}K = 0$. One the other hand, differentiating $K(\phi_C, \psi_C)$ given in Eq. (C.0.3) w.r.t. K, one has $1 = (\mathrm{d}\phi_C/\mathrm{d}K)/U'_C - (\mathrm{d}\psi_C/\mathrm{d}K)/W'_C$. These two relations give rise to

$$\frac{\mathrm{d}\phi_C}{\mathrm{d}K} = \frac{1}{U'_C}\left(\frac{1}{{U'_C}^2} + \frac{1}{{W'_C}^2}\right)^{-1}, \qquad \frac{\mathrm{d}\psi_C}{\mathrm{d}K} = -\frac{1}{W'_C}\left(\frac{1}{{U'_C}^2} + \frac{1}{{W'_C}^2}\right)^{-1}. \tag{C.0.6}$$

Combining these results, one obtains

$$\begin{cases} \dfrac{\partial \phi_C}{\partial \phi} = \dfrac{1}{U'(\phi)}\dfrac{U'_C {W'_C}^2}{{U'_C}^2 + {W'_C}^2}, & \dfrac{\partial \phi_C}{\partial \psi} = -\dfrac{1}{W'(\psi)}\dfrac{U'_C {W'_C}^2}{{U'_C}^2 + {W'_C}^2}, \\ \dfrac{\partial \psi_C}{\partial \phi} = -\dfrac{1}{U'(\phi)}\dfrac{{U'_C}^2 W'_C}{{U'_C}^2 + {W'_C}^2}, & \dfrac{\partial \psi_C}{\partial \psi} = \dfrac{1}{W'(\psi)}\dfrac{{U'_C}^2 W'_C}{{U'_C}^2 + {W'_C}^2}. \end{cases} \tag{C.0.7}$$

The coordinates of B are defined through the two conditions $K(\phi_B, \psi_B) = K(\phi, \psi)$ and $N_{BC} = N_S$. By differentiating these two equations w.r.t. ϕ and ψ, one obtains a linear system of four equations, from which, making use of Eq. (C.0.7), the four following quantities can be extracted[1]

$$\begin{cases} \dfrac{\partial \phi_B}{\partial \phi} = \dfrac{U'_B}{U'(\phi)V_B}\left(\dfrac{U_C {W'_C}^2 - W_C {U'_C}^2}{{U'_C}^2 + {W'_C}^2} + W_B\right), & \dfrac{\partial \phi_B}{\partial \psi} = \dfrac{U'_B}{W'(\psi)V_B}\left(\dfrac{W_C {U'_C}^2 - U_C {W'_C}^2}{{U'_C}^2 + {W'_C}^2} - W_B\right), \\ \dfrac{\partial \psi_B}{\partial \phi} = \dfrac{W'_B}{U'(\phi)V_B}\left(\dfrac{U_C {W'_C}^2 - W_C {U'_C}^2}{{U'_C}^2 + {W'_C}^2} - U_B\right), & \dfrac{\partial \psi_B}{\partial \psi} = \dfrac{W'_B}{W'(\psi)V_B}\left(\dfrac{W_C {U'_C}^2 - U_C {W'_C}^2}{{U'_C}^2 + {W'_C}^2} + U_B\right). \end{cases} \tag{C.0.9}$$

[1] In the forward formulation, the coordinates of B are defined through the two conditions $K(\phi_B, \psi_B) = K(\phi, \psi)$ and $N_{AB} = N_L - N_S$. By differentiating these two equations w.r.t. ϕ and ψ, on obtains [41]

$$\begin{cases} \dfrac{\partial \phi_B}{\partial \phi} = \dfrac{U'_B}{U'(\phi)}\dfrac{U(\phi) + W_B}{V_B}, & \dfrac{\partial \phi_B}{\partial \psi} = \dfrac{U'_B}{W'(\psi)}\dfrac{W(\psi) - W_B}{V_B}, \\ \dfrac{\partial \psi_B}{\partial \phi} = \dfrac{W'_B}{U'(\phi)}\dfrac{U(\phi) - U_B}{V_B}, & \dfrac{\partial \psi_B}{\partial \psi} = \dfrac{W'_B}{W'(\psi)}\dfrac{W(\psi) + U_B}{V_B}. \end{cases} \tag{C.0.8}$$

The other required derivatives can be obtained in the same way as with the backward formulation.

Then, to calculate the long-wavelength curvature perturbation $\delta N_{\rm L}$, the derivatives of the backward e-folds are needed. Differentiating $N = N_{AC}$ given by Eq. (C.0.4) (where $M_1 = A$ and $M_2 = C$) w.r.t. ϕ and ψ, one obtains

$$\frac{\partial N}{\partial \phi} = \frac{U(\phi)}{U'(\phi)} - \frac{W_C}{W'_C}\frac{\partial \psi_C}{\partial \phi} - \frac{U_C}{U'_C}\frac{\partial \phi_C}{\partial \phi}, \qquad \frac{\partial N}{\partial \psi} = \frac{W(\psi)}{W'(\psi)} - \frac{W_C}{W'_C}\frac{\partial \psi_C}{\partial \psi} - \frac{U_C}{U'_C}\frac{\partial \phi_C}{\partial \psi}, \tag{C.0.10}$$

which, combined with Eq. (C.0.7), gives rise to

$$\frac{\partial N}{\partial \phi} = \frac{1}{U'(\phi)}\left[U(\phi) + \frac{W_C U'^2_C - U_C W'^2_C}{U'^2_C + W'^2_C}\right], \qquad \frac{\partial N}{\partial \psi} = \frac{1}{W'(\psi)}\left[W(\psi) + \frac{U_C W'^2_C - W_C U'^2_C}{U'^2_C + W'^2_C}\right]. \tag{C.0.11}$$

In the following, the second derivatives of N are also needed. They can be obtained by differentiating the previous expressions one more time and making use of Eq. (C.0.7) again. One obtains

$$\begin{cases} \dfrac{\partial^2 N}{\partial \phi^2} = 1 - \dfrac{U''(\phi)}{U'^2(\phi)}\left[U(\phi) + \dfrac{W_C U'^2_C - U_C W'^2_C}{U'^2_C + W'^2_C}\right] + \dfrac{1}{U'^2(\phi)}\dfrac{U'^2_C W'^2_C}{(U'^2_C + W'^2_C)^2} \\ \qquad\qquad \times \left[2(U''_C W_C + U_C W''_C) - U'^2_C - W'^2_C + 2(U''_C + W''_C)\dfrac{U_C W'^2_C - W_C U'^2_C}{U'^2_C + W'^2_C}\right], \\ \dfrac{\partial^2 N}{\partial \psi^2} = 1 - \dfrac{W''(\psi)}{W'^2(\psi)}\left[W(\psi) + \dfrac{U_C W'^2_C - W_C U'^2_C}{U'^2_C + W'^2_C}\right] + \dfrac{1}{W'^2(\psi)}\dfrac{U'^2_C W'^2_C}{(U'^2_C + W'^2_C)^2} \\ \qquad\qquad \times \left[2(U''_C W_C + U_C W''_C) - U'^2_C - W'^2_C + 2(U''_C + W''_C)\dfrac{U_C W'^2_C - W_C U'^2_C}{U'^2_C + W'^2_C}\right], \\ \dfrac{\partial^2 N}{\partial \phi \partial \psi} = \dfrac{2}{U'(\phi)W'(\psi)}\dfrac{U'^2_C W'^2_C}{(U'^2_C + W'^2_C)^2} \\ \qquad\qquad \times \left[U'^2_C + W'^2_C - 2(U''_C W_C + U_C W''_C) + 2(U''_C + W''_C)\dfrac{W_C U'^2_C - U_C W'^2_C}{U'^2_C + W'^2_C}\right]. \end{cases} \tag{C.0.12}$$

The power spectrum of the scalar curvature perturbations realized between $A(\phi, \psi)$ and the constant energy hypersurface $\rho = \rho_{\rm c}$ is given by

$$\mathcal{P}_\zeta(\phi, \psi) = \left[\left(\frac{\partial N}{\partial \phi}\right)^2 + \left(\frac{\partial N}{\partial \psi}\right)^2\right]\left(\frac{H}{2\pi}\right)^2, \tag{C.0.13}$$

where $H^2 = V/3$ and $\partial N/\partial\phi$ and $\partial N/\partial\psi$ are given in Eq. (C.0.11). This gives rise to

$$\begin{cases} 6\pi^2 \dfrac{\partial \mathcal{P}_\zeta}{\partial \phi} = \left(\dfrac{\partial N}{\partial \phi}\dfrac{\partial^2 N}{\partial \phi^2} + \dfrac{\partial N}{\partial \psi}\dfrac{\partial^2 N}{\partial \phi \partial \psi}\right) V(\phi, \psi) + \dfrac{1}{2}\left[\left(\dfrac{\partial N}{\partial \phi}\right)^2 + \left(\dfrac{\partial N}{\partial \psi}\right)^2\right] U'(\phi), \\ 6\pi^2 \dfrac{\partial \mathcal{P}_\zeta}{\partial \psi} = \left(\dfrac{\partial N}{\partial \psi}\dfrac{\partial^2 N}{\partial \psi^2} + \dfrac{\partial N}{\partial \phi}\dfrac{\partial^2 N}{\partial \phi \partial \psi}\right) V(\phi, \psi) + \dfrac{1}{2}\left[\left(\dfrac{\partial N}{\partial \phi}\right)^2 + \left(\dfrac{\partial N}{\partial \psi}\right)^2\right] W'(\psi). \end{cases} \tag{C.0.14}$$

All the quantities required to evaluate Eq. (3.3.8) have now been specified, and $f_{\rm NL}$ can be computed. In practice, starting from $A_{\rm in}$, the following computational program should be used.

1. Compute the coordinates in field space of A_* by numerically solving $K(A_{\rm in}) = K(A_*)$ and $N_{A_*C} = N_{\rm L}$, where K is given by Eq. (C.0.3) and N by Eq. (C.0.4).
2. Compute the coordinates of B by numerically solving $K(A_{\rm in}) = K(B)$ and $N_{BC} = N_{\rm S}$, where K is given by Eq. (C.0.3) and N by Eq. (C.0.4).
3. Evaluate $\mathcal{P}_\zeta|_*$ making use of Eq. (C.0.13) and of the result of step 1.
4. Evaluate $\mathcal{P}_\zeta|_B$ making use of Eq. (C.0.13) and of the result of step 2.
5. Evaluate $\partial\mathcal{P}_\zeta/\partial\phi^I|_B$ making use of Eq. (C.0.14) and of the result of step 2.
6. Evaluate $\partial\phi^I_B/\partial\phi^J|_*$ making use of Eq. (C.0.9) and of the result of step 1.
7. Evaluate Eq. (3.3.8) with the results of steps 3–6.

Finally let us note that the case where $U = W$ is effectively equivalent to a single-field setup. Specifying the previous formula in this case, it is easy to see that $\partial\phi_B/\partial\phi = -\partial\phi_B/\partial\psi = -\partial\psi_B/\partial\phi = \partial\psi_B/\partial\psi$, and that $\partial\mathcal{P}_\zeta/\partial\phi = \partial\mathcal{P}_\zeta/\partial\psi$. From here it follows that $f_{\rm NL} = 0$ in this case, as it should.

Bibliography

[1] A. A. Starobinsky, *A New Type of Isotropic Cosmological Models Without Singularity*, *Phys. Lett.* **B91** (1980) 99–102.

[2] K. Sato, *First Order Phase Transition of a Vacuum and Expansion of the Universe*, *Mon. Not. Roy. Astron. Soc.* **195** (1981) 467–479.

[3] A. H. Guth, *The Inflationary Universe: A Possible Solution to the Horizon and Flatness Problems*, *Phys. Rev.* **D23** (1981) 347–356.

[4] A. D. Linde, *A New Inflationary Universe Scenario: A Possible Solution of the Horizon, Flatness, Homogeneity, Isotropy and Primordial Monopole Problems*, *Phys. Lett.* **B108** (1982) 389–393.

[5] A. Albrecht and P. J. Steinhardt, *Cosmology for Grand Unified Theories with Radiatively Induced Symmetry Breaking*, *Phys. Rev. Lett.* **48** (1982) 1220–1223.

[6] A. D. Linde, *Chaotic Inflation*, *Phys. Lett.* **B129** (1983) 177–181.

[7] Planck collaboration, P. A. R. Ade et al., *Planck 2015 results. XIII. Cosmological parameters*, *Astron. Astrophys.* **594** (2016) A13, [1502.01589].

[8] Planck collaboration, P. A. R. Ade et al., *Planck 2015 results. XVII. Constraints on primordial non-Gaussianity*, *Astron. Astrophys.* **594** (2016) A17, [1502.01592].

[9] Planck collaboration, P. A. R. Ade et al., *Planck 2015 results. XX. Constraints on inflation*, *Astron. Astrophys.* **594** (2016) A20, [1502.02114].

[10] https://www.skatelescope.org/.

[11] EUCLID collaboration, R. Laureijs et al., *Euclid Definition Study Report*, 1110.3193.

[12] A. Friedmann, *Über die Krümmung des Raumes*, *Zeitschrift fur Physik* **10** (1922) 377–386.

[13] G. Lemaître, *Expansion of the universe, A homogeneous universe of constant mass and increasing radius accounting for the radial velocity of extra-galactic nebulae*, *Monthly Notices of the RAS* **91** (Mar., 1931) 483–490.

[14] H. P. Robertson, *Kinematics and World-Structure*, *Astrophysical Journal* **82** (Nov., 1935) 284.

[15] A. G. Walker, *On milne's theory of world-structure*, *Proceedings of the London Mathematical Society* **s2-42** (1937) 90–127, [http://plms.oxfordjournals.org/content/s2-42/1/90.full.pdf+html].

[16] S. Weinberg, *Cosmology*. Oxford, UK: Oxford Univ. Pr. (2008) 593 p, 2008.

[17] H. Kodama and T. Hamazaki, *Evolution of cosmological perturbations in a stage dominated by an oscillatory scalar field*, *Prog. Theor. Phys.* **96** (1996) 949–970, [gr-qc/9608022].

[18] Y. Nambu and A. Taruya, *Evolution of cosmological perturbation in reheating phase of the universe*, *Prog. Theor. Phys.* **97** (1997) 83–89, [gr-qc/9609029].

[19] D. Polarski and A. A. Starobinsky, *Semiclassicality and decoherence of cosmological perturbations*, *Class. Quant. Grav.* **13** (1996) 377–392, [gr-qc/9504030].

[20] T. Fujita, M. Kawasaki, Y. Tada and T. Takesako, *A new algorithm for calculating the curvature perturbations in stochastic inflation*, *JCAP* **1312** (2013) 036, [1308.4754].

[21] T. Fujita, M. Kawasaki and Y. Tada, *Non-perturbative approach for curvature perturbations in stochastic δN formalism*, *JCAP* **1410** (2014) 030, [1405.2187].

[22] D. H. Lyth, K. A. Malik and M. Sasaki, *A General proof of the conservation of the curvature perturbation*, *JCAP* **0505** (2005) 004, [astro-ph/0411220].

[23] R. L. Arnowitt, S. Deser and C. W. Misner, *The Dynamics of general relativity*, *Gen. Rel. Grav.* **40** (2008) 1997–2027, [gr-qc/0405109].

[24] D. Wands, K. A. Malik, D. H. Lyth and A. R. Liddle, *A New approach to the evolution of cosmological perturbations on large scales*, *Phys. Rev.* **D62** (2000) 043527, [astro-ph/0003278].

[25] A. A. Starobinsky, *STOCHASTIC DE SITTER (INFLATIONARY) STAGE IN THE EARLY UNIVERSE*, *Lect. Notes Phys.* **246** (1986) 107–126.

[26] M. Morikawa, *Dissipation and Fluctuation of Quantum Fields in Expanding Universes*, *Phys. Rev.* **D42** (1990) 1027–1034.

[27] L. Perreault Levasseur, *Lagrangian formulation of stochastic inflation: Langevin equations, one-loop corrections and a proposed recursive approach*, *Phys. Rev.* **D88** (2013) 083537, [1304.6408].

[28] L. Perreault Levasseur, V. Vennin and R. Brandenberger, *Recursive Stochastic Effects in Valley Hybrid Inflation*, *Phys. Rev.* **D88** (2013) 083538, [1307.2575].

[29] A. K. Das, *Finite Temperature Field Theory*. World Scientific, New York, 1997.

[30] V. Vennin and A. A. Starobinsky, *Correlation Functions in Stochastic Inflation*, *Eur. Phys. J.* **C75** (2015) 413, [1506.04732].

[31] H. Assadullahi, H. Firouzjahi, M. Noorbala, V. Vennin and D. Wands, *Multiple Fields in Stochastic Inflation*, *JCAP* **1606** (2016) 043, [1604.04502].

[32] V. Vennin, H. Assadullahi, H. Firouzjahi, M. Noorbala and D. Wands, *Critical Number of Fields in Stochastic Inflation*, 1604.06017.

[33] S. E. Shreve, *Stochastic calculus for finance II: Continuous-time models*, vol. 11. Springer Science & Business Media, 2004.

[34] Y. Tada and V. Vennin, *Squeezed Bispectrum in the δN Formalism: Local Observer Effect in Field Space*, 1609.08876.

[35] D. Seery and J. E. Lidsey, *Primordial non-Gaussianities from multiple-field inflation*, *JCAP* **0509** (2005) 011, [astro-ph/0506056].

[36] J. M. Maldacena, *Non-Gaussian features of primordial fluctuations in single field inflationary models*, *JHEP* **05** (2003) 013, [astro-ph/0210603].

[37] Y. Urakawa and T. Tanaka, *Influence on observation from IR divergence during inflation: Multi field inflation*, *Prog. Theor. Phys.* **122** (2010) 1207–1238, [0904.4415].

[38] T. Tanaka and Y. Urakawa, *Dominance of gauge artifact in the consistency relation for the primordial bispectrum*, *JCAP* **1105** (2011) 014, [1103.1251].

[39] E. Pajer, F. Schmidt and M. Zaldarriaga, *The Observed Squeezed Limit of Cosmological Three-Point Functions*, *Phys. Rev.* **D88** (2013) 083502, [1305.0824].

[40] N. Bartolo, D. Bertacca, M. Bruni, K. Koyama, R. Maartens, S. Matarrese et al., *A relativistic signature in large-scale structure*, *Phys. Dark Univ.* **13** (2016) 30–34, [1506.00915].

[41] Z. Kenton and D. J. Mulryne, *The squeezed limit of the bispectrum in multi-field inflation*, *JCAP* **1510** (2015) 018, [1507.08629].

[42] C. T. Byrnes, D. Regan, D. Seery and E. R. M. Tarrant, *The hemispherical asymmetry from a scale-dependent inflationary bispectrum*, *JCAP* **1606** (2016) 025, [1511.03129].

[43] Z. Kenton and D. J. Mulryne, *The Separate Universe Approach to Soft Limits*, *JCAP* **1610** (2016) 035, [1605.03435].

[44] C. Armendariz-Picon, T. Damour and V. F. Mukhanov, *k - inflation*, *Phys. Lett.* **B458** (1999) 209–218, [hep-th/9904075].

[45] J.-O. Gong and M. Sasaki, *A new parameter in attractor single-field inflation*, *Phys. Lett.* **B747** (2015) 390–394, [1502.04167].

[46] G. Domenech, J.-O. Gong and M. Sasaki, *Consistency relation and inflaton field redefinition in the delta N formalism*, 1606.03343.

[47] J. Garriga and V. F. Mukhanov, *Perturbations in k-inflation*, *Phys. Lett.* **B458** (1999) 219–225, [hep-th/9904176].

[48] M. Sasaki, *Multi-brid inflation and non-Gaussianity*, *Prog. Theor. Phys.* **120** (2008) 159–174, [0805.0974].

[49] A. A. Starobinsky, *Multicomponent de Sitter (Inflationary) Stages and the Generation of Perturbations*, *JETP Lett.* **42** (1985) 152–155.

[50] S. Hawking, *Gravitationally collapsed objects of very low mass*, *Mon. Not. Roy. Astron. Soc.* **152** (1971) 75.

[51] B. J. Carr and S. W. Hawking, *Black holes in the early Universe*, *Mon. Not. Roy. Astron. Soc.* **168** (1974) 399–415.

[52] B. J. Carr, *The Primordial black hole mass spectrum*, *Astrophys. J.* **201** (1975) 1–19.

[53] K. Inomata, M. Kawasaki, K. Mukaida, Y. Tada and T. T. Yanagida, *Inflationary primordial black holes for the LIGO gravitational wave events and pulsar timing array experiments*, 1611.06130.

[54] K. Schwarzschild, *On the gravitational field of a mass point according to Einstein's theory*, *Sitzungsber. Preuss. Akad. Wiss. Berlin (Math. Phys.)* **1916** (1916) 189–196, [physics/9905030].

[55] S. W. Hawking, I. G. Moss and J. M. Stewart, *Bubble Collisions in the Very Early Universe*, *Phys. Rev.* **D26** (1982) 2681.

[56] M. Crawford and D. N. Schramm, *Spontaneous Generation of Density Perturbations in the Early Universe*, *Nature* **298** (1982) 538–540.

[57] H. Kodama, M. Sasaki and K. Sato, *Abundance of Primordial Holes Produced by Cosmological First Order Phase Transition*, *Prog. Theor. Phys.* **68** (1982) 1979.

[58] D. La and P. J. Steinhardt, *Bubble Percolation in Extended Inflationary Models*, *Phys. Lett.* **B220** (1989) 375–378.

[59] I. G. Moss, *Singularity formation from colliding bubbles*, *Phys. Rev.* **D50** (1994) 676–681.

[60] M. Yu. Khlopov, R. V. Konoplich, S. G. Rubin and A. S. Sakharov, *Formation of black holes in first order phase transitions*, hep-ph/9807343.

[61] R. V. Konoplich, S. G. Rubin, A. S. Sakharov and M. Yu. Khlopov, *Formation of black holes in first-order phase transitions as a cosmological test of symmetry-breaking mechanisms*, *Phys. Atom. Nucl.* **62** (1999) 1593–1600.

[62] C. J. Hogan, *MASSIVE BLACK HOLES GENERATED BY COSMIC STRINGS*, *Phys. Lett.* **B143** (1984) 87–91.

[63] S. W. Hawking, *Black Holes From Cosmic Strings*, *Phys. Lett.* **B231** (1989) 237–239.

[64] A. Polnarev and R. Zembowicz, *Formation of Primordial Black Holes by Cosmic Strings*, *Phys. Rev.* **D43** (1991) 1106–1109.

[65] J. Garriga and M. Sakellariadou, *Effects of friction on cosmic strings*, *Phys. Rev.* **D48** (1993) 2502–2515, [hep-th/9303024].

[66] H.-B. Cheng and X.-Z. Li, *Primordial black holes and cosmic string loop*, *Chin. Phys. Lett.* **13** (1996) 317–320.

[67] R. R. Caldwell and P. Casper, *Formation of black holes from collapsed cosmic string loops*, *Phys. Rev.* **D53** (1996) 3002–3010, [gr-qc/9509012].

[68] J. H. MacGibbon, R. H. Brandenberger and U. F. Wichoski, *Limits on black hole formation from cosmic string loops*, *Phys. Rev.* **D57** (1998) 2158–2165, [astro-ph/9707146].

[69] R. N. Hansen, M. Christensen and A. L. Larsen, *Cosmic string loops collapsing to black holes*, *Int. J. Mod. Phys.* **A15** (2000) 4433–4446, [gr-qc/9902048].

[70] M. Nagasawa, *Primordial black hole formation by stabilized embedded strings in the early universe*, *Gen. Rel. Grav.* **37** (2005) 1635–1649.

[71] T. Matsuda, *Primordial black holes from cosmic necklaces*, *JHEP* **04** (2006) 017, [hep-ph/0509062].

[72] M. Lake, S. Thomas and J. Ward, *String Necklaces and Primordial Black Holes from Type IIB Strings*, *JHEP* **12** (2009) 033, [0906.3695].

[73] V. A. Berezin, V. A. Kuzmin and I. I. Tkachev, *THIN WALL VACUUM DOMAINS EVOLUTION*, *Phys. Lett.* **B120** (1983) 91–96.

[74] R. R. Caldwell, A. Chamblin and G. W. Gibbons, *Pair creation of black holes by domain walls*, *Phys. Rev.* **D53** (1996) 7103–7114, [hep-th/9602126].

[75] S. G. Rubin, M. Yu. Khlopov and A. S. Sakharov, *Primordial black holes from nonequilibrium second order phase transition*, *Grav. Cosmol.* **6** (2000) 51–58, [hep-ph/0005271].

[76] M. Yu. Khlopov, R. V. Konoplich, S. G. Rubin and A. S. Sakharov, *First-order phase transitions as a source of black holes in the early universe*, *Grav. Cosmol.* **6** (2000) 153–156.

[77] S. G. Rubin, A. S. Sakharov and M. Yu. Khlopov, *The Formation of primary galactic nuclei during phase transitions in the early universe*, *J. Exp. Theor. Phys.* **91** (2001) 921–929, [hep-ph/0106187].

[78] V. Dokuchaev, Y. Eroshenko and S. Rubin, *Quasars formation around clusters of primordial black holes*, *Grav. Cosmol.* **11** (2005) 99–104, [astro-ph/0412418].

[79] J. H. Jeans, *The Stability of a Spherical Nebula*, *Philosophical Transactions of the Royal Society of London Series A* **199** (1902) 1–53.

[80] D. K. Nadezhin, I. D. Novikov and A. G. Polnarev, *The hydrodynamics of primordial black hole formation*, *Soviet Astronomy* **22** (Apr., 1978) 129–138.

[81] G. V. Bicknell and R. N. Henriksen, *Formation of primordial black holes*, *Astrophysical Journal* **232** (Sept., 1979) 670–682.

[82] J. C. Niemeyer and K. Jedamzik, *Near-critical gravitational collapse and the initial mass function of primordial black holes*, *Phys. Rev. Lett.* **80** (1998) 5481–5484, [astro-ph/9709072].

[83] J. C. Niemeyer and K. Jedamzik, *Dynamics of primordial black hole formation*, *Phys. Rev.* **D59** (1999) 124013, [astro-ph/9901292].

[84] I. Musco, J. C. Miller and L. Rezzolla, *Computations of primordial black hole formation*, *Class. Quant. Grav.* **22** (2005) 1405–1424, [gr-qc/0412063].

[85] I. Musco, J. C. Miller and A. G. Polnarev, *Primordial black hole formation in the radiative era: Investigation of the critical nature of the collapse*, *Class. Quant. Grav.* **26** (2009) 235001, [0811.1452].

[86] I. Musco and J. C. Miller, *Primordial black hole formation in the early universe: critical behaviour and self-similarity*, *Class. Quant. Grav.* **30** (2013) 145009, [1201.2379].

[87] I. Hawke and J. M. Stewart, *The dynamics of primordial black hole formation*, *Class. Quant. Grav.* **19** (2002) 3687–3707.

[88] T. Harada, C.-M. Yoo and K. Kohri, *Threshold of primordial black hole formation*, *Phys. Rev.* **D88** (2013) 084051, [1309.4201].

[89] T. Nakama, T. Harada, A. G. Polnarev and J. Yokoyama, *Identifying the most crucial parameters of the initial curvature profile for primordial black hole formation*, *JCAP* **1401** (2014) 037, [1310.3007].

[90] M. Shibata and M. Sasaki, *Black hole formation in the Friedmann universe: Formulation and computation in numerical relativity*, *Phys. Rev.* **D60** (1999) 084002, [gr-qc/9905064].

[91] A. M. Green, A. R. Liddle, K. A. Malik and M. Sasaki, *A New calculation of the mass fraction of primordial black holes*, *Phys. Rev.* **D70** (2004) 041502, [astro-ph/0403181].

[92] M. Kopp, S. Hofmann and J. Weller, *Separate Universes Do Not Constrain Primordial Black Hole Formation*, *Phys. Rev.* **D83** (2011) 124025, [1012.4369].

[93] T. Harada and B. J. Carr, *Upper limits on the size of a primordial black hole*, *Phys. Rev.* **D71** (2005) 104009, [astro-ph/0412134].

[94] S. Young, C. T. Byrnes and M. Sasaki, *Calculating the mass fraction of primordial black holes*, *JCAP* **1407** (2014) 045, [1405.7023].

[95] M. W. Choptuik, *Universality and scaling in gravitational collapse of a massless scalar field*, *Phys. Rev. Lett.* **70** (1993) 9–12.

[96] C. R. Evans and J. S. Coleman, *Observation of critical phenomena and selfsimilarity in the gravitational collapse of radiation fluid*, *Phys. Rev. Lett.* **72** (1994) 1782–1785, [gr-qc/9402041].

[97] C. Gundlach and J. M. Martin-Garcia, *Critical phenomena in gravitational collapse*, *Living Rev. Rel.* **10** (2007) 5, [0711.4620].

[98] F. Kühnel, C. Rampf and M. Sandstad, *Effects of Critical Collapse on Primordial Black-Hole Mass Spectra*, *Eur. Phys. J.* **C76** (2016) 93, [1512.00488].

[99] B. Carr, F. Kuhnel and M. Sandstad, *Primordial Black Holes as Dark Matter*, *Phys. Rev.* **D94** (2016) 083504, [1607.06077].

[100] S. W. Hawking, *Black hole explosions*, *Nature* **248** (1974) 30–31.

[101] S. W. Hawking, *Particle Creation by Black Holes*, *Commun. Math. Phys.* **43** (1975) 199–220.

[102] A. S. Josan, A. M. Green and K. A. Malik, *Generalised constraints on the curvature perturbation from primordial black holes*, *Phys. Rev.* **D79** (2009) 103520, [0903.3184].

[103] W. H. Press and P. Schechter, *Formation of Galaxies and Clusters of Galaxies by Self-Similar Gravitational Condensation*, *Astrophysical Journal* **187** (Feb., 1974) 425–438.

[104] B. J. Carr, K. Kohri, Y. Sendouda and J. Yokoyama, *New cosmological constraints on primordial black holes*, *Phys. Rev.* **D81** (2010) 104019, [0912.5297].

[105] Y. I. Izotov and T. X. Thuan, *The Primordial abundance of 4-He revisited*, *Astrophys. J.* **500** (1998) 188.

[106] Y. I. Izotov and T. X. Thuan, *Systematic effects and a new determination of the primordial abundance of He-4 and dY/dZ from observations of blue compact galaxies*, *Astrophys. J.* **602** (2004) 200–230, [astro-ph/0310421].

[107] K. A. Olive and E. D. Skillman, *A Realistic determination of the error on the primordial helium abundance: Steps toward non-parametric nebular helium abundances*, *Astrophys. J.* **617** (2004) 29, [astro-ph/0405588].

[108] M. Fukugita and M. Kawasaki, *Primordial helium abundance: a reanalysis of the izotov-thuan spectroscopic sample*, *Astrophys. J.* **646** (2006) 691–695, [astro-ph/0603334].

[109] M. Peimbert, V. Luridiana and A. Peimbert, *Revised Primordial Helium Abundance Based on New Atomic Data*, *Astrophys. J.* **666** (2007) 636–646, [astro-ph/0701580].

[110] Y. I. Izotov, T. X. Thuan and G. Stasinska, *The primordial abundance of He-4: A self-consistent empirical analysis of systematic effects in a large sample of low-metallicity HII regions*, *Astrophys. J.* **662** (2007) 15–38, [astro-ph/0702072].

[111] S. Burles and D. Tytler, *The Deuterium abundance toward QSO 1009+2956*, *Astrophys. J.* **507** (1998) 732–744, [astro-ph/9712109].

[112] J. M. O'Meara, D. Tytler, D. Kirkman, N. Suzuki, J. X. Prochaska, D. Lubin et al., *The Deuterium to hydrogen abundance ratio towards a fourth QSO: HS 0105 + 1619*, *Astrophys. J.* **552** (2001) 718–730, [astro-ph/0011179].

[113] J. Geiss and G. Gloeckler, *Isotopic Composition of H, HE and NE in the Protosolar Cloud*, *Space Science Reviews* **106** (Apr., 2003) 3–18.

[114] M. Asplund, D. L. Lambert, P. E. Nissen, F. Primas and V. V. Smith, *Lithium isotopic abundances in metal-poor halo stars*, *Astrophys. J.* **644** (2006) 229–259, [astro-ph/0510636].

[115] J. Hisano, M. Kawasaki, K. Kohri, T. Moroi and K. Nakayama, *Cosmic Rays from Dark Matter Annihilation and Big-Bang Nucleosynthesis*, *Phys. Rev.* **D79** (2009) 083522, [0901.3582].

[116] L. Zhang, X. Chen, M. Kamionkowski, Z.-g. Si and Z. Zheng, *Constraints on radiative dark-matter decay from the cosmic microwave background*, *Phys. Rev.* **D76** (2007) 061301, [0704.2444].

[117] X.-H. Fan, C. L. Carilli and B. G. Keating, *Observational constraints on cosmic reionization*, *Ann. Rev. Astron. Astrophys.* **44** (2006) 415–462, [astro-ph/0602375].

[118] K. J. Mack and D. H. Wesley, *Primordial black holes in the Dark Ages: Observational prospects for future 21cm surveys*, 0805.1531.

[119] D. J. Fixsen, E. S. Cheng, J. M. Gales, J. C. Mather, R. A. Shafer and E. L. Wright, *The Cosmic Microwave Background spectrum from the full COBE FIRAS data set*, *Astrophys. J.* **473** (1996) 576, [astro-ph/9605054].

[120] W. Hu and J. Silk, *Thermalization constraints and spectral distortions for massive unstable relic particles*, *Phys. Rev. Lett.* **70** (1993) 2661–2664.

[121] H. Tashiro and N. Sugiyama, *Constraints on Primordial Black Holes by Distortions of Cosmic Microwave Background*, *Phys. Rev.* **D78** (2008) 023004, [0801.3172].

[122] A. Kogut et al., *The Primordial Inflation Explorer (PIXIE): A Nulling Polarimeter for Cosmic Microwave Background Observations*, *JCAP* **1107** (2011) 025, [1105.2044].

[123] PRISM collaboration, P. Andre et al., *PRISM (Polarized Radiation Imaging and Spectroscopy Mission): A White Paper on the Ultimate Polarimetric Spectro-Imaging of the Microwave and Far-Infrared Sky*, 1306.2259.

[124] EGRET collaboration, P. Sreekumar et al., *EGRET observations of the extragalactic gamma-ray emission*, *Astrophys. J.* **494** (1998) 523–534, [astro-ph/9709257].

[125] J. H. MacGibbon and B. R. Webber, *Quark and gluon jet emission from primordial black holes: The instantaneous spectra*, *Phys. Rev.* **D41** (1990) 3052–3079.

[126] D. E. Gruber, J. L. Matteson, L. E. Peterson and G. V. Jung, *The spectrum of diffuse cosmic hard x-rays measured with heao-1*, *Astrophys. J.* **520** (1999) 124, [astro-ph/9903492].

[127] G. Weidenspointner et al., *The comptel instrumental line background*, *AIP Conf. Proc.* **510** (2004) 581–585, [astro-ph/0012332].

[128] A. W. Strong, I. V. Moskalenko and O. Reimer, *A new determination of the extragalactic diffuse gamma-ray background from egret data*, *Astrophys. J.* **613** (2004) 956–961, [astro-ph/0405441].

[129] Fermi-LAT collaboration, A. A. Abdo et al., *The Spectrum of the Isotropic Diffuse Gamma-Ray Emission Derived From First-Year Fermi Large Area Telescope Data*, *Phys. Rev. Lett.* **104** (2010) 101101, [1002.3603].

[130] Super-Kamiokande collaboration, M. Malek et al., *Search for supernova relic neutrinos at SUPER-KAMIOKANDE*, *Phys. Rev. Lett.* **90** (2003) 061101, [hep-ex/0209028].

[131] I. B. Zeldovich, A. A. Starobinskii, M. I. Khlopov and V. M. Chechetkin, *Primordial black holes and the deuterium problem*, *Soviet Astronomy Letters* **3** (June, 1977) 110–112.

[132] M. Lemoine, *Moduli constraints on primordial black holes*, *Phys. Lett.* **B481** (2000) 333–338, [hep-ph/0001238].

[133] J. H. MacGibbon, *Can Planck-mass relics of evaporating black holes close the universe?*, *Nature* **329** (1987) 308–309.

[134] B. J. Carr, J. H. Gilbert and J. E. Lidsey, *Black hole relics and inflation: Limits on blue perturbation spectra*, *Phys. Rev.* **D50** (1994) 4853–4867, [astro-ph/9405027].

[135] H. Niikura, M. Takada, N. Yasuda, R. H. Lupton, T. Sumi, S. More et al., *Microlensing constraints on $10^{-10}M_{\odot}$-scale primordial black holes from high-cadence observation of M31 with Hyper Suprime-Cam*, 1701.02151.

[136] K. Inomata, M. Kawasaki, K. Mukaida, Y. Tada and T. T. Yanagida, *Inflationary Primordial Black Holes as All Dark Matter*, 1701.02544.

[137] A. Barnacka, J. F. Glicenstein and R. Moderski, *New constraints on primordial black holes abundance from femtolensing of gamma-ray bursts*, *Phys. Rev.* **D86** (2012) 043001, [1204.2056].

[138] MACHO collaboration, C. Alcock et al., *The MACHO project: Microlensing results from 5.7 years of LMC observations*, *Astrophys. J.* **542** (2000) 281–307, [astro-ph/0001272].

[139] C. Hamadache et al., *Galactic bulge microlensing optical depth from eros-2*, *Astron. Astrophys.* **454** (2006) 185–199, [astro-ph/0601510].

[140] EROS-2 collaboration, P. Tisserand et al., *Limits on the Macho Content of the Galactic Halo from the EROS-2 Survey of the Magellanic Clouds*, *Astron. Astrophys.* **469** (2007) 387–404, [astro-ph/0607207].

[141] Macho collaboration, R. A. Allsman et al., *MACHO project limits on black hole dark matter in the 1-30 solar mass range*, *Astrophys. J.* **550** (2001) L169, [astro-ph/0011506].

[142] K. Griest, A. M. Cieplak and M. J. Lehner, *New Limits on Primordial Black Hole Dark Matter from an Analysis of Kepler Source Microlensing Data*, *Phys. Rev. Lett.* **111** (2013) 181302.

[143] P. N. Wilkinson, D. R. Henstock, I. W. A. Browne, A. G. Polatidis, P. Augusto, A. C. S. Readhead et al., *Limits on the cosmological abundance of supermassive compact objects from a search for multiple imaging in compact radio sources*, *Phys. Rev. Lett.* **86** (2001) 584–587, [astro-ph/0101328].

[144] P. W. Graham, S. Rajendran and J. Varela, *Dark Matter Triggers of Supernovae*, *Phys. Rev.* **D92** (2015) 063007, [1505.04444].

[145] F. Capela, M. Pshirkov and P. Tinyakov, *Constraints on Primordial Black Holes as Dark Matter Candidates from Star Formation*, *Phys. Rev.* **D87** (2013) 023507, [1209.6021].

[146] F. Capela, M. Pshirkov and P. Tinyakov, *Constraints on primordial black holes as dark matter candidates from capture by neutron stars*, *Phys. Rev.* **D87** (2013) 123524, [1301.4984].

[147] D. Gaggero, G. Bertone, F. Calore, R. M. T. Connors, M. Lovell, S. Markoff et al., *Searching for Primordial Black Holes in the radio and X-ray sky*, 1612.00457.

[148] K. Schutz and A. Liu, *Pulsar timing can constrain primordial black holes in the LIGO mass window*, 1610.04234.

[149] T. D. Brandt, *Constraints on MACHO Dark Matter from Compact Stellar Systems in Ultra-Faint Dwarf Galaxies*, *Astrophys. J.* **824** (2016) L31, [1605.03665].

[150] D. P. Quinn, M. I. Wilkinson, M. J. Irwin, J. Marshall, A. Koch and V. Belokurov, *On the reported death of the MACHO era*, *Monthly Notices of the RAS* **396** (June, 2009) L11–L15, [0903.1644].

[151] B. J. Carr and M. Sakellariadou, *Dynamical constraints on dark compact objects*, *Astrophys. J.* **516** (1999) 195–220.

[152] N. Afshordi, P. McDonald and D. N. Spergel, *Primordial black holes as dark matter: The Power spectrum and evaporation of early structures*, *Astrophys. J.* **594** (2003) L71–L74, [astro-ph/0302035].

[153] M. Ricotti, J. P. Ostriker and K. J. Mack, *Effect of Primordial Black Holes on the Cosmic Microwave Background and Cosmological Parameter Estimates*, *Astrophys. J.* **680** (2008) 829, [0709.0524].

[154] L. Chen, Q.-G. Huang and K. Wang, *Constraint on the abundance of primordial black holes in dark matter from Planck data*, 1608.02174.

[155] J. D. Bradford, M. Geha, R. Muñoz, F. A. Santana, J. D. Simon, P. Côté et al., *Structure and Dynamics of the Globular Cluster Palomar 13*, *Astrophys. J.* **743** (2011) 167, [1110.0484].

[156] R. Ibata, C. Nipoti, A. Sollima, M. Bellazzini, S. Chapman and E. Dalessandro, *Do globular clusters possess Dark Matter halos? A case study in NGC 2419*, *Mon. Not. Roy. Astron. Soc.* **428** (2013) 3648, [1210.7787].

[157] S. Bird, I. Cholis, J. B. Muñoz, Y. Ali-Haïmoud, M. Kamionkowski, E. D. Kovetz et al., *Did LIGO detect dark matter?*, *Phys. Rev. Lett.* **116** (2016) 201301, [1603.00464].

[158] S. Clesse and J. García-Bellido, *The clustering of massive Primordial Black Holes as Dark Matter: measuring their mass distribution with Advanced LIGO*, *Phys. Dark Univ.* **10** (2016) 002, [1603.05234].

[159] P. Pani and A. Loeb, *Tidal capture of a primordial black hole by a neutron star: implications for constraints on dark matter*, *JCAP* **1406** (2014) 026, [1401.3025].

[160] F. Capela, M. Pshirkov and P. Tinyakov, *A comment on "Exclusion of the remaining mass window for primordial black holes ...", arXiv:1401.3025*, 1402.4671.

[161] G. Defillon, E. Granet, P. Tinyakov and M. H. G. Tytgat, *Tidal capture of primordial black holes by neutron stars*, *Phys. Rev.* **D90** (2014) 103522, [1409.0469].

[162] Y. Ali-Haïmoud and M. Kamionkowski, *Cosmic microwave background limits on accreting primordial black holes*, 1612.05644.

[163] Virgo, LIGO Scientific collaboration, B. P. Abbott et al., *Observation of Gravitational Waves from a Binary Black Hole Merger*, *Phys. Rev. Lett.* **116** (2016) 061102, [1602.03837].

[164] M. Sasaki, T. Suyama, T. Tanaka and S. Yokoyama, *Primordial Black Hole Scenario for the Gravitational-Wave Event GW150914*, *Phys. Rev. Lett.* **117** (2016) 061101, [1603.08338].

[165] Virgo, LIGO Scientific collaboration, B. P. Abbott et al., *Binary Black Hole Mergers in the first Advanced LIGO Observing Run*, *Phys. Rev.* **X6** (2016) 041015, [1606.04856].

[166] Yu. N. Eroshenko, *Formation of PBHs binaries and gravitational waves from their merge*, 1604.04932.

[167] R. Saito and J. Yokoyama, *Gravitational wave background as a probe of the primordial black hole abundance*, *Phys. Rev. Lett.* **102** (2009) 161101, [0812.4339].

[168] R. Saito and J. Yokoyama, *Gravitational-Wave Constraints on the Abundance of Primordial Black Holes*, *Prog. Theor. Phys.* **123** (2010) 867–886, [0912.5317].

[169] S. Dodelson, *Modern Cosmology*. Academic Press, Amsterdam, 2003.

[170] L. Lentati et al., *European Pulsar Timing Array Limits On An Isotropic Stochastic Gravitational-Wave Background*, *Mon. Not. Roy. Astron. Soc.* **453** (2015) 2576–2598, [1504.03692].

[171] NANOGrav collaboration, Z. Arzoumanian et al., *The NANOGrav Nine-year Data Set: Limits on the Isotropic Stochastic Gravitational Wave Background*, *Astrophys. J.* **821** (2016) 13, [1508.03024].

[172] R. M. Shannon et al., *Gravitational waves from binary supermassive black holes missing in pulsar observations*, *Science* **349** (2015) 1522–1525, [1509.07320].

[173] C. J. Moore, R. H. Cole and C. P. L. Berry, *Gravitational-wave sensitivity curves*, *Class. Quant. Grav.* **32** (2015) 015014, [1408.0740].

[174] G. Janssen et al., *Gravitational wave astronomy with the SKA*, *PoS* **AASKA14** (2015) 037, [1501.00127].

[175] J. Kormendy and L. C. Ho, *Coevolution (Or Not) of Supermassive Black Holes and Host Galaxies*, *Ann. Rev. Astron. Astrophys.* **51** (2013) 511–653, [1304.7762].

[176] SDSS collaboration, X. Fan et al., *A Survey of $z > 5.8$ quasars in the Sloan Digital Sky Survey I: Discovery of three new quasars and the spatial density of luminous quasars at $z \sim 6$*, *Astron. J.* **122** (2001) 2833, [astro-ph/0108063].

[177] D. J. Mortlock et al., *A luminous quasar at a redshift of $z = 7.085$*, *Nature* **474** (2011) 616, [1106.6088].

[178] R. Bean and J. Magueijo, *Could supermassive black holes be quintessential primordial black holes?*, *Phys. Rev.* **D66** (2002) 063505, [astro-ph/0204486].

[179] B. J. Carr and J. E. Lidsey, *Primordial black holes and generalized constraints on chaotic inflation*, *Phys. Rev.* **D48** (1993) 543–553.

[180] J. Chluba, A. L. Erickcek and I. Ben-Dayan, *Probing the inflaton: Small-scale power spectrum constraints from measurements of the CMB energy spectrum*, *Astrophys. J.* **758** (2012) 76, [1203.2681].

[181] K. Kohri, T. Nakama and T. Suyama, *Testing scenarios of primordial black holes being the seeds of supermassive black holes by ultracompact minihalos and CMB μ-distortions*, *Phys. Rev.* **D90** (2014) 083514, [1405.5999].

[182] T. Nakama, T. Suyama and J. Yokoyama, *Supermassive black holes formed by direct collapse of inflationary perturbations*, *Phys. Rev.* **D94** (2016) 103522, [1609.02245].

[183] M. Kawasaki, A. Kusenko, Y. Tada and T. T. Yanagida, *Primordial black holes as dark matter in supergravity inflation models*, *Phys. Rev.* **D94** (2016) 083523, [1606.07631].

[184] K. Kumekawa, T. Moroi and T. Yanagida, *Flat potential for inflaton with a discrete R invariance in supergravity*, *Prog. Theor. Phys.* **92** (1994) 437–448, [hep-ph/9405337].

[185] K. I. Izawa, M. Kawasaki and T. Yanagida, *Dynamical tuning of the initial condition for new inflation in supergravity*, *Phys. Lett.* **B411** (1997) 249–255, [hep-ph/9707201].

[186] M. Kawasaki, M. Yamaguchi and T. Yanagida, *Natural chaotic inflation in supergravity*, *Phys. Rev. Lett.* **85** (2000) 3572–3575, [hep-ph/0004243].

[187] K. Harigaya, M. Ibe and T. T. Yanagida, *Lower Bound on the Garvitino Mass $m_{3/2} > O(100)$ TeV in R-Symmetry Breaking New Inflation*, *Phys. Rev.* **D89** (2014) 055014, [1311.1898].

[188] J. L. Evans, M. Ibe, J. Kehayias and T. T. Yanagida, *Non-Anomalous Discrete R-symmetry Decrees Three Generations*, *Phys. Rev. Lett.* **109** (2012) 181801, [1111.2481].

[189] F. Takahashi, *New inflation in supergravity after Planck and LHC*, *Phys. Lett.* **B727** (2013) 21–26, [1308.4212].

[190] K.-I. Izawa and T. Yanagida, *Dynamical supersymmetry breaking in vector - like gauge theories*, *Prog. Theor. Phys.* **95** (1996) 829–830, [hep-th/9602180].

[191] K. A. Intriligator and S. D. Thomas, *Dynamical supersymmetry breaking on quantum moduli spaces*, *Nucl. Phys.* **B473** (1996) 121–142, [hep-th/9603158].

[192] Z. Chacko, M. A. Luty and E. Ponton, *Calculable dynamical supersymmetry breaking on deformed moduli spaces*, *JHEP* **12** (1998) 016, [hep-th/9810253].

[193] M. Kawasaki and Y. Tada, *Can massive primordial black holes be produced in mild waterfall hybrid inflation?*, *JCAP* **1608** (2016) 041, [1512.03515].

[194] A. D. Linde, *Hybrid inflation*, *Phys. Rev.* **D49** (1994) 748–754, [astro-ph/9307002].

[195] G. R. Dvali, Q. Shafi and R. K. Schaefer, *Large scale structure and supersymmetric inflation without fine tuning*, *Phys. Rev. Lett.* **73** (1994) 1886–1889, [hep-ph/9406319].

[196] W. Buchmuller, L. Covi and D. Delepine, *Inflation and supersymmetry breaking*, *Phys. Lett.* **B491** (2000) 183–189, [hep-ph/0006168].

[197] W. Buchmuller, V. Domcke and K. Schmitz, *Spontaneous B-L Breaking as the Origin of the Hot Early Universe*, *Nucl. Phys.* **B862** (2012) 587–632, [1202.6679].

[198] W. Buchmüller, V. Domcke, K. Kamada and K. Schmitz, *Hybrid Inflation in the Complex Plane*, *JCAP* **1407** (2014) 054, [1404.1832].

[199] S. Clesse, *Hybrid inflation along waterfall trajectories*, *Phys. Rev.* **D83** (2011) 063518, [1006.4522].

[200] H. Kodama, K. Kohri and K. Nakayama, *On the waterfall behavior in hybrid inflation*, *Prog. Theor. Phys.* **126** (2011) 331–350, [1102.5612].

[201] D. Mulryne, S. Orani and A. Rajantie, *Non-Gaussianity from the hybrid potential*, *Phys. Rev.* **D84** (2011) 123527, [1107.4739].

[202] S. Clesse and B. Garbrecht, *Slow Roll during the Waterfall Regime: The Small Coupling Window for SUSY Hybrid Inflation*, *Phys. Rev.* **D86** (2012) 023525, [1204.3540].

[203] S. Clesse, B. Garbrecht and Y. Zhu, *Non-Gaussianities and Curvature Perturbations from Hybrid Inflation*, *Phys. Rev.* **D89** (2014) 063519, [1304.7042].

[204] J. Garcia-Bellido, A. D. Linde and D. Wands, *Density perturbations and black hole formation in hybrid inflation*, *Phys. Rev.* **D54** (1996) 6040–6058, [astro-ph/9605094].

[205] D. H. Lyth, *Contribution of the hybrid inflation waterfall to the primordial curvature perturbation*, *JCAP* **1107** (2011) 035, [1012.4617].

[206] D. H. Lyth, *The hybrid inflation waterfall and the primordial curvature perturbation*, *JCAP* **1205** (2012) 022, [1201.4312].

[207] E. Bugaev and P. Klimai, *Curvature perturbation spectra from waterfall transition, black hole constraints and non-Gaussianity*, *JCAP* **1111** (2011) 028, [1107.3754].

[208] E. Bugaev and P. Klimai, *Formation of primordial black holes from non-Gaussian perturbations produced in a waterfall transition*, *Phys. Rev.* **D85** (2012) 103504, [1112.5601].

[209] A. H. Guth and E. I. Sfakianakis, *Density Perturbations in Hybrid Inflation Using a Free Field Theory Time-Delay Approach*, 1210.8128.

[210] I. F. Halpern, M. P. Hertzberg, M. A. Joss and E. I. Sfakianakis, *A Density Spike on Astrophysical Scales from an N-Field Waterfall Transition*, *Phys. Lett.* **B748** (2015) 132–143, [1410.1878].

[211] S. Clesse and J. García-Bellido, *Massive Primordial Black Holes from Hybrid Inflation as Dark Matter and the seeds of Galaxies*, *Phys. Rev.* **D92** (2015) 023524, [1501.07565].

[212] J. Martin and V. Vennin, *Stochastic Effects in Hybrid Inflation*, *Phys. Rev.* **D85** (2012) 043525, [1110.2070].

[213] D. Jeong, *Cosmology with high ($z > 1$) redshift galaxy surveys*. PhD thesis, University of Texas at Austin <EMAIL>djeong@astro.as.utexas.edu</EMAIL>, Aug., 2010.